Max-Planck-Institut für Meteorologie
Max Planck Institute for Meteorology

A Subgrid Glacier Parameterisation for Use in Regional Climate Modelling

Sven Kotlarski


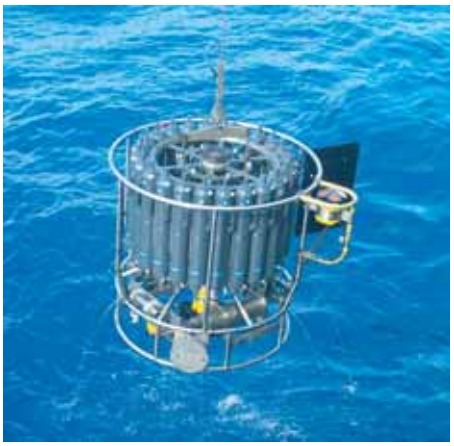


Berichte zur Erdsystemforschung 42/2007

Reports on Earth System Science

Hinweis

Die Berichte zur Erdsytemforschung werden vom Max-Planck-Institut für Meteorologie in Hamburg in unregelmäßiger Abfolge herausgegeben.

Sie enthalten wissenschaftliche und technische Beiträge, inklusive Dissertationen.

Die Beiträge geben nicht notwendigerweise die Auffassung des Instituts wieder.

Die "Berichte zur Erdsystemforschung" führen die vorherigen Reihen "Reports" und "Examensarbeiten" weiter.

Notice

The Reports on Earth System Science are published by the Max Planck Institute for Meteorology in Hamburg. They appear in irregular intervals.

They contain scientific and technical contributions, including Ph. D. theses.

The Reports do not necessarily reflect the opinion of the Institute.

The "Reports on Earth System Science" continue the former "Reports" and "Examensarbeiten" of the Max Planck Institute.

Anschrift / Address

Max-Planck-Institut für Meteorologie
Bundesstrasse 53
20146 Hamburg
Deutschland

Tel.: +49-(0)40-4 11 73-0
Fax: +49-(0)40-4 11 73-298
Web: www.mpimet.mpg.de

Layout:

Bettina Diallo, PR & Grafik

Titelfotos:
vorne:
Christian Klepp - Jochem Marotzke - Christian Klepp
hinten:
Clotilde Dubois - Christian Klepp - Katsumasa Tanaka

Berichte zur Erdsystemforschung 42/2007

A Subgrid Glacier Parameterisation for Use in Regional Climate Modelling

Dissertation zur Erlangung des Doktorgrades der Naturwissenschaften
im Departement Geowissenschaften der Universität Hamburg
vorgelegt von

Sven Kotlarski
aus Stadthagen

Hamburg 2007

Reports on Earth System Science 42/2007

ISSN 1614-1199

Sven Kotlarski
Max-Planck-Institut für Meteorologie
Bundesstrasse 53
20146 Hamburg
Germany

Als Dissertation angenommen
vom Departement Geowissenschaften der Universität Hamburg

auf Grund der Gutachten
von Prof. Dr. Hartmut Graßl
und Dr. Daniela Jacob
und Prof. Dr. Christoph Schär

Hamburg, den 4. April 2007
Prof. Dr. Kay-Christian Emeis
Leiter des Departements für Geowissenschaften

ISSN 1614-1199

A Subgrid Glacier Parameterisation for Use in Regional Climate Modelling

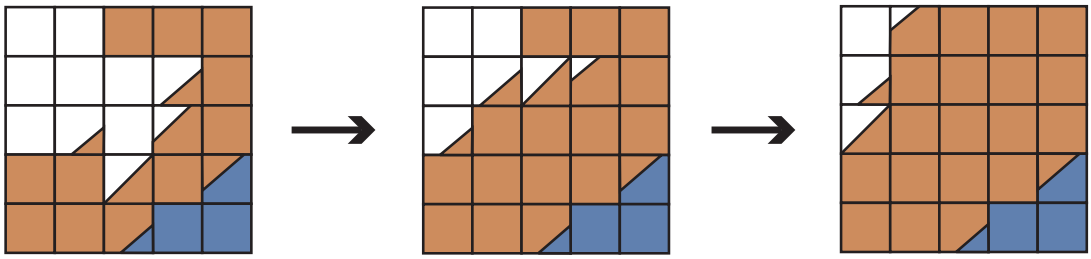

Sven Kotlarski

Hamburg 2007

Summary

Due to their unique surface characteristics and their function as hydrological reservoirs glaciers can be considered as an interacting component of the climate system. In alpine areas they often play a major role in determining regional water and energy budgets. Regional climate models (RCMs) are an important tool in the analysis of the corresponding water and energy cycles and for the prediction of future changes in the individual components. However, glaciers are only represented in an extremely simplified way (or even totally neglected) in state-of-the-art climate models. Their size is usually beyond grid box resolution and only the largest glaciers are treated as fixed surface boundary conditions with runoff generation on glaciated surfaces being simplified to a very high degree. The direct prediction of changes in glacier mass balance and glacier extent as a response to changing climatic conditions is therefore not possible. As a consequence, the feedback of changes in ice cover to the atmosphere and the influence of enhanced glacier melt (as generally expected for the next decades) on runoff conditions cannot be assessed.

To overcome these deficiencies and to represent glaciers in an appropriate way, a subgrid glacier parameterisation has been developed and implemented into the RCM REMO. The new scheme partly replaces the static glacier mask used so far and includes the explicit simulation of glacier mass and energy balance. The total ice mass within a climate model grid box is represented by a two-layer ice cuboid covering a certain fraction of the total grid box area. Surface fluxes are derived separately for glaciated and non-glaciated parts. The subgrid variability of snowfall and of global radiation within a climate model grid box is explicitly accounted for by simple redistribution concepts. The glaciated fraction of an individual grid box is adjusting dynamically depending on accumulation and ablation conditions and following simple volume-area relationships. Surface runoff and drainage originating from the glacier fraction are added to the total grid box runoff thereby closing the grid box water balance. In order to assess the effect of changing ice volumes on river discharge the routing scheme HD (Hydrological Discharge) is coupled to REMO in an offline mode. Several simulations with the new model system $\text{REMO}_{\texttt{glacier}}$ have been carried out for the period 1958-2003 for the European Alps, driven by the ERA40 re-analysis and the operational analysis of the ECMWF at the lateral boundaries. In all experiments a standard horizontal resolution of $^1/_6^\circ$ (approx. 18 x 18 km^2) has been used.

The temporal evolution and the general magnitude of the simulated glacier mass balance are in good accordance with observations, especially during the first half of the investigated period. However, the strong mass loss of Alpine glaciers towards the end of the 20$^{\text{th}}$ century is systematically underestimated by $\text{REMO}_{\texttt{glacier}}$. This is especially true for grid boxes along the northern slopes of the main Alpine ridge which experience a net gain of ice-covered area and ice volume. Probably, these shortcomings are associated with a strong positive bias of the simulated wintertime precipitation compared to observational datasets and with the assumption of a uniformly distributed snow layer on top of the grid box glacier cuboids. Depending on the chosen method for translating glacier mass changes into changes of the ice-covered area (volume-area relationship), the simulated total glaciated area in the Alps considerably decreases from 1958 to 2003 by -17.1 to -23.6% (ice volume: -15.5 to -16.7%).

Concerning the influence of glaciers on the regional climate, the effect of the new subgrid parameterisation on atmospheric parameters is generally restricted to the lower troposphere and to glaciated grid boxes themselves as well as their direct vicinity. The large scale flow conditions are not affected

significantly in the chosen model setup. In glaciated grid cells the incorporation of the glacier scheme into REMO causes a lowering of the near surface air temperature by several degrees Celsius and a less intense local recycling of water by reducing both precipitation and evapotranspiration. These effects are most pronounced in summer and autumn. Also the influence of the new parameterisation scheme on surface hydrology is mainly restricted to strongly glaciated areas in high-altitude regions of the Alps. Here, glacial meltwater can play an important role especially in late summer and early autumn by contributing a considerable fraction (more than 20%) to the total amount of grid box runoff and river discharge.

The simulated glacier mass balance and the corresponding changes of the ice-covered area strongly depend on the chosen value for a number of model parameters. Especially the adequate description of the subgrid variability of snow accumulation, global radiation (slope and shading effects) and air temperature is of high importance. The latter is so far not accounted for in the standard parameterisation scheme. Generally, the results obtained indicate that it is possible to approximately reproduce observed regional glacier mass balances within an RCM based on extremely simple concepts of glacier-climate interaction. However, it has also been shown that realistic results can only be achieved if the subgrid variability of atmospheric parameters within a climate model grid box is explicitly accounted for.

Zusammenfassung

Aufgrund ihrer besonderen Oberflächeneigenschaften und ihrer hydrologischen Speicherfunktion stellen Gletscher einen interaktiven Bestandteil des Klimasystems dar. Der Wasser- und Energiehaushalt vieler Gebirgsregionen wird entscheidend durch die Existenz von Gletschern beeinflusst und geprägt. Die Analyse der entsprechenden regionalen Kreisläufe und insbesondere die Abschätzung zukünftiger Veränderungen sind ein Hauptanwendungsgebiet regionaler Klimamodelle. Durch ihre im Vergleich zur Gitterboxgröße geringe räumliche Ausdehnung werden Gletscher in diesen Modellen jedoch, wenn überhaupt, nur in stark vereinfachter Form als statische untere Randbedingung berücksichtigt. Mit diesem Ansatz ist eine Abschätzung der Änderung von Gletschermassenbilanz und -ausdehnung als Reaktion auf veränderte klimatische Bedingungen nicht möglich. Folglich bleiben auch mögliche Rückkoppelungsmechanismen sowie der Einfluss einer verstärkten Gletscherschmelze auf das Abflussregime vergletscherter Einzugsgebiete unberücksichtigt.

Um die beschriebenen Defizite hinsichtlich der Berücksichtigung von Gletschern in Klimamodellen zu beheben wurde im Rahmen der vorliegenden Arbeit eine subskalige Parameterisierung für Gebirgsgletscher entwickelt und in das regionale Klimamodell REMO eingebaut. In Gebieten ausserhalb der polaren Eisschilde ersetzt die neue Parameterisierung die bisher verwendeten statischen Gletschermasken und berechnet explizit die Gletscherenergie- und -massenbilanz. Das gesamte innerhalb einer Klimamodellgitterbox befindliche Gletschervolumen wird durch einen einzelnen 2-Schichten Eiskörper repräsentiert, der einen zeitlich veränderlichen Anteil der Gitterboxgesamtfläche (entsprechend einer Volumen-Flächen-Beziehung) bedeckt. Durch einfache Umverteilungskonzepte wird die subskalige Varibilität von Schneeniederschlag und Globalstrahlung explizit berücksichtigt. Schnee- und Eisschmelze der vergletscherten Gitterboxfraktion werden dem Gesamtabfluss zugeschlagen, wodurch die Wasserbilanz vergletscherter Gitterboxen vollständig geschlossen wird. Zur Abschätzung des Einflusses der Gletscherschmelze auf das Abflussregime vergletscherter Einzugsgebiete wird zusätzlich ein laterales Transportschema für den Abfluss im Gerinnesystem (HD Modell) an REMO gekoppelt (1-Wege-Koppelung). Mit dem neuen Modellsystem $\text{REMO}_{\texttt{glacier}}$ wurden mehrere Simulationen für den Zeitraum 1958-2003 im Testgebiet der Europäischen Alpen mit einer horizontalen Gitterpunktsauflösung von $^1/_6^\circ$ (ca. 18 x 18 km^2) durchgeführt.

In Abhängigkeit der verwendeten Methode zur Gletscherflächenbestimmung (Volumen-Flächen-Beziehung) beläuft sich der simulierte Gletscherflächenschwund in den Alpen von 1958 bis 2003 auf insgesamt -17.1 bis -23.6% (Gletschervolumen: -15.5 bis -16.7%). Die generelle Größenordnung sowie die zeitliche Variabilität der simulierten alpenweiten Gletschermassenbilanz zeigen eine gute Übereinstimmung mit Beobachtungen, insbesondere in der ersten Hälfte des untersuchten Zeitraumes. Der starke Gletschermassenverlust gegen Ende des 20. Jahrhunderts wird in $\text{REMO}_{\texttt{glacier}}$ jedoch systematisch unterschätzt. Dies gilt besonders für Gitterboxen entlang der Alpennordabdachung, für die insgesamt eine Zunahme von Gletscherfläche und Gletschervolumen simuliert wird. Diese Unzulänglichkeiten werden zumindest teilweise durch eine deutliche Überschätzung der beobachteten Winterniederschläge in den entsprechenden Gebieten sowie durch die Annahme einer gleichmäßigen Schneebeckung auf den Eiskörpern hervorgerufen.

Die Verwendung der neuen Gletscherparameterisierung beeinflusst das simulierte Klima nur in den unteren atmosphärischen Modellschichten und fast ausschließlich in vergletscherten Gitterboxen sowie

direkt angrenzenden Gebieten. Die großskaligen Strömungsvorgänge werden in der gewählten Modellkonfiguration nicht verändert. In vergletscherten Boxen bewirkt das neue Schema einen Rückgang der bodennahen Lufttemperatur um mehrere Grad Celsius sowie eine verringerte Intensität des lokalen Wasserkreislaufs infolge eines Rückgangs von Niederschlag und Evapotranspiration. Beide Effekte sind im Sommer und Herbst am stärksten ausgeprägt. Auch der Einfluss der Gletscherparameterisierung auf den Abfluss beschränkt sich weitestgehend auf stark vergletscherte Einzugsgebiete. In diesen Regionen kann die Eisschmelze im Spätsommer und Frühherbst deutlich ($> 20\%$) zum simulierten Gesamtabfluss beitragen.

Die in $\text{REMO}_{\texttt{glacier}}$ simulierten Gletschermassenbilanzen und die daraus resultierenden Flächenänderungen sind stark abhängig von der gewählten Größe einiger Modellparameter. Insbesondere die Beschreibung der subskaligen Variabilität von Schneeakkumulation, Globalstrahlung und Lufttemperatur ist von entscheidender Bedeutung. In der Standardversion von $\text{REMO}_{\texttt{glacier}}$ ist die subskalige Variabilität der Lufttemperatur bisher noch nicht berücksichtigt. Generell zeigen die Ergebnisse der Modellexperimente, dass die angenäherte Reproduktion beobachteter Gletschermassenbilanzen in einem regionalen Klimamodell mit relativ einfachen und prinzipiell global anwendbaren Konzepten möglich ist. Zufriedenstellende Ergebnisse sind jedoch nur unter Berücksichtigung der subskaligen Variabilität atmosphärischer Parameter innerhalb einer Klimamodellbox möglich.

Contents

1 Introduction

1.1 Background

The 20th century has been a period of worldwide glacier retreat. Since the end of the "Little Ice Age" (in Central Europe around AD 1850) glaciated mountain regions all around the globe experienced a considerable decline of ice cover accompanied by substantial losses of corresponding ice volumes (see Figure 1.1 for an example). The European Alps, for instance, had lost about 50% of their original ice mass by the 1980s (Haeberli and Hoelzle, 1995) with melt rates significantly accelerating towards the end of the century (Paul et al., 2004b).

The observed widespread glacier retreat is consistent with 20th century global temperature increases and is rated as one of the most reliable natural indicators of ongoing warming trends (Haeberli, 1995; IPCC, 2001). Variations in glacier mass are generally determined by the balance between incoming (mass gain) and outgoing (mass loss) terms. The underlying processes are strongly controlled by atmospheric factors and, hence, changes in glacier mass balance can be considered as the direct, undelayed and unfiltered reaction to local atmospheric conditions (e.g., Haeberli, 1995; Reichert et al., 2001b). Via a complex series of changes in glacier flow and geometry, mass balance anomalies eventually result in an adjustment of the position of the terminus and, hence, in glacier length changes with response times varying considerably depending on the geometry and the specific climatic setting (Oerlemans, 2005). Due to the variety of involved time scales, the state of a glacier bears valuable information both on climatic changes in the past and on changes occurring at present (Singh and Singh, 2001; Smith and Budd, 1981). Applying inverse modelling techniques, glacier length variations can even be used to derive independent estimates of secular atmospheric warming trends (Oerlemans, 1994, 2005).

The link between glaciers and climate is not a simple, one-directional relationship though. Via a number of **feedback mechanisms**, changes in ice cover can potentially influence the ambient air and thus modify the local climate. The unique surface characteristics of ice, namely the comparatively high reflectivity in the solar spectrum and a surface temperature never exceeding 0°C, affect the components of the surface energy balance and near surface exchange processes. Depending on the extent of the ice cover and the magnitude of its variations, also larger regions can be affected. In case of the large polar ice sheets, a further feedback loop exists via ice thickness since the simple geometry and shape of an ice sheet alters the atmospheric circulation (Herterich, 2001). In addition to direct physical interactions between a surface ice cover and the overlying air mass a further feedback mechanism consists in freshwater originating from glacier melt entering the oceans and thereby modifying oceanic circulations and deep water formation and contributing to sea level rise (IPCC, 2001).

Besides their function as an interacting part of the climate system, glaciers play an important role in regional water cycles. Seasonal runoff patterns for instance are strongly influenced by the presence of glaciers (Singh and Singh, 2001; Beniston, 2003; Jansson et al., 2003; Verbunt et al., 2003). On a

Figure 1.1: Gepatschferner, Austria, in the years **1904** (left) and **2000** (right). Source: Gesellschaft für ökologische Forschung.

catchment scale, glaciers act as **natural hydrological buffers**, storing water in form of ice during wet and cold periods and releasing it in dry and hot times (Baumgartner and Liebscher, 1990). Glacier mass variations will therefore induce changes in the hydrological regime (i.e., in seasonal runoff patterns) which is likely to have major consequences for water resources management (Barry, 2003; Barnett et al., 2005). In many areas, water supply systems, agriculture, energy production and river transport strongly depend on this reservoir function since additional water is being released into river systems exactly during times when water is scarce and the need is largest. Even distant mountain glaciers can provide lowland rivers with the important hydrological base flow (Hall and Fagre, 2003). A striking example was the extraordinary hot and dry summer 2003 when a heat wave affected large areas in Central Europe (Beniston, 2004; Schär et al., 2004). At the same time, glaciers in the Alps experienced record-breaking negative mass balances. It is estimated that, during this single summer, the European Alps have lost between 5 and 10% of their remaining ice volume (Frauenfelder et al., 2005; EEA, 2005). Without this additional amount of meltwater, water scarcity in many European river systems would have been much more pronounced. Heavily glaciated catchments even experienced above-average amounts of summer discharge (BUWAL, 2004). If the observed trend of enhanced glacier melt continues, some of the most populated regions on Earth (e.g., the Himalaya-Hindu Kush area) can be expected to run out of water during the dry season (Barnett et al., 2005).

Although glaciers are clearly linked to regional and global climate processes via the described feedback loops, they are still poorly represented in climate models, even in the most sophisticated three-dimensional circulation models (see Figure 1.2 for illustration). Both state-of-the-art general circulation models (GCMs) and regional climate models (RCMs) make use of **static glacier masks** which define a land grid point as being either totally glaciated or totally ice free for the entire simulated period. Possible feedbacks via changes in ice extent triggered by changing climatic conditions are neglected. Furthermore, runoff generation on glaciated grid points is usually not accounted for (e.g., accumulation and melting of snow with subsequent generation of surface runoff or subsurface drainage) and grid point water balances are therefore not closed. If the runoff as simulated by a climate model is directly used in hydrological studies (e.g., in the analysis of changes in seasonal runoff patterns under climate change conditions) the contribution of glacial meltwater components is neglected.

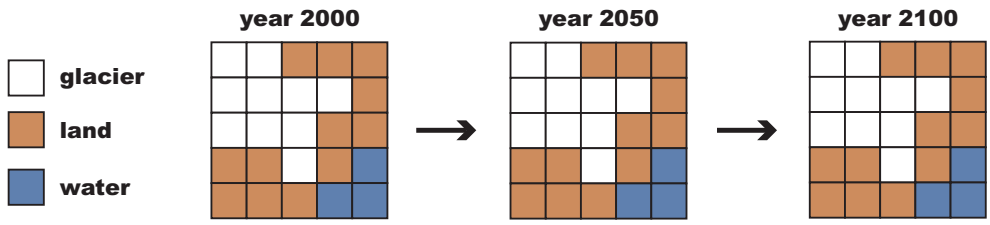

Figure 1.2: Land surface coverage in state-of-the-art climate models: Use of static 0-1 glacier masks.

The simple approach of representing glaciers by static glacier masks is suitable for short- to mid-term climate model integrations on a global scale, where a) the response of glacier extent to changing atmospheric conditions might still be small due to glacier response times and b) the feedback of changing glacier extent on large scale atmospheric flow conditions might be negligible. However, if

- ▷ the contribution of glaciers to global sea level rise is considered as non-negligible (due to their relatively short response time compared to the large ice sheets)
- ▷ regional climatic changes in glaciated areas are analysed
- ▷ a focus is laid on the investigation of runoff conditions in glaciated river basins

a more detailed approach seems to be highly desirable. It is evident that the proper description of processes attached to glaciers and of cryospheric processes in general is essential for simulating the complete terrestrial water cycle in climate models. Recently, the need for an appropriate treatment of the cryosphere in climate models has also been recognized within the *World Climate Research Programme* (WCRP), which led to the launch of the comprehensive *Climate and Cryosphere* (CliC) project (Barry, 2003).

Therefore, within the present study, the possibility of integrating an interactive glacier energy and mass balance scheme including the dynamic adjustment of glaciated areas into a regional climate model is investigated.

1.2 Objectives

Due to restrictions of computing time and a high demand of data, the implementation of existing high resolution mass balance and ice flow models into a climate model is not feasible. The complex chain of dynamic processes linking a meteorological forcing to glacier mass balance and resulting length changes can be numerically simulated only for a few glaciers which have been studied in great detail (Haeberli, 1995). Moreover, single glaciers are usually not resolved by current GCMs and RCMs and further downscaling techniques would have to be applied.

From a climate modelling point of view the exact response of single glaciers to changing climatic conditions does not lie in the focus of interest. The most important questions to be answered are related to regional and even global scales :

- ▷ Can we assess changes in ice cover characteristics by simple parameterisation schemes

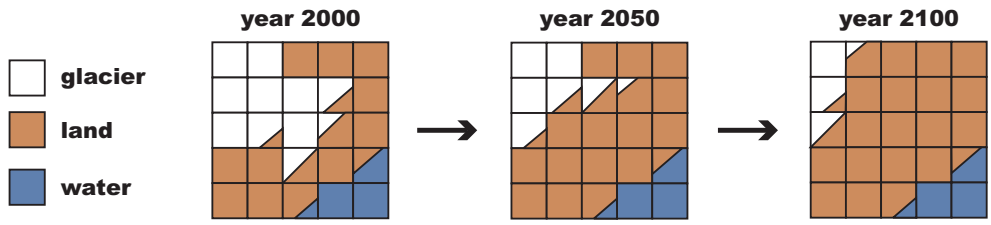

Figure 1.3: The new parameterisation scheme dynamically adjusts the glaciated fraction of each grid cell depending on the simulated climatic forcing (compare to Figure 1.2).

which require only a minimum amount of input data and which are potentially applicable on a global scale ?

- ▷ What is the (cumulative) reaction of total grid box ice cover and ice mass to variations in the simulated climate ?
- ▷ How does the presence of land ice influence surface energy and water exchange processes on a grid box scale ?
- ▷ How do changes in land ice cover feed back to the atmosphere, which atmospheric parameters are affected and on which spatial scale ?
- ▷ In which way is river discharge affected by the simulated changes in land ice cover ?

To answer these questions, a subgrid scale parameterisation of glaciers has been developed within the present study. The new parameterisation scheme has been implemented into the regional climate model REMO where it expands and partly replaces the static glacier mask used so far. In order to improve the simulation of climate relevant processes attached to glaciers and land ice cover in general, the new scheme should capture the most important processes governing the extent of glaciers and their potential influence on regional climate and runoff conditions. In particular, it should

- ▷ account for the influence of partial ice cover on grid box scale surface-atmosphere exchange processes
- ▷ interactively adjust the ice covered grid box fraction and thus enable the simulation of feedback loops via variations in ice cover as a response to climatic changes (see Figure 1.3 for illustration)
- ▷ explicitly account for runoff generation processes on glaciated areas and thus allow for a realistic simulation of runoff characteristics in glaciated catchments
- ▷ only require a minimum of additional input data
- ▷ be applicable in different parts of the world
- ▷ be computationally effective.

1.3 Methods

The general concept for reaching the goals described above is to set up a miniature coupled modelling system as shown schematically in Figure 1.4. The new glacier scheme is fully integrated into the

regional climate model REMO and is called each time step within the model physics. This approach allows for an online two-way interaction between the simulated climate and glacier related processes. The extended model will be referred to as $\text{REMO}_{\texttt{glacier}}$.

Additionally, a river routing scheme (the HD Model, *Hydrological Discharge*) is coupled to $\text{REMO}_{\texttt{glacier}}$. The routing scheme takes over the runoff components produced by REMO's soil scheme and accounts for the lateral transport of water within the surface river system. In this way, the simulation of river discharge on different spatial and temporal scales and, hence, the assessment of changes in runoff characteristics due to variations of glacier mass in glaciated catchments is possible. As the influence of river discharge on the simulated climate in downstream areas is considered as negligible and so far no regional ocean model is attached, the inclusion of possible feedbacks from the routing scheme to the climate model is not necessary. Therefore, the HD model is coupled to $\text{REMO}_{\texttt{glacier}}$ in an offline mode, i.e., the routing scheme is fed by REMO's runoff components but does not feed back to the simulated climate.

As initial test site for model development, the **European Alps** have been chosen (within this work also referred to as the *Alps*). Compared to other areas of the world, this region is only slightly glaciated with a total ice surface area in the mid 1970s of about 3000 km^2 and a total ice volume of about 100 to 130 km^3 (Paul et al., 2004b). A complete melting of this ice mass would lead to a sea level rise of less than 0.35 mm (after Haeberli and Hoelzle, 1995). However, a number of aspects clearly justify this choice:

- Continuous and coordinated glacier monitoring has its roots in the Alps (Haeberli and Zumbühl, 2003) and long-term, high quality datasets on past changes in glacier characteristics are available for this area. In Switzerland, systematic monitoring of glacier fluctuations began in 1880, earlier than in any other country, and has been continued consistently since then (Grove, 2001). Similarly, high resolution and high quality observational datasets exist for atmospheric quantities (e.g., precipitation) and for river discharge.
- Glaciers in the Alps showed a distinct signal to changing climatic conditions since the

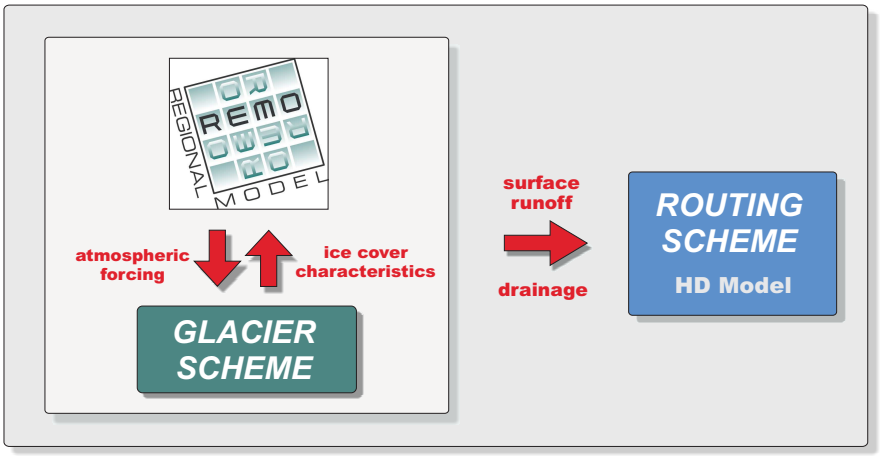

Figure 1.4: The general concept: Setup of a coupled modelling system.

end of the *Little Ice Age*.

- ▷ The regional climate model used in the present study has been developed with a focus on Northern and Central Europe and its general performance, its strengths and weaknesses have been intensively evaluated in this region.
- ▷ From a hydrological perspective, the Alps have an outstanding function as the "Water Tower of Europe" (Mountain Agenda, 1998; Beniston et al., 2003), supplying densely populated areas in the surroundings with water for domestic, industrial and agricultural use as well as for energy production and transportation. Some of the main European river systems originate in this area (Rhine, Danube, Rhone, Po).
- ▷ First-hand expertise on glacier related processes in the Alps has been available via a cooperation with the University of Zurich (Switzerland), which has been highly beneficial for the development of the new parameterisation scheme.

1.4 Structure of the Thesis

In order to provide the necessary background information and to present and discuss the results obtained, this thesis is organised in the following way:

After the introductory Chapter 1, an overview on glaciers and their relevance as a part of the climate system as well as on their influence on catchment hydrology is given in Chapter 2 (**Glaciers**). The most important characteristics of the basic modelling tool used within the present study, the standard version of the regional climate model REMO, are described in Chapter 3 (**The Regional Climate Model REMO**). This chapter also addresses the basic features and necessary modifications of the HD routing scheme, which is coupled to REMO in an offline mode in order to simulate river discharge. Afterwards, a detailed description of the new subgrid glacier parameterisation developed within the present study and its interface to the RCM REMO is given in Chapter 4 (**The New Subgrid Glacier Parameterisation**). The results of the model simulations carried out in the course of this study are presented and discussed in Chapter 5 (**Results**). Finally, the main conclusions of the work and an outlook regarding future perspectives and suggestions for further improvements of the new parameterisation scheme are given in Chapter 6 (**Conclusions and Outlook**).

2 Glaciers

2.1 Definition

The term *glacier* refers to a perennial natural body of surface ice which visibly moves under its own weight in response to gravitational force and which has been formed by metamorphism of snow. By internal deformation and by sliding on the underlying bedrock, glaciers move from upper reaches with a net gain of ice mass to lower regions where mass loss dominates (Singh and Singh, 2001).

In general, this definition applies to a large variety of surface land ice masses and, in a strict sense, also includes the large, continental scale ice masses of Greenland and Antarctica. The latter are usually clearly distinguished from smaller ice bodies and are referred to as *ice sheets*. Thus, fundamentally and in the simplest way, land ice masses can be classified into two basic categories according to their size, their shape and their relationship with the surrounding and underlying topography: **ice sheets** and **glaciers**. Following the UNESCO/WGMS standard classification scheme (UNESCO, 1970), the second category includes a number of subtypes, like mountain glaciers, valley glaciers, cirque glaciers, etc. The kind of ice body which develops in a given region depends partly on ground configuration, but even more on the local ratio of mass gain and mass loss (Singh and Singh, 2001). The present study and the new glacier parameterisation scheme focusses on ice bodies not larger than a couple of climate model grid cells and basically neglects large scale ice flow processes (here: ice flow between the climate model's grid boxes). Therefore, in this study the term *glacier* will simply be used as a synonym for all surface land ice masses except the Greenland and Antarctic ice sheets (see Figure 2.1).

In this section, the most important characteristics of the two basic types are presented.

2.1.1 Ice Sheets (and Ice Caps)

The large polar **ice sheets** of Greenland and Antarctica are continental scale masses of fresh water ice which were formed by the burial and the subsequent densification of accumulated snow (IPCC, 2001; Greve, 2003). Often, these two ice bodies are referred to as *inland ice*. Both ice sheets are dome-shaped with maximum ice thicknesses of more than 3000 m in their central parts. They are thick enough to cover underlying mountain ranges entirely and can thus be regarded as superior to topography. Their summits act as ice divides with ice flow in all directions. With an estimated volume of more than $25 \cdot 10^6$ km^3 and an area of $12 \cdot 10^6$ km^2 the Antarctic Ice Sheet is about eight times more extensive than its Greenland counterpart (Singh and Singh, 2001). It contains more than 90% of the world's ice and about 70% of the world's freshwater. The frozen water stored in both ice sheets corresponds to a sea level rise equivalent of nearly 70 m. That's why only a small fractional change in the volume of the polar ice sheets would have significant effects (IPCC, 2001). However, due to their size and the large ice mass involved in their dynamics, the geometry of ice sheets responds to

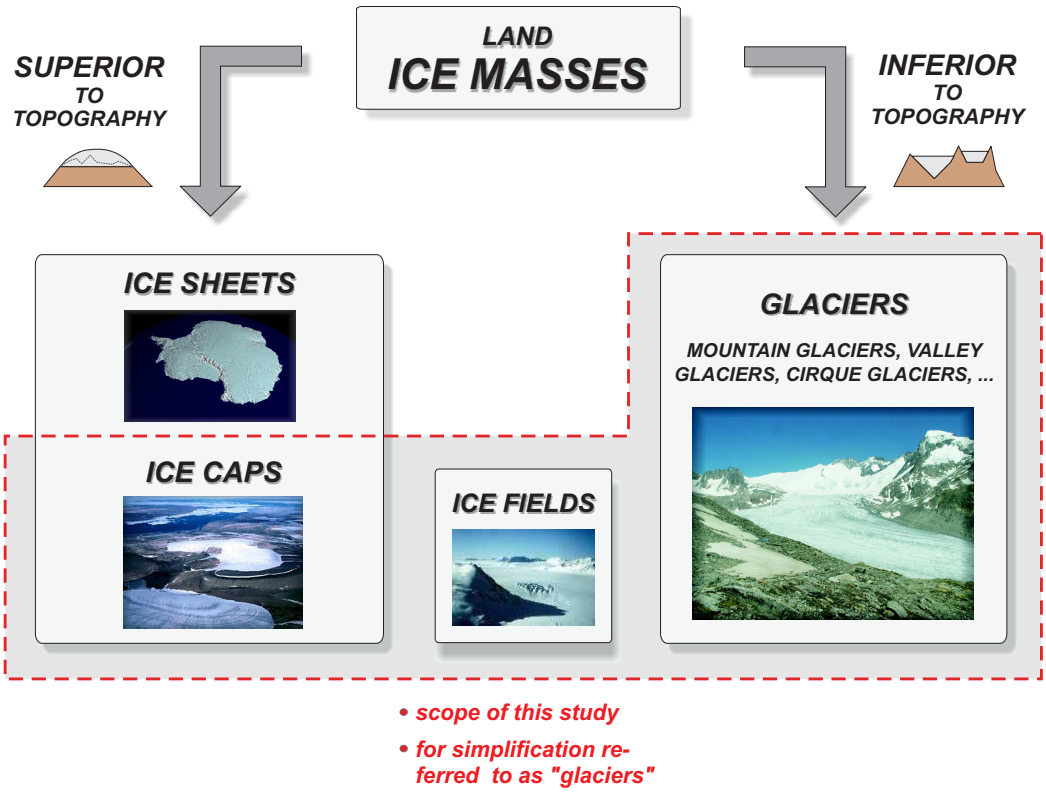

Figure 2.1: Classification of land ice masses according to the UNESCO/WGMS classification scheme (digit 1; UNESCO, 1970). Source of pictures: NASA, NSIDC, U.S. FWS, S. Kotlarski.

climatic changes with strong delays and response times can reach several thousand years. Dedicated modelling studies for the 21st century indicate that the effect of increased precipitation in Antarctica will dominate over the increased melting in Greenland, leading to a slight overall mass gain of polar ice sheets until 2100 (Huybrechts et al., 2004; Alley et al., 2005).

Ice shelves are the ungrounded or floating part of an ice sheet. They mainly occur in large bays along the margin of the Antarctic continent (e.g., the large *Ross Ice Shelf*). In addition to the large continental ice sheets of Greenland and Antarctica, smaller ice bodies with a similar geometry but an area of less than about 50.000 km^2 (i.e., not of continental size) are referred to as **ice caps**. They mostly occur in polar and sub-polar regions where they cover high altitude land areas in a dome shape (Singh and Singh, 2001).

2.1.2 Glaciers

In contrast to the large polar ice sheets and to ice caps, the size and position of **glaciers** is controlled by topographical features (i.e., they are confined by the surrounding mountain terrain). Glaciers usually form in high mountain ranges where temperatures are low enough to allow for the accumulation of snow (**mountain glaciers**). In some cases, they occur in places where ice sheets and ice caps cannot build because of existing land surface features (e.g., too high surface slopes).

If mountain glaciers are confined by valley walls and have formed a distinct tongue, which is quite often the case, they are also referred to as **valley glaciers**. Their shape is largely determined by the

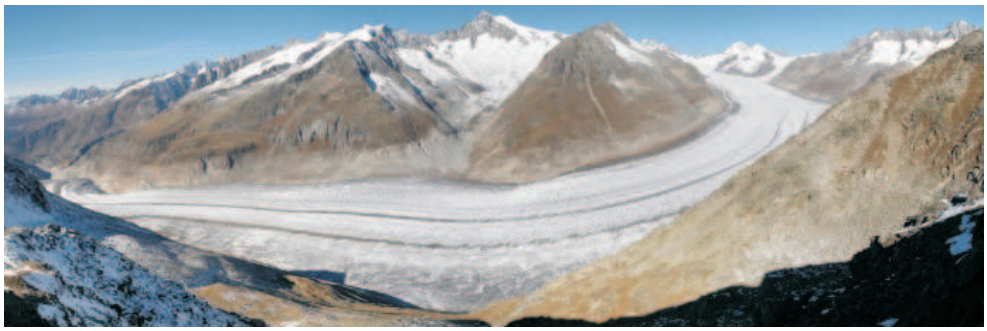

Figure 2.2: The Grosser Aletschgletscher in Switzerland, October 2005. Source: A. Schild, *http://en.wikipedia.org*.

pattern of the valleys. Typically, valley glaciers are 10 to 50 km long, flow into one direction (downhill) through rock valleys and possess no ice divide (Singh and Singh, 2001). They can exceptionally reach lengths of more than 70 km (like Fedtschenko Glacier in the Pamir Region, Asia). The largest glacier in the European Alps is Grosser Aletschgletscher in Switzerland, originating from the Jungfrau Region (at about 4200 m a.s.l.) and descending down towards the Rhone Valley with a length of more than 20 km (Figure 2.2). If, at the base of mountain ranges where valleys open onto large plains, glaciers spread out into wide lobes they are also referred to as **piedmont glaciers** (Hambrey and Alean, 2004). Due to their flatness and small altitudinal extent, a slight warming can be enough to melt the entire broad piedmont termini of a valley glacier (Singh and Singh, 2001).

Glaciers which originate from the continuous Greenland Ice Sheet, ice caps or semi-continuous ice fields (see below), from which they flow out in several directions, are termed **outlet glaciers**. A very common case are so-called **cirque glaciers** or **glacierets**, small ice masses which form in protected, bowl-shaped depressions in the bedrock near ridge crests (*cirques*) and which usually have a characteristic circular shape.

2.1.3 Intermediate Forms

In some cases, an exact distinction between ice caps and glaciers is not possible since some ice bodies show characteristics of both basic types, namely according to their relation to the surrounding and underlying topography. These intermediate types are referred to as **ice fields**, semi-continuous blankets of glacier ice which bury many features of the underlying landscape but still roughly mirror the topography beneath (Hambrey and Alean, 2004). They can consist of a number of large individual glaciers which are connected to each other to cover a large area (Oerlemans, 2001). Ice fields are most common in polar and sub-polar regions, but smaller ones can also be found in temperate latitudes.

2.1.4 Thermal Classification

Apart from their size and shape, glaciers can also be classified according to their internal thermal characteristics. On one side, **polar** or **cold glaciers** are substantially below the freezing point and melting only occurs in a thin layer at the surface during summer. They can be found in polar regions or at very high altitudes where the mean annual air temperature is at least several degrees below zero.

Conversely, **temperate** or **warm glaciers** are at or very near to the melting point throughout, except for a surface layer (up to some ten metres thick) in which the temperature falls below 0°C for part of the year. On such glaciers, the winter cold wave is completely eliminated by the end of the summer (Paterson, 1994). An essential feature of temperate glaciers is that the ice contains some part of liquid phase and that meltwater is abundant in summer, forming well-developed drainage networks within the glacier. Temperate glaciers are characteristic of most mountain regions outside the polar regions (Hambrey and Alean, 2004; Oerlemans, 2001). There are also intermediate cases, i.e., glaciers that have both warm and cold parts (**polythermal glaciers, sub-polar glaciers**). These glaciers are abundant in Arctic and in sub-Antarctic regions and some do also occur in dry high-mountain regions of the mid-latitudes.

2.2 Formation

The first step in the formation of glacier ice is the accumulation of snow. If in some location a part of the snow cover generally persists throughout the following melt season, snow gradually accumulates and is eventually turned into ice in a complex process known as *snow metamorphism* or *recrystallisation*. If finally the ice is thick enough, it starts to flow under the influence of gravity and can be referred to as a glacier.

The transformation of snow into glacier ice is often a long and complex process, during which snow crystals are being reshaped and rearranged through

- mechanical destruction (breaking of surface snow crystals by wind)
- pressure (weight of the overlying snow layers)
- cycles of melting and refreezing
- molecular diffusion and convection within the pore space of the snow

(Baumgartner and Liebscher, 1990).

These processes gradually transform the fine structured snowflakes into rounded grains of firn and ice (Figure 2.3), thereby compressing the material and reducing the volume of air in the pore space between the individual grains. As a consequence the density increases during the transformation process and with snow age (Table 2.1). The density of freshly fallen snow depends on temperature and wind conditions, a typical value for mid-latitude glaciers is 100 kg/m^3. After one year of metamorphism, in an intermediate stage between snow and ice, the material is called *firn*. Firn can be defined as wetted snow that has survived one summer without being transformed to ice (Paterson, 1994). It mainly consists of rounded grains with air spaces in between being still connected. As metamorphism proceeds, the firn grains begin to recrystallize and larger crystals of ice form at the expense of their smaller neighbours (Hambrey and Alean, 2004). When interconnecting volumes of air between the

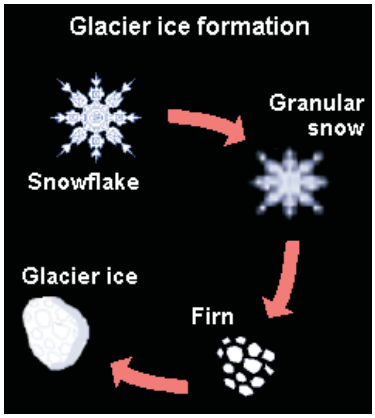

Figure 2.3: The process of glacier ice formation by metamorphism of snow. Source: *http://en.wikipedia.org*.

Snow type	Density [kg/m^3]
New snow	10 - 200
Settled snow	200 - 300
Depth hoar	200 - 300
Wind packed snow	350 - 400
Firn	400 - 650
Very wet snow and firn	700 - 800
Glacier ice	850 - 910

Table 2.1: Typical densities of snow and ice (after Singh and Singh, 2001)

grains are sealed off the state of *glacier ice* is reached. This occurs at a density of about 800 to 850 kg/m^3 (see Table 2.1), which is reached in a depth of about 60 to 70 m in cold polar regions and in 10 to 30 m depth in alpine glaciers (Baumgartner and Liebscher, 1990). The air content, or porosity, which can be higher than 90% in fresh fallen snow, has then reached a minimum of about 10%. This air is present only as bubbles trapped inside the ice and further increase in ice density results from compression of them (Paterson, 1994). Compact glacier ice is impermeable to air and water (Singh and Singh, 2001).

As glacier ice originates from snow which has survived at least one melting period, its formation requires two basic conditions: the accumulation of snow on a perennial surface during at least part of the year and sufficiently low temperatures in order to keep melt rates low. The time needed for transformation of snow into glacier ice is influenced by several factors and can reach from a few years to more than hundred years. Differences in the predominant transformation mechanisms exist between regions and even between different parts of the same glacier (Paterson, 1994). Strong winds, relatively high temperatures and alternating periods of melting and refreezing of snow generally accelerate the transformation process (Singh and Singh, 2001; Hambrey and Alean, 2004). In temperate regions, such as the Alps and the Western Cordillera of North America, transformation is most rapid and ice can be built within five to ten years. In the absence of surface melting (i.e., at high elevations and in high polar latitudes where temperature remains well below the freezing point throughout the year) the change from snow to ice may take hundreds of years (Hambrey and Alean, 2004).

2.3 Mass Balance

2.3.1 Mass Budget Terms

Variations in glacier mass are determined by the balance between incoming (mass gain) and outgoing (mass loss) terms. The former is referred to as **accumulation** and includes all processes by which material is added to a glacier. It normally takes place at or near a glacier's surface. Usually, the main accumulation process is snowfall and the subsequent transformation of snow into ice (see above). Avalanches, wind blown snow, rime formation and freezing of rain within the snowpack are further mechanisms by which mass is added to a glacier (Paterson, 1994; Singh and Singh, 2001). Geographically and seasonally the amount and distribution of snow accumulation may vary considerably.

Regions with high accumulation rates are maritime, mountainous areas with frequent winds blowing from the sea onland, like western North America, the west coast of New Zealand, western Patagonia, southern Iceland and western Scandinavia (Nesje et al., 2000).

Ablation refers to those processes by which snow and ice are removed from a glacier. This includes primarily melting followed by runoff but also evaporation, removal of snow by wind and avalanches and calving at the glacier tongue. Ablation of snow and ice almost entirely takes place at a glacier's surface or, in case of calving, at the terminus (Paterson, 1994). If meltwater of the current year's accumulated snowpack refreezes in deeper layers (cold firn or ice) it does not contribute to ablation since the total mass of the glacier remains unchanged (*internal accumulation*). The latent heat released during refreezing can be an important process in warming the layers near the surface in the accumulation zone of a glacier. Cogley and Adams (1998) state that the refreezing process should generally not be neglected in mass balance studies. But internal accumulation is very difficult to measure reliably. Evidence suggests that it has a typical magnitude of tens of millimeters per year on glaciers whose mass balance magnitude is a few times larger (Cogley and Adams, 1998). It is especially significant on sub-polar glaciers which are partly below freezing for the entire year (Kaser et al., 2006).

The difference between accumulation and ablation over a certain period of time is called **mass balance** (or *net balance*) b_n and the time is referred to as the *balance period*. The net balance b_n at a given point on a glacier is usually expressed as the volume change of the equivalent quantity of liquid water per unit area, i.e., in the thickness change of the corresponding water column (*metre water equivalent*, [m w.e.]). The mass balance B_n [m^3 w.e.] of an area (e.g., of a whole glacier surface) is the spatial integral of b_n:

$$B_n = \int_A b_n \, dA \tag{2.1}$$

Usually, this volume is related to the glaciated area A and the mass balance of a defined area can then be expressed as

$$\overline{b}_n = B_n \, / \, A \tag{2.2}$$

$\overline{b}_n$ has the unit [m w.e.] and is also referred to as the *mean specific mass balance* (or *mean specific net balance*), it is the most useful parameter for comparing mass changes of a glaciers in different regions (Paterson, 1994). The balance period is most commonly defined as the time interval between the minimum mass of a glacier in one calender year and the time of minimum mass in the following year, the so called *balance year* (Singh and Singh, 2001). For reasons of simplicity, the balance year is often assumed to start in October and to end in September of the next year. It can in many cases be subdivided into a winter period with net accumulation (positive winter mass balance b_w) and a summer season with ablation processes dominating (negative summer mass balance b_s). The net balance b_n at a given point can then be written as

$$b_n = b_w + b_s \tag{2.3}$$

(see also Figure 2.4).

2.3.2 Spatial Variability

Mass balance usually varies from place to place on a glacier, especially with elevation (Braithwaite, 2002). Spatially and for a given balance period, a glacier can be divided into an **accumulation area**

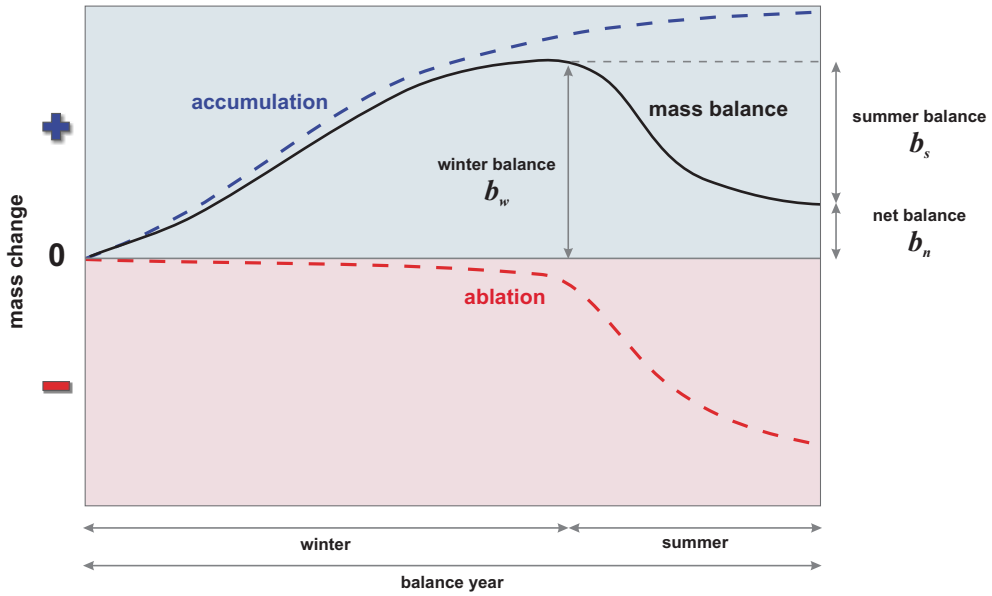

Figure 2.4: Idealised evolution of glacier mass balance terms over a balance year with a positive net balance b_n (modified after Paterson, 1994).

($b_n > 0$), located in the upper parts, and an **ablation area** ($b_n < 0$), located in the lower reaches and including the glacier's tongue. In the accumulation zone of a glacier, the annual snowfall is not entirely removed by ablation. This area is therefore covered by snow throughout the whole year and bare ice is not visible (Singh and Singh, 2001). Both regions are separated by the **equilibrium line**, a conceptual line where accumulation equals ablation in a balance year and consequently $b_n = 0$ (Figure 2.5).

On temperate glaciers, the equilibrium line approximately corresponds to the snow line at the end of a melt period and can be traced using remote sensing techniques (aerial photography, satellite imagery). Its altitude, the *equilibrium line altitude* (ELA), usually varies little for different parts of the same glacier. Often, the ELA is directly connected to the glacier mass balance of the corresponding balance period (Østrem, 1975; Braithwaite, 1984). In years of positive mass balance the equilibrium line will be found at a lower altitude than normal. Vice versa, negative mass balances are associated with a rise of the ELA. The altitude of the equilibrium line corresponding to a mean specific mass balance of zero ($\bar{b}_n = 0$) is called the *steady state equilibrium line altitude* or ELA_0. It varies widely over the globe, from greater than 4000 m in the subtropics, to about 2900 m in the Alps and to less than 1000 m in the subpolar and polar regions (Oerlemans and Fortuin, 1992). It is generally low in humid maritime regions with strong accumulation rates and high in dry continental areas. Similarly, relationships can be established between glacier mass balance and the *accumulation area ratio* (AAR) which is defined as the ratio between the accumulation area at the end of a balance period and the total area of the glacier. For Alpine glaciers, an AAR of about 0.6 corresponds to a mass balance of zero (AAR_0).

Moving from an individual glacier to a regional or even global scale, the question arises how net mass balance varies spatially over larger regions. Analysing measurement data from 129 glaciers, Cogley and Adams (1998) found that mass balance time series from nearby glaciers are highly correlated.

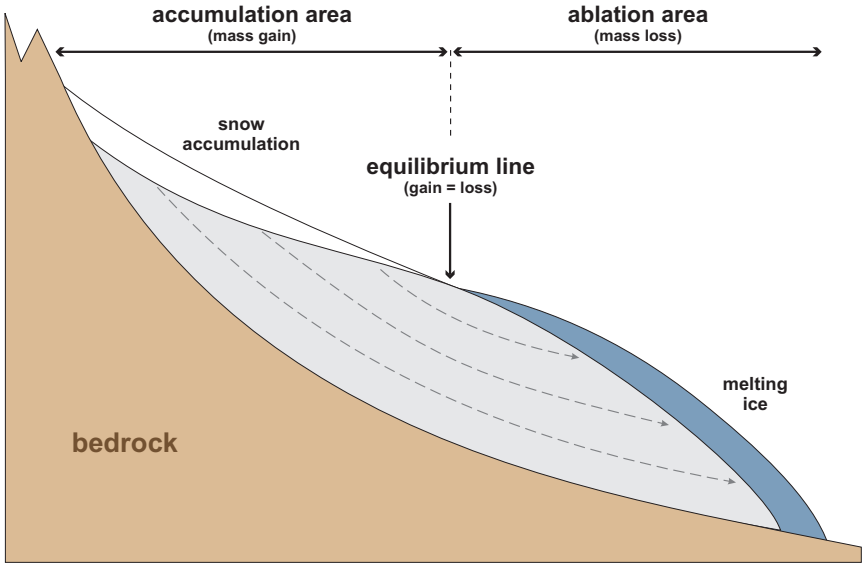

Figure 2.5: Length profile through a glacier showing accumulation and ablation areas (after Hambrey and Alean, 2004).

Correlation coefficients are higher than 0.8 at separations of a few kilometres and decrease to zero at a horizontal distance of about 1500 km. At separations of 2000 km and greater, a periodic structure appears in the correlogram (distance versus mean correlation) which is probably related to long wavelength atmospheric features (Cogley and Adams, 1998). When analysing mass balance series in the Northern Hemisphere, Letréguilly and Reynaud (1990) found that at the scale of a mountain range (distances less than 500 km), interannual mass balance fluctuations are highly comparable between individual glaciers. Haeberli et al. (1989) state that the temporal variation of mass balance within a mountain range (such as the Alps) is clearly predominant over the spatial variation. This spatial homogeneity reduces when a comparison between different mountain ranges or even different continents is made, and it reappears with the consideration of decadal mass balance trends only.

Nonetheless, under certain conditions the mass balances of adjacent glaciers can also react quite differently to the same climatic forcing (e.g., Kuhn et al., 1985). Such a scattering of mass balance evolution can for instance be caused by differences in the specific topographical setting (area-elevation distribution) and in the AAR, leading to different mass balance sensitivities. As glacier mass balance is partly influenced by the transient adjustment of the geometry to present climatic conditions (see below), also differences in the dynamic response time of two glaciers can lead to a different reaction of mass balances to a certain climatic forcing.

2.3.3 Vertical Profile

The simple division of a glacier's area into an accumulation zone with a positive mass balance and an ablation area where mass loss prevails often lacks important details. This is especially true when the response of a glacier to climatic changes is under investigation (see also Chapter 2.7). Here the *mass balance gradient*, i.e., the rate at which the specific mass balance changes with altitude, is an important parameter. It is linked to the climatic sensitivity of a glacier and constitutes the main

forcing function of glacier flow over long time intervals ("the higher the gradient the faster the flow").

Generally, mass balance is strongly negative on the lowest part of a glacier where temperatures are highest and the amount of snowfall is at its minimum. Moving further upwards the specific balance becomes less negative and ultimately positive once the equilibrium line is reached (Oerlemans, 2001). The most important factors determining the increase of mass balance with altitude and thus the mass balance gradient are

- the increase of precipitation (orographic effect plus snowdrift)
- the increase of surface albedo (see also Chapter 2.4)
- the decrease of air temperature (leading to a reduction of turbulent energy exchanges and of incoming longwave radiation at high elevations)
- the increase of the degree of snow and ice cover (leading to a reduced transfer of heat from ice free regions to the glacier at high elevations)
- topographic effects (increased shading at steep slopes).

Mass balance gradients are generally small for dry polar glaciers and ice caps (Oerlemans, 2001). In maritime environments with relatively high temperatures but also high amounts of precipitation mass balance gradients are usually much larger (strong accumulation in the upper reaches and strong ablation at the tongue) and mass turnover is high. Typical values of mass balance gradients in continental areas are normally less than 0.5 m w.e./100 m whereas gradients on maritime glaciers usually exceed 1.5 m w.e./100 m (Chinn, 1996). On most glaciers mass balance gradients are lower in the accumulation area than in the ablation area, i.e., the relation between mass balance and altitude is stronger in the ablation zone (Braithwaite, 1984). Generally, mass balance gradients cannot be expected to remain constant under climate change conditions (Oerlemans and Hoogendoorn, 1989).

2.4 Energy Budget

2.4.1 Surface Energy Balance

Variations in glacier mass balance are closely related to changes in air temperature and precipitation. On a global scale, air temperature alone is considered to be the most important factor reflecting glacier retreat (e.g., Gregory and Oerlemans, 1998; IPCC, 2001; Oerlemans, 2005). This relationship is not necessarily of a direct nature but includes indirect effects like the influence of air temperature on the partitioning of total precipitation into rainfall and snow. On a local scale, near surface air temperature is not the primary cause of ablation but is at least partly a result of the energy exchange processes at a glacier's surface (Figure 2.6). These in turn depend on a complex interplay between surface conditions on the glacier, external meteorological factors and the topography of the glacier surface itself and the surrounding terrain (Arnold, 2005).

Assuming a surface layer of infinitesimal thickness with zero heat capacity, the sum of all exchange processes, the *surface energy budget*, equals zero. For a snow-covered or snow-free glacier surface it can be expressed in terms of its different components (Hock, 2005):

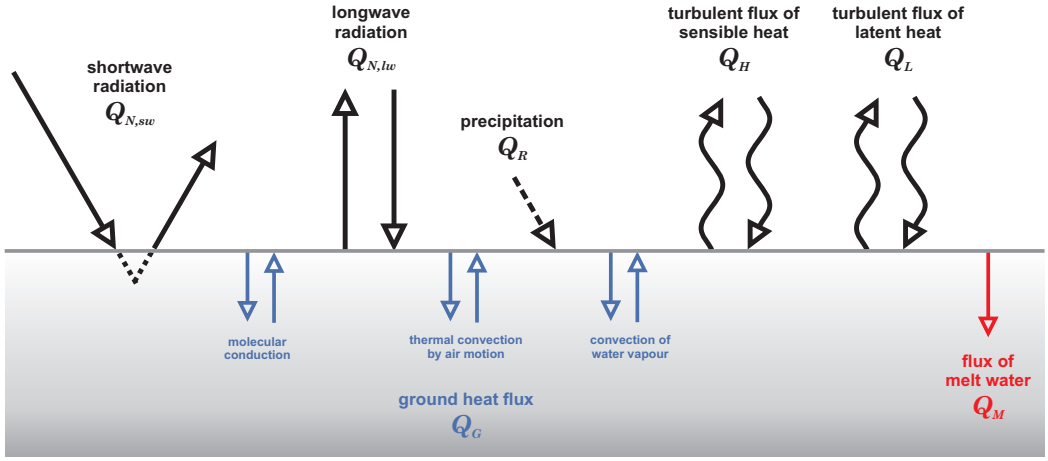

Figure 2.6: Schematic overview of the most important processes determining the surface energy balance of a glacier (modified after Oerlemans, 2001).

$$Q_N + Q_H + Q_L + Q_G + Q_R + Q_M = 0 \tag{2.4}$$

with positive values denoting a gain of energy for the surface and

Q_N : net radiation [W/m^2]

Q_H : turbulent flux of sensible heat [W/m^2]

Q_L : turbulent flux of latent heat [W/m^2]

Q_G : ground heat flux [W/m^2]

Q_R : sensible heat flux supplied by rain (when the temperature of precipitation differs from the surface temperature) [W/m^2]

Q_M : energy consumed by melt of snow or ice [W/m^2]

The heat flux due to precipitation Q_R is small, difficult to quantify and therefore usually ignored in energy balance models (Munro, 1990; Hock, 2005; Oerlemans, 2001; Singh and Singh, 2001). For temperate glacier ice, also the ground heat flux Q_G can be assumed to be negligible (Munro, 1990). Only for cold glacier ice or glaciers with a perennial cold surface layer, heat flux into the ice can be a substantial energy sink (Hock, 2005). Generally, the fluxes inside the glacier are much smaller than those between atmosphere and glacier surface, except for the flow of melt water through a snow pack which represents a flux of latent heat (Oerlemans, 2001).

The turbulent heat fluxes Q_H and Q_L are driven by the near-surface temperature and moisture gradients as well as by turbulence. The key surface condition is the surface roughness, which is normally higher for ice than for snow (Arnold, 2005). It is generally assumed that the relative contribution of the turbulent fluxes to the surface energy balance decreases with altitude (Oerlemans and Hoogendoorn, 1989). When air temperature is above freezing point Q_H is always positive (flux towards the surface). Under these conditions Q_L can go in both directions, depending on the humidity of the air (Oerlemans,

2001). If the surface is melting its temperature stays at 0°C and cannot rise further even if air temperature does. Therefore, with an increase of air temperature above 0°C, the vertical temperature gradient will increase and consequently also Q_H (Paterson, 1994). At the same time the cooling influence of the ice surface can create a stable atmospheric layering near the surface which suppresses the vertical exchange of energy by turbulence. Over glacier ice, Q_H and Q_L are generally small when averaged over weeks or months and compared to the net radiation flux Q_N. At high altitudes and high latitudes, sublimation ($Q_L < 0$) can be important and might be the only ablation component (Hock, 2005). This is for instance the case on glaciers in dry subtropical conditions, e.g., in southern Bolivia and northern Chile (Kaser, 2001). On tropical glaciers, the turbulent latent heat flux Q_L is usually the second largest energy flux in the energy balance (after net shortwave radiation) and is negative all year round, resulting in continuous sublimation (Mölg and Hardy, 2004).

The net radiation flux Q_N can be further split up into its shortwave (solar spectrum) and longwave (terrestrial spectrum) components:

$$Q_N = \underbrace{G\,(1-\alpha)}_{Q_{N,sw}} + \underbrace{L_{in} + L_{out}}_{Q_{N,lw}} \tag{2.5}$$

where

G : global radiation (incoming shortwave radiation), consisting of a direct and a diffusive part [W/m^2]

α : surface albedo integrated over the solar spectrum (ratio of reflected to incident solar radiation)

L_{in} : incoming longwave radiation [W/m^2]

L_{out} : outgoing longwave radiation (emitted by the surface) [W/m^2]

$Q_{N,sw}$: shortwave radiation balance [W/m^2]

$Q_{N,lw}$: longwave radiation balance [W/m^2]

The longwave energy fluxes L_{in} and L_{out} normally compensate each other to a large degree (Oerlemans, 2001). The remaining term G, the shortwave radiation entering a glacier surface, is often considered as the primary source of melt energy on glaciers (e.g., Oerlemans, 2001, 2005; Arnold, 2005). Consequently, the surface albedo α is a key control parameter and determines to a large extent the variability of the surface energy budget both in time and space (Oerlemans, 1991). On most glaciers, solar radiation typically provides about 75% of the melt energy (Oerlemans and Knap, 1998). The global radiation G generally depends on the latitude of a site, on the season and on atmospheric factors (scattering and absorption by air molecules, aerosols and clouds). Furthermore, on a local scale, the amount of incoming solar radiation can strongly depend on geometric factors such as the slope and aspect of the glacier surface and the shading by surrounding mountains (Oerlemans, 2001). Reflection from surrounding slopes can lead to an additional increase in the amount of solar radiation reaching a glacier surface (Oerlemans and Knap, 1998). Other authors also stress the importance of the longwave atmospheric radiation as a significant energy source for ice melt (Hock, 2003; Ohmura,

2001). On valley glaciers, also the longwave radiation emitted from non-glaciated surrounding slopes can considerably influence the surface radiation balance (Singh and Singh, 2001).

Melting of ice (or snow) occurs when the ice (or snow) temperature has been raised to 0°C. Up from this point any surplus of energy which would further increase the temperature above 0°C is used for melting instead. The amount of energy Q_M available for melting can thus be considered as a residual component controlled by the other terms of the surface energy budget. If meltwater percolates and refreezes in a deeper snow layer, it does formally not directly contribute to ablation since the total mass of the glacier is not changed.

The surface energy balance in summer determines to a large extent the specific mass balance of most glaciers outside the Antarctic continent (Oerlemans, 1993). As several components of the balance equation are strongly connected to air temperature (e.g., Q_H, Q_L, L_{in}), a high correlation is often observed between air temperature and melt rates (e.g., Braithwaite and Olesen, 1989). To a certain degree, temperature can therefore be considered as a proxy variable for surface energy fluxes (e.g., net radiation), determining the energy budget of a snow or ice surface. This relationship is the physical basis of *temperature-index models* (or *degree-day models*) in which air temperature is used as the sole index of melt energy, simplifying the complex variety of energy exchange processes to a high degree. On catchment scales, these models often match the performance of more detailed energy balance models (Hock, 2003).

2.4.2 Surface Albedo

With net radiation being the main contributor of melt energy, the surface albedo is a key control for melt rates and thus for a glacier's total mass budget (Arnold, 2005).

The surface albedo of a glacier depends in a complicated way on crystal structure (e.g., single snow crystals or compact ice body), surface morphology, dust and soot concentrations, morainic material, the presence of liquid water (both enclosed and at the surface), solar elevation, cloudiness etc. and of course on the presence of a snow layer at the surface (Oerlemans, 1993). As a consequence, the spatial and temporal variation of albedo is large and an accurate modelling including all important factors is difficult (Oerlemans, 2001). However, some basic dependencies can be derived from theoretical considerations and available data. These relations can be divided into two basic categories (Jonsell et al., 2003):

1. Dependency of surface albedo on the properties of the incident radiation (e.g., wavelength and incident angle) and on atmospheric factors (e.g., the presence of clouds with its effect on the spectral composition of the incident radiation).
2. Dependency of surface albedo on the characteristics of the surface layer.

A major control on glacier surface albedo is the depth of snow cover and its condition. Compared to ice, snow has a relatively high albedo which can reach values of more than 0.95 in case of fresh fallen snow. Snow albedo depends on the snow condition which in turn is strongly linked to the grain size. As described in Chapter 2.2, during the process of snow metamorphism snowflakes are gradually transformed into rounded grains of firn and ice. These structural and geometrical changes within the snowpack lead to an increase in density and also to an increase in grain size, the latter being responsible

Surface type	Albedo range	Mean value
Dry snow	0.80 - 0.97	0.84
Melting snow	0.66 - 0.88	0.74
Firn	0.43 - 0.69	0.53
Clean ice	0.34 - 0.51	0.40
Slightly dirty ice	0.26 - 0.33	0.29
Dirty ice	0.15 - 0.25	0.21
Debris-covered ice	0.10 - 0.15	0.12

Table 2.2: Typical albedos of snow and ice surfaces (after Paterson, 1994)

for a reduction in reflectivity. Snow albedo therefore generally decreases during the ageing process. The accumulation of impurities on the snow surface further enhances this ageing effect. Similarly, the presence of liquid water in the interstices between grains ("meltwater pockets") increases the *effective grain size* via a reduction in the surface area of snow in contact with air. This results in a reduction of refractive diffusion and a reduced value of the albedo of wet snow (Singh and Singh, 2001). Melting therefore reduces the albedo of a snow surface significantly and leads to relatively high values of the radiation balance Q_N (Paterson, 1994). Typical albedo values for different snow and ice surfaces are listed in Table 2.2. For glacier ice, the surface albedo usually lies in the range of 0.3 to 0.4 (Singh and Singh, 2001). Lower values arise in the presence of dust and debris on the ice surface.

Due to the large difference in the albedo of fresh fallen snow and glacier ice, the occurrence of summer snowfall can have a considerable impact on glacier mass balance by simultaneously adding mass to the glacier and increasing the amount of reflected solar radiation (Oerlemans and Klok, 2004). In this way, one or two summer snowfalls can be enough to considerably increase the annual mass balance (Paterson, 1994). For a summer snowfall event on Morteratschgletscher, Switzerland, Oerlemans and Klok (2004) found a feedback factor of 4 in the ablation zone, i.e., the total effect of the snowfall event on the annual mass balance was about four times the amount of mass added during the event. For the entire glacier, including the higher regions where snow cover was present also before the event, a much smaller factor of 1.6 was found.

2.4.3 Effect of Dust and Debris

The accumulation of atmospheric dust and morainic material (debris) on a glacier's surface can significantly decrease the albedo, particularly in the visible spectrum, and thus accelerate melting (Takeuchi et al., 2001). The ablation rate under a debris layer is governed by radiation, air temperature and physical characteristics of the debris such as thickness, albedo and thermal conductivity. With supraglacial debris having the same spectral characteristics as the surrounding terrain (Paul et al., 2004a) the albedo of debris-covered ice and ice with impurities embedded inside is lower than that of pure ice and the absorption of solar radiation is enhanced. On the other hand, a debris layer hinders the heat flow from the top surface of the debris to the ice surface underneath thus acting as an insulator (Nakawo and Rana, 1999). The effect of debris on melt rates therefore strongly depends on the thickness of the debris cover: a thin debris cover accelerates melting whereas a thick layer retards

it due the isolating effect. In case of a very thick cover, melting can even be totally suppressed (Singh and Singh, 2001). A maximum enhancement of melt rates has been observed at thicknesses of about 1 to 2 cm (Nakawo and Rana, 1999).

Debris-covered glaciers often exhibit a special behaviour. Due to the reduced melt rates under a thick debris cover they can "survive" at lower elevations than if they were debris-free which can significantly dampen the response of a glacier to climate forcing. Consequently, heavily debris-covered glaciers are often found to stagnate under climate warming conditions, and down-wasting (i.e., stationary thinning) is their primary response. Debris-covered glaciers are for instance abundant in the Himalayan region. Virtually all large glaciers in the Nepalese Himalayas, the Western Himalayas and the Karakoram are covered with dust and debris in their ablation area (Singh and Singh, 2001). Also many glaciers in the European Alps show a notable debris cover, especially in their lower reaches.

2.5 Dynamics

2.5.1 Glacier Motion and Flow Velocity

In locations where accumulation is continuously larger than ablation, snow and ice would accumulate more and more if they where inelastic and fixed to the underlying bedrock (Baumgartner and Liebscher, 1990). But this is not the case: If the ice cover has grown to a certain minimum thickness (usually some tens of metres), the ice starts to move under the influence of gravity, thereby reaching areas where mass loss (by melting or calving) exceeds mass gain. Downhill ice flow thus compensates between net accumulation at higher altitudes and net ablation in the lower areas of a glacier. The movement of ice generally consists of three basic modes (Paterson, 1994; Hambrey and Alean, 2004):

- plastic internal deformation
- basal sliding
- deformation of the bed

Glacier flow velocity is a result of all three motion processes and the total rate of movement varies considerably among glaciers. As described above, it is controlled by a variety of factors such as surface slope, ice thickness and basal thermal and physical conditions. Small glaciers and ice caps may flow only a few metres per year whereas ice flow velocities of valley glaciers can reach several kilometres per year (Hambrey and Alean, 2004). Typical velocities of valley glaciers range from 10 to 200 m/year for much of their length (Singh and Singh, 2001). A small percentage of the world's glaciers flow in an extremely variable and unpredictable manner, remaining relatively inactive for many years but suddenly accelerating to very high speeds of several metres per day. After a couple of months or years, the rapid movement then stops. These phenomena are called *surges* (or *galloping glaciers*) and can have catastrophic effects. They are frequently accompanied by major advances of the glacier's terminus. The mechanisms leading to glacier surges are not perfectly clear yet. Presumably, they are caused by some abrupt decoupling of a glacier from its bed (probably involving strong meltwater production at the base, thermal instability and deformation within the ice) and a subsequent rapid increase in basal slip (Singh and Singh, 2001).

2.5.2 Geometry and Response Time

Mass transfer across external surfaces by mass balance and across internal surfaces by motion act in combination to control the geometry of a glacier (Raymond, 1980). Simply speaking, an increase in glacier mass enlarges the thickness of the glacier which results in an increase in the rate of flow, thereby extending its length and area (Singh and Singh, 2001). A series of positive balance years therefore allows the glacier to grow and extend to lower altitudes, exposing a larger area to ablation (see Chapter 2.3). The resulting higher rate of ablation tends to compensate for the increase in mass balance in the previous years. Vice versa, a negative mass balance results in glacier retreat with a smaller area at higher elevations being subject to ablation. The dynamic response of glacier geometry to perturbations in mass balance triggered by climatic changes thus tends towards an equilibrium condition of ice geometry where the net mass balance is zero again (MBB, 2005). As the adjustment of glacier geometry is not an instantaneous process but continues for many years (see below), a glacier may advance or retreat in response to past conditions even though the net balance for the current year is zero (Paterson, 1994). If the net balance remains zero for many years, the dimensions of the glacier will, after an initial period of adjustment, eventually remain unchanged, the glacier is said to be in a *steady state*. Requiring a zero mass balance for many years, this state is only a theoretical concept and is never encountered in practice (Paterson, 1994). Based on theoretical considerations, Bahr et al. (1997) suggest that the glacier volume V and the area A in the steady state can be related to each other via a power law:

$$V \sim A^{\gamma} \tag{2.6}$$

with $\gamma = 1.375$ for valley glaciers and $\gamma = 1.25$ for ice caps and ice sheets. Equation 2.6 does not only hold for a theoretical steady state but seems to be valid for glaciers with observed volume and area too (Meier and Bahr, 1996; Chen and Ohmura, 1990a). Its validity for non-steady state conditions is also confirmed by numerical ice flow models (van de Wal and Wild, 2001). The power law 2.6 can therefore in principle be used to relate glacier volume to glacier area even in a non-steady state (see also Chapter 4.2.8). However, it has to be kept in mind that this law relates a variable (area) in parts to itself (volume = area · thickness). As a consequence, the large scatter of glacier volumes for glaciers of equal area (due to differences in mean ice thickness) is strongly suppressed in this formulation. Furthermore, in a physical way, glacier area is not the parameter that primarily controls glacier thickness. In the case of glaciers losing their thinnest parts (e.g., glacier tongues on steep slopes), mean ice thickness can even increase with decreasing glacier area (Zemp et al., 2006a).

The time that a glacier takes to adjust its geometry to mass balance perturbations (i.e., the time to reach a new (hypothetical) steady state after changes in the climatic forcing) is referred to as the **response time**. It is much larger than the time when the effect of a mass balance change is first observed at the terminus, which might happen immediately after a mass balance increase (Paterson, 1994). The response time of a glacier generally depends on its geometry and on the specific climatic setting (Oerlemans, 2005) and is one of the most important physical characteristics of glacier dynamics. It is therefore of fundamental importance when interpreting past glacier variations as a result of climatic history and for the prediction of glacier response to climatic changes (Johannesson et al., 1989). The typical response time of glaciers is in the order of 10 to 100 years. It tends to be longer for glaciers in

continental climates with a low mass turnover (IPCC, 2001; Raper et al., 2000). In case of the large polar ice sheets the response time reaches several thousand years (Paterson, 1994; Greve, 2003).

2.6 Global Distribution

In principle, a glacier can form wherever the annual accumulation of snow exceeds the amount of mass loss, i.e., in places where the surface elevation rises above the equilibrium line (Oerlemans, 1991). The occurrence of glaciers is therefore strongly related to climatic conditions, especially to mean annual air temperature and annual precipitation, with the latter usually showing much more complex spatial patterns. The global distribution of glaciers thus clearly reflects climate variability associated with latitude, altitude, continentality and large scale atmospheric regime (Oerlemans and Hoogendoorn, 1989). Ideal locations for glacier formation are the polar regions and high mountain ranges with their comparatively low temperatures and a large fraction of precipitation falling as snow. In mountainous areas, glaciers are located above the permanent snowline which lies at sea level at the poles and as high as 5000 to 6000 m a.s.l. in equatorial regions (Singh and Singh, 2001). The minimum altitude at which glaciers can exist generally decreases towards the poles. In maritime climatic zones with their high mass turnover and at high latitudes, glaciers extend down to sea level whereas in arid continental areas of the tropics, permanent ice occurs only at high altitudes (see Figure 2.7).

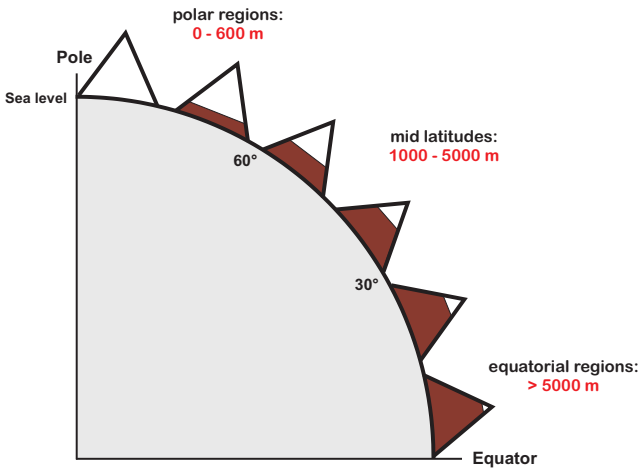

Figure 2.7: The altitude of permanent snow and ice cover at different latitudes (modified after Press and Siever, 1994).

Presently, land ice covers about 10% of the global land surface, an area more than $15 \cdot 10^6$ km^2 (Paterson, 1994; Hambrey and Alean, 2004) with Antarctica being by far the largest contributor ($>$ 80% of total glaciated area). About 99% of the total land ice is stored in the two polar ice sheets. The remaining glacier mass is concentrated in the Northern Hemisphere (Figure 2.8), most of it in the Central Asian mountains and in North America. Only 3% of the permanent snow and ice area is distributed over mountains outside the polar regions (Singh and Singh, 2001). For glaciers outside the Greenland and Antarctic ice sheets Dyurgerov and Meier (2005) derived a total area of about $785 \pm 100 \cdot 10^3$ km^2 and a total ice volume (water equivalent) of $260 \pm 65 \cdot 10^3$ km^3. Of the world's total glaciated area glaciers in the European Alps cover only about 0.0175% (approximately 2900 km^2), which corresponds to 3.5% of the total area of mountain glaciers and ice caps (Paul, 2004). During the last ice ages, glaciers covered an area about three times as large as today (Paterson, 1994).

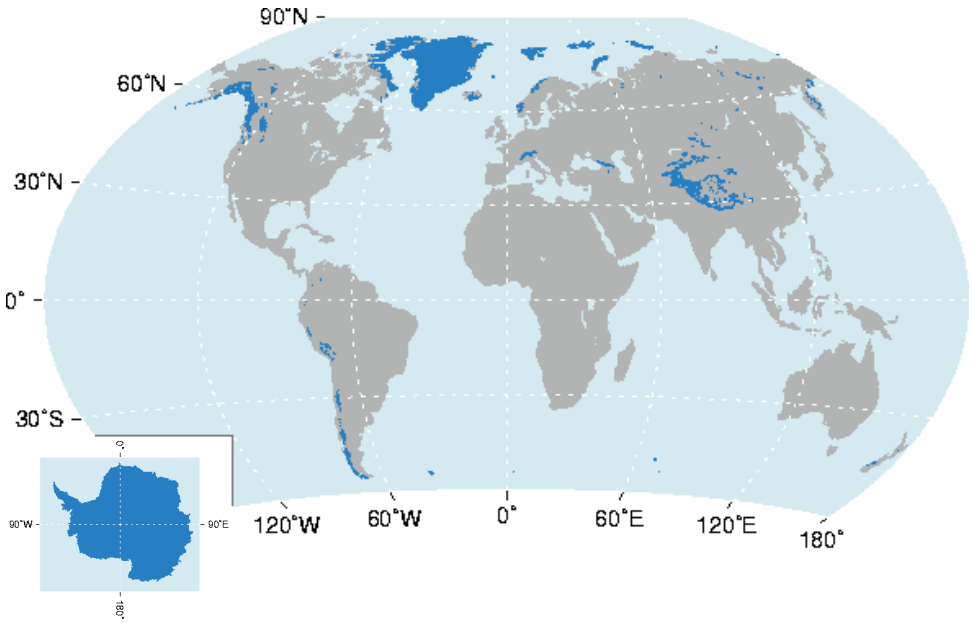

Figure 2.8: Global distribution of land ice masses (ice-covered surfaces in dark blue). Source: NSIDC / GLIMS.

2.7 Glaciers in the Climate System

2.7.1 Overview

As outlined in the previous sections, a glacier's energy and mass balance is strongly controlled by atmospheric factors. The climate, along with the physical properties of ice and the specific topographical setting, therefore determines the extent and behaviour of glaciers. The climatic forcing itself is of course not fixed but subject to random fluctuations as well as superimposed long-term changes. In principle, climatic changes can affect a glacier via

- ▷ changes in accumulation of glacier mass
- ▷ changes in the energy flux from the atmosphere through the surface into the glacier with the corresponding effects on ice temperature and melt rates
- ▷ changes in the geothermal heat flux

(Hutter, 1983).

Vice versa, due to their unique surface characteristics and their function as hydrological reservoirs, glaciers play an important role for local and regional water and energy budgets and can to a certain extent directly influence the local climate. Additional hemispheric to global scale feedbacks exist via the impact of glacial meltwater on the hydrology of mountain-fed river systems, on the freshwater balance of the oceans and on sea level rise (Dyurgerov and Meier, 2005). Furthermore, retreating glaciers will leave new terrain for plant colonisation (Hall and Fagre, 2003) with the corresponding impacts on surface-air exchange processes. These physical interactions constitute the role of glaciers

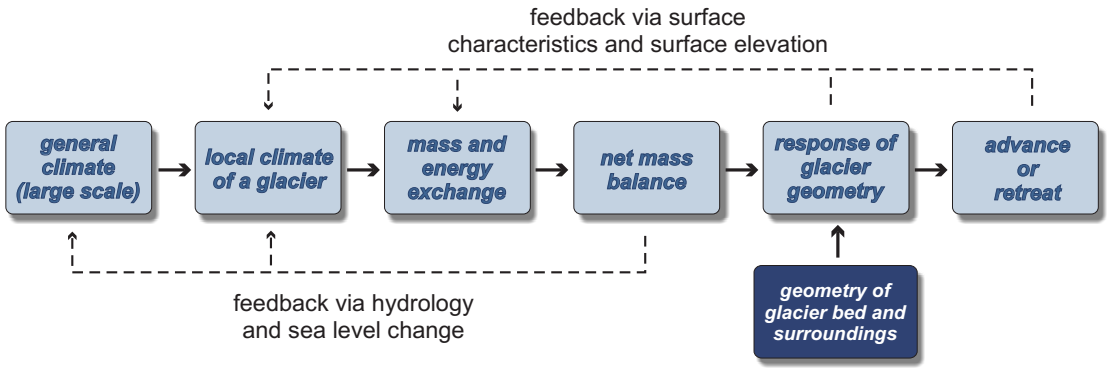

Figure 2.9: The relation between climate and glacier geometry, including feedback mechanisms (modified after Paterson, 1994 and Oerlemans, 2001).

as an interacting component of the climate system.

It is important to understand that the reaction of a glacier's geometry to climatic changes is the result of a complex chain of processes relating a climatic signal with its direct influence on surface mass balance to changes in the position of the terminus. Therefore, one should clearly distinguish between glacier mass changes as the direct and undelayed reaction to a changing climate and length variations as the indirect, filtered, delayed but also enhanced response (e.g., Haeberli and Beniston, 1998; Haeberli, 1995). Nevertheless, in a strict sense, only short-term fluctuations in glacier mass balance can be unambiguously related to meteorological quantities. On longer time scales, variations in mass balance may partly arise from changes in glacier geometry in the course of the dynamic adjustment to previous mass balance anomalies (Oerlemans, 2001, see also Chapter 2.5.2). The different steps by which climatic changes are translated into changes in glacier geometry, including possible feedbacks, are illustrated in Figure 2.9.

Due to the strong reaction of glaciers to comparatively small changes in the atmospheric forcing, glaciers are generally considered as sensitive indicators of climate change (Singh and Singh, 2001; IPCC, 2001) providing one of the clearest signals in nature for ongoing warming trends (Haeberli et al., 2001). Significance and robustness of a climatic signal deduced from glacier length fluctuations depend on the specific response characteristics. While the smallest, low-shear-stress glaciers reflect interannual changes in climate and mass balance almost without any delay, the dynamic reaction of large valley glaciers occurs with a delay of several decades and thus filters out the signal of high-frequency (interannual) climatic variations. Furthermore, their response can be considered as an enhanced signal since secular thickness changes of some metres are "amplified" into clearly detectable length changes of hundreds to thousands of metres (Haeberli, 1995).

Despite the direct link between meteorological conditions and mass balance and its impact on glacier geometry, there are special cases in which a glacier's areal extent can be partly decoupled from climatic influences. Factors other than climate can control the position of the terminus for instance in the case of glaciers calving into the sea or into a lake. Their terminal position is strongly controlled by the general water level. Also irregularities and obstacles in the bedrock topography, like steep drops in the valley floor, can influence the advance or retreat of a glacier's tongue. The isolating function of debris cover with its effect on glacier behaviour and the special case of glacier surges have already been

discussed in Chapters 2.4.3 and 2.5.1, respectively. Furthermore, the accumulation on avalanche-fed glaciers is influenced by climatic factors only as far as the size and frequency of avalanches is climatically controlled (Paterson, 1994). A further point is that with accelerated warming, the dynamic response of glacier geometry will probably not catch up with the speed of the induced mass balance changes and larger glaciers would continue down-wasting rather than retreating (Haeberli, 1995). In the European Alps, the corresponding disintegration of larger glaciers into smaller, separate parts with highly individual and non-uniform changes in glacier geometry has already been a typical element of glacier behaviour during the last decades (Paul et al., 2004b; Paul, 2004).

2.7.2 Direct Feedback Mechanisms

Due to its special surface characteristics a glacier can directly modify its own local climate though to what extent is often unclear (Paterson, 1994). While the vast ice masses of the polar regions are able to profoundly influence the atmospheric circulation and the earth's radiation budget, extrapolar glaciers are expected to have a comparatively small effect on the atmosphere (Kuhn, 1981) and are often regarded as passive components of the climate system (e.g., Maisch et al., 2000). The feedback of single glaciers is usually restricted to the atmospheric boundary layer and local circulation systems and does not affect the large scale circulation (Baumgartner and Liebscher, 1990). But, at least on a local scale, some basic feedback mechanisms can also be assumed for mid-latitude glaciers, especially when the overall effect of changes in glacier characteristics in a highly glaciated region is considered.

In wintertime, when the whole landscape is covered by snow, the contrasts between glaciated and non-glaciated surfaces are usually small. Differences can become very large in summer when those parts of a glacier which are not covered by debris have a relatively high albedo and absorb less solar energy. Furthermore, the temperature of the glacier surface cannot rise above 0°C whereas the surface temperature of glacier-free parts can be much higher. Therefore, on warm days, a glacier surface is a sink of energy for the overlying air (Oerlemans, 2001) and has a cooling effect on air temperature. This triggers the near-surface *glacier wind*, a catabatic wind in down-valley direction. The cooling effect of glaciers reduces and gradually vanishes towards high elevations where air temperature is constantly below zero (Singh and Singh, 2001).

The differential heating of air masses over glaciated and non-glaciated parts is also responsible for the so-called *oasis effect*. With ice surface temperatures being fixed at 0°C during melting, any increase in the radiation balance will lead to a larger temperature difference between the glacier and its direct surroundings. This temperature gradient can cause a larger advective flux of sensible heat towards the glacier tongue which in turn can significantly enhance the increase of melt rates (Oerlemans, 1989).

Besides the direct effect of a glacier surface on the overlying air mass two positive, second-order feedback mechanisms exist which amplify the response of a glacier to changing climatic conditions without necessarily affecting the overlying air masses in a significant way:

Snow and ice albedo feedback

On a global scale, the positive snow and ice albedo feedback is a major characteristic of the climate system. In a warmer climate snow and ice retreat, exposing land and ocean areas with a lower

albedo. The additionally absorbed solar radiation is leading to further warming, especially in the regions of snow and ice reduction (Hall, 2004; Pedersen and Winther, 2005). For a glacier's mass balance, a similar albedo feedback is active which does not close the full feedback loop via air temperature but which is able to enhance the response of glacier mass balance to a change in climate (Klok and Oerlemans, 2004). It is based on the difference in albedo between snow and ice as well as on the darkening process of glacier ice in the course of the melt season: A warmer climate will generally lead to larger melt rates, which in turn cause a faster disappearance of the winter snow pack and a longer period of bare ice exposed. Since ice is less reflective than snow (see Table 2.2) and the ice albedo will even further decrease during the melting period, the glacier will absorb more solar radiation, which in turn leads to more melt (Klok, 2003). This positive feedback can strongly enhance the mass balance sensitivity of a glacier to changes in temperature (Greuell and Böhm, 1998).

Surface elevation - mass balance feedback

Increased melt rates will eventually result in a thinning of a glacier. This will bring any particular point on the glacier surface to a lower elevation with a warmer climate and hence increase melt rates further (Braithwaite and Raper, 2002). Vice versa, a decrease of melt rates (e.g., due to lower temperatures or more snowfall) will result in an increase in surface elevation. With increasing height, the temperature decreases, which in turn will cause less melt and more snowfall. Generally, the surface elevation - mass balance feedback is stronger on glaciers with gentle slopes since, due to dynamical reasons, they can grow thicker than glaciers with steep slopes (Klok, 2003).

2.7.3 Climate Sensitivity

The response of a glacier to climatic changes generally depends on its geometry and on its specific climatic setting (Oerlemans, 2005). In this context, an important characteristic is the *climate sensitivity* of a glacier, i.e., its reaction to a certain change in a climatic parameter. It can be expressed in terms of changes in the mean specific mass balance $\overline{b}_n$ with respect to a climate parameter that affects it (*mass balance sensitivity*, e.g., Gregory and Oerlemans, 1998).

Although the primary source of energy for glacier melt is solar radiation, extensive meteorological experiments have shown that interannual fluctuations in glacier mass balance are mainly due to changes in temperature and precipitation (Oerlemans, 2005). Therefore, mass balance sensitivities are often defined with respect to uniform changes in mean annual air temperature (C_T) and to changes in annual precipitation (C_P):

$$C_T = d\overline{b}_n \,/\, dT \tag{2.7}$$

$$C_P = d\overline{b}_n \,/\, dP \tag{2.8}$$

C_T and C_P can be considered as basic quantities that characterise a glacier (Oerlemans, 2001). They can be markedly influenced by the albedo and surface elevation feedback mechanisms presented in Chapter 2.7.2. Modelling experiments have revealed that typically an increase in annual precipitation of more than 20% is needed to compensate for the mass loss due to a warming of 1°C (Braithwaite and Zhang, 2000; Oerlemans, 2001; Vincent, 2002). Combined with the evidence that precipitation anomalies normally have smaller spatial and temporal scales than temperature anomalies, one can assume that glacier fluctuations over decades to centuries on a continental scale are primarily driven

by temperature (Oerlemans, 2005) and that C_T thus dominates over C_P. One reason for this comparatively high sensitivity with respect to changes in air temperature is the direct influence of air temperature on the melt process: Since the melting point of ice is fixed at 0°C both the downward sensible heat flux and the longwave radiation balance increase when air temperature rises. Compensating effects like a corresponding increase in longwave emission (which would for instance occur in case of a warming soil layer) do not play a role (Oerlemans et al., 1998).

The climate sensitivity of glacier mass balance to changes in temperature strongly depends on the mass balance gradient (Chinn, 1996). It is generally larger for glaciers located in maritime climates (high balance gradients, long melt season, high temperature, high precipitation) than for continental glaciers. The corresponding values of C_T can vary by more than one order of magnitude (Oerlemans et al., 1998) and clearly depend on mean annual precipitation. Typical values range from 0.9 m w.e./°C for glaciers in moist climates to 0.23 m w.e./°C for dryer glaciers (Oerlemans, 1994). Investigating 37 glaciers in different parts of the world Braithwaite and Zhang (1999) found sensitivities ranging from about 0.1 to 1.3 m w.e./°C.

Instead of investigating the effect of climatic changes on an annual basis, mass balance sensitivities can also be calculated with respect to monthly perturbations in temperature and precipitation. The resulting *seasonal sensitivity characteristics* (SSC) give a much more structured description of the climate-mass balance relation which is a prerequisite for calculating future changes in glacier mass balance using climate sensitivities (Braithwaite and Zhang, 1999; Oerlemans and Reichert, 2000).

2.7.4 Sea Level Rise

In addition to direct physical interactions between a surface ice cover and the overlying air mass a further, indirect feedback mechanism exists in glacial meltwater entering the oceans and thereby modifying oceanic circulations and deep water formation (via changes in sea surface salinity) and contributing to sea level rise.

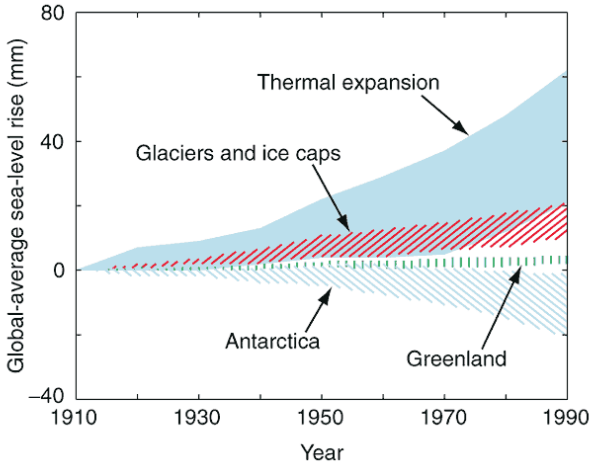

Figure 2.10: Estimated contribution of thermal expansion, glaciers & ice caps and Greenland & Antarctica to global 20th century sea level rise resulting from climate change; based on a range of AOGCM simulations (IPCC, 2001).

The *Intergovernmental Panel on Climate Change* (IPCC), based on the work of Meier and Bahr (1996), estimates a total ice volume (water equivalent) stored in glaciers and ice caps other than the two polar ice sheets of $180 \pm 40 \cdot 10^3$ km^3, corresponding to a sea level rise equivalent of 0.50 ± 0.10 m. This estimate explicitly includes glaciers and ice caps on the margins of Greenland and Antarctica, which probably contribute as much as 50% to the total value (Raper and Braithwaite, 2005). Such estimates are subject to large uncertainties since they involve assumptions on glacier-size distribution and volume-area scaling. A more recent study by Dyurgerov and Meier (2005) results in a somewhat larger estimate of glacier and ice cap

volume of $260 \pm 85 \cdot 10^3$ km^3 and a sea-level rise equivalent of 0.65 $\pm$ 0.16 m.

This value is still small compared to a potential contribution of about 70 m for the two polar ice sheets (IPCC, 2001). However, mountain glaciers and ice caps are relatively sensitive to climate change and have a shorter response time. Rapid changes in their mass are therefore possible, producing an important contribution to overall sea level rise on decadal and centennial time scales (see Figure 2.10; IPCC, 2001; Oerlemans and Fortuin, 1992). For the period 1910 to 1990, glaciers and ice caps may have contributed about 0.3 $\pm$ 0.1 mm/year to the observed total rate of sea level rise of 1.5 $\pm$ 0.5 mm/year. Their contribution is probably only surpassed by the thermal expansion of ocean water (0.5 $\pm$ 0.2 mm/year). The estimated contributions of Greenland and Antarctica (0.05 $\pm$ 0.05 mm/ year and -0.1 $\pm$ 0.1 mm/year respectively) are considerably smaller (IPCC, 2001). Furthermore, due to an increase of the sensitivity of glacier mass balance, the fraction of total sea level rise caused by the melting of glaciers and ice caps probably increased during the second half of the 20th century from about 10% (1961-1976) to as much as 27% (1988-1998; Dyurgerov, 2003). For the period 1991-2004 Kaser et al. (2006) estimate a glacier contribution to total sea level rise of 20-30%.

For the 21st century, thermal expansion of seawater is projected to continue being the major contributor to sea level rise, but increased melting of mountain glaciers and small ice caps may represent the second largest component, outbalancing the relatively small contributions of Greenland and Antarctica (IPCC, 2001; Braithwaite et al., 2002; Raper and Braithwaite, 2006, see also Chapter 2.1.1). Gregory and Oerlemans (1998) estimate that the largest contribution to total glacier melt will originate from north-west America (43%), whereas the intensively studied glaciers of the Alps will contribute only about 1%.

2.7.5 Recent Glacier Fluctuations

Global Picture

The retreat of mountain glaciers during the 20th century has been a worldwide phenomenon (see Figure 2.11) and is being considered as one of the clearest signals of ongoing climate change (Haeberli et al., 2002; IPCC, 2001). The observed retreat is probably outside the range of natural variability during the last several millennia (Meier et al., 2003) and climatic changes due to an additional anthropogenic forcing are likely to be an explanation for this (Reichert et al., 2002). Thus, for the first time in history, anthropogenic influences probably represent a major contributing factor to the observed glacier shrinkage (Haeberli et al., 1999).

In the low and mid-latitudes, glacier retreat has generally started in the mid of the 19th century at the end of the so-called "Little Ice Age"[1] and somewhat later at the high latitudes (IPCC, 2001). Applying an inverse modelling technique, Oerlemans (1994) derived a 20th century linear global warming trend of 0.66 $\pm$ 0.10 K/100 years based solely on observed glacier length fluctuations. Evidence furthermore suggests that the global warming signal derived from glacier length records does not depend on elevation, i.e., glaciers at different heights show similar signals (Oerlemans, 2005).

[1] A period with relatively low temperatures, lasting from about 1450 to 1850, during which glaciers extended globally with their fronts oscillating about advanced positions (Grove, 2001).

In many areas the general trend of glacier shrinkage has been interrupted by re-advances in response to decadal changes in temperature and precipitation (Hambrey and Alean, 2004). Well-known examples are the advances of glaciers in Norway and New Zealand from the early 1980s until around 2000. These glaciers are situated in humid, maritime climates in the belts of strong westerly circulation. In both cases, the positive mass balance anomalies in the late 20th century were caused by an increase in the strength of atmospheric circulation and an associated increase in precipitation together with, in the case of Norway, lower air temperatures during the ablation season (Chinn et al., 2005). In contrast, glaciers in continental-type climatic regions appear to have decreased steadily during the last century (Haeberli et al., 2002).

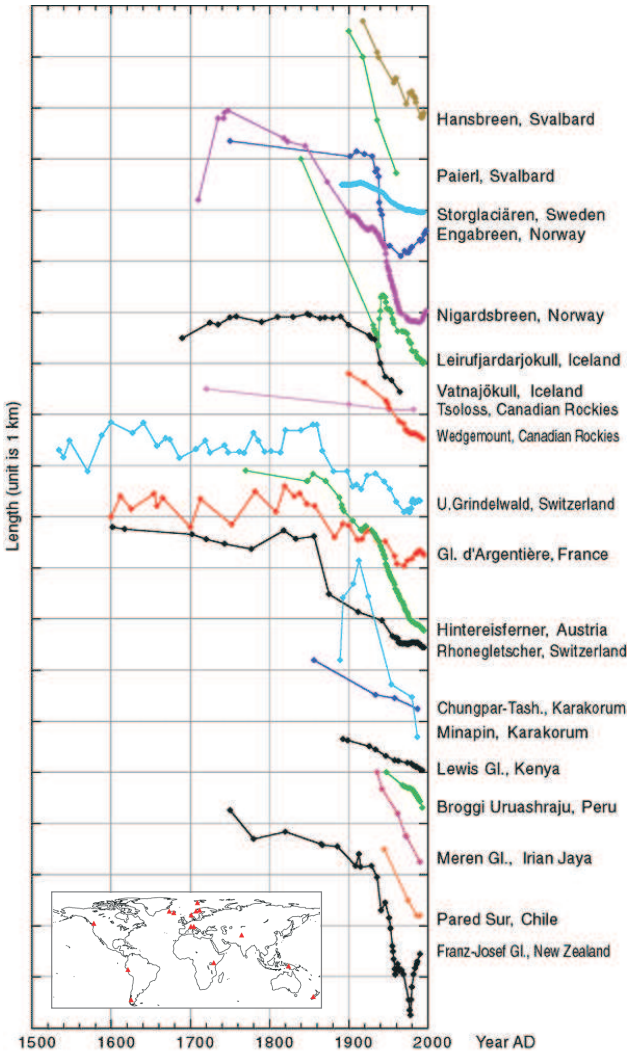

Figure 2.11: Length records of twenty glaciers around the globe for the last centuries (locations: see box in lower left corner; IPCC, 2001).

During the last decades of the 20th century, worldwide glacier volume losses showed clear signs of acceleration (Haeberli et al., 1999; Meier et al., 2003; MBB, 2005), corresponding to the unusually high mean temperatures during this period and consistent with other evidence of warming in the earth system (e.g., reduction of sea ice area and thickness, decreasing areal extent of snow cover, increased thawing of permafrost etc.; Dyurgerov and Meier, 2005). An analysis of continuous mass balance records for the period 1980-2003 for 30 glaciers worldwide even revealed a further acceleration during the first years of the 21st century: The mean glacier mass balance for the years 2000-2003 (-570 mm/year) has been twice that during 1980-1999 (-286 mm/year) and the mean proportion of glaciers with positive balances shrank to two thirds of the mean value during 1980-1999 (MBB, 2005). Empirical and energy-balance models indicate that 30 to 50% of the existing mountain glacier mass could disappear by 2100 if a global warming in the range of 2 to 4°C would occur (Beniston, 2003).

European Alps

The European Alps are among those regions that experienced the largest rates of glacier shrinkage during the 20th century. Haeberli and Hoelzle (1995) estimate that, by the 1980s, more than 35% of the glaciated surface area existing around 1850 had disappeared. Intermittent periods of glacier advance occurred (1890s and 1920s) but did not reverse the general trend of diminishing ice cover.

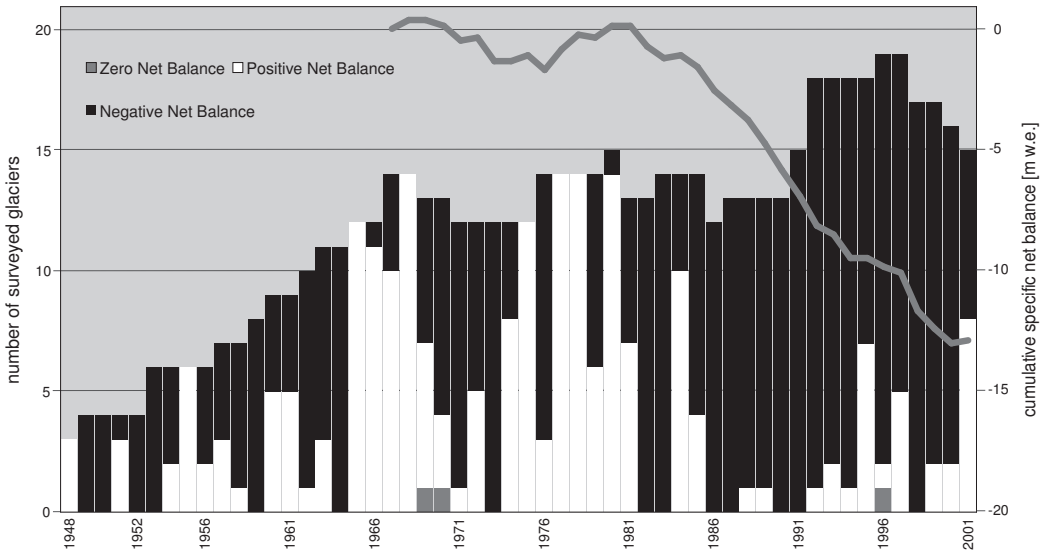

Figure 2.12: Alpine glacier mass balance measurements from 1948 to 2001. Annual numbers of glaciers (left axis) with a zero net balance (dark grey), positive net balance (white), or negative net balance (black). Grey: mean cumulative specific net balance (right axis) of nine Alpine reference glaciers (Careser (IT), Gries (CH), Hintereis (AT), Kesselwand (AT), Saint Sorlin (F), Sarennes (F), Silvretta (CH), Sonnblick (AT) and Vernagt (AT); Zemp et al., 2006b).

The corresponding loss of ice mass, about 50%, has been even larger. In the dry inner-alpine regions of Italy and Austria, glacier mass losses of up to 75% occurred (Braun and Weber, 2001). Assuming a continuous retreat (and thus neglecting the intermittent stabilisation periods) the average net mass balance lies in the range of -0.2 to -0.3 m w.e./year, which corresponds to an energy flux of 2-3 W/m^2 required for melting this amount of ice (Haeberli and Hoelzle, 1995; Hoelzle et al., 2003). The same authors estimate an overall ice volume in the Alps of 130 km^3 in the 1970s, which is equivalent to a global sea level rise of only 0.35 mm. A more recent study by Paul et al. (2004b) results in a considerably lower estimate of 100 km^3.

As a reaction to several years with positive net balances (Figure 2.12), many glaciers in the Alps started again to advance during the 1970s and 1980s. The last two decades of the 20^{th} century again brought strongly negative mass balances with an average value of about -0.6 m w.e./year (Figure 2.13). During that period, the warming in the European Alps has been larger than the global average (Haeberli and Beniston, 1998). By the year 2000, another 20 to 30% of the ice mass that remained in the 1970s had probably melted away (Haeberli et al., 2002). Compared to the period 1850-1973, the mean total area change per year has increased by a factor of three for the period 1973-1998 (-2.2%/decade and -6.4%/decade, respectively), and considering only the period 1985-1998 even by a factor of seven (-14.0%/decade). Relative area losses have generally been largest for the smaller glaciers (Paul et al., 2004b). The total Alpine glacier volume in 2000 is estimated to be close to one third of it's value in 1850 while almost 50% of the original area has been lost (Zemp et al., 2006a).

The strongly accelerating glacier wastage in the Alps towards the end of the century has not been the final stage of their recent retreat. In the year 2003 a record-breaking heat wave affected the European continent and especially the Alpine region. The climatological mean summer temperature (1961-1990)

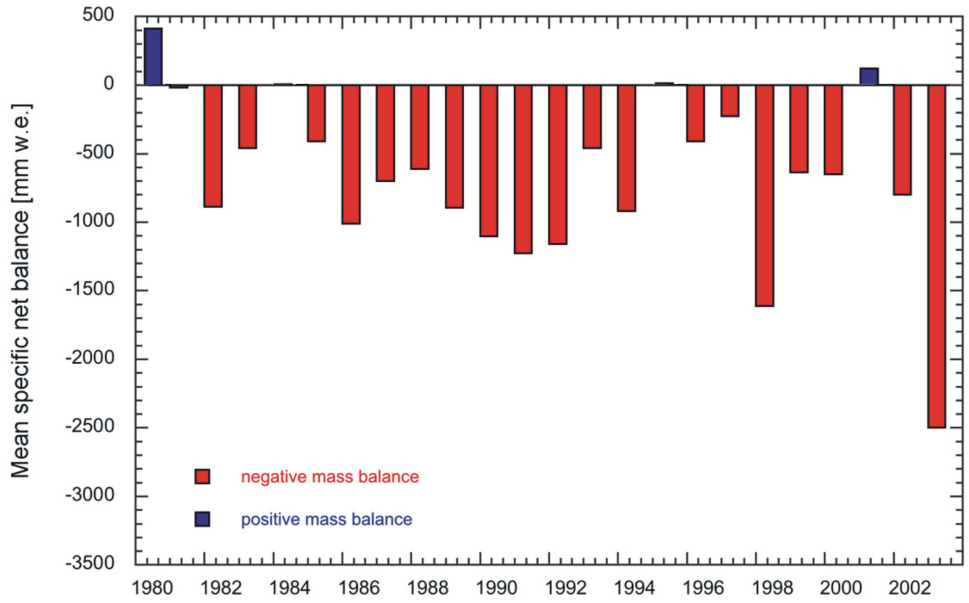

Figure 2.13: Mean specific net balance of nine Alpine reference glaciers (see Figure 2.12) in the European Alps for the period 1980-2003 (modified after Frauenfelder et al., 2005).

was exceeded by about 3°C over large areas (Schär et al., 2004) and Alpine glaciers lost about 5 to 10% of their remaining volume in a single summer (Frauenfelder et al., 2005; Zemp et al., 2006a). The average specific net balance of nine reference glaciers has been as high as -2.5 m w.e./year, clearly surpassing the previous record year 1998 (Figure 2.13).

2.8 Glaciers and Hydrology

2.8.1 Storage Characteristics

In alpine areas glaciers can exert a considerable influence on catchment hydrology by temporarily storing water as snow and ice on a variety of timescales (Hock, 2005). Even a low fraction of glacier cover within a catchment can have a large impact on its hydrological characteristics (Jansson et al., 2003). The reservoir function of a glacier involves the storage of water in the form of ice, snow and liquid water. These sub-reservoirs are associated with distinct time scales. On a sub-daily and sub-seasonal basis, the storage function is associated with the accumulation and melt of snow on a glacier surface as well as with the retention of liquid water, originating from melting at the surface or liquid precipitation, within (englacial) or underneath (subglacial) the glacier. On longer time scales (more than one year) the glacier ice itself constitutes the storage. A comprehensive review on glacier storage characteristics and the involved time scales is given in Jansson et al. (2003). The most important processes involved in glacier hydrology and their respective temporal scales are shown in Figure 2.14. Based on the mentioned study, a summary of the main aspects is being given in the following:

- **Long-term storage**
  The long-term hydrological effect of glaciers consists in the storage of water as ice and its

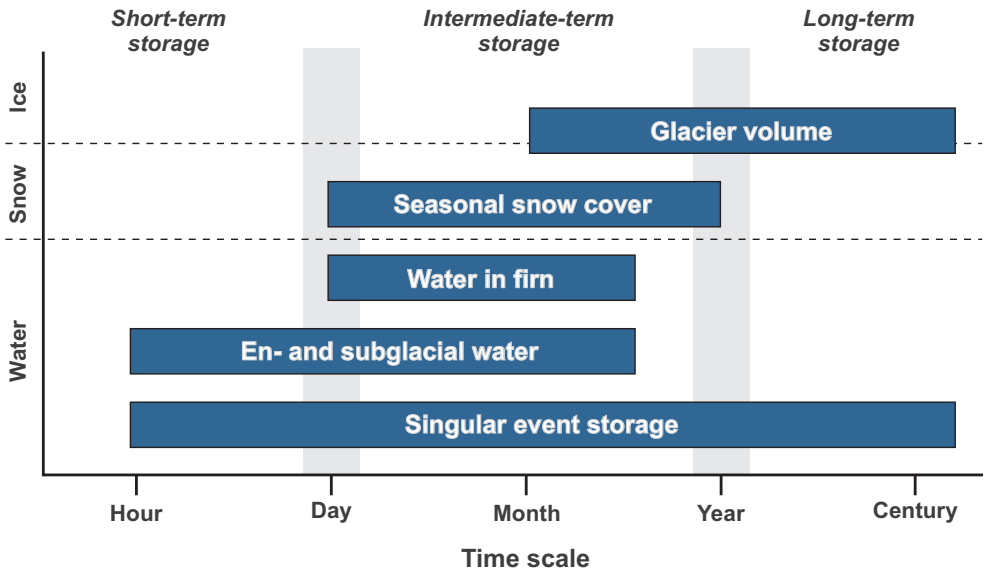

Figure 2.14: Different forms of glacier storage and their corresponding time scales (modified after Jansson et al., 2003).

release depending on climatic conditions. This process typically involves time scales larger than one year and strongly affects the interannual variability of discharge. In contrast to glacier-free catchments, the runoff from strongly glaciated catchments is not dominated by precipitation but by energy (Chen and Ohmura, 1990b). While in the glacier-free case the annual amount of runoff is directly related to (and always less than) the precipitation received, runoff from a glaciated basin can be either greater or less than total precipitation, according to the change in ice volume (Collins, 1989). During warm and dry periods, glaciers tend to melt more and glacier runoff is increased whereas under cool and wet conditions glacier runoff is reduced. The opposing responses of the ice-free and the glaciated parts of a catchment to the same hydrometeorological input tend to moderate year-to-year variations of runoff and, hence, constitute the regulating and compensating effect of glaciers on interannual streamflow variability (Singh and Singh, 2001; Collins, 2005). This effect can be of major importance for water resources management (Barry, 2003; Barnett et al., 2005). In many areas, water supply systems, agriculture, energy production and river transport strongly depend on the reservoir function of glaciers since additional water is being released into river systems exactly during times when water is scarce and the need is largest. It was found that the year-to-year variation of streamflow is lowest at moderate fractions of glacier cover in a catchment (about 40%) and that the streamflow variability increases as glacier cover both decreases and increases (since either precipitation or the supply of melt energy then strongly dominates the total amount of runoff throughout a year).

▷ **Intermediate-term storage**

As large volumes of precipitation are stored on glaciers in winter and are being released by summer melting, the presence of glaciers strongly modifies and enhances the seasonality of discharge. The ratio of summer runoff to total runoff generally rises with increasing glacier cover and the time of maximum discharge is shifted towards the summer months (see Figure 2.15). One reason for this shift is the fact that a glacier surface, in contrast to seasonal snow cover, produces melt

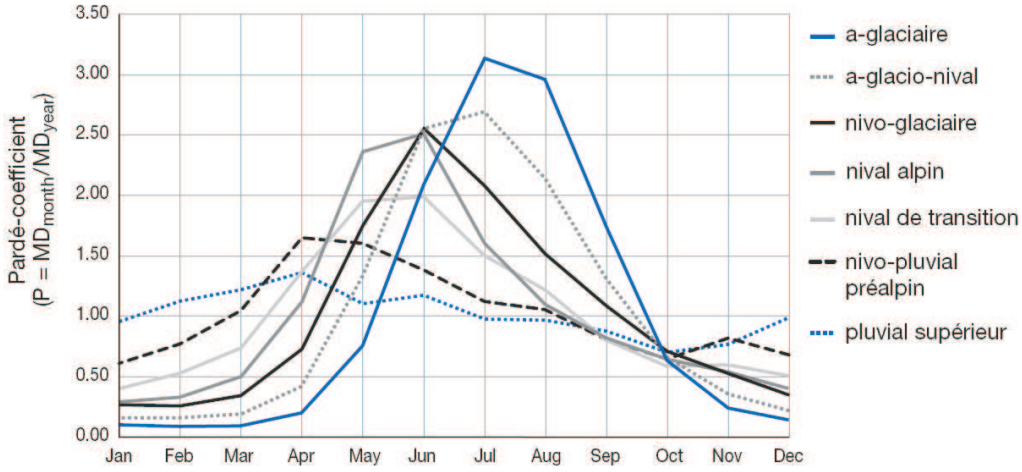

Figure 2.15: Average discharge patterns for Swiss catchments at varying elevations, ranging from "pluvial supérieur" (average elevation 800 m a.s.l., no glacier cover) to "a-glaciaire" (2700 m a.s.l., high degree of glacier cover), MD = mean discharge (Schädler, 2003).

water after the disappearance of snow (i.e., later during the melt season). A second point is the temporary storage of melt water and rain within the glacier itself, especially within the firn layers (*firn aquifer*). The delay in the timing of the discharge peak can be extremely important in regions where the summer is the driest period like in parts of Central Asia. Here, melt water from glaciers is virtually the only source of water in summer (Oerlemans, 2001). In many parts of the world, even distant mountain glaciers provide lowland rivers with the important hydrological base flow (Hall and Fagre, 2003).

▷ **Short-term storage**

Due to diurnal fluctuations in the amount of energy available for melting of snow and ice, glacier runoff is often subject to a pronounced variability on a diurnal time scale with runoff peaks in the afternoon. These variations are less pronounced in the beginning of the melt season due to percolation of melt water through the snow pack. As the melt season progresses, the drainage system of a glacier improves and is well developed by the mid or late melt season. Also, the area of exposed ice which can be efficiently drained by a moulin conduit system gets larger. Diurnal variations in the amount of meltwater produced at the surface will then also appear in the discharge at a glacier's snout (Singh and Singh, 2001). However, due to a certain retention capacity of the englacial and subglacial drainage system, a time lag of a few hours between maximum melt rates and the discharge peak will still occur. This lag generally decreases towards the end of the melt season because the drainage system of a glacier becomes more efficient at carrying large discharges through the ice body.

▷ **Singular storage release**

Under certain conditions, large volumes of water stored within or on the surface of a glacier can be released in single events which do usually not exhibit cyclic behaviour and have irregular occurrences. This description mainly refers to *outburst floods* (also called by the Icelandic term *jökulhlaups*), rapid discharges of water from a reservoir within a glacier or from an ice-dammed

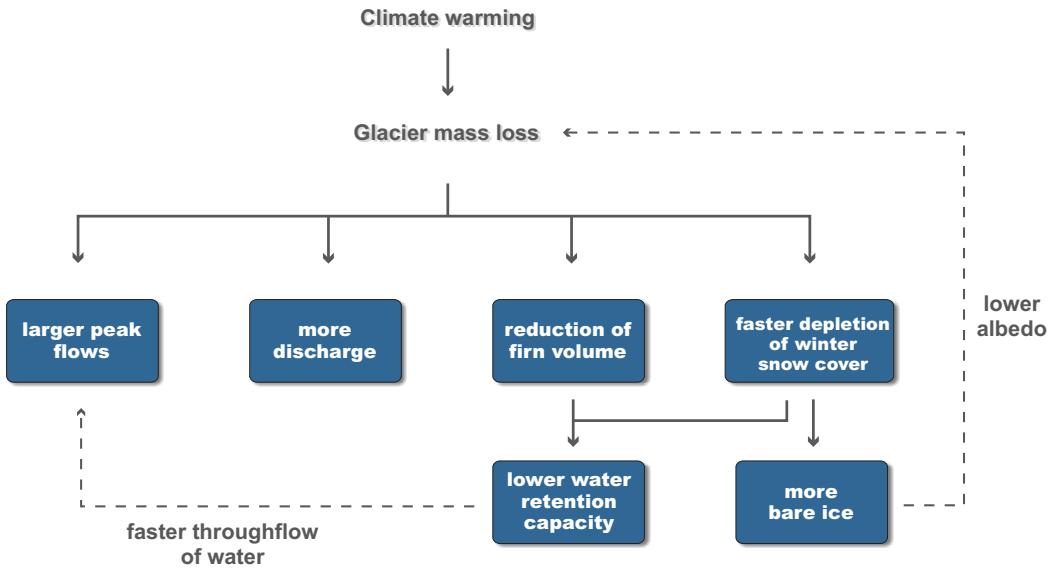

Figure 2.16: Short-term effects of climate warming on glacier discharge including feedback mechanisms (modified after Hock et al., 2005).

lake on its surface. These floods are characterised by a fast increase of discharge within minutes or hours and, due to their unpredictability, can be extremely dangerous (Hambrey and Alean, 2004). Also, *glacier surges* (see Chapter 2.5.1) can be associated with strongly increased amounts of discharge.

2.8.2 Impact of Climate Change

Due to the strong influence of glaciers on streamflow characteristics the expected future glacier wastage will have severe consequences for the discharge in glaciated catchments (Oerlemans, 2001). Generally, the response of glacier runoff to an increase of temperature is a matter of timescale. Although the response is immediate, a number of response characteristics will change sign at a later stage when glacier volume has decreased significantly. Hock et al. (2005) give a comprehensive overview of the involved processes and time scales. The major processes and feedback mechanisms that occur on short time scales are summarised schematically in Figure 2.16.

The initial effect of enhanced glacier melt will be an increase in discharge, especially during the summer months (see Figure 2.17). If glacier mass loss continues into the more distant future, the glaciated area will diminish and summer discharge will be gradually reduced again (Braun et al., 2000). By the time when most of the glaciers in a catchment have disappeared, the annual discharge may return to former levels, but summer discharge will be much lower. Assuming that conditions are now so warm that also the storage of water as snow has become less significant, the transition from a glacial to a pluvial regime type has been completed and discharge conditions will clearly reflect the annual cycle of precipitation (Oerlemans, 2001).

Changes in the year-to-year variability of runoff and hence in the compensating effect of glaciers will depend on the degree of initial (i.e., present) glaciation. Minimum variability occurs at glacier

coverages of about 40% or even less (Jansson et al., 2003; Hock et al., 2005). When glaciation falls below this threshold the year-to-year variability of runoff tends to increase and the compensating effect of glaciers diminishes. The general enlargement of bare ice areas and the reduction in the thickness and extent of firn and snow cover will furthermore lead to a reduced storage capacity of the glacier itself. Consequently, the transport of water on and through the glacier will speed up leading to enhanced diurnal discharge peaks and amplitudes (Hock et al., 2005). In the case that high melt rates and heavy summer rains coincide, the reduced storage capacity will result in higher flood peaks (Braun et al., 2000).

2.9 Glaciers and Climate Modelling

In today's state-of-the art global and regional climate models glaciers are represented in a strongly simplified way (see also Chapter 1). In most cases static 0-1-glacier masks are used which define each land grid point as either totally glaciated or totally ice free at the time of initialisation (see Figure 1.2). They do neither allow for the simulation of changes in ice extent due to changing climatic conditions nor for a reliable estimate of changes in total ice volume. This simplistic approach originally stems from the necessity to represent the surface characteristics of large, slowly reacting ice masses, especially the polar ice sheets, as lower atmospheric boundary conditions. Glaciers and smaller ice caps are usually beyond grid box resolution and are not accounted for explicitly. The only way in which they are considered is via their contribution to the mean grid box surface characteristics (e.g., albedo, surface roughness length, leaf area index) as defined by the underlying land surface parameter dataset on "non-glaciated" model grid points.

Static 0-1-glacier masks are for instance applied in the Max Planck Institute's most recent GCM ECHAM5 (Roeckner et al., 2003) and in the original version of the RCM REMO (REMO 5.3, see Chapter 3). An extension of this simple concept is the use of fractional glacier masks by considering several land cover types (including one type for glaciers/ice caps) on a subgrid level, as it is for instance done in the global climate system model CCSM 3.0 (Collins et al., 2006) using the CLM 3.0 land surface scheme (Oleson et al., 2004; Dickinson et al., 2006). Nonetheless, the subgrid fraction covered by glaciers is still static (i.e., does not change in time) and changes in ice volume are disregarded. A provisional dynamical approach on the resolved grid scale (i.e., a 0-1-glacier mask which is allowed to

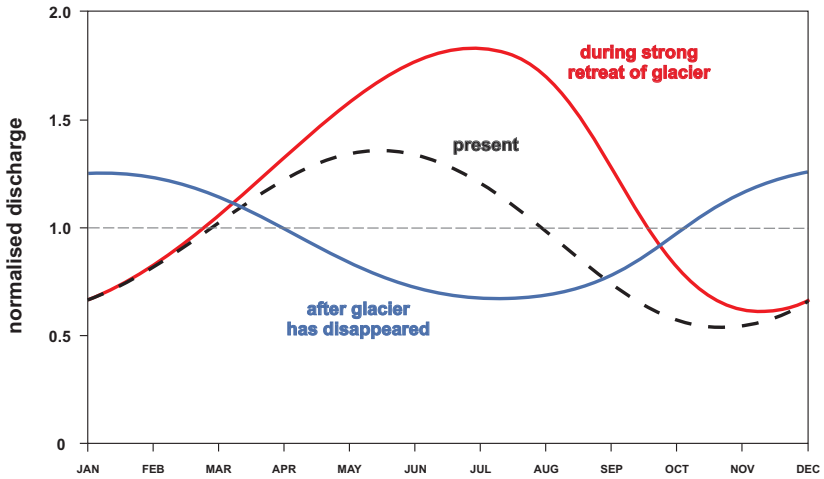

Figure 2.17: Expected changes in discharge regime in a strongly glaciated catchment under climate warming conditions (idealised). Precipitation has a seasonal cycle with a summer minimum and the total amount of precipitation does not change (modified after Oerlemans, 2001).

change in time) has been implemented in the RCM HIRHAM (Christensen et al., 1996): If the snow depth on a formerly non-glaciated grid point exceeds 10 m w.e. the model switches to "glacier mode" at the respective grid point. Once the snow/ice water equivalent drops again below 10 m (by ice ablation exceeding snow accumulation) the model switches back to the regular "snow mode" (J.H. Christensen, pers. comm.). However, the total ice volume stored in the respective grid box is still disregarded.

To our knowledge no effort has been undertaken so far to dynamically include glaciers and small ice caps (i.e., land ice masses other than the two polar ice sheets) on a subgrid level in climate models. Only in case of the large continental ice sheets, and especially in paleo-climate studies, dynamical ice sheet models have been bi-directionally coupled to GCMs (e.g., Ridley et al., 2005; Winguth et al., 2005; Vizcaino, 2006) or have been implemented into Earth System Models of Intermediate Complexity (EMICs; e.g., Wang and Mysak, 2002; Kageyama et al., 2004; Calov et al., 2005). Recently, downscaled climate model output has also been used to drive glacier mass balance models and to assess changes in glacier mass balance and glacier geometry as a response to climatic changes (e.g., Schneeberger et al., 2001, 2003; Reichert et al., 2001a, 2002; Radić and Hock, 2006). Such one-way coupling techniques do not allow for any feedback of changes in glacier characteristics and extent to the simulated climate. Furthermore, they are typically restricted to a small sample of individual glaciers for which calibrated mass balance models are available.

3 The Regional Climate Model REMO

3.1 Introduction

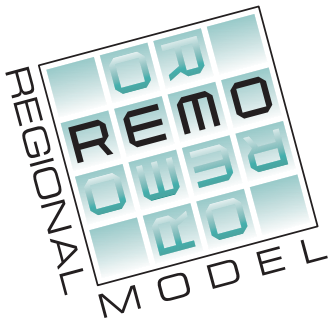

The basic modelling tool for the development and the assessment of the new glacier subgrid parameterisation is the regional climate model REMO (an acronym for *REgional MOdel*). In the course of the present study, the most recent model version REMO 5.3 has been extended and modified in order to account for the energy and mass balance of mountain glaciers. These changes primarily concern the physical parameterisations of the model, especially the treatment of land surface processes. The new model version (REMO 5.3 plus the subgrid glacier parameterisation) will be termed $\text{REMO}_{\texttt{glacier}}$. This section presents the most important features of the basic version 5.3 with a special focus on the land surface. A detailed description of all modifications and extensions that have been implemented within the present study, including technical issues, will follow in Chapter 4.

In recent years, regional climate models (RCMs) have proved to be useful tools for the analysis of regional energy and water cycles as well as for the prediction of climatic changes on a regional scale (e.g. Jacob et al., 2007, 2001; Déqué et al., 2005). In contrast to general circulation models of the atmosphere (AGCMs, or simply GCMs), the model domain of an RCM does not cover the entire globe but is typically restricted to some hundred to some thousand kilometers in x- and y-direction. This feature allows the long-term simulation of atmospheric processes with a high horizontal resolution at comparatively low computational costs. Generally, a fine resolution is important to resolve small-scale atmospheric circulations, for instance those affected by orography or by details of the land surface (McGregor, 1997). The restriction to a certain geographical region and the aim to simulate atmospheric processes on climatological time scales (i.e., for much longer than just a few hours or days) implies that information on the large-scale state of the atmosphere outside the regional model domain has to be provided by another source. These *lateral boundary conditions* (LBCs) can in principle be derived from GCM simulations or, based on observations, from global-scale analysis and re-analysis products. The latter are also referred to as *perfect boundary conditions* (Jacob, 2001) since they are based on the observed state of the atmosphere and represent the best estimate of multi-decadal time series of large-scale conditions. The RCM is said to be *nested into* the respective large-scale forcing, a technique which is also referred to as *physically based downscaling* and which is usually carried out in a one-way mode (no feedback to the large scales). Recently, also two-way nesting methods have been developed (e.g., Lorenz and Jacob, 2005). Within the present study, LBCs for REMO are provided by the ERA-40 Re-analysis (Uppala et al., 2005) and by the operational analysis of the ECMWF applying the one-way nesting technique.

3.2 General Characteristics

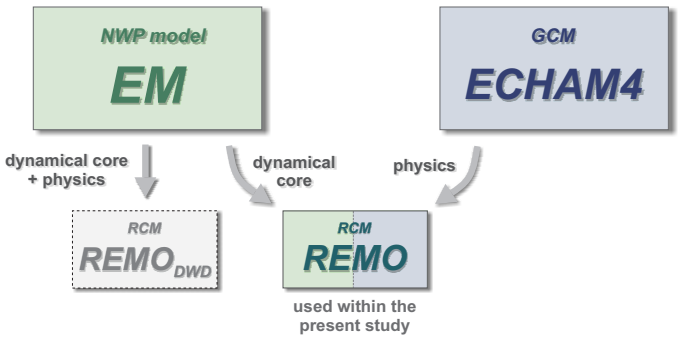

Figure 3.1: Origins of the regional climate model REMO.

The regional climate model REMO (Jacob, 2001; Jacob et al., 2001; Jacob and Podzun, 1997) is a three-dimensional, hydrostatic atmospheric circulation model which solves the discretised primitive equations of atmospheric motion. Like most other RCMs, REMO has been developed starting from an existing numerical weather prediction (NWP) model: the Europa-Modell (EM) of the German Weather Service DWD (Majewski, 1991). Additionally, the physical parameterisation package of the general circulation model ECHAM4 (Roeckner et al., 1996) has been implemented, optionally replacing the original EM physics. In numerous studies, the latter combination (i.e., the EM dynamical core plus the ECHAM4 physical parameterisation scheme) proved its ability to realistically reproduce regional climatic features and is therefore used as the standard setup in recent applications, including the present study (see Figure 3.1).

The atmospheric prognostic variables of REMO are the horizontal wind components, surface pressure, temperature, specific humidity and cloud liquid water. The temporal integration is accomplished by a leap-frog scheme with semi-implicit correction and time filtering after Asselin (1972). In the vertical, variations of the prognostic variables (except surface pressure) are represented by a hybrid vertical coordinate system (Simmons and Burridge, 1981). For horizontal discretisation REMO uses a spherical Arakawa-C grid in which all variables except the wind components are defined in the centre of the respective grid box. The grid box centres themselves are defined on a rotated latitude-longitude coordinate system. In its standard setup, REMO uses a horizontal grid spacing of $^1/_6^\circ$ or $^1/_2^\circ$, corresponding to horizontal resolutions of about 18 km and 55 km, respectively. The time step length is usually set to 100 seconds in the first case and to 240 seconds in the latter. Recently, also simulations using higher resolutions of about 10 km have been successfully carried out (D. Jacob, pers. comm.).

As described in Chapter 3.1, the lateral boundary conditions can either be provided by a GCM simulation or by re-analysis or analysis products. In all cases, the relaxation scheme according to Davies (1976) is applied: The prognostic variables of REMO are adjusted towards the large-scale forcing in a lateral sponge zone of 8 grid boxes with the LBC influence exponentially decreasing towards the inner model domain. At the lower boundary, REMO is forced by the land surface characteristics (see Chapter 3.3) and, over sea, by the sea surface temperature (SST) and sea ice distribution. The SST can either be interpolated from the large-scale forcing (if existent in there) or observational datasets, or can be calculated online by a regional ocean model coupled to REMO (e.g., Lehmann et al., 2004). The same is true for the sea ice extent, which can as a further option also be diagnosed from the SST.

3.3 Land Surface Treatment

3.3.1 Overview

In REMO as well as in any other RCM, the land surface is treated with special care. It plays a key role within the climate system, controlling the partitioning of available energy into terrestrial radiation and sensible and latent heat as well as the partitioning of available water into evaporation and runoff over land areas. Furthermore, it is the location of the terrestrial carbon sink. Due to this important role in determining surface-atmosphere exchanges, it is necessary to represent the land surface in an appropriate way in climate models which is usually achieved by the incorporation of a more or less sophisticated land surface scheme (LSS). The recent work by Pitman (2003) provides a comprehensive review on the different types of LSS used in climate models, ranging from simple first-generation models (e.g., Manabe, 1969) to complex third-generation schemes which include the modelling of the terrestrial carbon cycle.

According to the mentioned study, the LSS used in REMO can be classified as a second-generation scheme, though the treatment of soil hydrology is still based on the simple bucket scheme proposed by Manabe (1969). In principle, the parameterisation of land surface processes in REMO is derived from the parameterisation scheme of the GCM ECHAM4 (Roeckner et al., 1996), which in turn is almost identical to the one used in the former version ECHAM3 (DKRZ, 1994). However, a number of modifications of the original ECHAM4 physics have been carried out in recent years, especially related to subgrid surface coverage, snow processes and the phase transformation of soil water (Semmler, 2002) as well as to vegetation characteristics (Rechid and Jacob, 2006). This chapter will give a summary of the most important points with respect to the objectives of the present study. For further details, the reader is referred to the publications mentioned above.

3.3.2 Fractional Surface Cover and Turbulent Fluxes

In the original ECHAM4 parameterisation, a model grid box consisted of only one single surface type, i.e. was either covered by land, water or sea ice (or permanently by glacier ice, see Chapter 3.3.6). Semmler (2002) extended this concept for REMO by introducing subgrid fractions for each of the three basic types (see Figure 3.2 for an example). These fractions are not assumed to be located in a specific

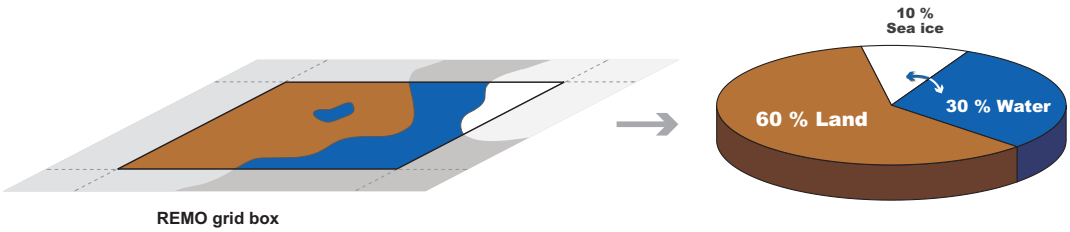

Figure 3.2: The tile approach. Example for a grid box covered by land (60%), water (30%) and sea ice (10%).

area of a grid box but do simply cover a certain percentage of the total grid box area, summing up to a total of 100% (*tile approach*). Applying this technique, the consideration of a smoothed transition from land to sea along the coastlines as well as from ice-covered to ice-free ocean surfaces is possible. The water fraction of a grid box includes both ocean surfaces and inland lakes. While the general land-sea distribution remains constant throughout the model integration, the partitioning of the total water fraction of a grid box into open water and sea ice-covered parts can vary in time.

During the model integration, each surface fraction is characterised by its own roughness length, its own albedo and its own, time-varying surface temperature. The land fraction is further divided into a part covered by vegetation and a bare soil fraction (see Chapter 3.3.3). Based on these characteristics, the turbulent surface fluxes and the surface radiation flux are calculated separately for each fraction and are subsequently averaged within the lowest atmospheric level using the respective areas as weights.

On each fraction and within each time step, the turbulent fluxes of momentum and latent and sensible heat are derived from the well-established bulk transfer relations with the transfer coefficients being obtained from Monin-Obukhov similarity theory Louis (1979) with a higher order closure scheme. Over land surfaces, the roughness length z_0 is geographically prescribed as a function of subgrid-scale orography and vegetation type. For the turbulent fluxes of sensible and latent heat z_0 is restricted to a maximum value of 0.1 m. Over open water, the relation after Charnock (1955) with a minimum value for z_0 of $1.5 \cdot 10^{-5}$m with subsequent reduction of the heat transfer coefficient is applied. Over sea ice a constant value of $z_0 = 0.001$ m is prescribed.

3.3.3 Vegetation and Land Use

Surface-atmosphere exchange processes over land are to a large extent controlled by the physical properties of the soil and of the vegetation. These characteristics include for instance the surface roughness length (see above), the soil field capacity, the water holding capacity of the vegetation, the background albedo (i.e., the albedo of a snow-free surface), the fractional vegetation cover, the *leaf area index* (LAI), etc. Some of these parameters strongly depend on the physiological state of the vegetation and are therefore subject to a pronounced seasonal variability (between growing and dormancy season) in many regions. Nevertheless, a number of RCMs still neglect the annual cycle of vegetation characteristics. In REMO, a seasonal variation of the parameters

- ▷ fractional vegetation cover
- ▷ LAI (the ratio of one-sided leaf area to surface area)
- ▷ background albedo

in each grid box has been introduced by Rechid and Jacob (2006).

3.3.4 Soil Processes

Heat Budget

The temperature profile in the soil is calculated applying a heat conduction equation for five soil layers with increasing thicknesses from the surface downwards (Figure 3.3). A zero heat flux condition is applied at the lowest boundary. Heat conductivity and heat capacity of the soil layers depend on the respective soil type. Additionally, a dependency of these two parameters on the soil water content has been implemented by Semmler (2002). Due to some spurious influences on the model results, this feature has been switched off in recent applications, including all simulations carried out within the present study. Semmler (2002) also introduced the freezing and thawing of soil water with the corresponding release and consumption of latent heat.

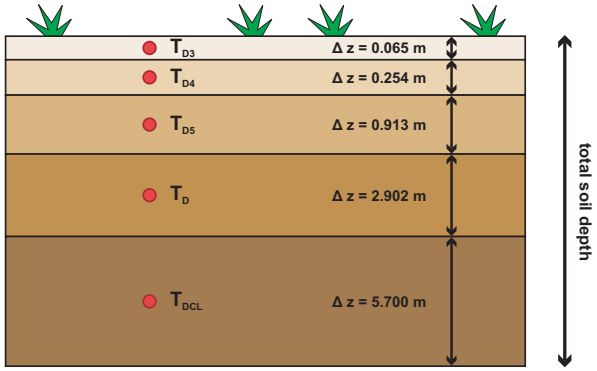

Figure 3.3: Soil temperatures and layering in REMO.

Hydrology

The parameterisation of soil hydrology in REMO consists of budget equations for the following three reservoirs:

- the amount of snow accumulated on the surface (Chapter 3.3.5)
- the amount of water in the skin reservoir (i.e., rain water and melting snow that is intercepted by the vegetation until its water holding capacity is reached)
- the amount of water in the soil

The latter is filled by infiltrating water (i.e., the amount of rain or snow melt that does not enter the skin reservoir and does not run off on the surface). The partitioning of the total amount of water available for runoff generation into surface runoff and infiltration follows the so-called *Arno-Scheme* (Dümenil and Todini, 1992) in which surface runoff is computed as infiltration excess from a bucket-type reservoir. However, in contrast to the simple bucket scheme originally proposed by Manabe (1969), the subgrid-scale heterogeneity of field capacities (i.e. of the total amount of water that

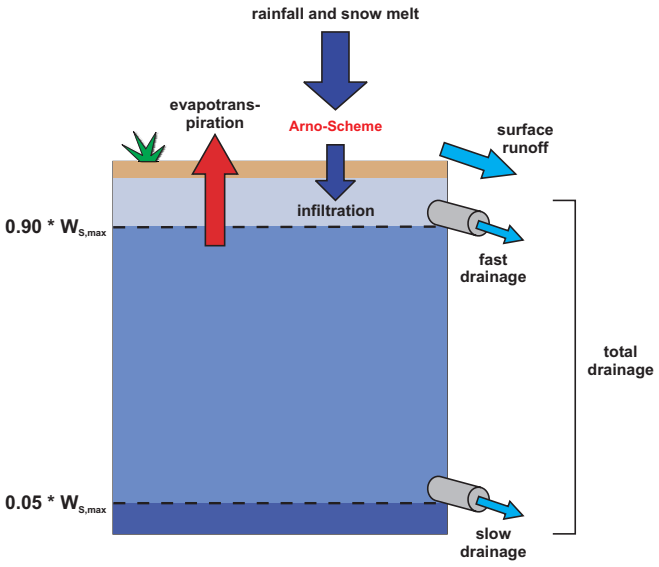

Figure 3.4: Soil hydrology in REMO.

can be stored within a soil column) within
a climate model grid box is accounted for.

The amount of rainfall and snow melt that has passed the Arno-Scheme and infiltrates into the soil is used to fill the soil water reservoir. From here, subsurface drainage occurs independent of the water input if the soil wetness is larger than 5% of the field capacity $W_{S,max}$ (slow drainage). Once the relative soil water content reaches 90%, a second, fast drainage component is additionally activated (Figure 3.4). The sum of both drainage components equals the total drainage, which is the subsurface counterpart of surface runoff. Furthermore, soil water can be extracted by surface evaporation / evapotranspiration which is computed from atmospheric demand and plant physiological characteristics (see Chapter 3.3.2).

3.3.5 Snow Cover

The original snow parameterisation, which has been adopted from the GCM ECHAM4, was substantially modified by Semmler (2002) in order to improve the model performance in high-latitude regions. The current parameterisation is still simple and computationally effective compared to more complex, comprehensive snow schemes (e.g., Loth, 1995).

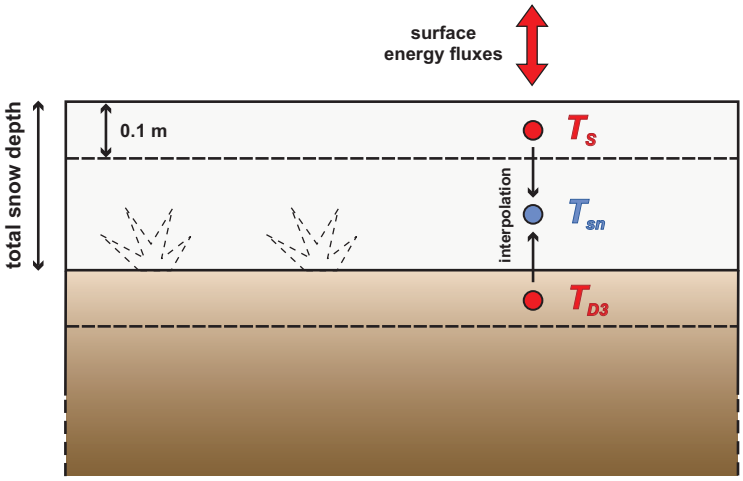

Figure 3.5: Snow layers and corresponding temperatures in REMO.

In terms of heat conduction, an extra snow layer is considered up from a critical snow depth of SN_{cri} = 0.01 m w.e.. In each time step, the residual of the surface energy fluxes is then used to warm or to cool an upper snow layer of SN_{up} = 0.1 m thickness (or less if the total snow depth is smaller). The corresponding upper layer snow temperature is considered as the surface temperature T_S of the snow layer and serves as interface to the atmosphere (see Figure 3.5). The temperature T_{sn} in the centre of the whole snow pack is being interpolated from T_S and the temperature T_{D3} of the uppermost soil layer. If T_S or T_{D3} have reached the melting point T_{melt} = 0°C, further energy input is used for snow melt. Snow density and heat conductivity depend on the snow temperature T_{sn} with both parameters increasing with rising temperatures.

The snow albedo α_{snow} is a function of the snow surface temperature T_S and of the forest fraction f_{forest} in a grid cell. For $T_S \leq$ -10°C the albedo is fixed at a maximum value $\alpha_{snow,max}$. For -10°C $\leq T_S \leq$ 0°C it decreases linearly until the minimum value of $\alpha_{snow,min}$ is reached at T_S = 0°C (Figure 3.6). This dependency on snow temperature accounts for the fact that wet snow usually has a higher temperature and a lower albedo than completely frozen snow (Hall, 2004, see also Chapter 2.4.2). $\alpha_{snow,max}$ and $\alpha_{snow,min}$ in turn depend on the forest fraction f_{forest} and vary from 0.4 to 0.8 and from 0.3 to 0.4 respectively (with the lower value for $f_{forest} = 1$ and the higher value for

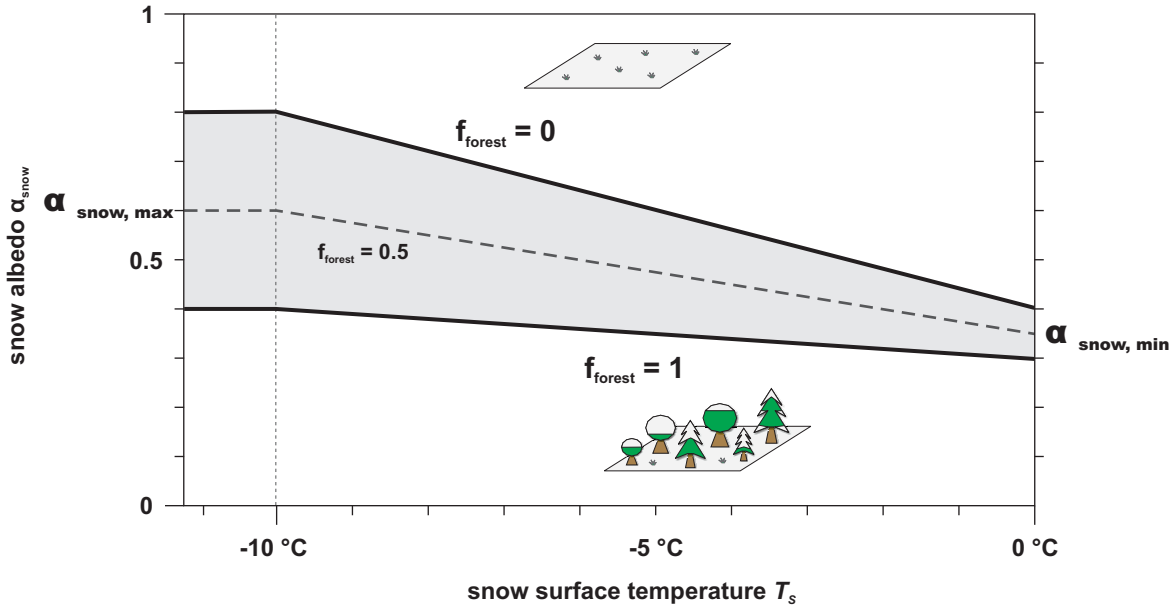

Figure 3.6: Dependency of the snow albedo α_{snow} on snow surface temperature T_S and forest fraction f_{forest} in a REMO grid box.

$f_{forest} = 0$).

The final albedo of a snow covered land surface α_{surf} is a function of the background albedo α_b (see Chapter 3.3.3), the snow albedo α_{snow} and the actual snow depth Sn:

$$\alpha_{surf} \;=\; \alpha_b \;+\; (\alpha_{snow} - \alpha_b) \cdot \frac{Sn}{Sn \;+\; Sn^*} \tag{3.1}$$

with a critical snow depth $Sn^* = 0.01$ m w.e. and α_{surf} approaching α_{snow} for $Sn \gg Sn^*$.

3.3.6 Glaciers

As most state-of-the-art climate models (see Chapter 2.9), REMO in its default version uses a static glacier mask *GLAC* which is allocated at the start of the simulation and which does not change with time. In the standard setup, the mask is diagnosed at the very first model time step from the snow depth interpolated from the driving field (LBC) during preprocessing. If in a REMO grid box this interpolated snow depth is larger than 9.5 m w.e., the box is marked as glaciated (*GLAC*=1), otherwise as non-glaciated (*GLAC*=0). Normally, this is only the case in regions which are marked as "glacier" also in the driving model (e.g., over the Greenland Ice Sheet). In REMO simulations over Europe, typically no single grid cell on the European Continent is considered as being glaciated (Figure 3.7).

Grid boxes marked as "glacier" are assumed to be totally covered by ice. The soil heat equations are solved for five layers (see Chapter 3.3.4), but assuming the thermal characteristics of ice. The process of runoff generation on glacier ice is neglected. Both surface runoff and drainage are set to zero in each time step. A snow pack on top of the ice surface is not considered and therefore also snow melt does not occur. Consequently, the water balance of these grid boxes is not closed: The amount of solid and liquid precipitation does neither accumulate on the surface nor run off but is simply lost. In the model output, the snow depth does remain at its initial value larger than 9.5 m w.e. (which is important if double nesting is applied and a glacier mask must also be derived for a subsequent model simulation at higher resolution). Similarly to the snow albedo on the land fraction of non-glaciated boxes, the albedo of a glaciated grid box is a function of the surface temperature T_S (see Figure 3.6), varying between $\alpha_{ice,max} = 0.8$ (for $T_S \leq$ -10°C) and $\alpha_{ice,min} = 0.6$ (for $T_S = 0$°C).

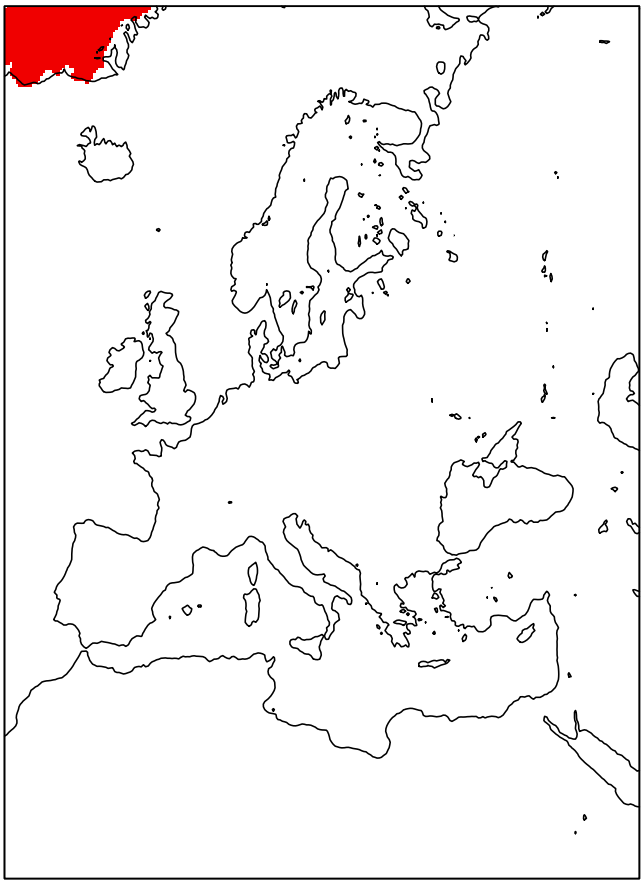

Figure 3.7: Static glacier mask used in a standard REMO simulation ($^1/_6$° horizontal resolution, 289 x 321 grid boxes), glaciated boxes are marked in red colour.

Also in grid boxes marked as "non-glaciated" (GLAC=0), surface ice cover is in principle accounted for via its proportional contribution to the mean grid box surface characteristics (e.g., mean surface roughness length and mean leaf area index) as defined by the underlying, static land surface parameter dataset (Hagemann et al., 1999; Hagemann, 2002). The latter is based on a satellite-derived 1 x 1 km^2 global map of major ecosystem types (Loveland et al., 2000), including one type for "glacier ice". It reflects the spatial distribution of ecosystem types and the associated land surface characteristics for the period 1992-1993. A special treatment has been implemented for the surface background albedo (albedo of a snow-free land surface). In REMO version 5.3 a mean monthly climatology of this parameter is computed based on another high-resolution, satellite-derived albedo dataset (MODIS) and monthly values of the leaf area index. In the Alps, the methodology applied basically neglects the presence of glaciers on a subgrid level since snow- and ice-covered pixels in the respective MODIS scenes are excluded from the analysis. These pixels do not contribute to the mean REMO grid box background albedo. Hence, the background albedo of glaciated REMO grid cells in the Alps is systematically underestimated. This fact is of major importance for the analysis of differences in the simulated atmospheric parameters between REMO 5.3 and REMO$_{\texttt{glacier}}$ (Chapter 5).

3.4 Coupling of the HD Model

3.4.1 Introduction

As long as climate models have mainly been concerned with atmospheric processes and oceans were represented in a strongly simplified way (e.g., by prescribed SSTs or slab ocean models) the transport of water in the horizontal direction within the river system has usually been ignored. The runoff components that were produced by one-dimensional land surface schemes (compare Figure 3.4) have not been treated further but were simply extracted from the system. Consequently, the hydrological cycle was not completely closed in these models. With the development of AOGCMs, coupled models of the atmospheric and oceanic circulation, the need for a more adequate treatment of river discharge as a major contributor of freshwater flux into the ocean has been widely recognised. Furthermore, the validation of the simulated river discharge against river gauge measurements can provide a useful independent and integrating measure of the performance of the simulated hydrological cycle of a climate model (Hagemann and Dümenil, 1998b), both on a continental scale (GCM scale) and for individual, meso-scale river basins (RCM scale). However, a direct comparison of the runoff produced at the individual climate model grid boxes against observations without accounting for the lateral routing of water towards the river mouths is not feasible (Graham and Jacob, 2000).

In order to provide the missing link and to account for the travel time of water in the horizontal direction, so-called *routing schemes* (or *routing models*) have been developed for global and regional climate model applications (e.g., Hagemann, 1998; Coe, 2000; Miller et al., 1994; Lohmann et al., 1996), often based on algorithms already existing in catchment-based hydrological models. Routing schemes link the individual climate model grid boxes by taking over the runoff components produced by the vertical soil schemes and by transporting the respective amount of water in the horizontal plane, thereby mapping the natural river network. In this way, also catchment boundaries are implicitly defined: Grid boxes draining to a common outlet at the coastline, or a common interior basin, belong to the same catchment (see Figure 3.8). Usually, the retarding function of different types of reservoirs (e.g., lakes and wetlands) that have to be traversed along the way towards the catchment outlet is accounted for by the concept of linear reservoirs (see below). The simulated discharge at the river mouths can subsequently be used to provide an ocean model with the necessary freshwater inflow. Additionally, the discharge simulated by the routing scheme at specific sites, corresponding to the location of gauging stations, can be compared to gauge measurements and hence can be used for model validation purposes. A direct feedback of the simulated river flow to the atmospheric model component, for instance by surface evaporation or by re-infiltration of water over inundated areas with its influence on soil moisture and evapotranspiration, is typically neglected (one-way coupling).

Within the present study the HD routing scheme has been coupled to REMO in order to assess the influence of glaciers on river discharge. The following two sections give a short overview on the basic characteristics of the HD model and on the modifications that have been implemented in order to enable the coupling to REMO.

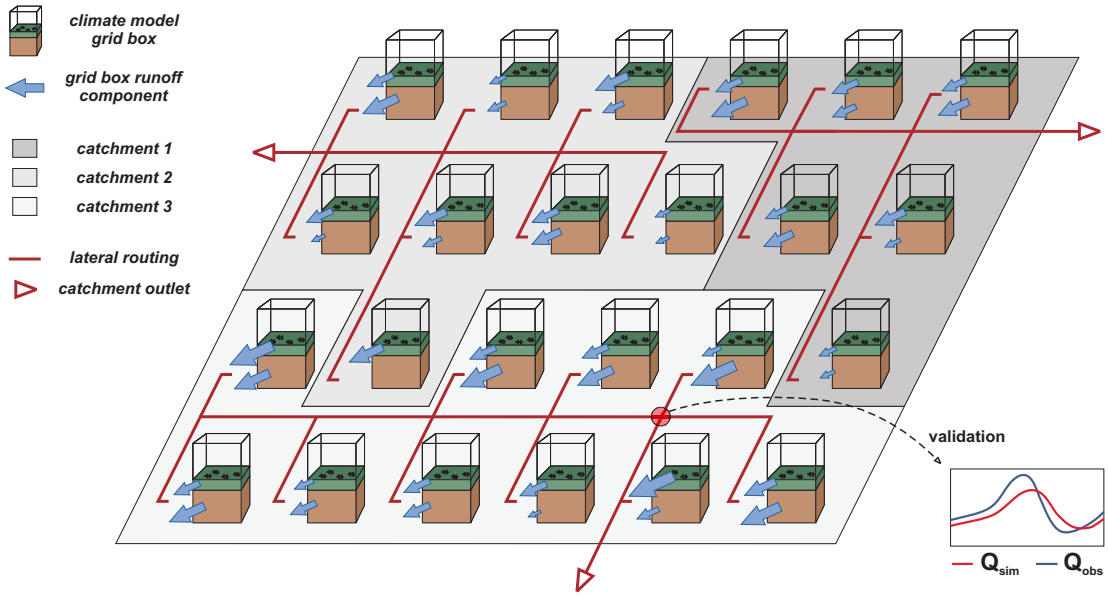

Figure 3.8: Overview on the functioning of a routing scheme: The runoff components of the individual climate model grid boxes (here: surface runoff and subsurface drainage) are transported horizontally towards the catchment outlets.

3.4.2 Model Description

General Characteristics

The HD Model (*Hydrological Discharge*) is a routing scheme which has been developed at the Max Planck Institute for Meteorology by Hagemann and Dümenil (1998b). It accounts for the lateral waterflow on the land surface in global climate model applications. It is part of the coupled atmosphere-ocean GCM ECHAM5/MPI-OM (Jungclaus et al., 2006; Latif et al., 2003), providing the ocean component with freshwater input from the surface river system.

The model describes the translation and retention of the lateral discharge within the river system as a function of spatially distributed land surface characteristics. In it's original version, the HD Model is applied on a global scale with a fixed horizontal resolution of $^1/_2^\circ$ on a regular, non-rotated spherical grid, corresponding to an average grid box size of about 55 x 55 km^2. The model requires daily time series of surface runoff and subsurface drainage as input parameters. These quantities are typically derived from global climate model simulations and are interpolated from the respective GCM grid to the $^1/_2^\circ$ grid used by the HD Model. The same technique can be used to simulate the lateral transport of runoff produced by RCM simulations (e.g., Hagemann and Dümenil, 1999; Hagemann and Jacob, 2007). In both cases, the fixed resolution of $^1/_2^\circ$ for river routing is used. This value has originally been chosen as a compromise between the GCM scale and the scale of topography-driven hydrological processes.

The HD model generally uses a daily time step. Only for riverflow (see below) a time step of six hours is applied in order to take into account a minimum travel time of river discharge through a $^1/_2^\circ$ grid

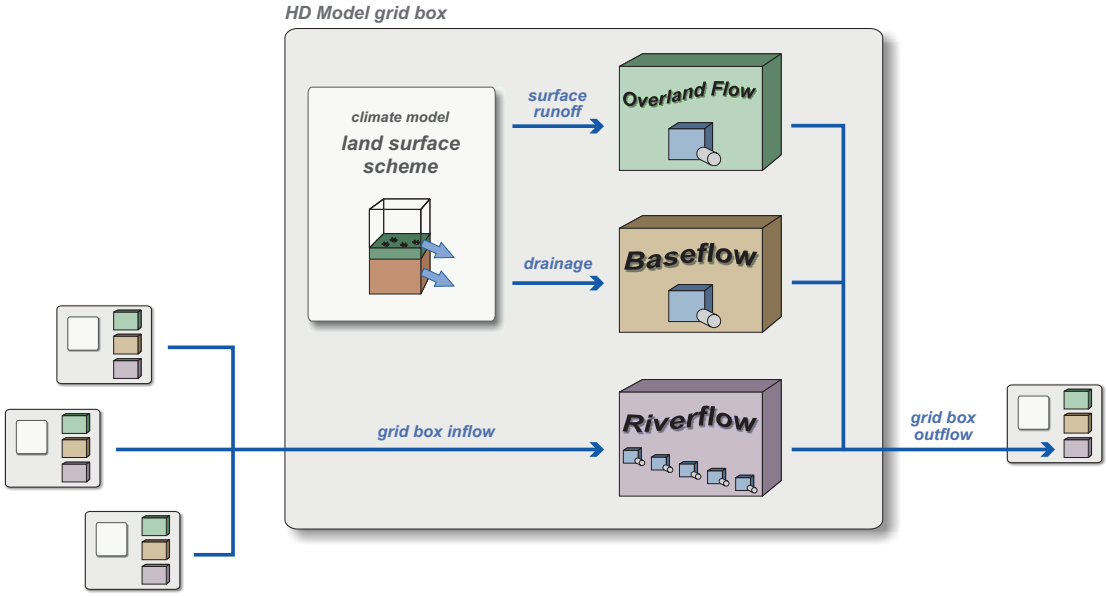

Figure 3.9: General structure of the HD Model. The total horizontal flow of water in a grid box is separated into the three flow processes overland flow, baseflow and riverflow.

box of less than one day. If, for some reason, GCM surface runoff and drainage are not available in the necessary temporal resolution but only atmospheric parameters (precipitation, 2m temperature), a simplified land surface scheme (SL scheme) can be used to compute the required runoff components from the pure atmospheric forcing. In the same way, HD Model input can also be derived from climatological datasets (Hagemann and Dümenil, 1998b).

Details about the model structure can be found in Hagemann (1998), Hagemann and Dümenil (1998a) and Hagemann and Dümenil (1998b). The remaining part of this section will only give a brief overview of the most important features.

Flow Processes

The horizontal movement of water within a catchment takes place both on the surface (mostly confined to rivers and creeks) and in the unsaturated and saturated zone within the ground. These different modes of lateral flow are associated with distinct flow velocities and hence distinct mean residence times of water. In the absence of large lakes, the transport of water within the surface river system is normally the fastest component. The HD Model accounts for this variety of involved time scales by separating the lateral waterflow within a model grid box into three flow processes:

- **overland flow**, representing the horizontal, surface-near transport of water, which has not yet reached the major river system, within a single grid box
- **baseflow**, representing the sub-surface horizontal transport of water in the saturated zone (groundwater flow) within a single grid box
- **riverflow**, representing the transport of water in the major river system within and

between grid boxes

(see Figure 3.9). Their specific influence on translation and retention of water in the horizontal direction is parameterised in terms of *linear reservoirs*, a commonly used concept in catchment hydrology. A linear reservoir relates the discharge $Q(t)$ out of the reservoir linearly to the actual filling $S(t)$ via a retention time (or retention constant) k:

$$Q(t) = \frac{1}{k} \cdot S(t) \tag{3.2}$$

The constant k thus defines the retention characteristics of the reservoir, with a large value denoting a strong retention. k is equal to the mean residence time of water within the reservoir.

In the HD Model, the overland flow and the baseflow component within a grid box are both represented by a single linear reservoir with the respective retention constants k_o and k_g. Riverflow is accounted for by a cascade of n_r (typically $n_r = 5$) equal linear reservoirs, i.e., by the serial arrangement of n_r reservoirs which have the same retention constant k_r. The amount of surface runoff which has been computed by the climate model's LSS (or an attached SL scheme, see above) for the respective time step and which has been interpolated to the HD Model grid serves as input for the overland flow reservoir. Input for the baseflow reservoir is provided by the climate model's subsurface drainage component. Finally, riverflow is fed by the inflow from other grid boxes. In each time step, the sum of the outflow of the three basic flow reservoirs equals the total outflow of a grid box and enters the down-stream box in the next time step (Figure 3.9). It is thus implicitly assumed that both surface runoff and drainage produced within a grid box have reached the surface river system by the end of a time step. The storage characteristics of the different flow reservoirs in a grid box, expressed in terms of the retention constants k_o, k_r and k_g, exclusively depend on physiographic grid box characteristics (e.g., average slope, wetland fraction, land fraction) and therefore vary in space (i.e., from grid box to grid box). A further calibration of the model parameters is not carried out.

Drainage Network

Besides the parameterisation of the grid box retention characteristics, a further key element of a routing scheme is the underlying drainage network. It defines the direction of water flow on the surface and as a consequence also the catchment boundaries in the model (see Figure 3.8). It is generally controlled by the surface topography. In the ideal case, the model's drainage network should match the existing surface river system. Similarly, the size of a specific model catchment should be equal to the real catchment size. Due to the relatively coarse resolution of global scale routing schemes, this is difficult to achieve and the real conditions can only be approximated to a certain degree.

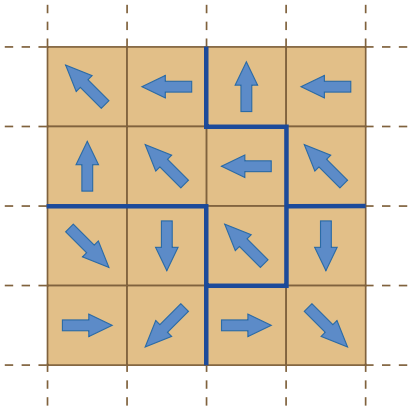

Figure 3.10: Fictitious drainage network with flow directions and catchment boundaries delineated by blue lines.

In the HD Model, the discharge produced in a grid box within

a certain time step has eight possibilities to leave the box: the four main geographical directions (N, E, S, W) and the four diagonal directions (NE, SE, SW, NW). Only one outflow direction is permitted for a specific grid box (i.e. the total amount of discharge produced in a box only drains to one single neighbouring box). A splitting of the total discharge into several directions is not possible and the model catchment boundaries are exactly following the grid box margins (Figure 3.10). The outflow direction of each grid box is constant in time and has to be defined prior to the model simulation.

3.4.3 Modifications

The HD Model has originally been designed for global applications. However, the required input fields can also be provided by regional climate simulations. In this case, the RCM results are interpolated to the standard HD Model grid and the discharge simulation is carried out on a global scale, with "empty" input fields over areas outside the RCM domain. Even if the RCM resolution is higher, the simulation of river discharge is thus restricted to a horizontal resolution of $^1/_2{}^\circ$ and a daily time step.

In order to enable the discharge simulation on higher spatial and temporal scales using high resolution REMO results as input, the HD Model has been modified and reshaped in the course of the present study. The modifications mainly concern the model domain of HD simulations (global $\Rightarrow$ regional), the horizontal resolution (regular $^1/_2{}^\circ$ $\Rightarrow$ rotated $^1/_6{}^\circ$ REMO grid) and the model time step including the required temporal resolution of input fields (daily $\Rightarrow$ hourly). In detail, the following steps have been carried out:

- ▷ **Change of HD model domain**
  In it's original version, the HD Model computes the lateral discharge on a global $^1/_2{}^\circ$ grid. In a first step, this global coverage has been replaced by a regional domain, i.e., discharge simulations are no more carried out for the entire global land surface but only for a sub-domain. The respective location and the number of grid boxes in x and y direction can now be specified within the model code.

- ▷ **Change of horizontal resolution and grid system**
  The global $^1/_2{}^\circ$ resolution on a regular, non-rotated grid used by the original HD version has been replaced by a rotated RCM grid system with a default resolution of $^1/_6{}^\circ$ and a corresponding grid box size of about 18 x 18 km^2. The horizontal resolution of HD applications is thus approximately increased by a factor of 3. The grid boxes of the $^1/_6{}^\circ$ REMO simulations carried out within this study exactly match the new HD default grid. Consequently, the runoff components produced by the REMO land surface scheme can be directly fed into the HD Model, without interpolation of the RCM results prior to the lateral routing. It is furthermore assumed that the influence of the chosen grid box size on the retention constants k_o, k_r and k_g is included in the respective equations. In this respect, no scale adjustment has been carried out.

- ▷ **Change of time step**
  In order to account for the reduced grid box size (rotated $^1/_6{}^\circ$ instead of regular $^1/_2{}^\circ$), the possible minimum travel of water through a grid box has been adjusted by reducing the HD Model time step from 1 day in the original version (or 6 hours for riverflow) to

1 hour. Accordingly, the runoff input fields as derived from climate model simulations have to be provided in hourly resolution.

- **Change of model topography and flow directions**
  A major task during the modification of the HD Model has been the construction of a new discharge network, i.e., the definition of new river flow directions with the corresponding adjustment of the model topography. The flow directions and catchment boundaries originally derived for the regular $^1/_2^\circ$ grid could not simply be adopted since the new grid has a much finer resolution and is defined on a rotated system. Via a semi-automatic procedure, updated flow directions and model catchment boundaries have been derived for the new $^1/_6^\circ$ default resolution for a total of 9 European catchments, including the four main Alpine catchments Rhine, Danube, Rhone and Po.

4 The New Subgrid Glacier Parameterisation

4.1 Overview

A new glacier parameterisation scheme has been developed and implemented into the regional climate model REMO in order to account for the mass and energy balance of mountain glaciers and their influence on climate and hydrology. Over glaciated mountain ranges, the new scheme replaces the static glacier mask used so far. Only over the Greenland and Antarctic Ice Sheets the previous static mask is still used in case that they are part of the regional model domain. The new model system is referred to as $\text{REMO}_{\texttt{glacier}}$.

For various reasons the European Alps have been chosen as a test region (see Chapter 1.3). In this area, as well as in most other regions, the current RCM grid box resolution of about 10 to 50 km is beyond the scale of individual mountain glaciers (see Figure 4.1 for an example). Hence, the overall behaviour of glaciers contained within a grid box has to be described on a subgrid scale in terms of the atmospheric fields as resolved by the RCM (i.e., by the simulated mean grid box values of temperature, precipitation, radiation etc.). A detailed, spatially resolved simulation of a glacier's surface energy and mass balance, as it is done using high-resolution, distributed models for individual glaciers, and the subsequent consideration of ice flow dynamics is not possible. This is especially true when the large amount of data required by these models, for instance information on the specific topographical setting of a glacier or the bedrock topography, is considered. These datasets can hardly be provided for all existing glaciers contained within a typical regional climate model domain. Furthermore, an explicit treatment of each individual glacier would result in a considerable increase in computing time, which is still a limiting factor in regional and global climate simulations. None the less, to a certain extent it is still possible to account for the heterogeneity of processes within a climate model grid box by applying simple concepts such as a fractional surface coverage or the redistribution and scaling of atmospheric parameters within a grid cell.

Due to the restrictions mentioned above, the representation of mountain glaciers in $\text{REMO}_{\texttt{glacier}}$ is simplified to a high degree. A number of processes and characteristics which influence a glacier's mass and energy balance and hence its reaction to climatic changes and which have been outlined in Chapter 2 are not treated explicitly. Others are only described in a strongly simplified way. Nevertheless, it is assumed that the major processes and dependencies are accounted for in an appropriate manner regarding the objectives of this study. The present work has to be seen as an attempt to simulate the overall behaviour of glaciers contained in a climate model grid box by more or less simple concepts and to include their interaction with the prevailing climate and their influence on runoff conditions.

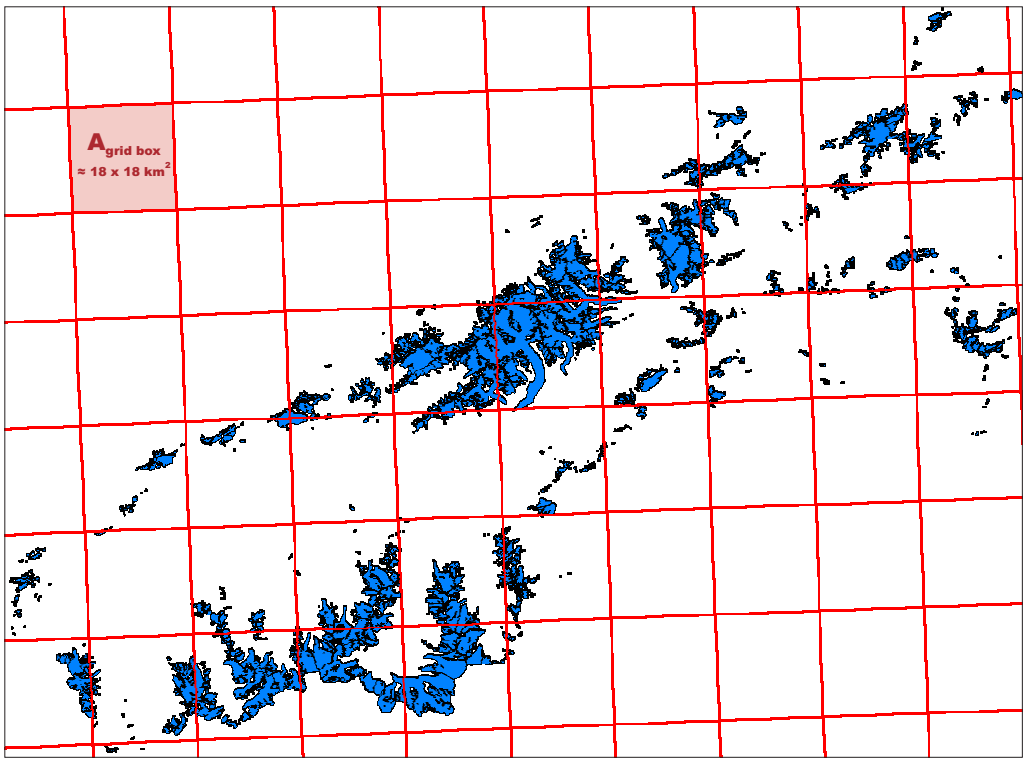

Figure 4.1: Glaciated areas in Switzerland (blue) derived from the Swiss glacier inventory 1973 (Müller et al., 1976) and REMO grid box boundaries (red) of the rotated $^1/_6^\circ$ grid used within this study. The figure has been prepared by F. Paul, University of Zurich.

4.2 Processes and Parameterisations

4.2.1 A Fourth Surface Fraction

The basic modification in $\text{REMO}_{\texttt{glacier}}$ with respect to the original REMO version consists in the extension of the tile approach as presented in Chapter 3.3.2. In order to account for mountain glaciers on a subgrid scale, covering a certain fraction of a climate model grid box, a fourth surface fraction "glacier ice" has been introduced (Figure 4.2). The new fraction represents the total area covered by glaciers in the respective grid box. It's extent is allowed to grow or to shrink depending on accumulation and ablation conditions but is restricted to the total land surface area of a grid box. Glacier ice is not allowed to expand over water surfaces. The characteristics and the behaviour of the glaciated fraction (e.g., areal extent, albedo and surface temperature) are controlled by the new glacier parameterisation which has been implemented in REMO's land surface scheme. As before, the turbulent surface fluxes are calculated separately for each surface fraction contained in a grid box and are subsequently averaged within the lowest atmospheric level (see Chapter 3.3.2).

4.2.2 The Single-Cuboid Concept

A major simplification in the new parameterisation scheme concerns the treatment of the glacier population in a specific grid box. In $\text{REMO}_{\texttt{glacier}}$ all individual glaciers located within a climate

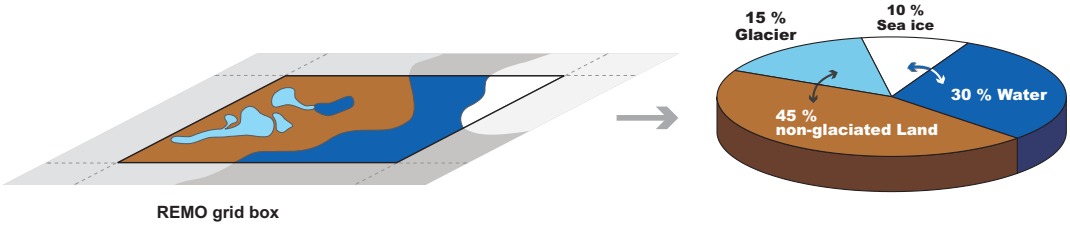

Figure 4.2: The extended tile approach. Example for a grid box covered by non-glaciated land (45 %), glacier ice (15 %), water (30 %) and sea ice (10 %); compare to Figure 3.2.

model grid box are represented by one single ice body in form of a cuboid with a well-defined surface area A and a thickness h (Figure 4.3). The corresponding volume V equals the sum of the estimated volumes of all individual glaciers contained within the respective grid box. Similarly, the surface area A of the cuboid is the sum of all individual glacier areas and determines the glacier-covered fraction of the total grid box area (see Figure 4.2). Initially, the ice thickness h can thus be considered as a residual parameter which is determined by the total volume V and the total area A originally derived from information on individual glaciers. Only for the purpose of area adjustment, the ice cuboid is temporarily split up into single glaciers again (see Chapter 4.2.8). The idea to group individual glaciers in "pools", defined by the extent of a climate model grid box, is supported by the observation that nearby glaciers often show a similar response to a given climatic forcing in terms of their mass balance evolution (Chapter 2.3.2). In REMO$_{\texttt{glacier}}$, the glacier cuboids of adjacent grid boxes are independent of each other and do not interact directly. Each grid box contains its "own" sample of glaciers (represented by a single cuboid), and direct mass transfer and, hence, large scale ice flow across grid box boundaries are neglected. Considering the fact that the size of mountain glaciers is usually much smaller than a typical REMO grid box this simplification seems to be justifiable. Furthermore, the independence of processes in the horizontal direction is important for an effective parallelisation of the physical subroutines in REMO$_{\texttt{glacier}}$ and a high performance on vector architectures.

The altitude of the glacier cuboid surface is assumed to be identical to the mean grid box altitude (in this point, Figure 4.3 might be misleading). For each grid box it is fixed throughout the entire model simulation. The effect of a possible surface elevation - mass balance feedback (Chapter 2.7.2) is therefore not taken into account. A constant ice density of $\rho_{ice} = 880$ kg/m^3, the mean value for glacier ice according to Table 2.1, is assumed for the entire cuboid. In terms of the surface heat budget, glacier ice is taken into account starting from a critical ice depth of 0.1 m w.e.. Up to a total depth of 0.6 m (real ice depth, not water equivalent), only one single ice layer is considered. As soon as this value is surpassed, the cuboid is split into an upper layer of a thickness of 0.2 m ice, representing the interface to the atmosphere or the overlying snow cover respectively, and a lower layer, representing the remaining ice volume.

4.2.3 Snow Cover and Surface Energy Balance

As for all other surface fractions within a climate model grid box, the full surface energy balance of the glaciated fraction is calculated in each time step, according to Equations 2.4 and 2.5. The

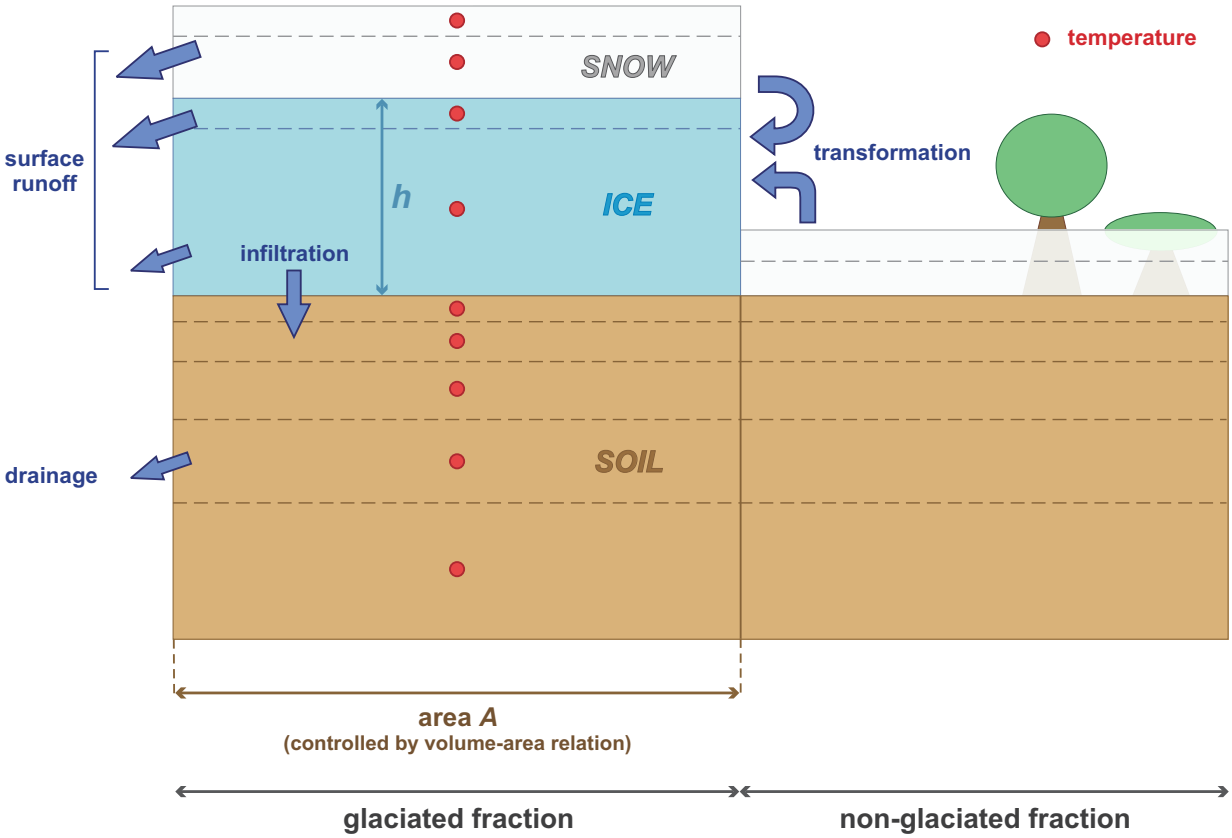

Figure 4.3: 2-D profile through the land fraction of a partly glaciated grid box in $\text{REMO}_{\texttt{glacier}}$.

calculation of the different flux terms basically follows the parameterisations already applied in the standard REMO version (DKRZ, 1994; Roeckner et al., 1996). However, in order to account for the special surface characteristics of glacier ice, a number of modifications concerning for instance surface albedo and surface roughness length have been implemented. The corresponding atmospheric forcing is directly provided by the climate model's atmospheric component.

A basic surface characteristic with a strong influence especially on net surface radiation is the presence or absence of snow (see Chapter 2.4.2). Similarly to the non-glaciated land fraction, the glaciated part of a grid box in $\text{REMO}_{\texttt{glacier}}$ can be covered by a snow layer (Figure 4.3). In both cases, snow is treated in the same way as in the standard REMO version (see Chapter 3.3.5) except for the calculation of snow albedo on the glaciated part (see below). The snow cover characteristics of the glaciated and the non-glaciated fraction are calculated separately without a direct interaction. It is thus possible that the glaciated grid box fraction is covered by a snow layer while the non-glaciated fraction is snow-free (due to differences in snow ablation or accumulation, see below).

Snow on the glaciated fraction directly covers the underlying ice cuboid, the presence of a firn layer in between is neglected. Hence, once the snow has completely melted, the upper ice layer immediately becomes exposed. It is further assumed that the snow cover thickness is constant over the whole glacier surface and that the glacier cuboid is either completely covered by snow or completely snow-free. This is a strong simplification regarding the elevation range of real glaciers and the corresponding variability of snow depth with glacier tongues usually becoming exposed during the summer while snow is still present in the accumulation area (Chapter 2.3.2). A further simplification concerns the influence of

supraglacial debris cover on the surface energy balance. Due to a general lack of data on the scale of whole mountain ranges and the diverse influence on a glacier's energy balance depending for instance on the debris cover thickness (see Chapter 2.4.3), supraglacial debris is not explicitly accounted for in $\text{REMO}_{\texttt{glacier}}$.

In case that a snow cover is present on the glaciated fraction and it's depth is larger than 0.01 m w.e., the residual of the surface energy fluxes is used to warm or to cool an upper snow layer with a maximum thickness of 0.1 m. Similarly, if no snow overlays the glacier cuboid and the ice is exposed, the surface energy budget directly changes the heat content and thereby the temperature of the upper ice layer. In either case, the sensible heat flux supplied by rain Q_R is assumed to be zero. If the temperature of the upper snow or ice layer has been raised to the melting point of 0°C any excess energy input is used for melting. Altogether, the surface energy balance of the glacier surface, for the snow-free as well as for the snow-covered case, is thus determined by a modified version of Equation 2.4:

$$Q_N + Q_H + Q_L + Q_G + Q_M = dQ_{snow/ice} \tag{4.1}$$

with

Q_N : net radiation [W/m^2]

Q_H : turbulent flux of sensible heat [W/m^2]

Q_L : turbulent flux of latent heat [W/m^2]

Q_G : ground heat flux [W/m^2]

Q_M : energy consumed by melt of snow or ice [W/m^2]

$dQ_{snow/ice}$: change of the heat content of the upper snow or ice layer [W/m^2]

Here, Q_M and $dQ_{snow/ice}$ can be considered as the residual of the surface energy budget determined by the terms Q_N, Q_H and Q_L. A short description of the calculation of these energy fluxes will be given in the following.

Net Radiation (Q_N)

The radiation budget at the glacier surface is calculated according to Equation 2.5. The longwave components L_{in} and L_{out} are directly computed by the atmospheric radiation scheme and from surface temperature conditions assuming a longwave emissivity of snow and ice surfaces of $\epsilon = 0.996$. Longwave radiation emitted from surrounding slopes is not accounted for. The incoming shortwave radiation flux G as provided by the radiation scheme is modified in order to account for subgrid shading effects (see Chapter 4.2.6).

With shortwave radiation being the primary source of energy on many glaciers, an important control on the total surface energy budget is exerted by the surface albedo α. As outlined in Chapter 2.4.2, the albedo of snow and ice surfaces depends in a complex way on factors such as grain size, liquid water content and the presence of impurities. Generally, a fundamental difference exists between the relatively high albedo of snow surfaces and the lower albedo of ice (Table 2.2). In order to account for this fact and to include a possible snow and ice albedo feedback (Chapter 2.7.2), the surface albedo of

the glaciated grid box fraction in REMO$_{\texttt{glacier}}$ depends on the presence of snow on top of the glacier cuboid. If a snow cover exists, the snow albedo (integrated over the solar spectrum) is computed as a simple function of the snow surface temperature T_S [°C] (see Figure 4.4):

$$\alpha_{snow} = \begin{cases} 0.8 & \text{if } T_S \leq \text{-10°C} \\ 0.6 + 0.02 \cdot (-T_S) & \text{if -10°C} < T_S < \text{0°C} \\ 0.6 & \text{if } T_S = \text{0°C} \end{cases} \tag{4.2}$$

This parameterisation basically corresponds to the calculation of the snow albedo on the non-glaciated land fraction (Chapter 3.3.5) with fixed values of $\alpha_{snow,min} = 0.6$ and $\alpha_{snow,max} = 0.8$. The same method has so far also been used to calculate the surface albedo of grid boxes marked as "glaciated" by the static glacier mask. It accounts for the fact that a melting snow layer has a comparatively high temperature and a low albedo due to the presence of meltwater pockets (Chapter 2.4.2). An aging effect, i.e., the decrease of snow albedo with snow age, is not considered. The final albedo α_{surf} of a snow-covered glacier surface is subsequently calculated as a function of the snow depth SNG [m w.e.], the albedo α_{ice} of the underlying ice layer and the critical snow depth $SN^* = 0.01$ m w.e.:

$$\alpha_{surf} = \alpha_{ice} + (\alpha_{snow} - \alpha_{ice}) \cdot \frac{SNG}{SNG + SN^*} \tag{4.3}$$

With respect to Equation 4.3, the background albedo of a vegetation-covered land surface α_b is thus replaced by the albedo of glacier ice α_{ice}.

In case that a snow cover does not exist, the ice albedo α_{ice} equals the surface albedo α_{surf} of the glaciated fraction. Two different methods have been implemented in REMO$_{\texttt{glacier}}$ for the calculation of α_{ice} (see also Figure 4.4) :

- **Method A** (default, used in all simulations if not stated otherwise)
  In the standard setup a constant ice albedo of $\alpha_{ice} = 0.4$, the mean value for clean ice according to Table 2.2, is prescribed. Any influence of ice temperature, the presence of surface meltwater, dust and debris or ageing is neglected. A value of 0.4 has to be considered as an upper limit of the surface albedo of real mountain glaciers, but yields reasonable results in the present work as well as in other studies. It has for instance successfully been applied by Escher-Vetter (2000) for modelling the surface energy balance of Vernagtferner in the Oetztal Alps, Austria.

- **Method B**
  In order to account for the presence of liquid water at the surface of a glacier with its lowering effect on albedo, a second parameterisation has been implemented following the method already used for the calculation of the albedo of snow (see above). Here, α_{ice} is assumed to linearly decrease with a rising temperature $T_{ice,up}$ [°C] of the upper ice layer from a maximum value $\alpha_{ice,max} = 0.4$ for temperatures lower than -10°C to a minimum of $\alpha_{ice,min} = 0.3$ at 0°C :

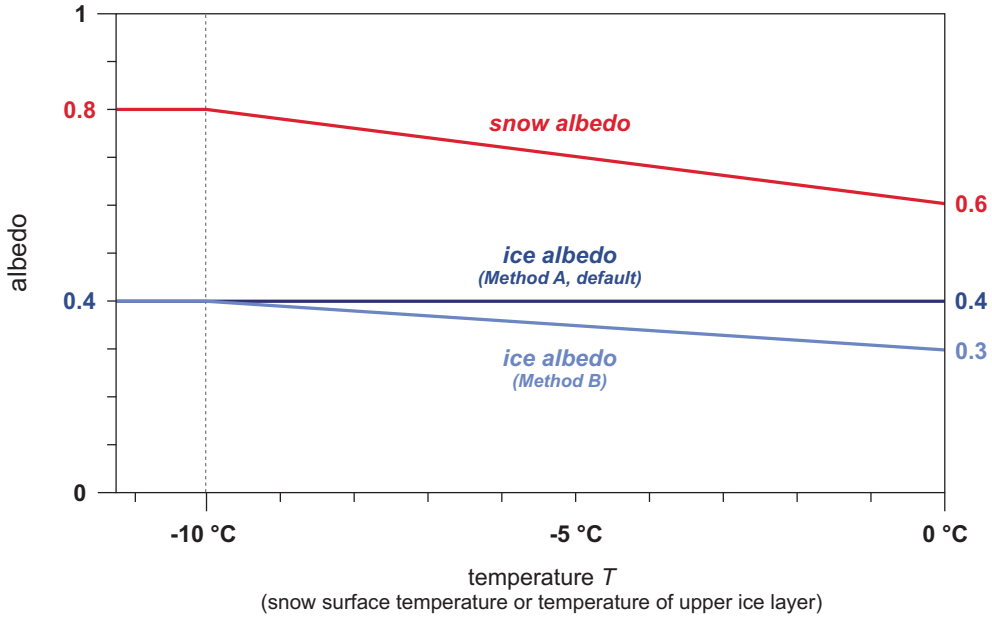

Figure 4.4: Calculation of snow albedo and ice albedo (methods A and B) in REMO$_{\texttt{glacier}}$ as a function of snow / ice temperature T.

$$\alpha_{ice} = \begin{cases} 0.4 & \text{if} \quad T_{ice,up} \leq \text{-10°C} \\ 0.3 + 0.01 \cdot \ (-T_{ice,up}) & \text{if} \quad \text{-10°C} < T_{ice,up} < \text{0°C} \\ 0.3 & \text{if} \quad T_{ice,up} = \text{0°C} \end{cases} \tag{4.4}$$

Thus, the albedo-reducing effect of surface meltwater is accounted for by fixing the surface albedo to its minimum value of 0.3 during the melt of an exposed ice surface ($T_{ice,up} = 0$°C).

Turbulent Fluxes (Q_H and Q_L)

The calculation of the turbulent fluxes of sensible and latent heat at the glacier's surface basically follows the parameterisations already used in the standard REMO version (DKRZ, 1994; Roeckner et al., 1996, see also Chapter 3.3.2). The turbulent flux Q_χ of a variable χ (here: temperature or humidity) depends on the near surface vertical gradient of the respective quantity, the horizontal wind speed $|V_L|$ and a transfer coefficient C_χ. It is calculated in each time step according to the bulk transfer relation

$$Q_\chi \ = -C_\chi \ \cdot \ |V_L| \ \cdot \ (\chi_L - \chi_S) \tag{4.5}$$

The subscripts L and S refer to the values at the lowest model level and at the surface, respectively. With regard to the turbulent flux of latent heat, the saturation specific humidity q_S (depending on the surface temperature T_S and the surface pressure p_S) is generally assumed over the glacier surface, whether it is covered by snow or not. The transfer coefficient C_χ is derived from Monin-Obukhov similarity theory (despite the fact that the usefulness of this method is limited under extremely stable

conditions, which often prevail over a melting glacier surface; Paterson, 1994; Weber, 2005). The roughness length of glacier ice $z_{0,ice}$, used for calculation of C_χ, is the analogue to the vegetation roughness length on the non-glaciated land fraction. For calculation of the turbulent heat fluxes it is set to a constant value of 0.001 m, regardless of the presence of a snow layer on top of the ice. In REMO the same value is used for the sea ice fraction per default. It approximately corresponds to the roughness length commonly applied for a flat, snow-covered surface but underestimates the value for a melting ice surface in the ablation zone (0.001 to 0.007 m; e.g., Oke, 1978; Kuhn, 1979; Paterson, 1994; Arya, 2001). The spatial variability of the aerodynamic roughness length over a glacier's surface, especially with respect to snow-covered and snow-free areas (e.g., Arnold, 2005), is so far not considered in REMO$_{\texttt{glacier}}$.

Ground Heat Flux (Q_G)

The ground heat flux Q_G (i.e., the transfer of energy by heat conduction between the centres of the respective snow, ice and soil layers) is computed applying the same heat conduction equation as used in REMO's soil scheme (see Chapter 3.3.4 and DKRZ, 1994). For the ice layers, a constant heat capacity c_{ice} = 2093 J kg^{-1}K^{-1} and a thermal conductivity λ_{ice} = 2.3 W m^{-1}K^{-1} are assumed, following already existing parameterisations in REMO (e.g., for grid boxes with permanent ice cover and for frozen soil water) and the ranges given by Paterson (1994). The influence of ice temperature, water content and impurities on both parameters is neglected. Heat diffusion in the soil is calculated separately for the glaciated and the non-glaciated land fraction, i.e., the total soil volume of a grid box is split up into two parts (glaciated and non-glaciated) which do not interact directly in terms of their heat budget.

4.2.4 Surface Mass Balance

Similarly to the surface energy fluxes, mass balance processes are assumed to occur uniformly over the entire glacier surface in REMO$_{\texttt{glacier}}$. A partitioning of the cuboid surface into sub-areas experiencing different accumulation and/or ablation conditions is not carried out. Again, this is a strong simplification with regard to the spatial variability of mass balance on real glaciers (see Chapter 2.3.2, especially Figure 2.5). In a defined balance period, the entire glacier cuboid surface experiences either net accumulation or net ablation (or, in an unlikely case, a zero net balance). The modelled glacier mass balance is thus assumed to represent the mean specific mass balance $\overline{b}_n$ in Equation 2.2, averaged over all individual glaciers contained in the respective climate model grid box.

Accumulation

REMO generally discriminates between liquid and solid precipitation, i.e., between rainfall and snowfall at the surface with both quantities representing grid box averages. In order to account for subgrid scale variability of snow accumulation, the total amount of snowfall in a time step is redistributed between the glaciated and the non-glaciated land fraction in an REMO$_{\texttt{glacier}}$ grid box. The amount of snow which is assumed to fall onto the glaciated fraction directly increases the snow depth and thereby adds mass to the system glacier cuboid + snow cover. A further accumulation process is rime

formation which is directly added to the upper ice layer. The refreezing of rain on the glacier surface is not accounted for.

As described in Chapter 2.2, snow is gradually transformed into ice during the snow metamorphism process. In $\text{REMO}_{\texttt{glacier}}$ both snow and ice are represented by the respective layers, as illustrated in Figure 4.3. The intermediate stage of firn (i.e., of snow that has survived an ablation period) is not accounted for. The complexity of processes involved in snow metamorphism, like cycles of melting and freezing in different depths, cannot be explicitly represented by the concept of a single ice cuboid overlaid by a two-layer snow pack. Therefore, the transformation of snow on both land fractions into ice is parameterised in a rather simple way using a snow age threshold. For this purpose, two additional variables have been introduced in REMO, both for the glaciated (...G) and the non-glaciated (...L) land fraction (see also Chapter 4.3):

- the age of the snow layer (SNAGEG, SNAGEL), i.e., the time [days] that has passed since the last snow-free state and
- the mean snow depth [m w.e.] over this period (SNMDG, SNMDL).

If the snow layer on any of the two fractions has reached a critical snow age threshold of $ZACRIT$ = 730 days (2 years), it is assumed that parts of the snow volume on this fraction have passed the metamorphism process from snow to ice. This part of the total snow volume is defined as a fraction $ZFTRANS$ = 0.5 of the mean snow depth (SNMDG or SNMDL, respectively). It is transformed from snow into ice (i.e., substracted from the snow layer and added to the ice cuboid) if, as an additional condition, the total snow depth would not decrease to a value lower than the critical snow depth SN_{cri} = 0.01 m w.e. by substraction of the transformed quantity. The latter is necessary in order to avoid the total disappearance of snow from one time step to another by the transformation process.

In case that a transformation has been carried out, the snow age and the mean snow depth are reset to zero and the next transformation on the respective fraction will, at the earliest, be possible after 730 days. This critical snow age has been chosen as a compromise between the time it takes for snow to be transformed into firn (about one year) and the total time necessary for the transformation of snow into ice in temperate regions (five to ten years at minimum, see Chapter 2.2). It is a model parameter which can be adjusted (increased) if regional particularities have to be considered, e.g., for simulations in polar climates where the transformation process takes much longer. The same is true for the parameter $ZFTRANS$ (currently set to 0.5).

Ablation

Snow and ice ablation is calculated in a straightforward way. Generally, the temperature of the snow and ice layers are not allowed to exceed the melting point of T_{melt} =0°C. If this threshold is surpassed as a result of a positive surface energy balance or of heat diffusion the temperature is adjusted back to 0°C. The released energy is used for melt in the respective layer or, in case that not enough snow/ice is available and the whole layer has already disappeared, for warming the layer underneath. If the glacier cuboid is covered by snow which is not treated explicitly in terms of temperature (snow depth $<$ 0.01 m w.e.), snow melt is possible if the temperature $T_{ice,up}$ of the underlying ice layer exceeds

0°C. In this case, 50% of the energy released by cooling $T_{ice,up}$ back to 0°C is used for snow melt, the other half for melt in the upper ice layer. Ablation is furthermore possible by sublimation at the surface ($Q_L < 0$ in Equation 4.1). Internal accumulation (i.e., the refreezing of meltwater within the snow or ice) is neglected as it does not change the total snow and ice mass and its accelerating effect on the elimination of a winter's cold wave in the glacier (see Chapter 2.3.1) could hardly be resolved using a two-layer scheme. Furthermore, calving processes and the removal of snow by wind are not accounted for.

4.2.5 Runoff Generation and Soil Hydrology

The new parameterisation scheme explicitly accounts for the contribution of glacial meltwater to the total amount of grid box runoff which serves, at a later stage, as input for the HD Model. Melt water originating from a snow layer on top of the ice cuboid and from the upper ice layer is assumed to directly contribute to grid box surface runoff in the respective time step (see Figure 4.3). The same is true for liquid precipitation falling onto the glaciated fraction. If melt occurs in the lower ice layer, the respective amount of water is divided into surface runoff and infiltration according to the Arno-Scheme and dependent on the soil moisture content (see Chapter 3.3.4). Concerning soil hydrology and the formation of subsurface drainage, the glaciated and the non-glaciated land fraction of a grid box share a "common" soil bucket, which is treated in the same way as in the standard REMO version (see Chapter 3.3.4). The input at the soil surface is provided by the infiltrating amount of water from both fractions.

As snow and ice melt directly contribute to surface runoff and drainage in the respective time step, the short-term storage function of the englacial and subglacial drainage system as well as a temporary storage of melt water within a firn aquifer (Chapter 2.8.1) are not directly considered in REMO$_{\texttt{glacier}}$. At a later stage, the inclusion of an additional reservoir (or several reservoirs) representing glacier specific storage processes and being fed by snow and ice melt is still possible. In contrast, the long-term and intermediate-term storage of water in form of snow and ice, as outlined in Chapter 2.8.1, are explicitly represented.

4.2.6 Subgrid Radiation

Radiation, the main source and sink of energy at the earth's surface, is significantly influenced by topographical features (e.g., Müller and Scherer, 2005). In mountainous terrain, the variability of topography and of radiative properties of the surface often generate complex patterns of surface radiation budgets (Oliphant et al., 2003). Especially solar radiation has to be treated with care in glacier mass balance models since it is, in most cases, the main source of energy with a dominant influence on ablation (see Chapter 2.4). Modelling the mass balance of Morteratschgletscher, Switzerland, Klok and Oerlemans (2002) found that mean shortwave radiation on the glacier surface would be 37% larger if the effects of topography were discounted, leading to a decrease of 0.34 m w.e. in the mean specific mass balance. Against this background, the authors conclude that topographic effects on shortwave radiation should in principle be taken into account in glacier mass balance modelling.

For a given surface, the incoming flux of shortwave radiation consists of three different components:

direct irradiance from the sun, radiation reflected from nearby terrain and diffuse irradiance from the sky (Ranzi and Rosso, 1995). The amount of direct radiation received by an inclined surface strongly depends on its slope and aspect and also on shadowing effects caused by the surrounding topography. A point on the surface will be shaded if the angle of the surface away from the sun exceeds the solar elevation (self-shadowing). Points that do not fulfil this criterion will still be shaded if the sun lies below the local horizon as defined by the surrounding terrain (Essery, 2004). Also the diffuse sky radiation varies with the orientation of the surface and may be reduced due to the hemispherical sky dome being partially obstructed by the surrounding terrain and the tilt of the surface itself (Wang et al., 2000).

In standard REMO, topographic effects on the incoming radiation flux are not accounted for, neither on the resolved grid scale nor on a subgrid level. The grid box surface is treated as a horizontal, non-shaded plane which is located at the mean grid box altitude and which receives both direct and diffuse radiation from the hemispherical sky dome. Even if the mean radiation fluxes as computed by this method and averaged over a whole grid box surface area would be realistic, they can still be expected to strongly vary on a subgrid scale. This is especially true for the difference in incoming direct solar radiation between exposed, non-shaded surfaces and low-lying valley floors, where the sky view can be restricted to a high degree. As the tongues of mountain glaciers are often located in topographic depressions (see Figure 4.5), the latter also applies to the ablation area of many glaciers in the study area, with the corresponding effects on their total surface energy budget. An example for the shading of a glacier tongue is shown in Figure 4.6 for the case of Morteratschgletscher, Switzerland.

In order to account for the spatial variability of solar radiation within an RCM grid box and its effect on glacier surface energy balance, the radiation model SRAD (Moore et al., 1993; Wilson and Gallant, 2000) has been used in the present study. SRAD is an approximate method for estimating the spatial distribution of radiation fluxes in complex terrain based on a gridded digital elevation model (DEM). The model has recently been applied in a number of glacier mass balance and permafrost studies (e.g., Machguth et al., 2006; Paul et al., 2005; Gruber and Hoelzle, 2001). Among other quantities, SRAD computes the potential solar radiation G_{pot} (in the present case the sum of direct and diffuse shortwave radiation for clear-sky, i.e., cloud-free conditions) for each DEM grid cell as a function of latitude, slope, aspect, topographic shading and time of year. Internally, the model distinguishes between direct-beam and diffuse fluxes. For each DEM grid cell both components are computed in 12-min intervals from sunset to sunrise and are subsequently summed up to daily totals of potential solar radiation.

Applying the SRAD radiation scheme on a resampled 100 x 100 m^2 cell size DEM (derived from the 25 x 25 m^2 DEM of SWISSTOPO, 2001) in combination with the digitised glacier outlines of the Swiss glacier inventory of 1973 (Müller et al., 1976), two radiation fluxes have been computed for each month of the year and for each REMO grid box in the Swiss part of the model domain (see also Figure 4.7):

A The mean potential solar radiation [W/m^2] over all **glaciated** 100 x 100 m^2 DEM boxes contained in a REMO grid box (including the effects of terrain shading, slope and aspect).

B The potential solar radiation [W/m^2] on a 2 x 2 km^2 horizontal, non-shaded

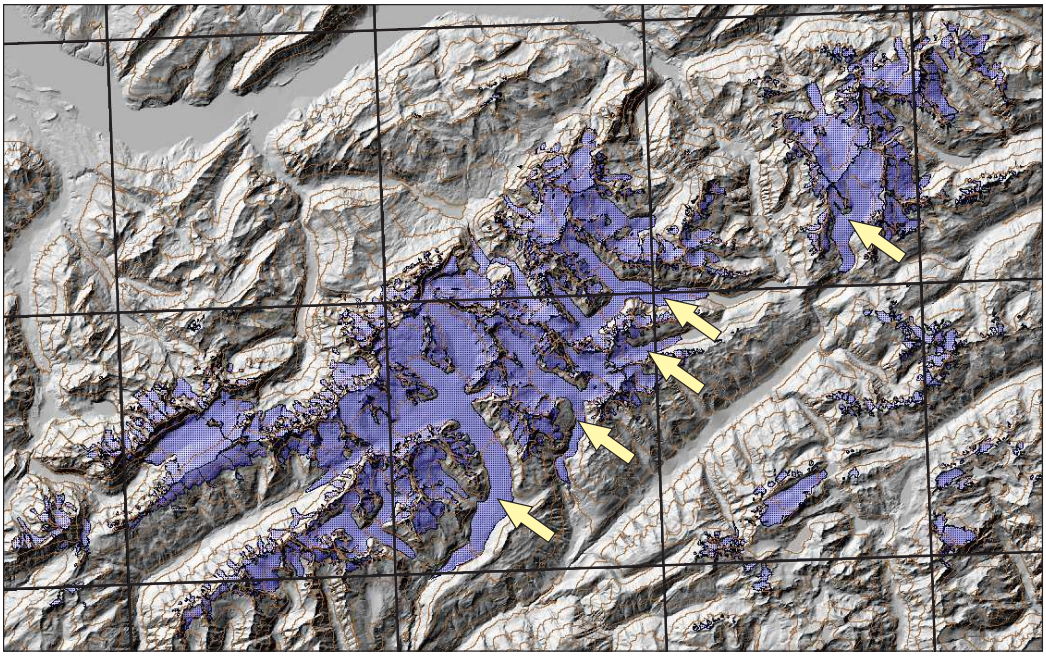

Figure 4.5: Shaded relief of the Aletsch / Grimsel Region, Switzerland, based on a 25 m DEM (SWISSTOPO, 2001). The relief is overlaid by the glacier outlines of the Swiss glacier inventory of 1973 (Müller et al., 1976, blue shaded), the $^1/_6^\circ$ REMO grid box delineations (black) and terrain isohypses (brown). A number of glacier tongues which are located in topographic depressions and which are subject to considerable shading are marked by yellow arrows. The figure has been prepared by F. Paul, University of Zurich.

Figure 4.6: The tongue of Morteratschgletscher, Switzerland, shaded by surrounding terrain. The photo was taken in August 2005 at 7.30 a.m. (S. Kotlarski).

surface located in the center of a REMO grid box and at the REMO grid box altitude.

Flux **B** can be considered to represent the incoming shortwave radiation flux (clear-sky) at the surface of a REMO grid box, if REMO's radiative transfer scheme would be identical to the one used in SRAD and the same atmospheric transmission properties were assumed.

In a second step, the monthly varying *SRAD ratio*

$$r_{G,i} = \frac{\mathbf{A}}{\mathbf{B}} \qquad , i = 1, 2, .., 12 \tag{4.6}$$

has been computed for each REMO grid box in the Swiss part of the model domain. A ratio $r_{G,i}$ larger than 1 denotes a mean shortwave radiation flux on the glaciated area of a grid box which is larger than the flux onto a non-shaded horizontal surface at mean grid box altitude in the respective month i. Vice versa, a value lower than 1 indicates a smaller shortwave radiation flux on glaciated surfaces. The annual variation of $r_{G,i}$ is shown in Figure 4.8 for each investigated grid box. In most cases the ratio is lower than 1 throughout the entire year, which means that the glaciated parts within the grid cells receive less solar radiation than a horizontal plane. The annual cycle usually exhibits a sinusoidal structure with a maximum in the summer months and a minimum in wintertime, when the solar zenith angle is largest (sun closest to the horizon) and shading effects are most pronounced. In a number of grid boxes a second maximum occurs in December/January with values larger than 1 in two cases. These boxes are only slightly glaciated with glaciers located at very high altitudes compared to the grid box mean elevation and shading and slope effects are not pronounced. The positive effect of a higher altitude on G_{pot} and thus on flux **A** (due to a thinner atmospheric column that has to be traversed by radiation) compensates the reduction of G_{pot} due to shading and slope effects. Especially in wintertime, when the atmosphere has a higher density and a lower transmissivity, this effect can lead to a ratio $r_{G,i}$ larger than 1.

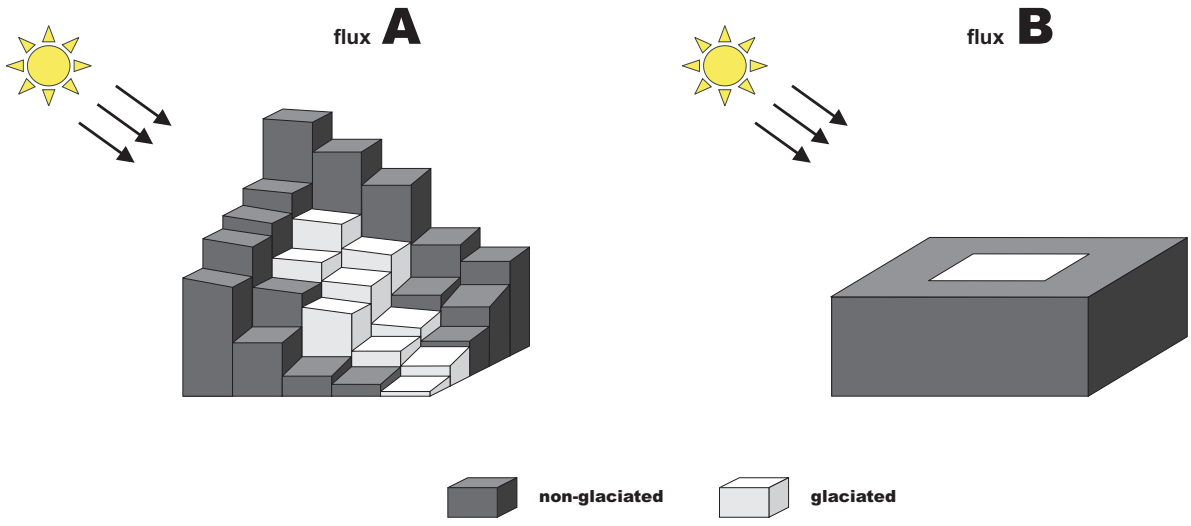

Figure 4.7: Overview on the calculation of the potential solar radiation fluxes **A** (mean over all glaciated DEM boxes, including topographic effects) and **B** (horizontal, non-shaded surface) using the SRAD model.

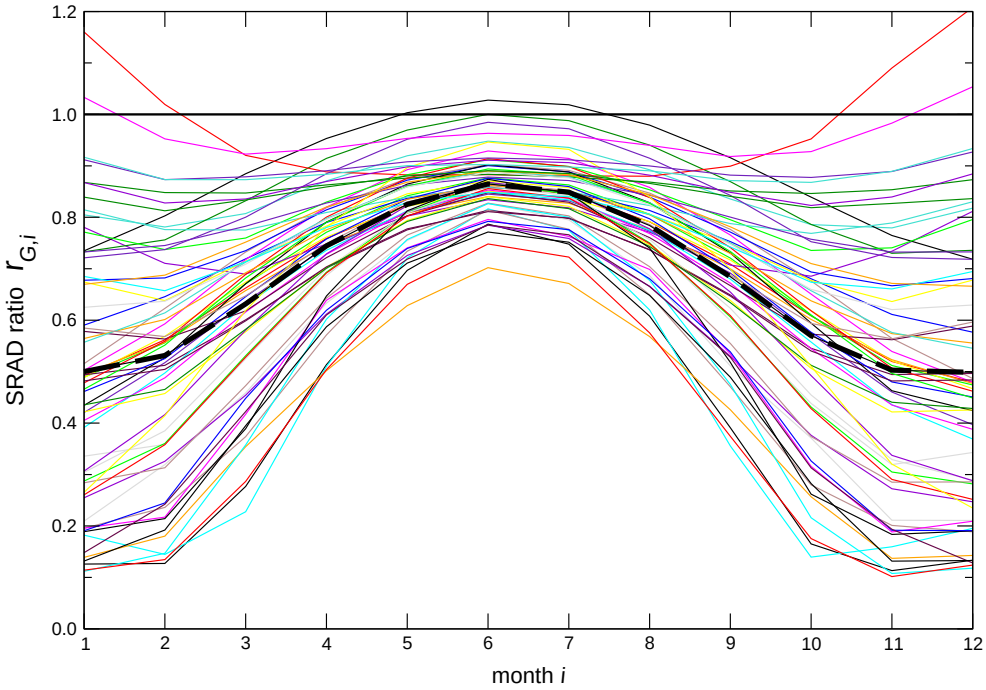

Figure 4.8: Annual cycles of the SRAD ratio $r_{G,i}$. Each line represents one glaciated REMO box in Switzerland. The dashed black line corresponds to the arithmetic mean of all individual grid boxes under investigation. The data has been compiled by F. Paul, University of Zurich.

Assuming that

a) $r_{G,i}$ is valid both for clear-sky conditions and for overcast skies and

b) $r_{G,i}$ is valid for the entire simulated period

the ratio can be used to scale the incoming solar radiation on glaciated surfaces in REMO$_{\texttt{glacier}}$. Especially the first assumption is a strong simplification since the presence of clouds will increase the proportion of diffuse radiation and will lead to less pronounced shading effects. Also assumption b) might be critical as, for example, an advancing and thickening glacier may gradually become subject to different shading conditions (Oerlemans and Hoogendoorn, 1989). Nonetheless, in a first approach, both effects are neglected in REMO$_{\texttt{glacier}}$ and the incoming solar radiation on the glaciated surface fraction $G_{glaciated}$ [W/m^2] at any point in time t is scaled using the ratio $r_{G,t}$ for the respective grid box:

$$G_{glaciated} = G \cdot r_{G,t} \tag{4.7}$$

with the global radiation G on a horizontal, non-shaded surface at mean grid box altitude, i.e., the standard incoming shortwave radiation flux as used in REMO. For a specific grid box, $r_{G,t}$ is derived by linear interpolation between the respective values $r_{G,i}$ of the previous and the following mid-month. For grid boxes outside Switzerland, the SRAD ratio could not be computed because digitised glacier outlines were not available. In these boxes, the non-weighted, mean annual cycle $\overline{r}_{G,i}$ as derived from all grid boxes for which both flux **A** and flux **B** could be computed is prescribed (dashed black line in Figure 4.8). Clear relationships between the shape of the annual cycle of $r_{G,i}$ and physical grid box characteristics (e.g., variance of orography and mean grid box altitude), which would allow a regionalisation of the SRAD ratios without explicit flux computation, could not be established (not

shown).

In order to account for energy conservation and to ensure the validity of G as mean grid box global radiation, the incoming shortwave radiation flux on the non-glaciated surface fraction $G_{non-glaciated}$ is adjusted accordingly (i.e., increased if $r_{G,t} < 1$ and decreased if $r_{G,t} > 1$). In principle, this "redistribution" of the incoming solar radiation flux on a subgrid level leads to a differential heating of the two surface fractions (glaciated and non-glaciated) with corresponding influences, for instance, on the surface energy balance and the turbulent surface fluxes.

4.2.7 Subgrid Snow Accumulation

Similarly to shortwave radiation, the accumulation of snow cannot be expected to occur uniformly within an RCM grid box. Even on the scale of single glaciers, snow accumulation can vary considerably in space, especially with elevation, which is one reason for the general increase of glacier mass balance with altitude (Chapters 2.3.2 and 2.3.3). The spatial variability of snow accumulation is mainly controlled by two factors:

1 **The spatial variability of the amount and the phase of precipitation**
Precipitation is an atmospheric quantity which is subject to strong variations in space. This is especially true in mountainous terrain where regional and local-scale topographic features exert a strong influence on the distribution of precipitation by various orographically-controlled precipitation mechanisms (e.g., Häckel, 1999). Often, a general increase of precipitation with altitude can be observed. The reason, in principle, is a decreasing temperature and increasing condensation with altitude on windward slopes (Sevruk, 1997). In the European Alps, the relationship between precipitation and altitude itself shows a high spatial variability, non-linearities and a general dependence on the spatial scale under consideration (Frei and Schär, 1998). In addition to variations in the total amount of (liquid plus solid) precipitation, also spatial variations in its phase are possible: While precipitation often falls as rain in the relatively warm valleys, high-elevation sites can receive snowfall at the same time. The total amount and the phase of precipitation, provided as a grid box average by the RCM, can therefore be expected to considerably vary in space on a subgrid scale. Both effects subsequently lead to differences in the direct accumulation of snow. Generally, glaciers tend to form in the wettest parts of terrain with a pronounced topography (Oerlemans and Fortuin, 1992). Braithwaite et al. (2002) state that the relatively high amount of precipitation should be taken into account in any effort to include glaciers in high-resolution climate models.

In the course of the present study, the subgrid variability of precipitation within REMO grid boxes has been assessed by overlaying a high-resolution, 2 x 2 km^2 precipitation dataset for the Alpine region (Schwarb, 2000; Schwarb et al., 2001, provided through a cooperation with the Department of Geography, University of Zurich) with REMO grid box delineations. By additionally including glacier outlines of the Swiss glacier inventory of 1973 (Müller et al., 1976), the difference between precipitation on glaciated and non-glaciated fractions within a grid box could be assessed for the Swiss part of the Alps. The first visual impression in terms of the annual sum of precipitation (Figure 4.9) is that

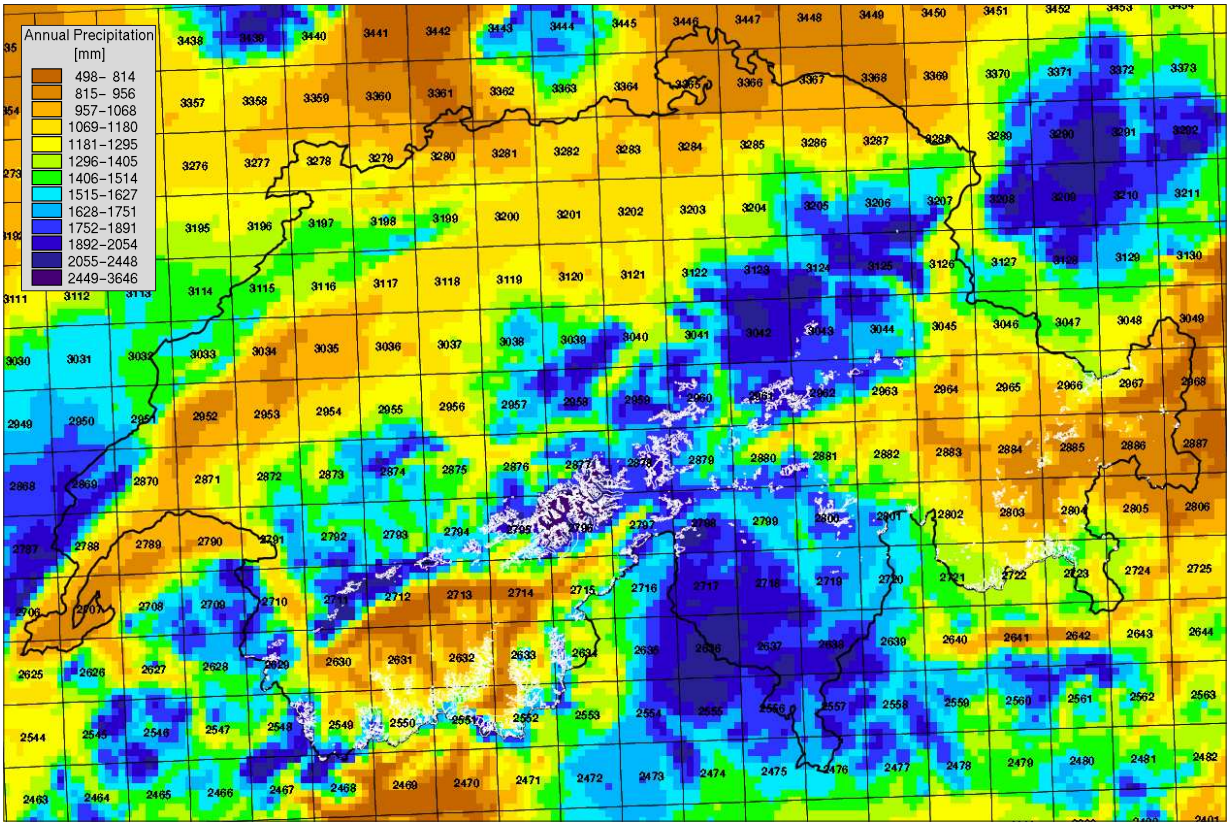

Figure 4.9: Mean annual precipitation [mm/year] for the period 1971-1990 from a high-resolution 2 x 2 km^2 dataset derived from observations (Schwarb, 2000; Schwarb et al., 2001). The grid cells of the precipitation dataset are overlaid by the $^1/_6^\circ$ REMO grid box delineations (black, including grid box number), the Swiss borderline (black) and the glacier outlines of the Swiss glacier inventory of 1973 (Müller et al., 1976, white). The precipitation dataset is not corrected with respect to the systematic bias of rain-gauge measurements. The figure has been prepared by F. Paul, University of Zurich.

a) in many REMO grid boxes precipitation is highly variable on a subgrid scale

b) in most cases glaciers are found in the wettest part of a REMO grid box.

In order to quantify especially point b) and to additionally consider seasonal shifts in subgrid precipitation variability, the ratio $r_{P,i}$, defined as the mean precipitation in month i (i = 1,2,..,12) on the glaciated part of a grid box ($\overline{P}_{i,glaciated}$) divided by the mean precipitation over the entire grid box area ($\overline{P}_{i,total}$), has been calculated for each glaciated $^1/_6^\circ$ REMO box in Switzerland using the mentioned datasets:

$$r_{P,i} = \frac{\overline{P}_{i,glaciated}}{\overline{P}_{i,total}} \quad , i = 1, 2, .., 12 \tag{4.8}$$

A positive value of $r_{P,i}$ denotes a mean monthly precipitation on glaciated surfaces which is higher than the grid box average in the respective month. A negative value indicates lower-than-average precipitation on glaciers. The annual cycles of $r_{P,i}$ for the investigated grid boxes (Figure 4.10) reveal that in most cases glacier precipitation is higher than mean grid box precipitation throughout the entire year. Only a few slightly glaciated grid boxes located in the Engadine area (eastern part of Figure 4.9) show below-average precipitation on glaciers. For most boxes the ratio $r_{P,i}$ lies in the range 1 to 1.5. A characteristic

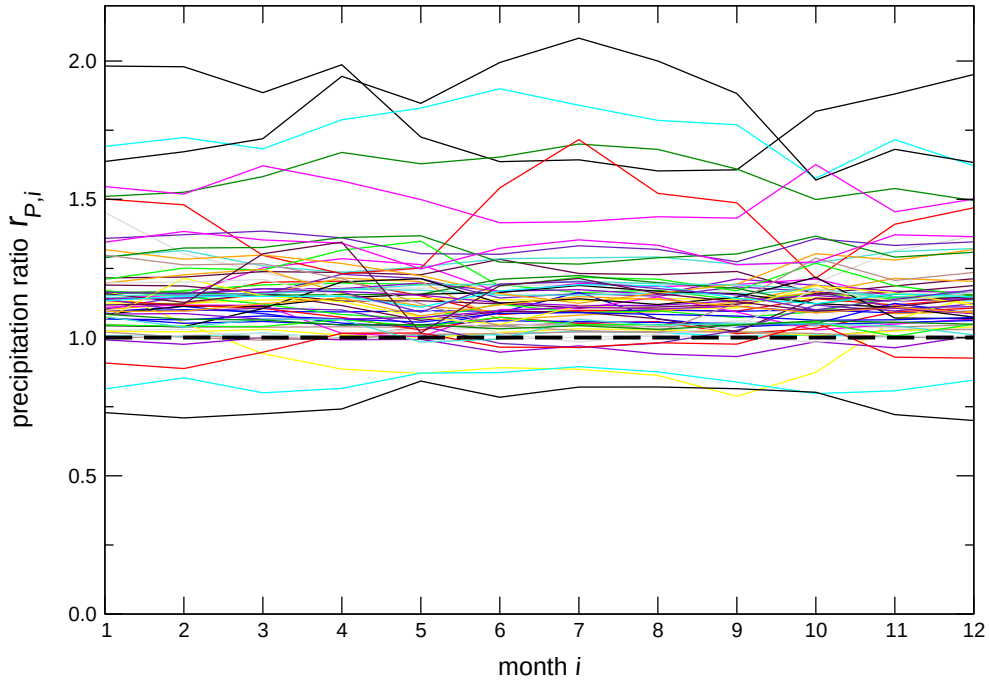

Figure 4.10: Annual cycles of the ratio $r_{P,i}$ of mean monthly precipitation on glaciated surfaces within a $^1/_6^\circ$ REMO grid box to mean grid box precipitation. Each line represents one glaciated REMO box in Switzerland. The dashed line denotes a ratio of 1. The data has been compiled by F. Paul, University of Zurich.

shape of the annual cycle of $r_{P,i}$ cannot be identified. Some boxes show highest ratios in summertime, while others have maximum values in the winter months. It has to be noted that the precipitation dataset is not corrected for the systematic measurement bias. Due to a higher snowfall fraction and higher wind speeds, this bias can be expected to be larger in the upper parts of a grid box where the glaciers are located in most cases. Hence, a correction of the measurement bias would probably lead to larger values of $r_{P,i}$.

2 The redistribution of snow by wind and avalanches

In mountainous terrain, the redistribution of fallen snow by wind and avalanches can play an important role. Once the snow has reached the ground it is redistributed at the 100 to 1000 m scale from exposed erosion areas (ridges and steep slopes) to accumulation areas (valleys and cirques), forming a snow distribution pattern which is typical for the terrain and the prevailing wind conditions (Jaedicke and Sandvik, 2002; Kuhn, 2003). These processes commonly result in an additional mass gain of glaciated surfaces while snow is removed from surrounding crests and ridges. By modelling glacier mass balance in a strongly glaciated catchment in the Austrian Alps (area $\approx$ 100 km^2, ice cover $\approx$ 40%), Kuhn (2003) found that, if the effect of snow redistribution is not considered, large amounts of accumulation occur outside the glacier area while the glaciers themselves exhibit unrealistic negative mass balances. Consequently, in order to obtain realistic results, snow has to be removed from the ice free areas and added to the glacier surface. This can be done in a straightforward way by introducing a *snow redistribution factor* which determines how much the amount of solid precipitation is increased on the glacier surface compared to the catchment average

and which generally depends on basin topography. In the mentioned study, this factor has been tuned to a value of 2.15 (independent of altitude and time of year) and is applied separately for each altitude interval. It does therefore not include the spatial variability and the elevation dependency of snowfall itself but only the redistribution effect.

In order to account for the subgrid variability of snow accumulation as a result of the processes described above, the simple concept of redistributing snow within a climate model grid box using a snow redistribution factor κ has been adopted in REMO$_{\texttt{glacier}}$. However, in contrast to its original meaning as outlined in point **2**, κ includes both the effect of subgrid scale variability of precipitation itself (point **1**) and the redistribution of snow by wind and avalanches after having reached the ground (point **2**). If the latter would be neglected, the ratios $r_{P,i}$ (Equation 4.8) could simply be used as a monthly varying factor κ for the investigated grid boxes (i.e., for those boxes where both a high-resolution precipitation dataset and glacier outlines are available). As shown in Figure 4.10, $r_{P,i}$ mostly lies within the range 1 to 1.5. In order to additionally consider the redistribution of fallen snow from non-glaciated to glaciated surfaces (see point **2**), the ratios have to be further increased, depending on the local characteristics of topography and the local wind conditions. As both factors can hardly be assessed in an appropriate manner on an RCM scale, it was decided to generally prescribe a snow redistribution factor of $\kappa = 2$ for all grid boxes, independent of the time year. This value lies well above the subgrid precipitation ratios $r_{P,i}$ for most grid boxes, but is lower than the redistribution factor of 2.15 as found by Kuhn (2003) for a catchment of a size comparable to a $^1/_6^\circ$ REMO grid box. In the mentioned study, the value of 2.15 does not include the variability of precipitation itself and would probably be even larger if the latter had been considered. Concerning the parameterisation in REMO$_{\texttt{glacier}}$ it is thus implicitly assumed that the study of Kuhn (2003) represents an extreme case which cannot be expanded to the whole model domain. Nonetheless, κ can formally be considered as a tuning parameter in REMO$_{\texttt{glacier}}$. Its influence on the simulated glacier mass balance will be assessed in additional sensitivity studies (Chapter 5.5).

The concept of snow redistribution in REMO$_{\texttt{glacier}}$ is shown schematically in Figure 4.11. In each time step, the amount of snow falling on the glaciated fraction of a grid box ($P_{snow,glaciated}$, [m w.e.]) is generally computed as

$$P_{solid,glaciated} \;=\; \kappa \;\cdot\; \overline{P}_{solid} \tag{4.9}$$

with the mean grid box snowfall $\overline{P}_{solid}$ [m w.e.] as provided by the atmospheric component of REMO. In order to ensure mass conservation (i.e., to conserve $\overline{P}_{solid}$) the amount of snowfall on the non-glaciated fraction $P_{solid,non-glaciated}$ is decreased accordingly. With regard to the redistribution factor κ, two basic restrictions apply:

- κ must not be larger than the ratio of the total grid box area A_{total} to the glaciated area $A_{glaciated}$:

$$\kappa \;\leq\; \frac{A_{total}}{A_{glaciated}} \tag{4.10}$$

  If this would be the case, the amount of snowfall on the non-glaciated fraction $P_{solid,non-glaciated}$ would have to be negative in order to ensure mass conservation and to keep $\overline{P}_{solid}$ unchanged.

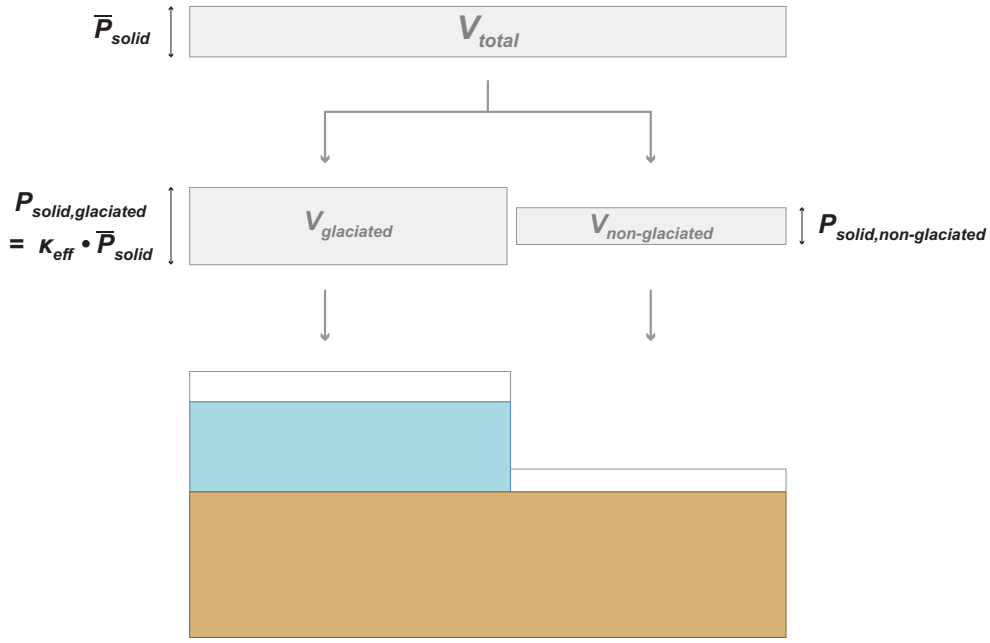

Figure 4.11: Concept of snow redistribution in REMO$_{\texttt{glacier}}$. κ_{eff} = snow redistribution factor. V_{total} = total snow volume falling in the current time step onto the grid box surface.

- ▷ In order to avoid very small snowfall rates on the non-glaciated part of a grid box while mean grid box snowfall is high, it is ensured that the non-glaciated part always receives a minimum fraction $ZSNLFMIN = 0.1$ of mean grid box snowfall, i.e.

$$P_{solid,non-glaciated} \geq ZSNLFMIN \cdot \overline{P}_{solid} \tag{4.11}$$

To guarantee the conditions 4.10 and 4.11, the maximum redistribution factor $\kappa = 2$ might have to be lowered in some cases. The new factor κ_{eff} (which is always equal to or lower than κ) is used instead:

$$P_{solid,glaciated} = \kappa_{eff} \cdot \overline{P}_{solid} \quad , \kappa_{eff} \leq \kappa \tag{4.12}$$

As liquid precipitation does not contribute to accumulation and is also not subject to a marked redistribution once it has reached the ground, rainfall is not redistributed in REMO$_{\texttt{glacier}}$. The glaciated and the non-glaciated fraction receive the same amount of liquid precipitation.

4.2.8 Volume-Area Relation

A key element of the new glacier subgrid parameterisation is the calculation of the areal extent of the glacier cuboid representing the total ice volume contained within a climate model grid box (see Figure 4.3). Changes in the glaciated area of a grid box ($A_{glaciated}$) will ultimately lead to changes of land surface characteristics, thereby directly affecting surface-air exchange processes. Variations in the areal extent of ice cover are thus one possibility for closing the glacier-climate feedback loop (Figure 2.9). As a general rule, negative glacier mass balances will gradually lead to a retreat of glaciers and consequently to a decrease of the ice-covered area. Vice versa, positive balances will result in an enlargement of a glacier's surface area (see Chapter 2.5.2).

In $\text{REMO}_{\texttt{glacier}}$ the dynamic response of glacier geometry to a given mass balance forcing is not computed explicitly. Instead, simplifying assumptions are used which relate a glacier's volume V [m^3] to its area A [m^2]. As described in Chapter 2.5.2, a simple power law can in principle be used for this purpose:

$$V = c \cdot A^{\gamma} \tag{4.13}$$

with a dimensionless scaling coefficient $\gamma = 1.375$ for mountain glaciers and a calibrated constant c. The corresponding relation between the glacier area and the mean ice thickness $\overline{h}$ [m] is obtained by dividing both sides in Equation 4.13 by the area A:

$$\overline{h} = c \cdot A^{\gamma-1} \tag{4.14}$$

Assuming that this simple geometric model always holds (i.e., for steady states as well as for non-steady states, for retreating as well as for advancing glaciers and with γ being constant in time), it can be used to deduce the area of a glacier as its volume changes (IPCC, 2001). It should be noted that, in a strict sense, γ cannot generally be expected to remain constant under changing climatic conditions (Bahr et al., 1997). Also the assumption that the shape of a glacier for a given volume is the same irrespective of whether it is in advance or retreat is not necessarily the case in reality (Raper et al., 2000). Nonetheless, Equation 4.13 has successfully been applied in a number of modelling studies (e.g., Raper et al., 2000; van de Wal and Wild, 2001; Raper and Braithwaite, 2005). Based on data from 63 glaciers in different regions of the world, including 15 glaciers in the Alps, Chen and Ohmura (1990a) tuned the scaling parameter γ to a slightly different value of **1.357** and the parameter c to **0.206** (or 28.5 if A and V are given in [10^6 m^2] and [10^6 m^3], respectively), obtaining a correlation coefficient of 0.98. In the present study, these values will be used to relate the glacier volume V and the mean ice thickness $\overline{h}$ to the glacier area A via Equations 4.13 and 4.14. Both relations exhibit a strictly monotonic behaviour and an increase in glacier area A will at any time result in an increase of both V and $\overline{h}$ (red curve in Figures 4.12 and 4.13).

Besides the power law relation further methods exist to derive the glacier volume V from other physical glacier characteristics, including for instance average surface slope and mean basal shear stress. An overview is given in Paul (2004). Some of these methods are based on physical relationships, others are empirically derived. Among these is the relation between the mean glacier thickness $\overline{h}$ [m] and the glacier area A [m^2] by Maisch (1992):

$$\overline{h} = 15.0 \cdot \sqrt{\frac{A}{10^6}} + 10.6 \tag{4.15}$$

Accordingly, the glacier volume V [m^3] can be calculated as

$$V = A \cdot \left(15.0 \cdot \sqrt{\frac{A}{10^6}} + 10.6\right) \tag{4.16}$$

This relationship has been empirically derived by a regression analysis based on ice thickness and glacier area datasets of 16 existing glaciers in the Alps and 63 late glacial ice bodies. For glacier areas smaller than about 50 km^2 it is very similar to the power law relation, while larger volumes and mean ice thicknesses are obtained for areas exceeding 50 km^2 (see Figures 4.12 and 4.13). In addition to the power law, the relation after Maisch (1992) is used as an alternative method for relating glacier volume to the ice-covered area in $\text{REMO}_{\texttt{glacier}}$ and hence to translate the simulated glacier mass and volume changes into changes of the glaciated area.

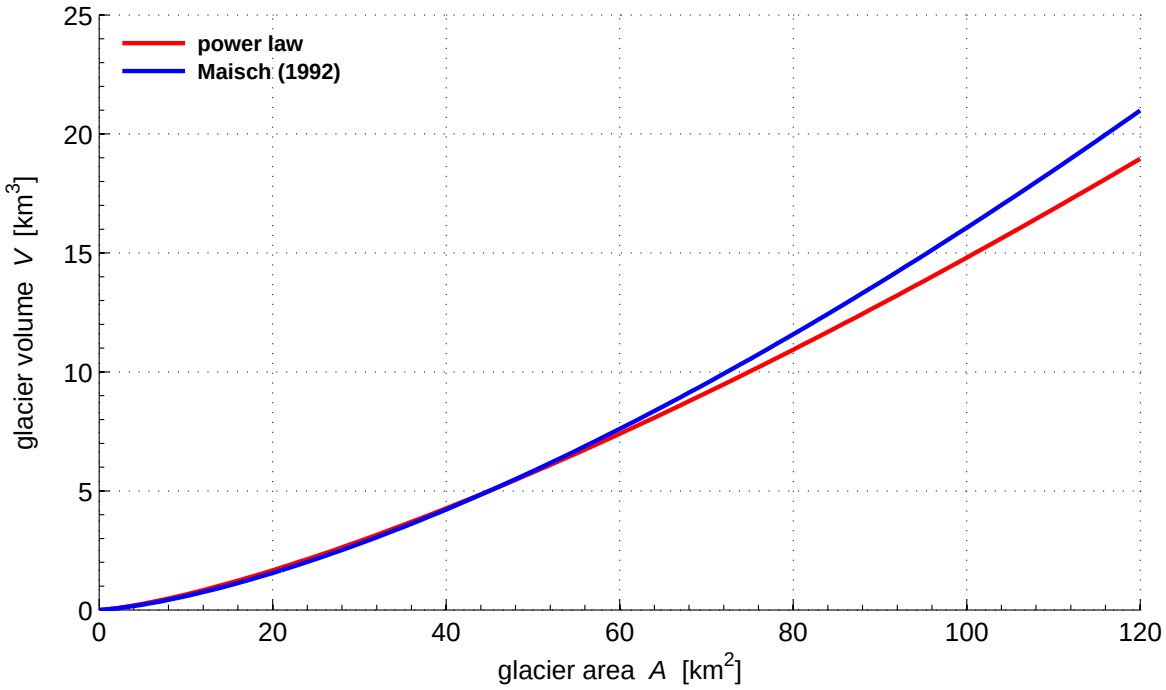

Figure 4.12: Relation between glacier area A [km^2] and glacier volume V [km^3] according to the power law (red, Equation 4.13 with $\gamma = 1.357$ and $c = 0.206$) and after Maisch, 1992 (blue, Equation 4.16).

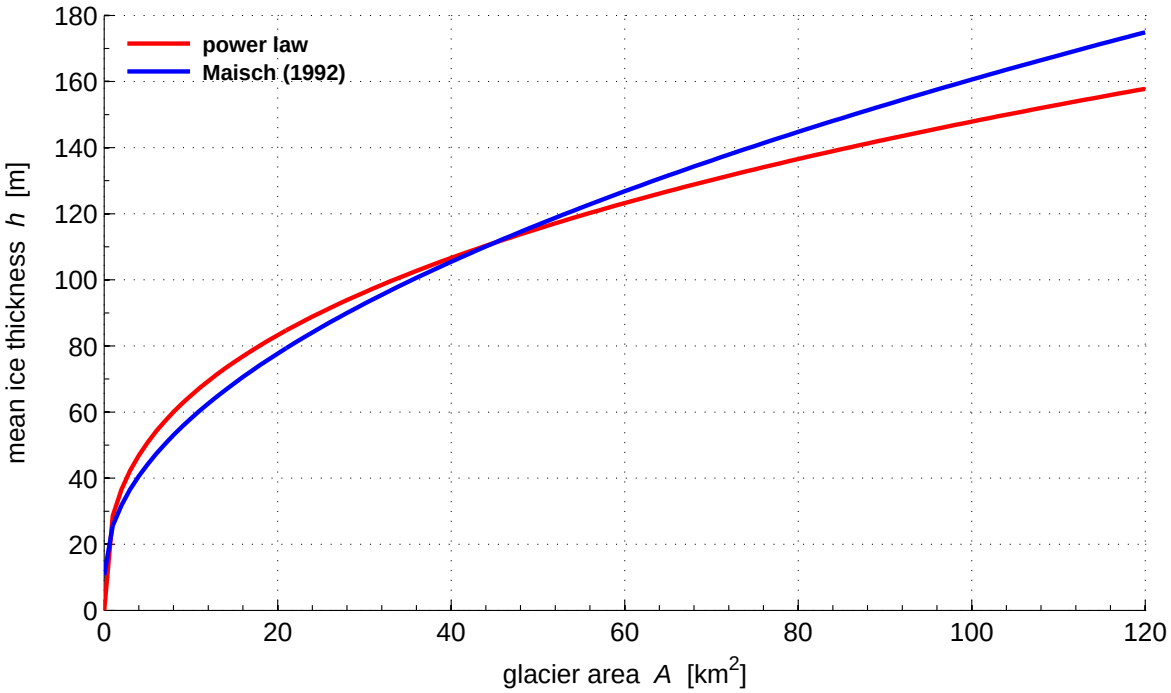

Figure 4.13: Relation between glacier area A [km^2] and mean ice thickness $\overline{h}$ [m] according to the power law (red, Equation 4.14 with $\gamma = 1.357$ and $c = 0.206$) and after Maisch, 1992 (blue, Equation 4.15).

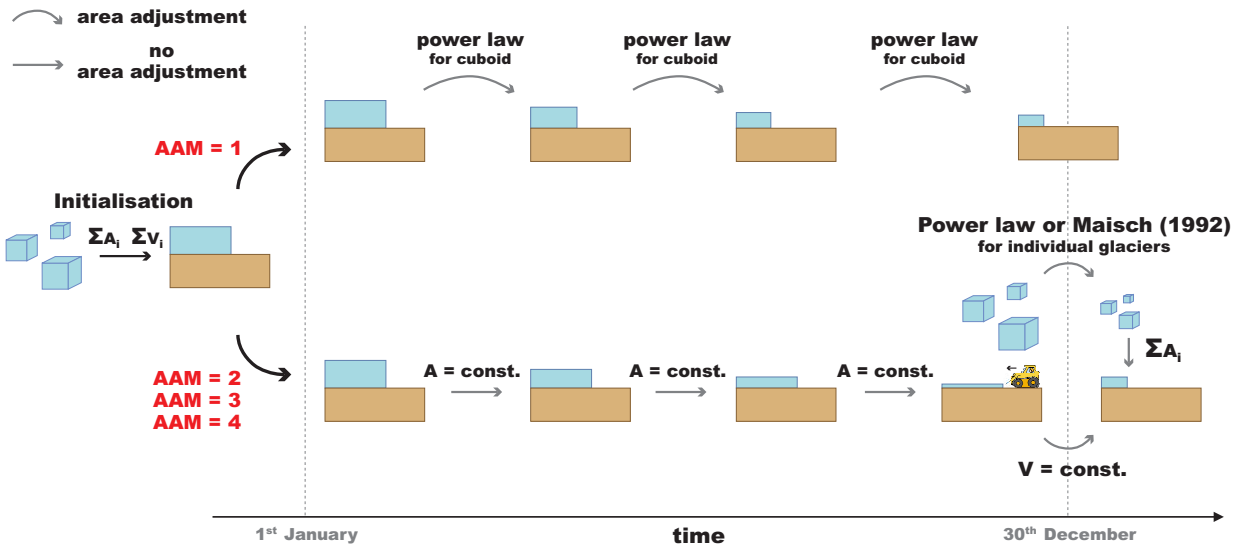

Figure 4.14: Schematic overview of the concept of glacier area adjustment in REMO$_{\texttt{glacier}}$. Example of a grid box with a negative net balance $\overline{b}_n$ in the first year of simulation. AAM 1 to 4 refer to the different area adjustment methods. See text for further explanations.

In REMO$_{\texttt{glacier}}$ both the power law relation and the relation after Maisch (1992) can be used in order to adjust the glacier surface area in case that changes of the total ice volume (i.e., non-zero mass balances) occur. In detail, three different *area adjustment methods* (AAMs; AAM 1, AAM 2, AAM 4) plus an option for including response times at a later stage (AAM 3) have been implemented (see also Figure 4.14):

- **AAM 1: Power law for glacier cuboid** (default if not stated otherwise)
  The simplest area adjustment method of all does not consider the variety of individual glaciers that are contained within a REMO grid box but treats the glacier cuboid as one single glacier with an area A and a volume V. At the time of model initialisation, both quantities are derived from information on the areal extent A_i of the individual glaciers in a grid box and by applying the power law (Equation 4.13, with $\gamma = 1.357$ and $c = 0.206$) to derive the individual glacier volumes V_i. The grid box totals A and V equal the sum of the individual contributions (N = number of glaciers contained in the respective climate model grid box):

$$A = \sum_{i=1}^{N} A_i \tag{4.17}$$

$$V = \sum_{i=1}^{N} V_i \tag{4.18}$$

  The ratio V/A equals the mean grid box ice depth h (compare to Figure 4.3). At this stage the power law, which has originally been applied to the individual glaciers, is no more valid for the grid box sums A and V. Or, if the validity of the scaling exponent $\gamma = 1.357$ is still assumed, the parameter c now has a different value.

  After the initialisation procedure, the information on individual glaciers is completely for-

gotten. The entire glacier cuboid is treated as one single glacier which is assumed to follow the power law 4.13 in terms of its geometrical behaviour. At the end of each model time step, the ice covered area A is adjusted in case that a change in the ice volume V occurred (by ice ablation or by transformation of snow into ice):

$$A_t \;=\; A_{t-1} \;\cdot\; \left(\frac{V_t}{V_{t-1}}\right)^{1-\gamma} \tag{4.19}$$

where the subscript "t" represents the new value at the current time step whereas "t-1" refers to the last time step or, alternatively, to the respective value at the time of initialisation. The adjustment of glacier area as a response to a change in ice volume (i.e., of a non-zero mass balance) is thus carried out instantaneously, an additional response time is not considered. As the vast majority of Alpine glaciers ($> 80\%$) is smaller than 0.5 km^2 (Zemp et al., 2007) and will therefore only show a limited dynamic reaction to climatic change, this approach seems to be feasible in a first stage. Equation 4.19 can be directly derived from the power law 4.13 by replacing the parameter c with the term ${V_{t-1}/A_{t-1}}^{\gamma}$ of the previous time step. The knowledge of c for the respective grid box glacier cuboid is not necessary. If an area adjustment is carried out, the total ice volume V_t must still be valid in order to ensure mass conservation, which means that the mean ice depth h has to be adjusted accordingly. Furthermore, as the total land area of a grid box is constant in time, an enlargement of the glaciated part is associated with a reduction of the extent of the non-glaciated fraction and vice versa. In the course of the area adjustment the total snow volume of each fraction remains constant, i.e., snow depths are adjusted similarly to the ice depth on the glaciated fraction in order to account for mass conservation.

▷ **AAM 2: Power law for individual glaciers**

In contrast to the treatment of the glacier cuboid as one single glacier obeying the power law in AAM 1, this method keeps the information on the individual glaciers within a climate model box throughout the entire simulation. Area A and volume V of the glacier cuboid are initialised in the same way as in AAM 1. However, the area and the volume of each individual glacier as well as the respective grid box number are stored in an external file. During the model simulation, the glaciated area A of a grid box (i.e., the area of the glacier cuboid in Figure 4.3) is kept fixed for one year, only the mean ice depth h and consequently also the total ice volume V are allowed to vary depending on accumulation and ablation conditions.

After one year, in the current model setup on 30$^{\text{th}}$ December, the area adjustment is carried out. The external file containing A_i and V_i of each individual glacier at the time of the last area adjustment (or, in case of the first year of the simulation, at the time of model initialisation) is read and the mean specific net balance of the glacier cuboid $\overline{b}_n$ for the previous 12 month period is applied to each individual glacier. The sum of the updated glacier volumes V_i in a specific grid box now exactly corresponds to the current volume V of the glacier cuboid. Applying the power law and equation 4.19, the new area A_i is now computed for each individual glacier and the areas A_i are summed up grid box-wise (Equation 4.17). The updated glaciated area A of each grid box is then used to change the geometry of the glacier cuboid and to adjust the relation between glaciated and non-

glaciated fraction in each grid box (see AAM 1). A new external file containing the updated individual A_i and V_i is compiled and will be read in at the time of the next area adjustment.

The main modifications with respect to AAM 1 can be summarised in the following way:

- The adjustment of the glaciated area A of a grid box is carried out only once a year and not in each time step, meaning a lower computational burden.
- The power law 4.13 is applied to each individual glacier in a grid box and not for the whole glacier cuboid. This is a major advantage of AAM 2 since, in a strict sense, the validity of the power law has only been shown for single glaciers. It is not necessarily applicable for the total sums of ice-covered area and ice volume in a certain region (RCM grid box).
- Implicitly, a short response time of glacier geometry of less than 1 year is assumed. At the time of area adjustment, i.e., at the end of a balance year (30$^{\text{th}}$ December), the geometry of each individual glacier is expected to have adjusted to the applied mass balance forcing during the previous 12 months and to obey the power law. In contrast, an instantaneous adjustment of glacier geometry is assumed in AAM 1.

Despite these advantages of AAM 2, a number of restrictions still apply. These mainly concern the total number of glaciers contained in a specific grid box since both the disintegration of large glaciers into smaller ones and the joining of small, growing glaciers into larger ice bodies are not considered. Individual glaciers can disappear if negative mass balances result in an ice volume of zero, but new glaciers cannot form and the maximum number of individual glaciers in a grid box is therefore restricted to their number N at the time of initialisation. In the special case, that snow is transformed into ice in a formerly non-glaciated grid box, new glaciers are formed. The total ice volume V is then allocated to individual glaciers with increasing areas A_i of 0.01 km^2, 0.1 km^2, 1 km^2, 10 km^2 etc. of volumes V_i according to the power law 4.13. Once the remaining ice volume to be allocated is less than the volume required for a glacier of the next size category, a glacier of intermediate size is created which comprises the remaining volume.

▷ **AAM 3: Power law for individual glaciers, including response time**
As AAM 2, but including a response time for the adjustment of geometry. The updated individual glacier areas as obtained by Equation 4.19 are not reached instantaneously at the time of area adjustment. Only a certain fraction of the total area change as calculated from the power law is carried out. So far, details of this method (especially the calculation of glacier response times) have not been implemented. It is an additional option for including response times into the concept of AAM 2 at a later stage.

▷ **AAM 4: Relation after Maisch (1992) for individual glaciers**
As AAM 2, but instead of the power law 4.13 the volume-area relation after Maisch (1992, Equation 4.16) is applied both for initialisation of the total grid box ice volume V and for

the update of the individual glacier areas A_i at the time of area adjustment. The latter is achieved by applying an iterative procedure in order to compute the area A_i for a given volume V_i according to equation 4.16.

4.3 Technical Aspects

The new glacier parameterisation scheme has been integrated in the physical parameterisation package of REMO via the inclusion of three additional FORTRAN subroutines plus a number of further modifications in already existing routines. The glacier scheme can be turned on or completely off by setting a dedicated switch in the job control script. In total, 46 new variables have been defined, describing the state of the glaciated fraction of a grid box and its interaction with the atmosphere (see Appendix A). For simulations in the Alpine area the increase of the total computing time due to the inclusion of the new subroutines amounts to about 1%. The following listing gives a short overview of the new subroutines:

- **subroutine INIDGLA**
  This routine initialises the glacier state variables in each grid box (glaciated fraction, mean ice depth, ice temperature, snow depth etc.). It is called during the model initialisation procedure.

- **subroutine GLADJUST**
  If AAM $= 2$, 3 or 4 (area adjustment based on individual glaciers) this routine is called once a year (default: 30$^{\text{th}}$ December). It reads the data file containing volume and area information on individual glaciers at the time of the last area adjustment (or, in case of the first year of simulation, at the time of model initialisation) and computes the updated individual glacier areas A_i as well as the total glaciated area A for each grid box (see Chapter 4.2.8). A new external file containing the updated individual A_i and V_i is created.

- **subroutine DYNAMICE** (*DYNAMic ICE cover*)
  Most processes involving the glaciated fraction of a grid box are represented by this subroutine. DYNAMICE is the central part of the new glacier subgrid parameterisation. It is called each time step out of REMO's land surface routine SURF. Input to DYNAMICE are the turbulent surface fluxes over the glaciated fraction (computed beforehand in the vertical diffusion scheme), the radiation fluxes (computed in the radiation scheme) and the amounts of liquid and solid precipitation (see Figure 4.15). DYNAMICE itself accounts for

  - the surface energy balance of the glacier cuboid
  - the surface mass balance of the glacier cuboid (i.e., for accumulation of snow, for transformation of snow into ice on both the glaciated and the non-glaciated fraction and for ablation by melting and sublimation)

- temperature diffusion in the snow, ice and soil layers
- runoff generation on the glaciated grid box fraction
- the adjustment of the glaciated area, if AAM $= 1$

It returns updated values of snow and ice temperature on the glaciated fraction, snow and ice depth, snow age, glaciated area (if AAM $= 1$) and the glacial runoff components.

As most of the processes involved in glacier mass and energy balance and glacier area adjustment are handled by these three subroutines, a transfer of the new parameterisation scheme into RCMs other than REMO (or even GCMs) is, from a technical point of view, possible with a reasonable amount of additional workload. Generally, the interface to the glacier scheme would have to be implemented in the land surface routine of the respective model. An already existing concept of fractional surface coverage (see Chapter 3.3.2) would be highly beneficial since "glaciers" could then be incorporated as an additional land cover type which is allowed to dynamically change its areal extent (as it is done in REMO$_{\texttt{glacier}}$).

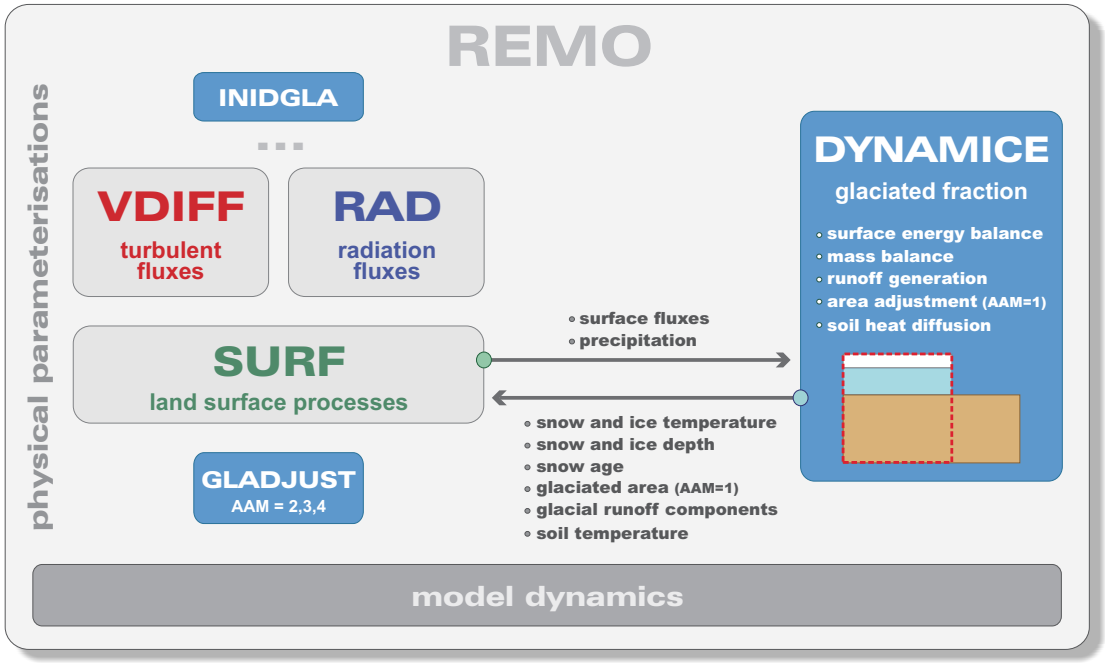

Figure 4.15: Schematic overview on the technical implementation of the new glacier parameterisation in REMO (blue: the new subroutines).

5 Results

This chapter presents and discusses the results of the model simulations ($\text{REMO}_{\texttt{glacier}}$ and standard REMO, plus HD) that have been carried out in the course of the present study. All experiments start in the year 1958 and span a time period of several decades. The first section (5.1) gives an overview on the chosen model setup (model domain, initialisation procedure) and on the baseline simulations that have been carried out. The results concerning the characteristics of the simulated Alpine glacier cover (glacier mass balance, number of glaciers, ice-covered area and ice volume) are presented in Section 5.2. Afterwards, the quality of the simulated atmospheric parameters is evaluated via a comparison against observational datasets in Section 5.3. Biases in these parameters can, in principle, have a strong influence on the simulated glacier mass balance. The modification of the simulated climatic conditions in the Alpine area due to the inclusion of the new glacier subgrid parameterisation is investigated in Section 5.4 by comparing simulations of $\text{REMO}_{\texttt{glacier}}$ and standard REMO. Section 5.5 presents the analysis of the model sensitivities with respect to individual model parameters and the inclusion of specific processes. Finally, the influence of glaciers on local runoff and on river discharge (coupling of the HD model) is investigated in Section 5.6.

5.1 Model Setup

5.1.1 Model Domain

All REMO simulations that have been carried out within the present study were performed on a regional model domain consisting of 81 x 61 grid boxes and completely covering the European Alps as well as further parts of central, western and southern Europe (Figure 5.1).

The arc-shaped Alps are the highest mountain range in central Europe, peaking at 4808 m a.s.l. at the Mont Blanc in their western part. Due to their scale and geometry they exert a strong influence on the regional climate by modifying and triggering weather systems and thereby establishing distinct climatic characteristics (e.g., orographic precipitation enhancement and orographically related flow phenomena like meso-scale wind systems and Alpine lee cyclogenesis; Schär et al., 1998). The general climate of the Alps is characterised by the transition between two major climatic zones: the mid-latitude temperate type to the North and the Mediterranean type to the South. Consequently, distinct thermal regimes and a strong latitudinal temperature gradient can be identified between the north and the south sides of the main Alpine crest. At elevations below 1500 m a.s.l. air temperatures in the southern Alpine area exceed those in the North by about 2 to 4°C, both in winter and in summer. Also precipitation in the Alps is subject to a pronounced spatial variability, from the scale of the entire mountain range to that of single slopes. It is strongly controlled by topographical features. Prominent effects include the enhancement of precipitation along the Alpine foothills and the shielding of the inner-Alpine valleys. The annual sum of precipitation ranges from less than 600 mm in some inner-

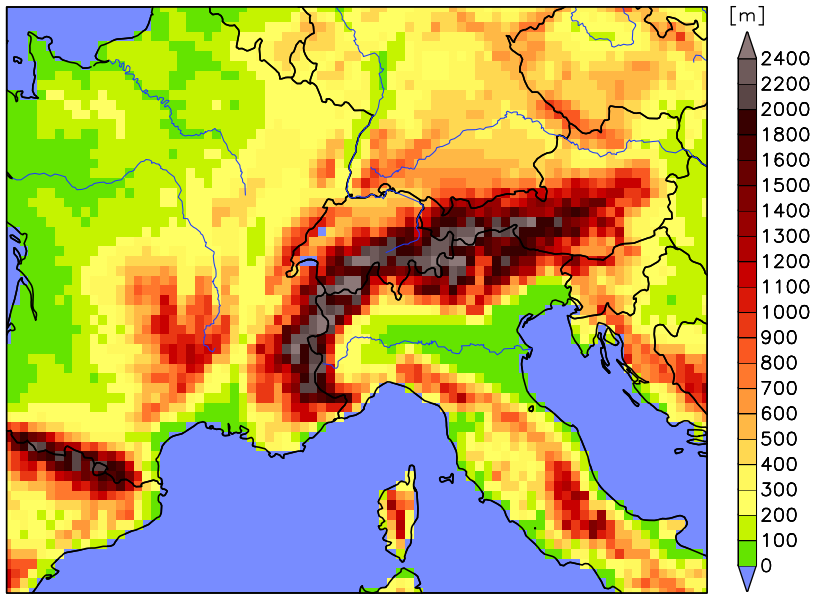

Figure 5.1: Model domain (81 x 61 grid boxes) and grid box orography [m] used for all regional climate simulations performed within this study. The horizontal resolution is $^1/_6^\circ$ on a rotated spherical grid.

Alpine valleys to more than 2000 mm along the northern rim and in some areas south of the main crest. In general, precipitation totals increase with altitude, but much of the topographic signal is associated with slope and shielding rather than height effects (Schär et al., 1998). In situations with pure convection, decreasing altitude gradients are often found due to the preferred location of the convection centres in valleys and in the flatland and due to the decrease in precipitable water content with altitude (Schwarb, 2000). As a consequence, the relation between precipitation and altitude strongly varies with respect to location and season. Concerning the seasonal cycle of precipitation, pronounced differences exist between different sub-regions. Generally, the winter season is relatively dry whereas summer is the main rainy season in the Alps. A more detailed description of the Alpine climate and the influence of the Alps on atmospheric circulation can be found in Schär et al. (1998).

5.1.2 Simulations

In order to assess the performance of the new glacier parameterisation scheme, four baseline simulations (plus several sensitivity studies, see Chapter 5.5) have been carried out for the period 1958-2003 (Table 5.1). Three of them (GlacA, GlacB, GlacC) include the new parameterisation scheme with the ice albedo fixed at 0.4 (Method A, see Chapter 4.2.3), but differ with respect to the area adjustment method used. The fourth simulation (CTRL) is a standard REMO 5.3 experiment and does not account for glaciers in the model domain. It is used in order to assess the effect of the new glacier parameterisation on the simulated climate and on river discharge. The experiments GlacA and CTRL are subsequently coupled to the HD routing scheme in an offline mode.

In all experiments, the standard horizontal resolution of $^1/_6^\circ$ on a rotated spherical grid, corresponding to a grid box size of approximately 18 x 18 km^2 (see Figure 5.1), and 20 vertical levels were used. The lateral boundary forcing was directly provided by the ERA40 re-analysis (01/1958 to 07/2002; Uppala et al., 2005) and the operational analysis of the ECMWF (08/2002 to 12/2003). The internal model time step was 100 seconds. In all simulations, the atmospheric concentrations of greenhouse gases and of aerosols did not vary in time but have been prescribed at values corresponding to the

Name	Version	Period	AAM	Ice albedo	HD ?
GlacA	$REMO_{glacier}$	1958 - 2003	1	Method A	yes
GlacB	$REMO_{glacier}$	1958 - 2003	2	Method A	no
GlacC	$REMO_{glacier}$	1958 - 2003	4	Method A	no
CTRL	REMO 5.3	1958 - 2003			yes

Table 5.1: Baseline simulations carried out within the present study.

1990s. Nonetheless, rising greenhouse gas concentrations towards the end of the 20th century are implicitly accounted for since, due to the comparatively small model domain, the lateral boundary forcing generally exerts a strong influence on the simulated regional climate. The effect of increased greenhouse gas concentrations is therefore forced upon the RCM via the characteristics of the air masses in the driving fields (re-analysis and analysis). Even for large model domains covering the entire European continent, dedicated sensitivity studies with REMO have shown that the effect of time-varying greenhouse gas concentrations in the RCM itself (compared to prescribed mean values) on the simulated near-surface air temperature is generally smaller than 0.2°C (P. Lorenz, pers. comm.).

5.1.3 Initialisation

At the start of each REMO simulation (1st January 1958, 0h) the standard initialisation procedure was applied for most parameters. The prognostic atmospheric fields (temperature, specific humidity, surface pressure, etc.) in each grid box and in each vertical level were directly initialised with the interpolated large-scale forcing, i.e., the ERA40 re-analysis interpolated to the REMO grid. Initial values for the land surface parameters (surface temperature, soil temperatures, snow depth, soil water content, etc.) were extracted from an already existing REMO simulation (here: 1st January 1999, 0h). The ice temperature in glaciated grid boxes (upper and lower layer) was initialised with -2°C in the entire model domain, which is assumed to roughly represent the temperature of temperate glacier ice in wintertime (i.e., the penetration of a winterly cold wave into ice which is close to the melting point for most of the time; see Chapter 2).

A more complicated procedure was necessary for initialising the glaciated grid box fraction and the mean ice depth (see Figure 4.3). For this purpose, glacier area information extracted from the database of the *World Glacier Inventory* (WGI)[1] was used (WGI, 1989; NSIDC, 1999). The WGI contains information for more than 67.000 glaciers throughout the world, and parameters within the

[1] available from http://nsidc.org/data/glacier_inventory

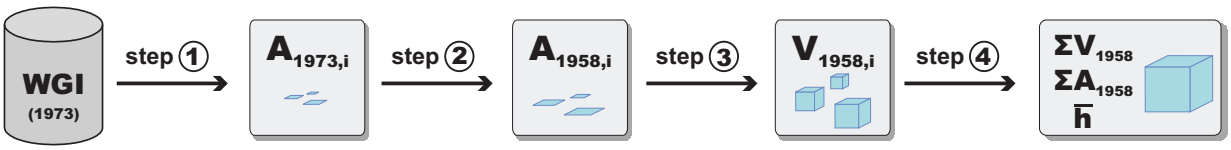

Figure 5.2: Four-step procedure for initialisation of glaciated area and mean ice depth of each REMO grid box (see text for explanation of the individual steps).

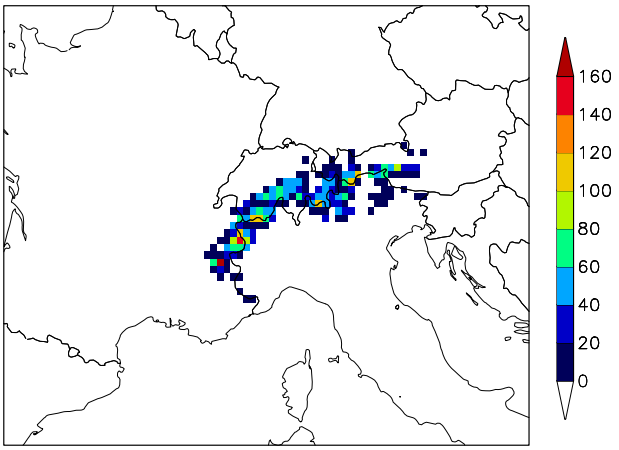

Figure 5.3: Total number of glaciers per REMO grid box as extracted from the WGI.

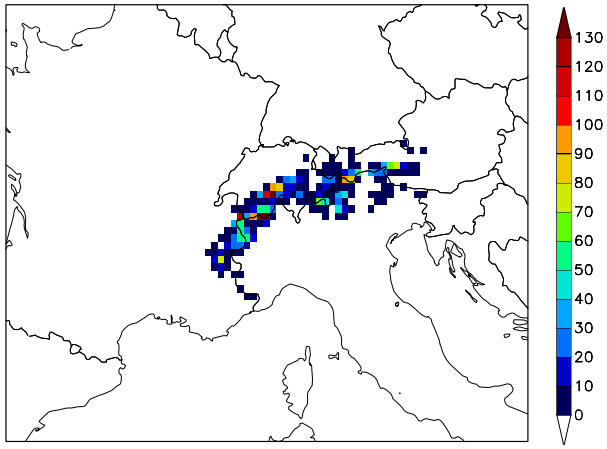

Figure 5.4: Total glaciated area per REMO grid box [km^2] as extracted from the WGI.

inventory include geographic location, area, length, orientation, elevation, and classification of the morphological type and moraines. All inventory entries are based upon a single observation in time and can therefore be viewed as a snapshot of the respective glacier at this time. The core of the WGI is data collected by the World Glacier Monitoring Service (WGMS) in Zurich. For the European Alps, the inventory includes more than 5000 individual glaciers and comprises the national inventories for Austria (1969), France (1967 to 1971), Switzerland (1973), Germany (1979) and Italy (1975 to 1984). While the inventories of Austria, Switzerland and Germany refer to one single reference year, the records of France and Italy have been compiled over a longer period of time in order to achieve a total coverage (Zemp et al., 2006b). As Swiss glaciers contribute the largest fraction to the Alpine part of the inventory (both with respect to total number and total area), it is assumed in the present study that the glacier area information extracted from the WGI is representative for the year 1973.

In order to derive the initialisation fields for the glaciated grid box fraction and the mean ice depth, the following four-step procedure has been applied (see also Figure 5.2):

step ① **Extraction of individual glacier areas from the WGI and attribution to REMO grid boxes**

In a first step, the area of each individual glacier in the Alps was extracted from the WGI and assigned to the respective REMO grid box (using the geographic location as provided by the WGI). Glaciers in the Pyrenees, which are part of the model domain (see Figure 5.1), were not considered. By this procedure, glaciers have been assigned to 168 REMO grid boxes (out of 4941) with more than 100 glaciers per REMO grid box along the main Alpine crest (Figure 5.3). The glaciated area per REMO grid box (sum of all individual glacier areas) exceeds 100 km^2 in a number of grid boxes located in south-western Switzerland and close to the French and Italian borders (Figure 5.4). The total glaciated area in the Alps amounts to approx. 3040 km^2, which represents less than 0.2% of the total surface area of the REMO model domain.

step ② **Scaling of individual glacier areas (1973 → 1958)**

The individual glacier areas as extracted from the WGI are assumed to be valid for the year 1973 (see above). In order to obtain the respective values for the time of model

initialisation (1st January 1958), the general retreat of Alpine glaciers between the late 1950s and the early 1970s (see Chapter 2.7.5) has to be accounted for. As glacier area information for the 1950s is only available for very few Alpine glaciers, a simple scaling procedure has been applied. The method is based on 17 glaciers in the Alps of different size for which glacier area in the balance period 1956/57 (A_{1957}) could be obtained from the *Fluctuations of Glaciers* Series (FoG, 1967). Relating A_{1957} to the glacier area in 1973 as extracted from the WGI (A_{1973}), the relative area change from 1957 to 1973 Z (here: with respect to the 1973 area) has been calculated for the 17 glaciers and has been related to A_{1973} by a logarithmic regression (Figure 5.5, r=0.72):

$$Z(A_{1973}) \;=\; \frac{A_{1973} - A_{1957}}{A_{1973}} \;=\; -0.111 \;+\; 0.031 \;\cdot\; ln(A_{1973}) \tag{5.1}$$

In the investigated sample small glaciers generally experienced a larger percentage retreat than large glaciers, which is in line with more comprehensive studies by other authors (e.g., Paul et al., 2004b; Zemp et al., 2006b). In order to obtain glacier areas for the year 1958 a linear area decay for the 17-year period 1957 to 1973 was assumed and the corresponding area change $Z^\star$ was calculated as

$$Z^\star(A_{1973}) \;=\; \frac{A_{1973} - A_{1958}}{A_{1973}} \;=\; \frac{16}{17} \cdot\; Z(A_{1973}) \tag{5.2}$$

$Z^\star(A_{1973})$ was then used to derive the glacier area in 1958 for each individual glacier i in the Alps:

$$A_{1958,i} \;=\; A_{1973,i} \;\cdot\; (1 - Z^\star(A_{1973,i})) \tag{5.3}$$

Only for Grosser Aletschgletscher, the largest glacier in the Alps, a different procedure was applied. This glacier experienced a slight retreat from 1958 to 1973 (upper right marker in Figure 5.5). However, the fitted regression (Equation 5.1) results in a positive value of Z for this size category, i.e., an increase of glacier area, which is unrealistic. Therefore, based on the area information originally derived from FoG (year 1957) and WGI (year 1973), $Z^\star$ = -0.0049 was used for this glacier.

Applying the described procedure, the total glaciated area in the Alps in 1958 amounts to approx. 3280 km^2, which is 7.9% more than the area in 1973 as directly extracted from the WGI.

step (3) Calculation of individual glacier volumes

The WGI contains information on mean ice depth only for very few glaciers. For this reason, in order to obtain the total ice volume per REMO grid box and the mean ice depth of the glacier cuboids (Figure 4.3), the ice volume V_i for the year 1958 of each individual glacier contained in the WGI was calculated applying

- ▷ Equation 4.13 (power law) if AAM 1, 2 or 3 was used for area adjustment in the respective model simulation (see Chapter 4.2.8)
- ▷ Equation 4.16 (relation after Maisch, 1992) in case of AAM=4

using the respective glacier area $A_{1958,i}$. The resulting total ice volume in the Alps is 156 km^3 for the first case and 145 km^3 for the latter. This is slightly more than the 130 km^3

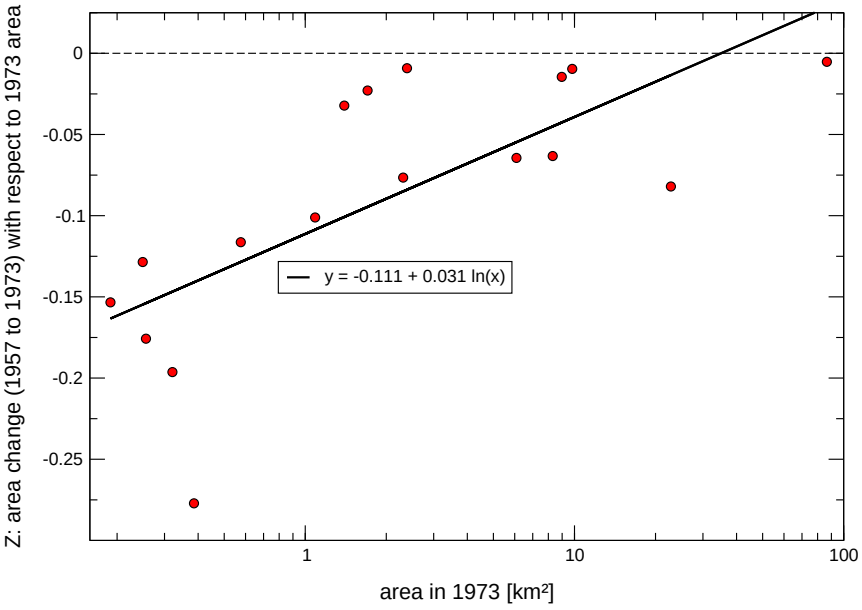

Figure 5.5: Relative area change from 1958 to 1973 (with respect to the area in 1973) of 17 Alpine glaciers and logarithmic regression.

suggested by Haeberli and Hoelzle (1995) and clearly exceeds the value of 100 km^3 given by Paul et al. (2004b). However, both studies refer to the 1970s and do not include the Alpine glacier retreat from 1958 to to 1973.

step ④ **Computation of total glacier area, glaciated grid box fraction, total ice volume and mean ice depth for each REMO grid box**

After step ③, the individual areas A_i and volumes V_i of all glaciers in the Alps for the year 1958 were available. In a final step, A_i and V_i were summed up for each REMO grid box (Equations 4.17 and 4.18), resulting in the total glaciated area A and the total ice volume V for the respective grid box. The glaciated grid box fraction a has then been obtained by dividing A by the total grid box area $A_{grid\,box}$:

$$a = \frac{A}{A_{grid\,box}} \tag{5.4}$$

For most parts of the Alps, this fraction lies below 5% (Figure 5.6). Still, maximum glaciations of more than 45% are obtained in south-western Switzerland. In general, there is a clear dependence of the degree of ice cover on grid box altitude with maximum glacier-covered fractions occurring along the main Alpine ridge (Figure 5.8).

The mean ice depth $\overline{h}$ [m] of the glacier cuboid in a glaciated grid box was obtained by dividing the total ice volume V by the glaciated area A:

$$\overline{h} = \frac{V}{A} \tag{5.5}$$

Maximum mean ice depths of slightly more than 100 m are obtained for grid boxes with high fractions of ice cover (Figure 5.7).

5.1.4 Catchments

The evaluation of the REMO$_{\texttt{glacier}}$ model results has in most cases been carried out for the entire Alps as well as for the four main catchments draining the Alpine area (Figure 5.9):

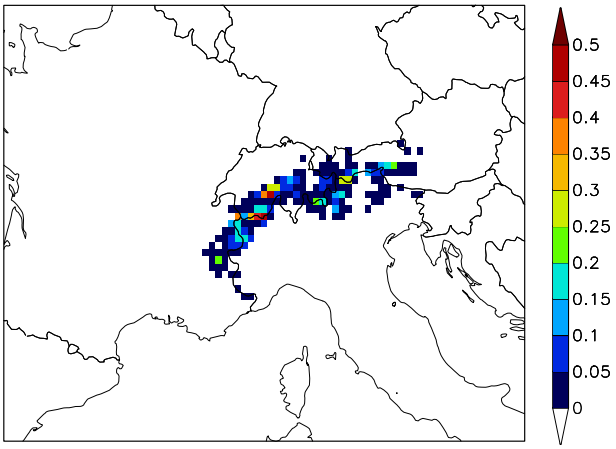

Figure 5.6: Glaciated grid box fraction a at initialisation (1st January 1958).

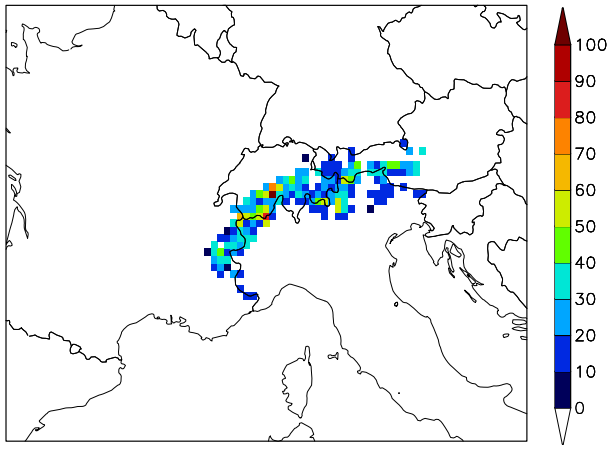

Figure 5.7: Mean ice depth [m] at initialisation (1st January 1958).

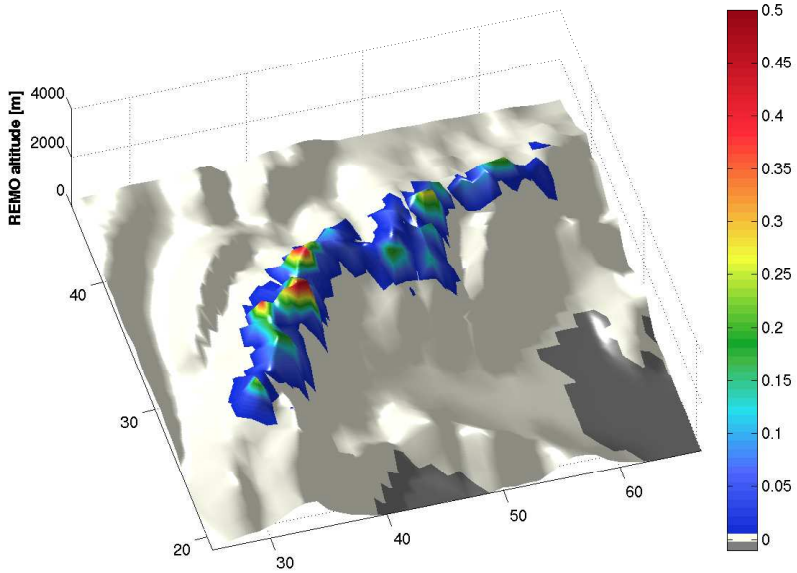

Figure 5.8: REMO orography (view from South-West) coloured by the glaciated grid box fraction a at initialisation (1st January 1958). Note that only the central part of the model domain is shown.

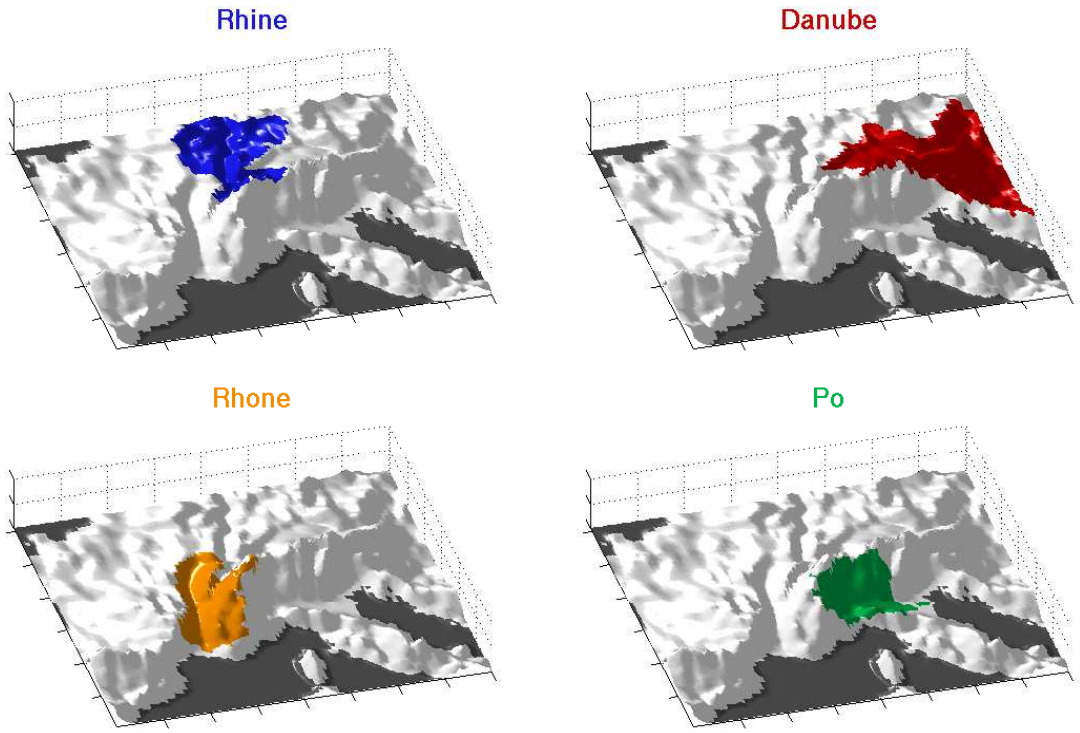

Figure 5.9: 3D-view of the entire model domain and the four main river catchments draining the Alpine area.

- The **Rhine** catchment, draining the north-western part of the Alps towards the North Sea (not part of model domain). Catchment area in model domain: 144293 km^2.
- The **Danube** catchment, draining the north-eastern Alpine region into the Black Sea (not part of model domain). Catchment area in model domain: 234776 km^2.
- The **Rhone** catchment, draining large parts of the Western Alps into the Gulf of Lion. Catchment area in model domain: 98186 km^2.
- The **Po** catchment, draining major parts south of the main Alpine ridge towards the Adriatic Sea. Catchment area in model domain: 73179 km^2.

In 1958, these four catchments contained about 96.6% of the total glaciated area in the Alps and about 97.8% of the total ice volume (both values as derived by the model initialisation procedure). The remaining ice cover (i.e., less than 4% of the total Alpine glacier area) is mainly located in the Adige (Etsch) catchment which also drains into the Adriatic Sea. Due to the small fraction of total glacier cover this catchment has not been analysed in detail.

5.2 Simulated Glacier Cover

In the following section the results of the three baseline experiments GlacA, GlacB and GlacC with respect to the characteristics of the Alpine ice cover are presented. In this regard, one of the most

important parameters is the simulated glacier mass balance. It's spatial distribution, its evolution in time and its dependence on simulated atmospheric quantities (temperature, precipitation, radiation) are investigated in Section 5.2.1, both for the entire model domain and for the individual main Alpine catchments. The simulated glacier mass balance exerts a direct control on the ice volume and, via the implemented volume-area-relationships, indirectly affects the evolution of the ice-covered area. These parameters are assessed in Section 5.2.2. Afterwards, Section 5.2.3 presents the temporal evolution of the total number of glaciers in the simulations GlacB and GlacC (AAM 2 and AAM 4). Finally, the obtained results concerning the simulated Alpine ice cover are discussed in Section 5.2.4.

5.2.1 Glacier Mass Balance

Entire Domain

The mean specific mass balance $\overline{b}_n$ is the basic parameter for the assessment of glacier mass changes (see Chapter 2.3). Figures 5.10 and 5.11 show the evolution of $\overline{b}_n$ and of the corresponding cumulative mass balance $\sum \overline{b}_n$ for the entire Alpine region for the three baseline simulations as well as for the recent estimate of Dyurgerov and Meier (2005). In case of the model simulations $\overline{b}_n$ has been obtained by dividing the total volume change of snow and ice on the glaciated grid box fractions by the total ice-covered area in the Alps. The balance period is assumed to last from October (last year) to September (current year). Hence, the balance year 1958 (October 1957 to September 1958) is not totally covered by the simulations and is therefore excluded from the analysis. The observation-based dataset of Dyurgerov and Meier (2005) has been computed by weighting all available individual glacier mass balance values in the Alps by the respective glacier surface areas.

The simulated mean mass balance only slightly differs between the three baseline experiments. Apparently, the choice of the area adjustment method has virtually no influence on the spatial mean of the simulated Alpine glacier mass balance. Only in the early 1980s small differences occur, with slightly higher values for GlacA. At any time the differences of the annual mass balance values between the three simulations are lower than 0.1 m w.e./year. The general temporal evolution of the simulated mass balance is in good accordance with the observation-based dataset. In both cases the most positive values appear in the late 1970s and the early 1980s, which is in line with the interim stabilisation and advance period of Alpine glaciers during that time (assuming small response times; see Chapter 2.7.5). Before and after that period annual mass balances are mainly negative, both in the simulations and in the observation-based dataset. The periods of positive mass balances in the late 1960s and around 1980 are, however, not very well captured by the model. This fact is responsible for the clear negative bias of the simulated cumulative mass balance until the 1990s (Figure 5.11). Furthermore, the strong glacier mass loss towards the end of the 20$^{\text{th}}$ century and especially the extremely negative mass balance in 2003 are underestimated by the model simulations. This shortcoming more than compensates for the negative bias of the simulated annual mass balance before 1985 and, as a consequence, leads to a clear underestimation of cumulative glacier mass loss over the entire investigated

Simulation	$\sum \bar{b}_n$ **Alps**	$\sum \bar{b}_n$ **Rhine**	$\sum \bar{b}_n$ **Danube**	$\sum \bar{b}_n$ **Rhone**	$\sum \bar{b}_n$ **Po**
	1961 - 2003	1959 - 2003			1987 - 2003
GlacA	- 3.53	11.76	- 6.41	- 1.78	- 14.58
GlacB	- 3.96	10.44	- 5.88	- 2.53	- 10.87
GlacC	- 3.47	10.08	- 5.27	- 2.14	- 10.04
D&M 2005	- 7.92	-6.95	- 15.00	- 7.28	- 11.08

Table 5.2: Mean cumulative specific mass balance $\sum \bar{b}_n$ [m w.e.] of the entire Alps and of the four main catchments as simulated by the three baseline simulations (GlacA, GlacB, GlacC) and as derived from Dyurgerov and Meier (2005, D&M 2005).

period (Table 5.2 and Figure 5.11).[2]

Still, the general course of Alpine glacier mass balance is relatively well reproduced. In a number of balance years the simulated values are very close to the observations (e.g., 1964, 1975, 1984, 1987, 2001) and the observed interannual variability of glacier mass balance is, in principle, reproduced by REMO$_{\texttt{glacier}}$ except for the period 1986 to 1995 (correlation coefficient $r = 0.66$ / 0.67 / 0.67 between GlacA / GlacB / GlacC and observations for the period 1961-2003). The amplitude of interannual mass balance variations is, however, underestimated by the model. This can at least partly be explained by the relatively small number of individual glaciers with mass balance measurements in the Dyurgerov and Meier (2005) sample (less than 20 in any balance period). In contrast, $\bar{b}_n$ in the simulations is based on the entire Alpine glacier cover, i.e., on a much larger sample of individual glaciers, which can be thought to generally dampen interannual fluctuations.

Due to the single-cuboid concept (see Chapter 4.2.2) the glacier mass balance is not allowed to vary on a subgrid scale in REMO$_{\texttt{glacier}}$. However, as accumulation and ablation processes are simulated independently for each glaciated grid box, glacier mass balance can be subject to a pronounced spatial variability on the resolved scale (for instance, due to differences in the atmospheric forcing). This fact is reflected by a varying percentage f_{area} of the total glaciated area in the Alps experiencing a positive mass balance in the respective balance year (Figure 5.12). The time series of f_{area} basically follows the temporal evolution of the mean specific mass balance (Figure 5.10). In years of positive mean Alpine mass balance more than 60% of the total glaciated area in the Alps have a positive balance value (e.g., 1975, 1978, 1984). On the other side, in the year 1964 with its high glacier mass loss, less than 10% of the total glaciated area show a positive mass balance (or, vice versa, more than 90% of

[2] At this point it has to be noted that the estimate of mean cumulative Alpine glacier mass balance as derived from Dyurgerov and Meier (2005) clearly differs from the estimate of Zemp et al. (2006a, see also Figure 2.12). Averaging mass balance values of nine Alpine "reference" glaciers, Zemp et al. (2006a) computed a mean cumulative mass balance of about -13 m w.e. for the period 1967-2001. For the same period of time the mean cumulative mass balance as derived from Dyurgerov and Meier (2005) only amounts to -4.05 m w.e., i.e., a considerably smaller glacier mass loss. The difference between both data sources can be explained by sampling effects and by the area-weighting applied in order to obtain mean mass balance values. For instance, the dataset of Dyurgerov and Meier (2005) includes a number of large glaciers (e.g., Grosser Aletschgletscher, Mer de Glace, Rhonegletscher) which dominate the average value due to their large surface area but which are not contained in the underlying dataset of Zemp et al. (2006a). The estimate of Dyurgerov and Meier (2005), which is used for validation purposes in the present study, should therefore be seen as a lower boundary of the probable "real" Alpine glacier mass loss in the last two decades. The differences between both datasets also clearly highlight the large uncertainty associated with estimates of mean regional glacier mass balance.

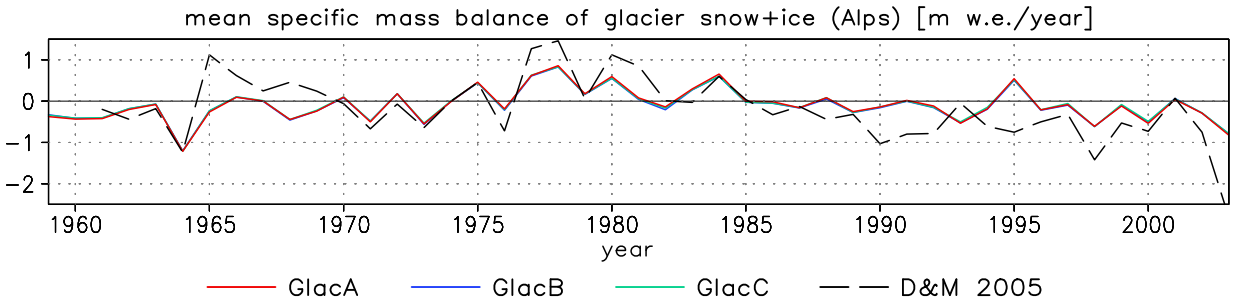

Figure 5.10: Mean specific mass balance $\overline{b}_n$ [m w.e./year] for the entire Alpine area as simulated by the three baseline simulations (GlacA, GlacB, GlacC) and as compiled by Dyurgerov and Meier (2005, D&M 2005).

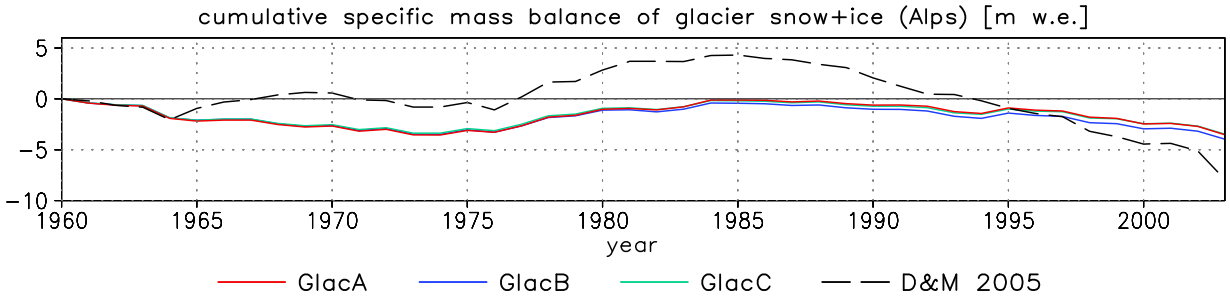

Figure 5.11: Mean cumulative specific mass balance $\sum \overline{b}_n$ [m w.e.] for the entire Alpine area as simulated by the three baseline simulations (GlacA, GlacB, GlacC) and as compiled by Dyurgerov and Meier (2005, D&M 2005).

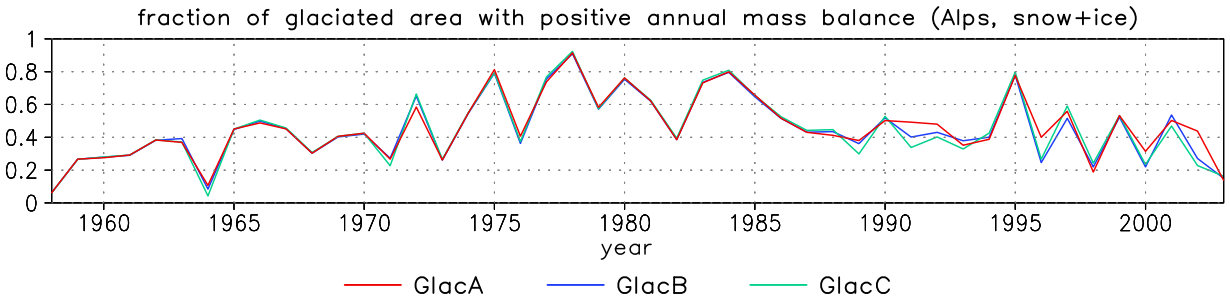

Figure 5.12: Fraction f_{area} of the total glaciated area in the Alps experiencing a positive mass balance in the respective balance year in the three baseline simulations.

the glaciated area experience net ablation).

Main Catchments

Similarly to the presented procedure for the entire Alps, the simulated mean specific mass balance has also been calculated separately for the four main Alpine catchments. Observation-based time series of $\overline{b}_n$ on a catchment basis are, however, not available from Dyurgerov and Meier (2005).

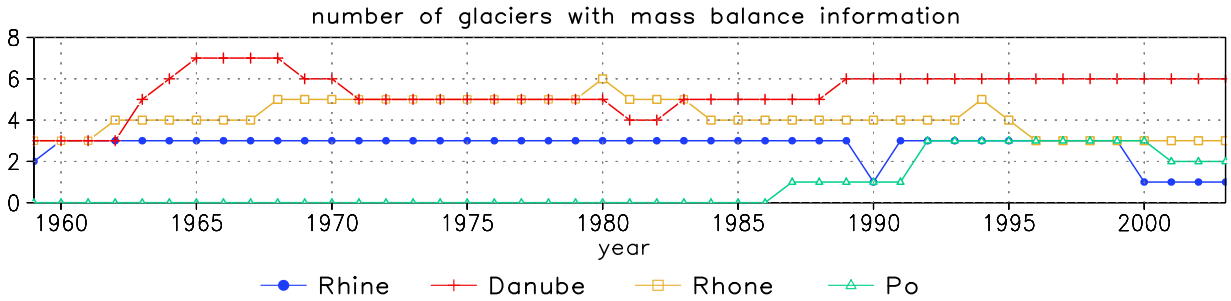

Figure 5.13: Number of glaciers in the four main Alpine catchments with annual mass balance information available in Dyurgerov and Meier (2005).

Therefore, individual glacier mass balance values have been extracted from the same source and have been weighted by the respective glacier surface area in order to obtain time series of mean specific mass balance for the four investigated Alpine catchments. Figure 5.13 shows the number of individual glaciers with mass balance information available in the respective balance year and the respective catchment. Simply speaking, the accuracy of and the confidence in the calculated catchment mean of $\overline{b}_n$ decreases with a decreasing number of contributing glaciers. For the Po catchment the database contains no single surveyed glacier until the balance year 1987. A better data coverage exists in the Danube and in the Rhone catchment where, in any balance year, mass balance information from at least three surveyed glaciers is available.

The comparison of the simulated and the observation-based time series of $\overline{b}_n$ (Figure 5.14) and $\sum \overline{b}_n$ (Figure 5.15) reveals a number of similarities as well as some clear shortcomings of the model simulations:

Rhine catchment

During the first half of the simulation period (until about 1980), simulated mass balances are relatively close to the observation-based values, though the model shows a positive bias in most years. Especially the interannual variability of $\overline{b}_n$ is realistically reproduced. Comparatively large deviations occur in the following period from about 1980 to 1995, in which the observed negative mass balances are not captured by the model. This fact is reflected in the strong positive bias of the simulated mean cumulative mass balance $\sum \overline{b}_n$ (Table 5.2 and Figure 5.15). While, at the end of the investigated period, the observation-derived dataset shows a negative cumulative balance of -7.81 m w.e. (i.e., a net mass loss in case of a constant total glacier area) all simulations produce a positive cumulative balance of more than +9 m w.e. (i.e., a net mass gain).

Danube catchment

While the model shows a relatively good skill in reproducing the observed mass balances from 1958 until about 1978, the observed mass loss in the last two decades of the 20$^{\text{th}}$ century is clearly underestimated. Consequently, the simulated cumulative mass balance for the entire period (-6.63 to -7.76 m w.e.) is considerably less negative than the cumulative balance as derived from the observations (-15.81 m w.e., Table 5.2). Compared to the Rhine catchment the interannual variability of both the simulated and the observed annual

mass balance is significantly smaller.

Rhone catchment
A relatively good agreement between simulated and observation-based annual mass balances exists until about 1987. Still, the observed mass balance is underestimated in most years. Similarly to the Rhine and the Danube catchment the strong glacier mass loss towards the end of the century is not accurately reproduced and glacier mass balances are overestimated by the model. The same is true for the cumulative mass balance for the entire period (-3.16 to -3.91 m w.e. compared to -7.92 m w.e., Table 5.2 and Figure 5.15).

Po catchment
The assessment of the model performance in the Po catchment is difficult as observation-based mass balance information is only available from 1987 onwards and the validation period is comparatively short. Furthermore, the observational dataset only relies on a small number of individual glaciers (1 to 3, see Figure 5.13). If, however, the observation-derived mass balance values are trusted in, the model performs relatively well in the last 17 years of the simulation and roughly reproduces the observed glacier mass loss. The simulated cumulative mass balance for the period 1987 to 2003 (-10.04 to -14.57 m w.e.) is relatively close to the observation-based value (-11.08 m w.e., Table 5.2 and Figure 5.15). The simulated mass balance is negative in most years and the glacier mass loss is therefore comparatively strong. In contrast to the other catchments, notable differences of the simulated glacier mass balance occur between the three baseline simulations. Up from about 1987 GlacA shows a larger glacier mass loss than GlacB and GlacC. This probably has to be attributed to relatively large differences in the total glaciated area of the Po catchment between GlacA on one side and GlacB / GlacC on the other side (see Chapter 5.2.2).

Sensitivities

Interannual fluctuations in glacier mass balance are primarily controlled by variations in temperature and precipitation, although the primary source of energy for glacier melt is solar radiation (Oerlemans, 2005). An important characteristic of the climate-glacier relationship is the mass balance sensitivity of a glacier, i.e., the change of $\overline{b}_n$ as a reaction to variations in a certain climatic parameter (see also Chapter 2.7.3). In order to analyse the corresponding relationships in REMO$_{\texttt{glacier}}$ the simulated annual specific mass balance $\overline{b}_n$ (catchment mean values) has been related to various forcing parameters, including precipitation and air temperature.

- **2m Temperature**
  The simulated mean specific mass balance shows a clear dependency on the mean summer (April - September) air temperature (Figure 5.16): The higher the temperature the larger the glacier mass loss. In all baseline simulations and for all investigated catchments a significant linear relation between both parameters exists. The Pearson product moment correlation coefficient r is negative in all cases (inverse relationship) and ranges from -0.50 (Rhine catchment, GlacC) to -0.75 (Rhone

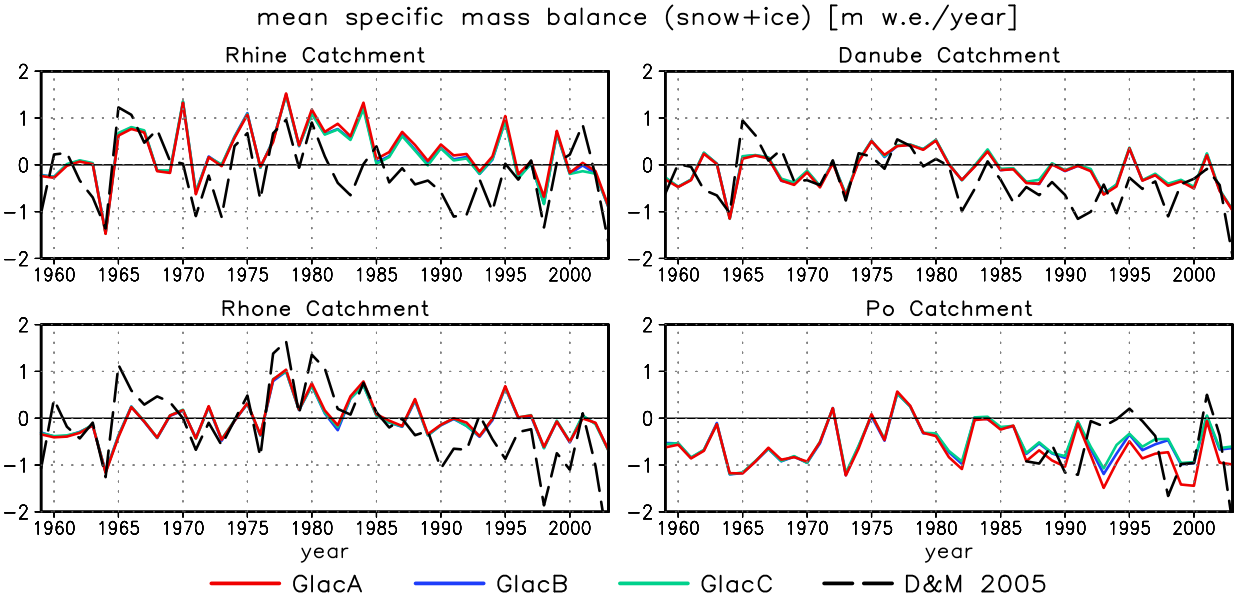

Figure 5.14: Mean specific mass balance $\overline{b}_n$ [m w.e./year] for the main Alpine catchments as simulated by the three baseline simulations (GlacA, GlacB, GlacC) and as computed from mass balance data compiled by Dyurgerov and Meier (2005, D&M 2005).

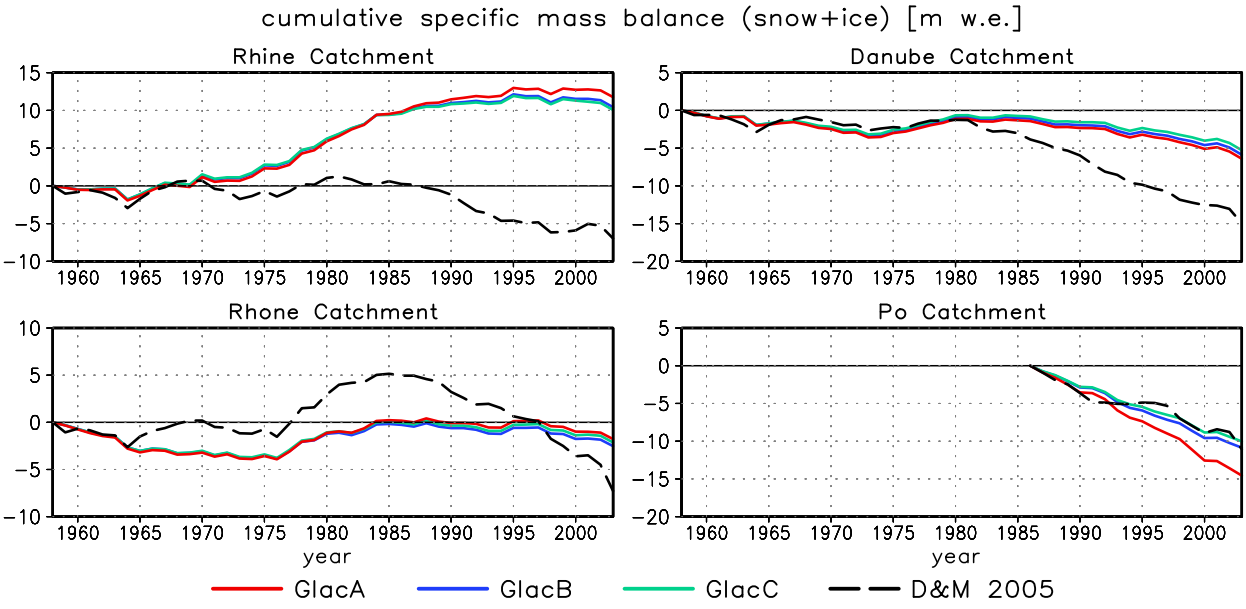

Figure 5.15: Mean cumulative specific mass balance $\sum \overline{b}_n$ [m w.e.] for the main Alpine catchments as simulated by the three baseline simulations (GlacA, GlacB, GlacC) and as computed from mass balance data compiled by Dyurgerov and Meier (2005, D&M 2005).

catchment, all simulations)[3]. These values correspond well to those found by Braithwaite and Zhang (2000) for four Swiss glaciers based on observational data (-0.58 to -0.70). The slope of the linear regression curve, expressed by the regression coefficient b, is largest in the Rhone and lowest in the Po catchment. For a given catchment it only varies little between the three simulations, except for the Po. Here, GlacA shows a considerably steeper slope which is due to the larger glacier mass loss towards the end of the century compared to GlacB and GlacC (see above). The regression coefficient b ranges from -0.27 to -0.47 m w.e./°C and can, with some care, be interpreted as the climate sensitivity of simulated glacier mass balance with respect to mean summer air temperature. This range roughly corresponds to the sensitivity of glacier mass balance to summer temperature as derived from Oerlemans and Reichert (2000) and Reichert et al. (2001a) for the two Alpine glaciers Hintereisferner ($\sim$ -0.35 m w.e./°C) and Rhonegletscher ($\sim$ -0.34 m w.e./°C)[4]. Applying multiple linear regression, Braithwaite and Zhang (2000) derived larger mass balance sensitivities with respect to mean JJA (June - August) air temperature of -0.44 to -0.64 m w.e./°C for four Swiss glaciers. The sensitivities obtained by the application of a degree-day model for the same sample of glaciers are even higher (-0.69 to -0.89 m w.e./°C).

Hence, there is some indication that the mass balance sensitivity with respect to summer air temperature is underestimated in $\text{REMO}_{\texttt{glacier}}$. A higher summer temperature leads to a decrease of the simulated mass balance (enhanced mass loss), but this decrease is not as pronounced as it could be expected based on modelling studies for individual glaciers. However, it has to be noted that the mass balance sensitivity in $\text{REMO}_{\texttt{glacier}}$ as derived by linear regression is not a "pure" sensitivity with respect to air temperature as it might, implicitly, also include changes in atmospheric parameters other than temperature. For instance, summer temperature in $\text{REMO}_{\texttt{glacier}}$ is negatively (though less strongly) correlated with total annual precipitation in all catchments (not shown). A high summer temperature is therefore often associated with below-average annual precipitation sums which, simply speaking, leads to less snow accumulation and a larger net glacier mass loss.

▷ **Precipitation**

A clear positive relation exists between the simulated mean specific mass balance and mean annual precipitation (Figure 5.17). The correlation coefficients r range from 0.60 (Po catchment, GlacB and GlacC) to 0.85 (Rhine catchment, GlacC) and are significant in all cases. They are larger than those found by Braithwaite and Zhang (2000) for four Swiss glaciers analysing observational data (0.39 to 0.61). The corresponding regression coefficients b which can, again, be interpreted as mass balance sensitivities with respect to changes in annual precipitation are largest for the Rhine and the Rhone catchment (0.0324 to 0.0326 m w.e./1% and 0.0211 to 0.0220 m w.e./1%, respectively) and lowest in the Danube and Po catchment (0.0176 to 0.0178 m w.e./1% and 0.0155 to 0.0184 m w.e./1%, respectively). Except for GlacA in the Po catchment, the values of b only slightly differ between the three simulations. Especially in case of the Rhine catchment the obtained values of b tend to overestimate those calculated by other authors for individual

[3]The dependency of glacier mass balance on the mean **annual** 2m temperature is less pronounced (not shown here). Values of r range from -0.15 to -0.56 and are significant (99% confidence level) only in the Po catchment.

[4]The mentioned studies are based on modelled mass balance sensitivities with respect to monthly perturbations in temperature. The sensitivity of $\bar{b}_n$ to mean summer temperature, as presented here, has been derived by summing up the respective monthly sensitivities for the months April to September.

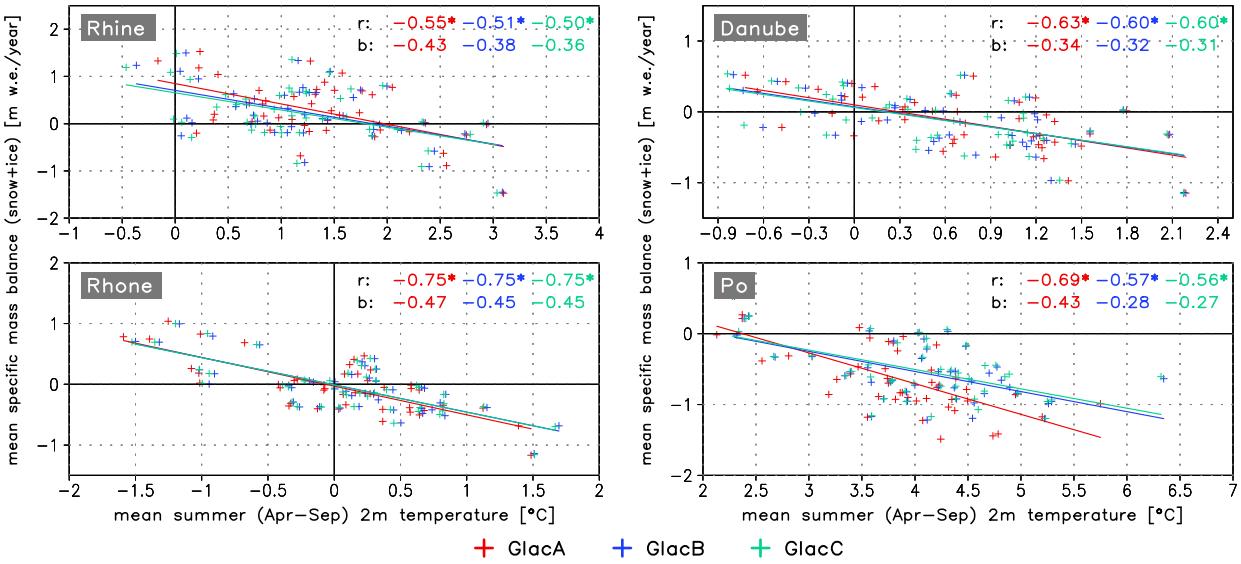

Figure 5.16: Relation between mean summer (April-September) 2m temperature [°C] and mean annual specific mass balance $\bar{b}_n$ [m w.e./year] for the three baseline simulations and the four main Alpine catchments. Values correspond to catchment mean values, weighted by the respective glaciated grid box area. r: correlation coefficient (the $\star$ indicates a significant linear correlation, 99% confidence level). b: regression coefficient, i.e. slope of line of best fit.

Alpine glaciers (e.g., 0.17 m w.e./10% for Griesgletscher by Braithwaite et al. (2002), 0.14 to 0.17 m w.e./10% for Morteratschgletscher by Klok and Oerlemans (2004), $\sim$ 0.25 m w.e./10% for Hintereisferner by Oerlemans and Reichert (2000), $\sim$ 0.26 m w.e./10% for Rhonegletscher by Reichert et al. (2001a); the last two values have again been calculated by summing up monthly sensitivities as extracted from the respective studies).

Hence, in contrast to the temperature sensitivity of glacier mass balance (see above), the dependency of $\bar{b}_n$ with respect to precipitation seems to be overestimated in REMO$_{\texttt{glacier}}$. An increase in the annual precipitation sum leads to a comparatively large increase of the simulated mass balance. Generally, the sensitivity of glacier mass balance to a 10% change in precipitation has been found to roughly follow the same spatial pattern as the sensitivity to a 1°C temperature change (i.e., clearly decreases from maritime to continental conditions; see also Chapter 2.7.3) but to be of opposite sign and much smaller (Braithwaite et al., 2002; Braithwaite and Zhang, 2000). Consequently, very large precipitation increases between 25 and 40% would be needed to offset the effects of a 1°C temperature increase (Braithwaite et al., 2002; Oerlemans, 2005). In REMO$_{\texttt{glacier}}$, according to the calculated values of the regression coefficient b, an increase in annual precipitation of less than 20% would be sufficient in all catchments. This means that the effect of interannual variations of precipitation on the simulated glacier mass balance is probably too large compared to the influence of variations in air temperature.

▷ **Snow Accumulation**

The link between total precipitation (rain + snow) and glacier mass balance is established via the direct relation between precipitation and the accumulation of snow on a glacier's surface. This process mainly takes place in wintertime, but can also become important during summer (see Chapter 2.4.2). In contrast to snowfall, an increase of precipitation in the form of rain has

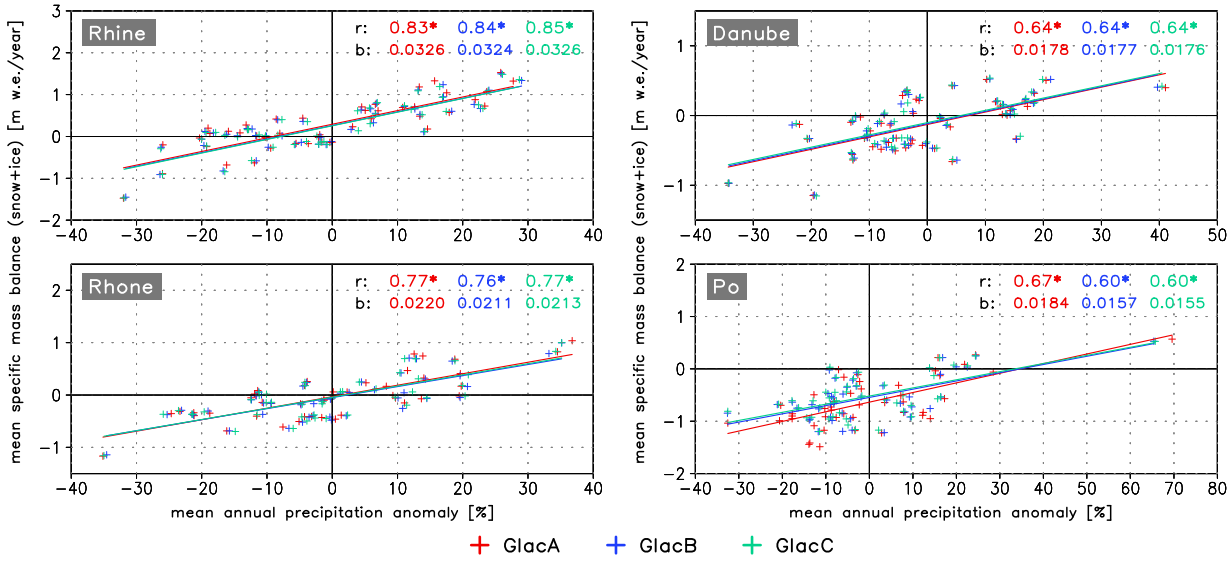

Figure 5.17: Relation between annual (October-September) total precipitation anomaly [%] and mean annual specific mass balance $\overline{b}_n$ [m w.e./year] for the three baseline simulations and the four main Alpine catchments. Values correspond to catchment mean values, weighted by the respective glaciated grid box area. r: correlation coefficient (the $\star$ indicates a significant linear correlation, 99% confidence level). b: regression coefficient, i.e. slope of line of best fit.

no direct influence on a glacier's mass balance. Therefore, the relation between annual snow accumulation and glacier mass balance can be expected to be even stronger than that for annual precipitation and mass balance. In $\text{REMO}_{\texttt{glacier}}$ this is the case: The simulated glacier mass balance shows a strong positive correlation with annual snow accumulation which is significant in all catchments and for all baseline simulations (Figure 5.18). The correlation coefficient r ranges from 0.80 (Danube and Po catchment) to values as high as 0.91 (Rhine catchment). If snow accumulation is expressed in terms of the annual sum (and not as anomaly with respect to the mean value) the slope of the regression curve b varies between 1.17 and 1.44 m w.e./ m w.e. and is similar for all cases except GlacA in the Po catchment. Values of b larger than 1.0 generally denote an amplified increase in glacier mass balance compared to the "pure" effect of an increase of snow accumulation. This result can partly be explained by the albedo effect, i.e., the fact that snow has a higher albedo than ice. An increase in snowfall does not only directly increase accumulation (by the respective snow water equivalent) but also reduces the amount of absorbed solar radiation and thus melt rates, leading to an amplification of the net mass balance signal (see Chapter 2.4.2). Apart from this, years of high snow accumulation tend to have comparatively low summer temperatures in $\text{REMO}_{\texttt{glacier}}$ (weak negative correlation between mean summer temperature and annual snow accumulation; not shown) which also amplifies the net mass balance signal via a reduction of summer ablation.

The strong dependence of glacier mass balance on the annual snow accumulation is also clearly illustrated by a comparison of the temporal evolution of both parameters over the entire Alpine region (Figure 5.19, only shown for GlacA). The corresponding correlation coefficient amounts to 0.86. Hence, the relation is considerably stronger than the dependence of glacier mass balance on the annual sum of precipitation ($r = 0.72$).

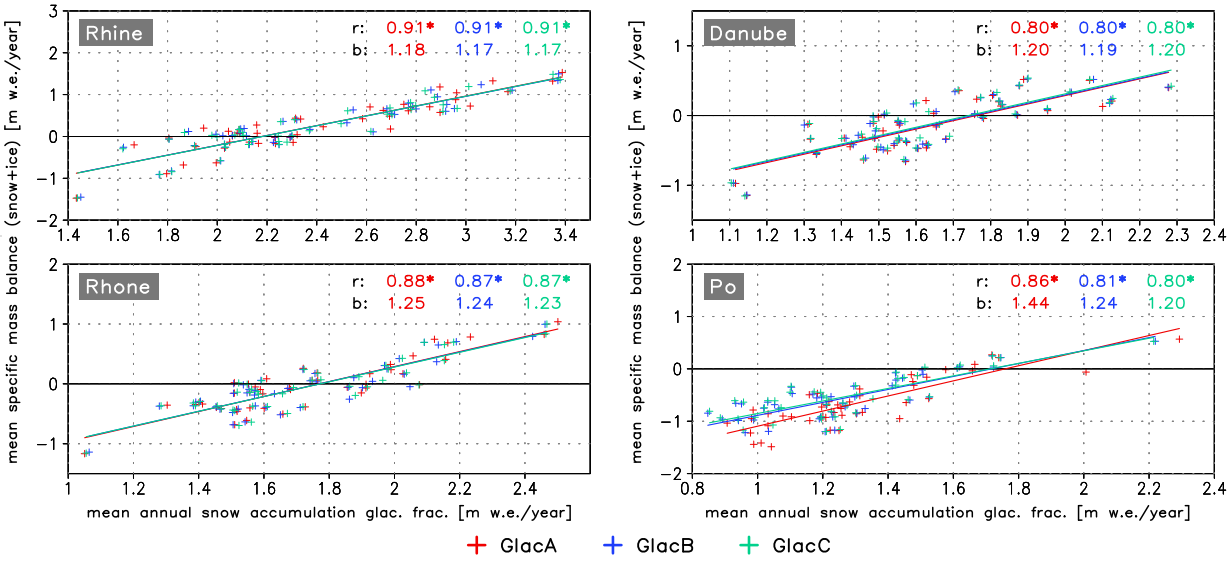

Figure 5.18: Relation between annual (October-September) snow accumulation on glaciated fraction [m w.e./year] and mean annual specific mass balance $\bar{b}_n$ [m w.e./year] for the three baseline simulations and the four main Alpine catchments. Values correspond to catchment mean values, weighted by the respective glaciated grid box area. r: correlation coefficient (the ★ indicates a significant linear correlation, 99% confidence level). b: regression coefficient, i.e. slope of line of best fit.

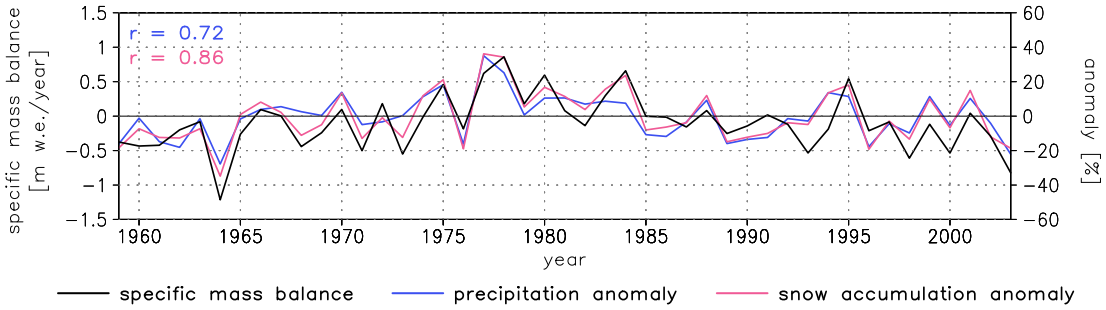

Figure 5.19: Temporal evolution of the simulated mean Alpine glacier mass balance [m w.e./year] and the anomalies of annual precipitation and annual snow accumulation [%] as simulated by GlacA.

▷ **Radiation**

On most glaciers, solar radiation typically provides the largest part of the available melt energy, the flux of sensible heat towards the glacier surface is usually much smaller (see Chapter 2.4). Hence, the relation between air temperature and glacier mass balance is often primarily an indirect one. It is established via the influence of air temperature on the fraction of precipitation falling as snow and via the positive relationship between (summer) air temperature and incoming solar radiation. The latter is also found in $\text{REMO}_{\texttt{glacier}}$ (not shown) and, as expected, glacier mass balance is also significantly correlated to the annual mean of incoming solar radiation (Figure 5.20). Correlation coefficients range from 0.41 (Po catchment, GlacC) to 0.68 (Rhine catchment, GlacB and GlacC). The relation between glacier mass balance and incoming thermal radiation is less strong (not shown).

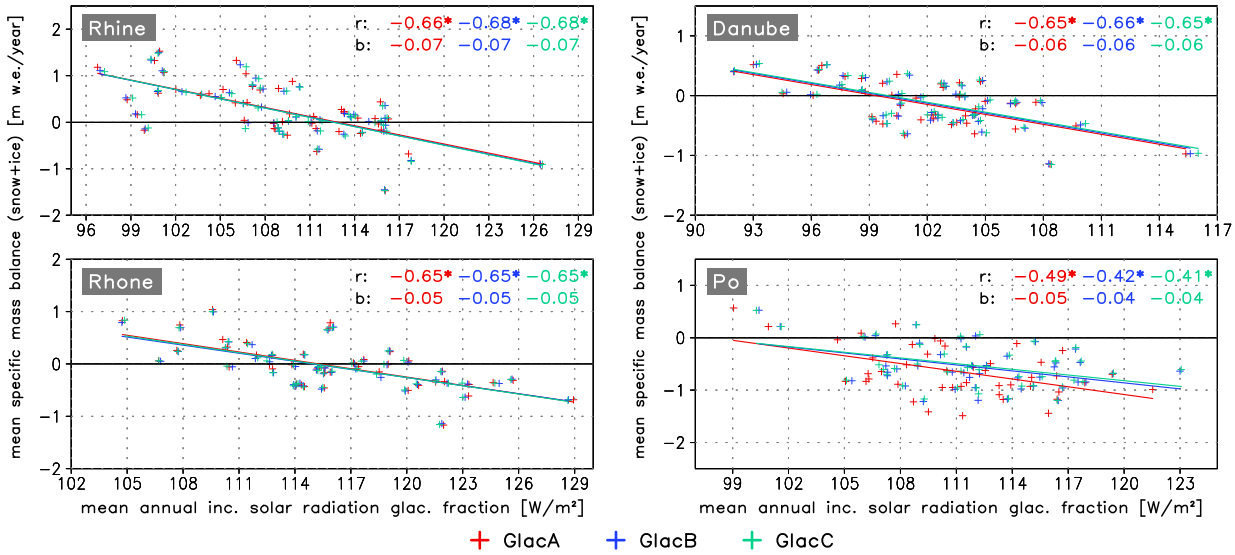

Figure 5.20: Relation between mean annual (October-September) incoming solar radiation on glaciated fraction [W/m^2] and mean annual specific mass balance $\overline{b}_n$ [m w.e./year] for the three baseline simulations and the four main Alpine catchments. Values correspond to catchment mean values, weighted by the respective glaciated grid box area. r: correlation coefficient (the $\star$ indicates a significant linear correlation, 99% confidence level). b: regression coefficient, i.e. slope of line of best fit.

Synthesis: Glacier Mass Balance

In general, the temporal evolution of the simulated mean Alpine glacier mass balance is in good accordance with the observation-based dataset of Dyurgerov and Meier (2005). This is especially true for the first half of the investigated period (1958 to about 1985). Towards the end of the 20$^{\text{th}}$ century the strong mass loss of Alpine glaciers is systematically underestimated by REMO$_{\texttt{glacier}}$. Also the catchment-based analysis reveals a comparatively good performance of the model in the first half of the simulated period. However, a common feature of all catchments except the Po catchment with its relatively small glacier surface area is the clear underestimation of the observed glacier mass loss towards the end of the century. Especially in the Rhine catchment the cumulative mass balance over the entire period is strongly overestimated. Only small differences occur between the three baseline simulations, i.e., the simulated mean specific mass balance only slightly depends on the choice of a specific area adjustment method. Distinct differences only occur in the Po catchment towards the end of the century. Concerning the sensitivity of the simulated mass balance with respect to atmospheric quantities, a clear dependency on mean annual precipitation and on snow accumulation exists. These parameters exert the primary control on interannual variations of $\overline{b}_n$. Probably, their influence is overestimated by the model. In contrast, the sensitivity of the simulated glacier mass balance with respect to summer air temperature appears to be too low.

5.2.2 Ice Area and Ice Volume

Entire Domain

In December 2003, after 46 years of continuous model simulation, both glacier area and glacier volume in the Alps have considerably decreased with respect to the initial state in all three baseline simulations (Figure 5.21, Table 5.3). The total loss of glacier area from 1958 to 2003 lies between -17.1% (GlacC) and -23.6% (GlacA). In all experiments a major loss of ice area occurs during the first part of the simulation from 1958 until about 1975 as a result of negative mass balances (compare to Figure 5.10). In the following period of strongly positive annual mass balances the total ice area increases and reaches a secondary maximum in 1986. The increase is far less pronounced in GlacA than in GlacB and GlacC. This phase approximately corresponds to the documented stabilisation and advance period of Alpine glaciers in the 1970s and 1980s (e.g., Zemp, 2006, see also Chapter 2.7.5). Towards the end of the simulation negative mass balances again cause a decrease of total ice cover which is clearly less pronounced than in the first part of the simulation. While the temporal evolution of the total ice area is similar in GlacB and GlacC (i.e., in those simulations which rely on an area adjustment method based on individual glaciers), GlacA shows a stronger overall reduction of glacier area up from about 1970. Two basic features of the model formulation are responsible for this discrepancy:

- The non-linear character of the underlying volume-area relationships (Equations 4.13 and 4.16) and the corresponding increase of the mean ice depth $\overline{h}$ with increasing glacier area A (see Figure 4.13). Due to these characteristics a given mean grid box mass balance (i.e., an imposed change in ice thickness) leads to different changes in total ice area depending on whether the thickness change is applied to the entire glacier cuboid (with a comparatively large area; GlacA) or to each individual glacier in the respective grid box (with comparatively small areas; GlacB and GlacC).
- In GlacA the parameter c in Equation 4.13 is not equal to the default value of 0.206 (as it is the case in GlacB and GlacC) and can, in principle, vary form grid box to grid box (see Chapter 4.2.8).

Besides percentage changes in the total ice area A_{tot} and the total ice volume V_{tot} for the entire simulated period (1958-2003) Table 5.3 also shows the respective changes for the sub-periods 1958-1972 and 1973-2000. After the first 15 years of model simulation the decrease of A_{tot} ranges from -14.5% (GlacB) to -16.0% (GlacA). In December 1972 the total ice area in GlacA, GlacB and GlacC amounts to 2754, 2804 and 2786 km^2, respectively. These values can now be compared to the total Alpine glacier area as derived from the WGI which is assumed to be representative for the year 1973 (see Chapter 5.1.3). This area is 3040 km^2, it is considerably larger than the simulated values. Therefore, if the scaling of the WGI glacier areas (which has been carried out in order to obtain glacier areas for the year 1958, see Chapter 5.1.3) is assumed to be valid, the simulated loss of ice area from 1958 to 1972 is too large (-14.5 to -16.0% compared to -7.3% obtained from area scaling). Furthermore, the simulated loss of ice area from 1973 to 2000 can be compared to the estimates of Paul et al. (2004b) and Zemp et al. (2006b). Both studies are based on the WGI and the satellite-

derived Swiss glacier inventory of the year 2000 (Paul, 2004) and estimate a total loss of Alpine glacier area from 1973/1975 to 1998/2000 of about -22%. The simulated area loss only ranges from -0.6% (GlacC) to -5.7% (GlacA). Hence, the strong and accelerating retreat of Alpine glaciers in the last two decades of the 20th century is clearly underestimated by REMO$_{\texttt{glacier}}$. From 1973 to 2000 the total Alpine ice volume even slightly increases in all simulations (see below) which is contradictory to the estimated net mass loss (e.g., Paul et al., 2004b). Also, the total loss of ice area from 1958 to 2000 is underestimated by REMO$_{\texttt{glacier}}$: For the three baseline simulations it amounts to -20.8%, -16.5% and -15.5%, respectively, compared to -27.7% as derived from the combination of the area scaling (1958-1972) and the estimate of Paul et al. (2004b) and Zemp et al. (2006b) (1973-2000).

Generally, the evolution of the total ice volume contained in the model domain clearly follows the changes in ice area which is, basically, a direct consequence of the monotonous character of the underlying volume-area relationships. For any individual REMO grid box in GlacA and for any individual glacier in GlacB and GlacC the relation between ice area A and ice volume V is unambiguous and strictly monotonous. However, due to

- ▷ the non-linear character of the volume-area relationships (Equations 4.16 and 4.13)
- ▷ sampling effects, like the coexistence of growing and shrinking glaciers / grid box cuboids of different size and the varying number and size of glaciers / grid box cuboids forming the same total ice area at different points in time

this is not necessarily the case if the total ice area A_{tot} and the total ice volume V_{tot} in the entire model domain (or in individual catchments) are analysed. Therefore, it is possible that an identical value of A_{tot} can be associated with different total ice volumes as it is, for instance, the case for GlacB and GlacC around 1976 and 1995. Furthermore, it is possible that A_{tot} decreases between two points in time while V_{tot} increases (GlacA between 1975 and 2003). This uncommon behaviour is a direct result of the implemented area adjustment methods and of the spatial distribution of the simulated glacier mass balance. It has to be considered as a shortcoming of the model formulation.

Another point which is astonishing at first sight is the fact that in all simulations the percentage decrease of A_{tot} between 1958 and 2003 is larger than the decrease of V_{tot} (Table 5.3). If the mean ice thickness in the entire domain $\overline{h}_{tot}$ is defined as V_{tot} divided by A_{tot} a larger percentage decrease of A_{tot} implies an increase of the mean ice thickness $\overline{h}_{tot}$. Again, this feature has to be attributed to sampling effects when averaging ice and area and ice volume over a larger region (see above). Especially the simulated disappearance of glaciers in only slightly glaciated grid cells with a small ice thickness (see below) contributes comparatively more to area loss than to volume loss. For any individual REMO grid box in GlacA and for any individual glacier in GlacB and GlacC, the relation between ice area A and mean ice thickness $\overline{h}$ is strictly monotonous and a decrease of ice area would always be accompanied by a decrease of the mean ice thickness (see Figure 4.13). The larger simulated percentage decrease of the total ice area compared to the decrease of the total ice volume for the period 1958 to 2003 is questionable and, again, indicates shortcomings in the model formulation. It is commonly assumed that the percentage loss of Alpine glacier volume exceeds the corresponding loss of ice area since 1850 and that, accordingly, also the mean glacier thickness over the entire Alps decreased as a result of predominantly negative mass balances (e.g., Haeberli and Hoelzle, 1995;

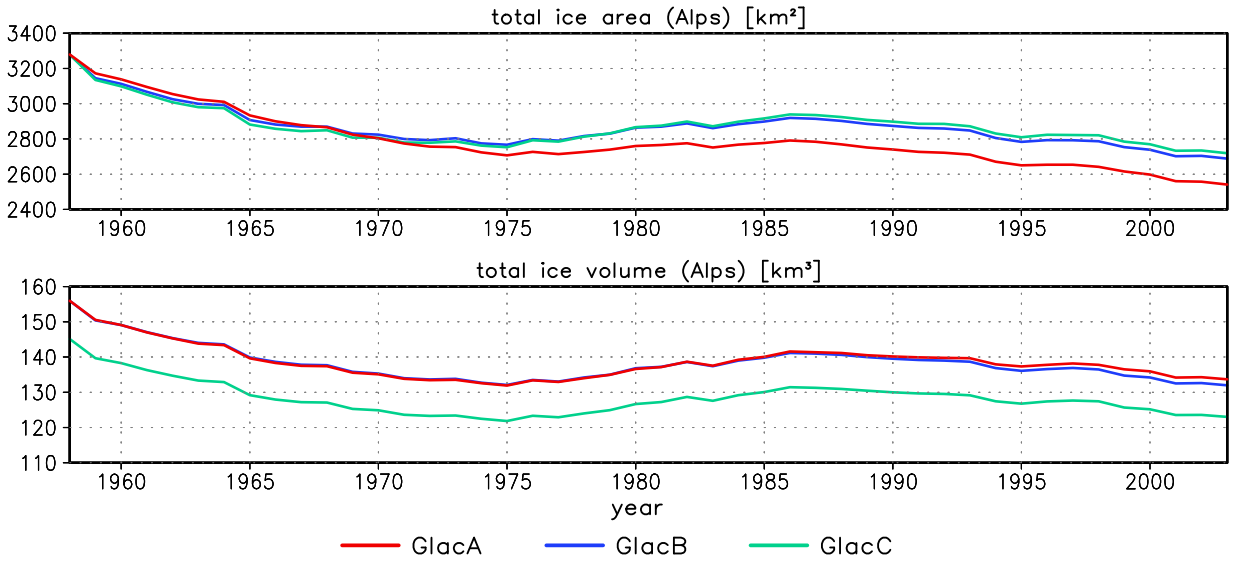

Figure 5.21: Evolution of the total ice area A_{tot} [km^2] (upper panel) and the total ice volume V_{tot} [km^3] (lower panel) in the Alps in the three baseline simulations (values refer to the beginning of the respective year).

Simulation	$\triangle A$ [%]			$\triangle V$ [%]		
	1958-2003	1958-1972	1973-2000	**1958-2003**	1958-1972	1973-2000
GlacA	**-23.6**	-16.0	-5.7	**-15.5**	-14.4	+1.8
GlacB	**-18.1**	-14.5	-2.3	**-16.7**	-14.8	+0.3
GlacC	**-17.1**	-15.0	-0.6	**-16.7**	-15.0	+1.5

Table 5.3: Simulated changes of total ice area ($\triangle A$) and total ice volume ($\triangle V$) in the entire model domain for the three periods 1958-2003, 1958-1972 and 1973-2000 (January of first year to December of last year) in the three baseline simulations.

Haeberli et al., 2002; Paul et al., 2004b; Zemp et al., 2006a).

The temporal evolution of the total ice volume in the model domain is similar for all model simulations.[5] From about 1990 onward the volume reduction is slightly smaller in GlacA compared to GlacB and GlacC. This discrepancy results from the smaller total ice area in GlacA during this period while the specific mass balances are comparable to GlacB and GlacC (Figure 5.10).

Main Catchments

Figures 5.22 and 5.23 show the evolution of the total ice-covered area and the total ice volume for the main Alpine catchments. In all catchments and in all simulations a strong decrease of the glacier area is simulated until about 1975 (in the Rhine catchment the minimum is already reached in the late 1960s). From then on, strong differences between the four catchments appear. In the Rhine and the Rhone catchment, i.e., in the north-western and western parts of the Alps, a strong increase of glacier

[5] Note that, due to the application of the volume-area relation after Maisch (1992) instead of the power law, the total ice volume at initialisation is lower in GlacC than in GlacA and GlacB (see Chapter 5.1.3).

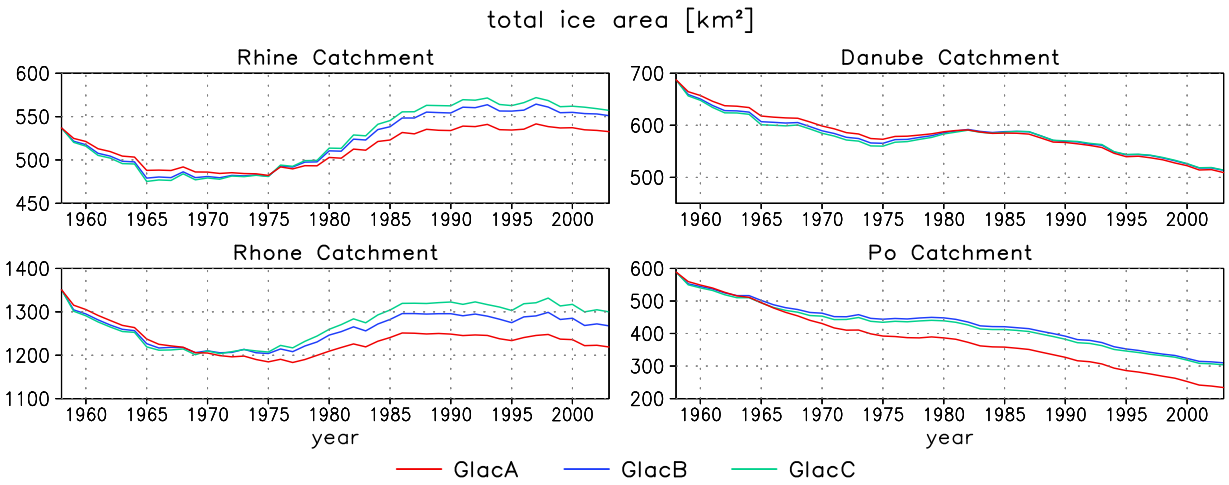

Figure 5.22: Evolution of the ice area A [km^2] in the main Alpine catchments in the three baseline simulations (values refer to the beginning of the respective year).

Simulation	$\triangle A_{1958-2003}$ [%]				$\triangle V_{1958-2003}$ [%]			
	Rhine	Danube	Rhone	Po	Rhine	Danube	Rhone	Po
GlacA	-2.4	-27.4	-10.6	-61.5	+15.5	-19.9	-8.0	-62.6
GlacB	+2.5	-25.4	-6.2	-47.5	+12.4	-18.7	-9.7	-63.3
GlacC	+3.6	-25.4	-3.9	-48.5	+12.8	-18.7	-9.3	-66.0

Table 5.4: Ice area change $\triangle A$ and ice volume change $\triangle V$ from 1958 to 2003 for the main Alpine catchments in the three baseline simulations.

area is simulated until the mid 1990s, following predominantly positive net mass balances in this period (Figure 5.14). Afterwards, negative mass balances again cause a slight decrease of the ice area towards the end of the simulation. However, the minimum of the mid-1970s is not reached anymore, i.e., a net increase of glacier area from about 1975 to 2003 is simulated. GlacB and GlacC even simulate a net increase of glacier area for the Rhine catchment for the entire simulated period 1958-2003 (Table 5.4). In contrast to this, the ice-covered area in the Danube and Po catchment (southern and north-eastern parts of the Alps) strongly decreases in the course of the model simulation. Largest and continuous losses of ice area are simulated for the Po catchment (more than -45% from 1958-2003, Table 5.4) as a result of strongly negative mass balances. Except for the Danube catchment the ice-covered area at the end of the simulation is lowest in GlacA.

Again, the evolution of the total ice volume approximately follows the variations of the ice-covered area. A special feature appears in the Rhine catchment, though. While a net decrease of ice volume is simulated for the Danube, Rhone and Po catchments for the entire period (more than -60% in the Po), the Rhine catchment shows an increase in ice volume of more than 12% (Table 5.4). This fact is consistent with the positive cumulative specific mass balance $\sum \bar{b}_n$ simulated for this catchment (Table 5.2).

The results described above point to the fact that the overall underestimation of the Alpine glacier area and volume loss in the 1980s and 1990s in REMO$_{\texttt{glacier}}$ is primarily due to the evolution of both

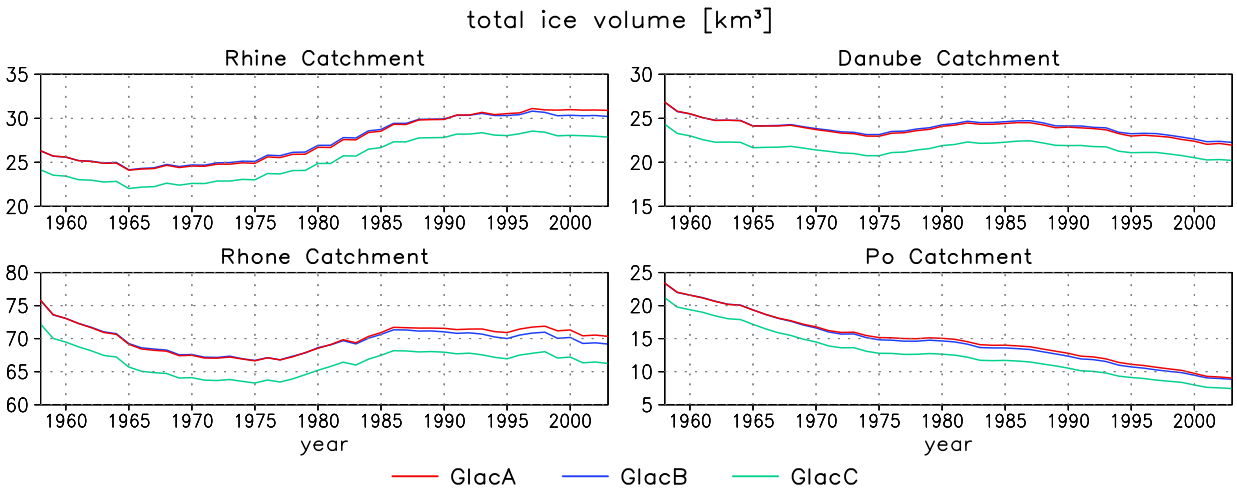

Figure 5.23: Evolution of the ice volume V [km^3] in the main Alpine catchments in the three baseline simulations (values refer to the beginning of the respective year).

parameters in the Rhine and the Rhone catchment. For both catchments a net increase of ice area and volume is simulated up from the mid 1970s. This increase is associated with a clear positive bias of the simulated mass balance compared to the observation-based estimates (Figure 5.14). In contrast, the simulated area and volume loss in the Danube and especially in the Po catchment seem to be much closer to the observed rates. The inter-catchment differences are most pronounced between the Rhine (increase of area and volume, except for the area in GlacA) and the Po catchment (strong decrease of both area and volume). Recalling the sensitivities of the simulated glacier mass balance with respect to the atmospheric forcing parameters the large discrepancy between both catchments can be explained by the considerably higher amount of snow accumulation and, at the same time, a lower temperature level in the Rhine catchment (see x-axis scale in Figures 5.16 and 5.18). As a result of the pronounced differences in the evolution of the total ice area between the four catchments, the percentage contribution to the total Alpine glacier cover is shifted towards the Rhine and Rhone catchment in the course of all three baseline simulations (not shown).

Grid Box Scale

Besides investigating the simulated changes in ice area and ice volume on the scale of the entire Alps or on catchment scale, the analysis can also be carried out for the individual REMO$_{\texttt{glacier}}$ grid boxes. This approach gives a much more detailed picture of the spatial variability of the simulated glacier area and volume changes as well as of the underlying processes.

Figure 5.24 shows the spatial distribution of the net changes of ice area from the beginning until the end of the respective simulation. The majority of the glaciated grid boxes experiences a strong net loss of ice area. In contrast, a number of grid cells in the north-western part of the Alps as well as in the central part show a considerable increase of ice area of more than 100%. The general picture of glacier area change, i.e., the spatial distribution of grid boxes with net gain and with net loss of ice area, is very similar between the three simulations. Only in boxes with a net decrease of ice area

the percentage loss is usually larger in GlacA than in GlacB and GlacC and amounts up to -100% (total loss of glacier cover). This is especially true in the south-western part of the Alpine ridge and is consistent with the stronger decrease of the total ice area in GlacC (Figure 5.21). By combining the horizontal distribution of ice area changes with the regional topography (Figures 5.25 and 5.26) a more detailed analysis of the topographical control on the simulated glacier area change is possible. Those grid boxes experiencing a net gain in ice area (and ice volume) are exclusively located along the northern Alpine ridge as defined by the model topography. All grid boxes south of the main ridge, i.e., the entire Po catchment, show a net decrease of glacier area (and volume). The general spatial distribution of ice volume changes is very similar to the changes of ice area (i.e., grid boxes with a net increase of ice area also show a gain of ice volume and vice versa) and the differences between the three simulations are considerably less pronounced (not shown).

The described changes of the glaciated grid box area directly lead to changes in the glaciated grid box fraction a. In many areas south of the main Alpine ridge the ice cover virtually disappears and values of a close to 0 are reached by the year 2003 (Figure 5.27). However, maximum values of more than 0.4 are still present and isolated areas in the north- western and central part of the Alps show an increase of the glaciated grid box fraction (following the increase in the total grid box ice area, see above). The percentage change in a (and thus the percentage change in the glaciated grid box area A) does not strictly depend on the glaciated grid box area at initialisation (Figure 5.28). While the three grid boxes with the largest ice area at initialisation (> 140 km^2) experience a net loss of glacier area in all simulations, grid boxes with an intermediate initial degree of ice cover (90-140 km^2) show a net gain. Again, grid boxes with an initial ice cover of less than 90 km^2 mostly show a substantial decrease of the glaciated area, which amounts up to -100% for a large number of grid cells. Furthermore, some boxes (north of the main Alpine ridge, not shown) with a very small initial glacier area experience a very strong increase of ice area due to predominantly positive mass balances (not shown). The latter points to shortcomings in the simulated atmospheric forcing, especially in the amount of snow accumulation, or in the parameterisation scheme itself (snow redistribution) since a strong growth of glaciers in only slightly glaciated areas in the Alps during the second half of the 20$^{\text{th}}$ century has not been observed in reality.

Synthesis: Ice Area and Ice Volume

In all baseline experiments both the total glaciated area and the total ice volume in the model domain considerably decrease from 1958 to 2003 (area: -17.1 to -23.6%, volume: -15.5 to -16.7%). Largest loss rates occur in the first part of the simulations until about 1975, followed by a growth period in the late 1970s and the 1980s. This phase approximately corresponds to the documented stabilisation and advance period of Alpine glaciers. The subsequent period of strong and accelerating glacier retreat towards the end of the 20$^{\text{th}}$ century is not fully reproduced by REMO$_{\texttt{glacier}}$. The observed loss of ice area in the Alps is clearly underestimated by the model which is primarily caused by a net growth in the Rhine and the Rhone catchment. Especially grid boxes along the northern slopes of the main Alpine ridge experience a pronounced net gain in ice area and volume.

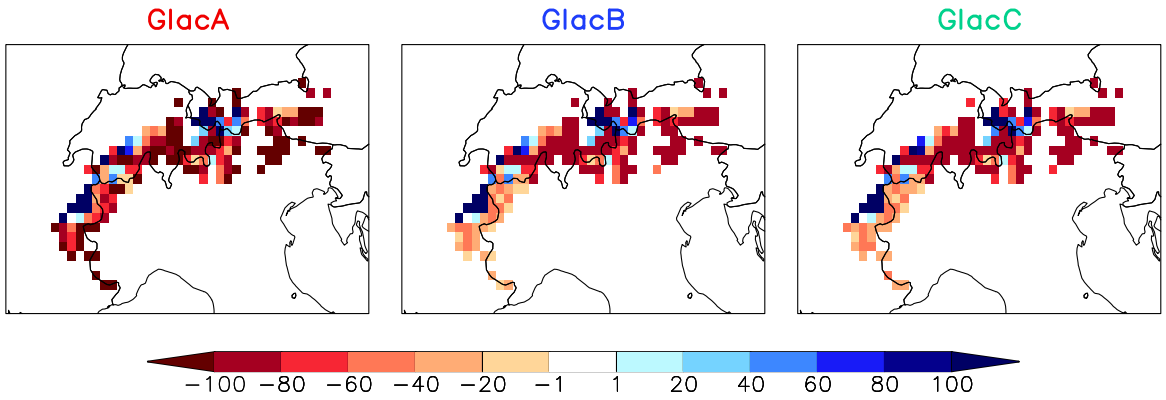

Figure 5.24: Net change of the glaciated grid box area (1958-2003) [%] for the three baseline simulations. Note that only the central part of the model domain is shown (compare to Figure 5.1).

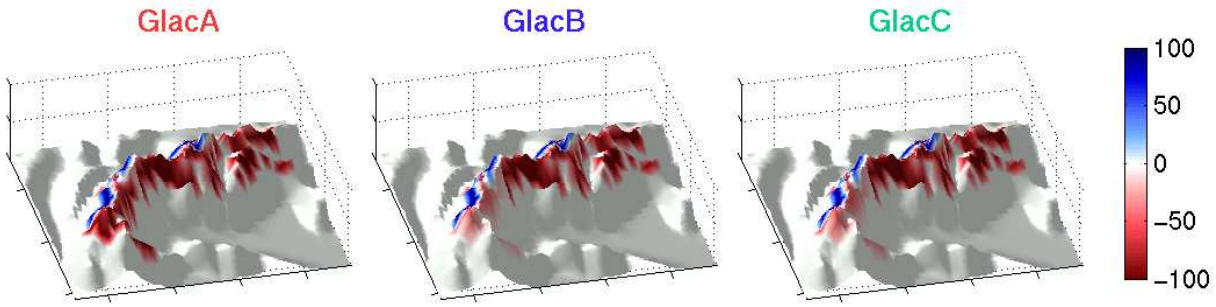

Figure 5.25: REMO orography (view from South-West) coloured by the net change of the glaciated grid box area (1958-2003) [%] for the three baseline simulations. Note that only the central part of the model domain is shown.

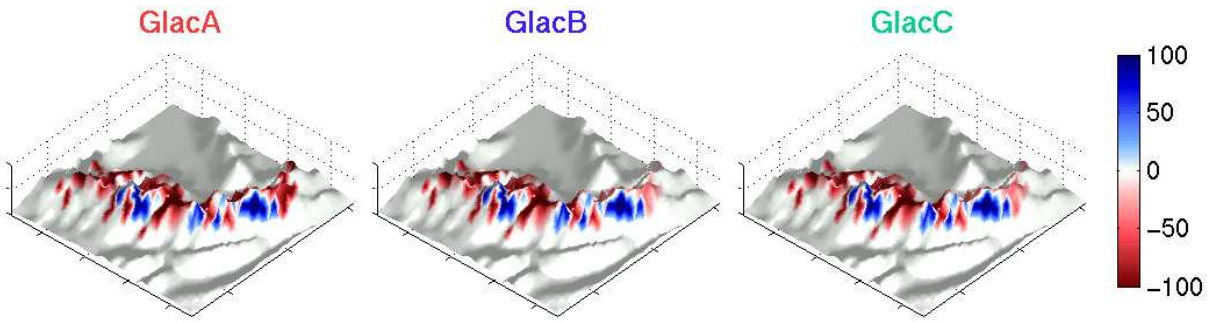

Figure 5.26: REMO orography (view from North-West) coloured by the net change of the glaciated grid box area [%] from the beginning to the end of the three baseline simulations. Note that only the central part of the model domain is shown.

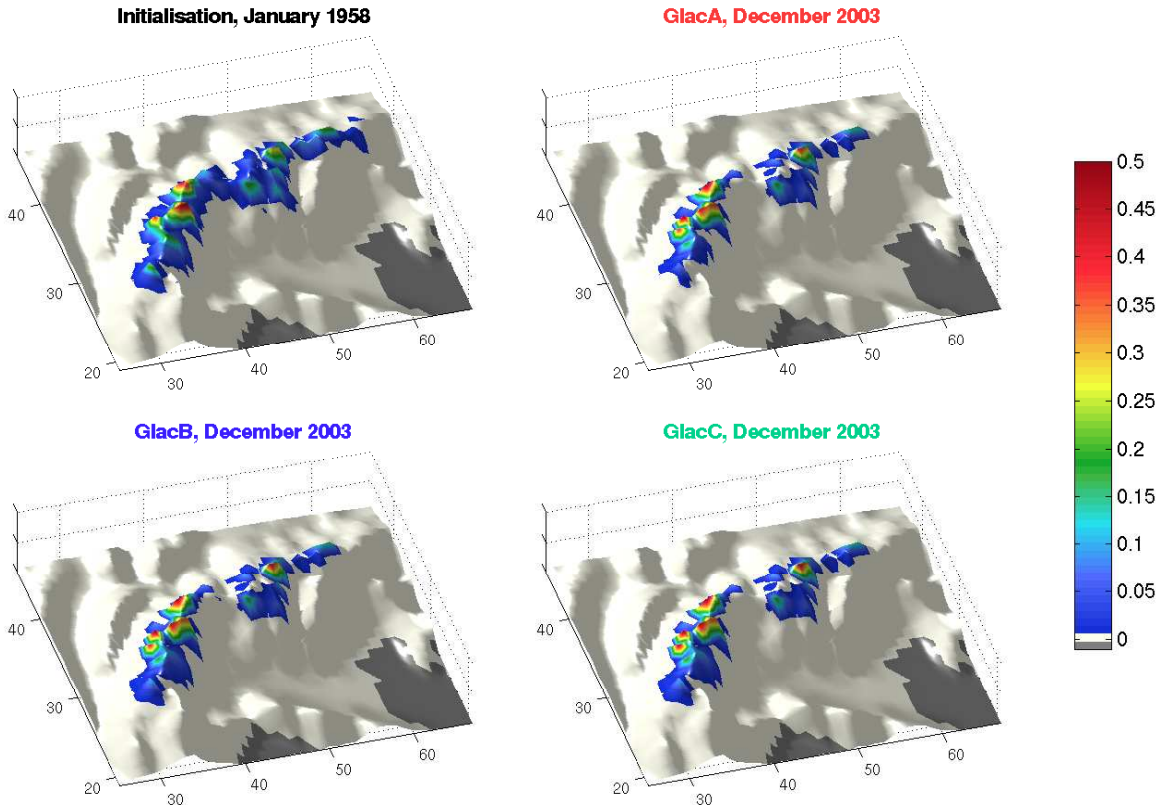

Figure 5.27: REMO orography (view from South-West) coloured by the glaciated grid box fraction a at initialisation (January 1958, upper left) and at the end of the three baseline simulations (December 2003). Note that only the central part of the model domain is shown.

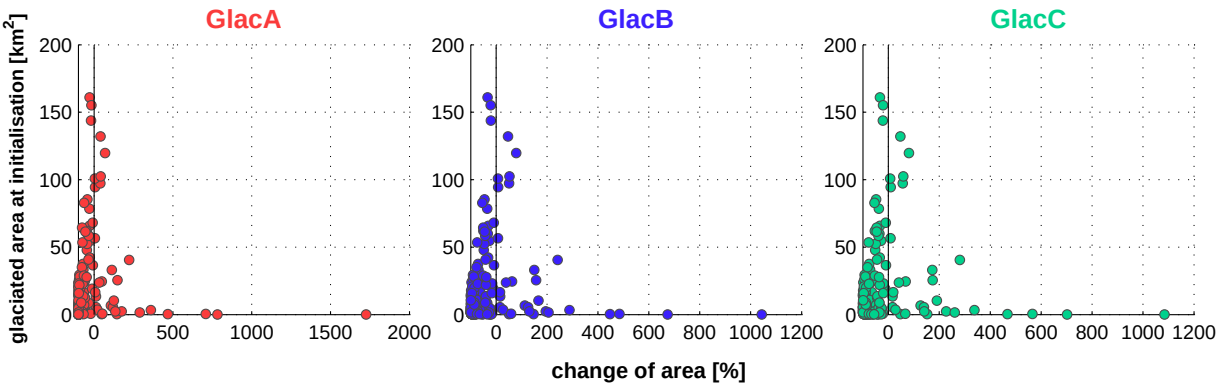

Figure 5.28: Percentage change of glaciated area from January 1958 to December 2003 versus glaciated grid box area at initialisation [km^2] for the three baseline simulations. Each circle represents one single REMO$_{\texttt{glacier}}$ grid box. Note the differing x-axis scale.

5.2.3 Number of Glaciers

In contrast to GlacA, information on the surface area and ice volume of all individual glaciers that contribute to the ice cuboid in a glaciated grid box is kept in the simulations GlacB and GlacC. After each year of model simulation the area adjustment is carried out based on individual glaciers. During this process, glaciers can completely disappear if the respective grid box experienced a negative mass balance $\overline{b}_n$ during the last balance period and if a glacier's thickness is smaller than $|\overline{b}_n|$. Vice versa, new glaciers can be created in formerly non-glaciated grid boxes (see Chapter 4.2.8). Hence, the total number of glaciers in the model domain is allowed to vary in time and can be traced in GlacB and GlacC (Figure 5.29).

In both simulations the number of individual glaciers decreases with time, but the reduction is far less pronounced in GlacC (5268 to 5051, -4.1%) than in GlacB (5268 to 3826, -27.4%). At first sight this large difference between the two simulations is astonishing since the simulated specific mass balance is very similar (see above). However, if one recalls the underlying volume-area and ice thickness-area relationships and especially when investigating the glacier size distributions (Figure 5.30) the phenomenon becomes clearer. The individual glacier areas in GlacC are based on the relationship after Maisch (1992) in which the mean thickness $\overline{h}$ of glaciers approaching a surface area of 0 is still larger than 10.6 m (Equation 4.15). In the (theoretical) case of a glacier with a surface area of 0 the mean ice thickness would still be 10.6 m. From a natural point of view this behaviour is not realistic and leads to a strong persistence of small glaciers with a comparatively large ice thickness in

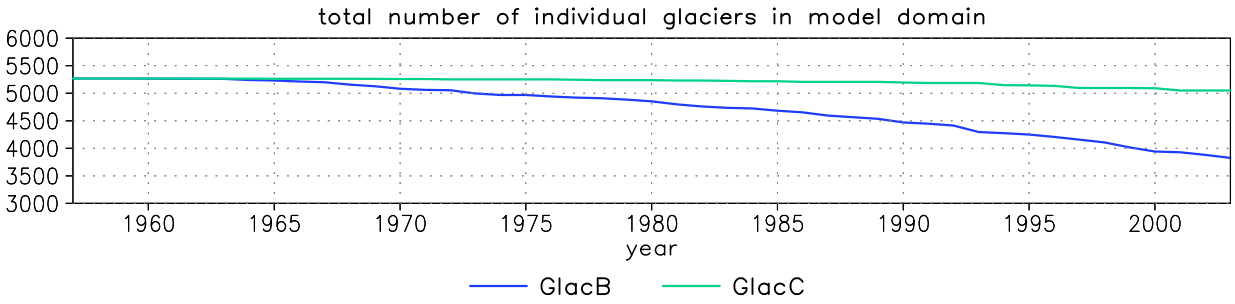

Figure 5.29: Temporal evolution of the total number of glaciers in the entire model domain (simulations GlacB and GlacC).

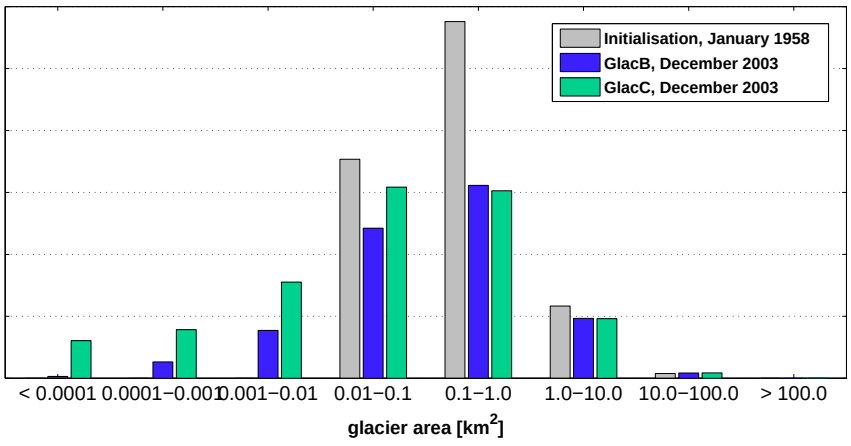

Figure 5.30: Total number of glaciers in different size classes at model initialisation (grey) and at the end of the simulations GlacB (blue) and GlacC (green).

the course of the model simulation. This is reflected in the high number of glaciers with areas of less than 0.1 km^2 in GlacC (Figure 5.30). Practically, these glaciers can only disappear if the mean ice thickness or the total ice surface area in a grid box falls below a critical threshold as implemented in REMO$_{\texttt{glacier}}$ (0.1 m w.e. or 1/10000 of total grid box area, respectively). But, due to their very small surface area, these glaciers only contribute little to the total grid box ice volume and have a negligible influence on the simulated grid box mass balance. In GlacB, on the other hand, the mean ice thickness $\overline{h}$ approaches 0 for a shrinking surface area (Equation 4.14) and small glaciers can disappear more rapidly.

5.2.4 Discussion

The analysis of the simulated Alpine glacier cover as presented above reveals that the interannual variability and the general magnitude of glacier mass balance in the second half of the 20$^{\text{th}}$ century can be approximately reproduced by the model. This is true both for the entire Alpine area and for individual catchments. Still, large biases appear in individual years especially towards the end of the century. The strong observed glacier mass loss in this period is not captured by the model simulations, resulting in a clear positive bias of the cumulative mass balance in most areas by the year 2003. In this respect, the most striking feature is the net growth of glaciers in the Rhine catchment compared to the observed glacier mass loss. There is some indication that these shortcomings of the modelled glacier mass balance are related to inaccuracies in snow accumulation. The latter is determined by the amount of solid precipitation as simulated by the atmospheric component of the RCM and the subsequent redistribution of snowfall on a subgrid scale. It is the main factor determining the simulated annual glacier mass balance $\overline{b}_n$ in REMO$_{\texttt{glacier}}$. Generally, the sensitivity of $\overline{b}_n$ with respect to precipitation seems to be overestimated while the influence of air temperature is comparatively weak. This fact is presumably in parts responsible for the underestimation of the observed glacier mass loss in the warm period up from about 1980, which results in an underestimation of the decrease of the glaciated area towards the end of the century. In the Rhine catchment, two baseline simulations even show a net increase of the glaciated area during the 46 years of continuous model simulation which is mainly caused by a strong growth of glaciated surfaces on the north-facing slopes of the main Alpine ridge. Again, the clear dependency of the simulated area changes on the location of the grid cell with respect to the main ridge points to shortcomings in the simulated amount of snowfall. Generally, the amount of (solid) precipitation can be assumed to strongly differ between north-west- and south-east facing slopes depending on the direction of atmospheric flow, triggering distinct topographic signals of glacier mass balance.

A further point which presumably contributes to the underestimation of the observed glacier mass loss towards the end of the 20$^{\text{th}}$ century is the assumption of a uniformly distributed snow layer on top of the glacier cuboids and the neglection of the equilibrium line concept (i.e., the coexistence of accumulation and ablation areas on the same glacier). Figure 5.31 shows the temporal evolution of the fraction of the total glaciated area in the four main Alpine catchments which is permanently covered by snow in the experiment GlacA (snow depth > 0 m w.e. in all months of the respective year). As a consequence of comparatively large amounts of snow accumulation in the 1970s this fraction is close to 100% in the Rhine and the Danube catchment in the second half of the simulated period. This means that in this period the glacier cuboids are almost entirely covered by a snow layer and the ice

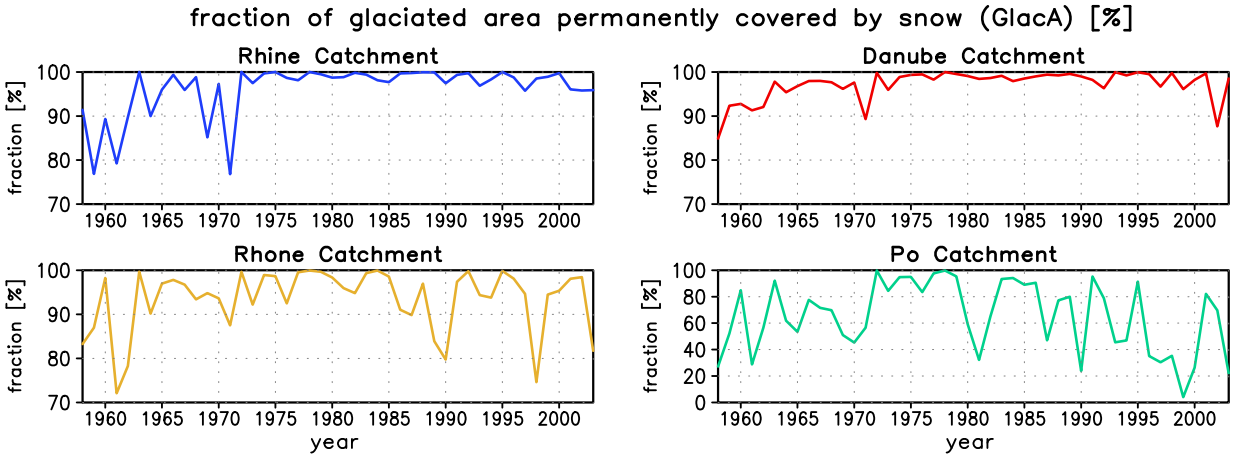

Figure 5.31: Evolution of the permanently snow-covered fraction of the total glaciated area [%] in the four main Alpine catchments in the baseline simulation GlacA (snow depth > 0 m w.e. in all months of the respective year).

cuboids themselves do not get exposed, not even in summer and autumn. Hence, ablation on the glaciated grid box fractions in mainly due to snow melt. The enhancement of ablation due to the exposure of the darker ice surfaces after the winterly snow layer has melted (snow and ice albedo feedback, see Chapter 2.7.2), a process which takes place in the ablation zone of real-world glaciers in almost every year, only occurs in a small number of $\text{REMO}_{\texttt{glacier}}$ grid boxes in this period. In principle, this fact can lead to an underestimation of ablation rates and, hence, to an overestimation of the net balance. Towards the very end of the simulation period, the snow depths on the glaciated grid box fractions considerably decrease (i.e., the snow which has accumulated during the previous years diminishes following predominantly negative glacier mass balances, see Figure 5.14) and the glacier cuboids start to get exposed again. This allows the feedback mechanism described above to come into play again, which could trigger enhanced ice ablation in the period after 2003.

In terms of the simulated mass balance, the choice of a specific area adjustment method in $\text{REMO}_{\texttt{glacier}}$ only has a minor influence on the model results. Clear differences between the experiments GlacA, GlacB and GlacC only occur in the case of the simulated evolution of the glaciated area in the Alps. The net decrease of glacier area in the course of the model simulation is most pronounced in the simulation GlacA. Given the general underestimation of net glacier area loss, GlacA obviously performs most realistic in this respect. This indicates that the consideration of individual glacier areas and volumes (as it is done in GlacB and GlacC) is not mandatory in the current model setup.

5.3 Simulated Climate

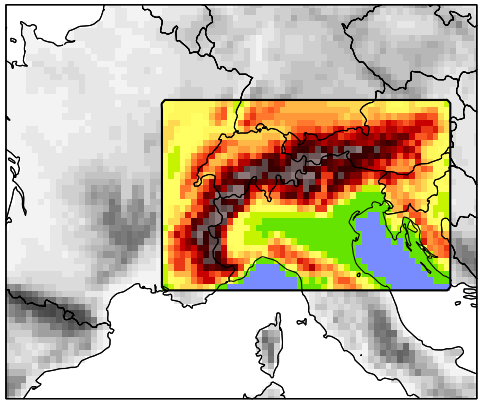

Figure 5.32: Location of the sub-domain "Alps" (coloured part) in which the validation of the simulated atmospheric parameters has been carried out.

As the new glacier parameterisation scheme has been fully implemented into the RCM REMO the atmospheric forcing for the calculation of glacier mass and energy balance is directly derived from the model's atmospheric component (including a number of modifications of atmospheric parameters in order to account for subgrid effects, see Chapter 4). Therefore, any bias in an atmospheric parameter involved in glacier mass and energy balance with respect to observations will inevitably influence the behaviour of the glaciated grid box fraction. Even if a perfect functioning of the glacier parameterisation scheme itself is assumed (e.g., the general applicability of the cuboid concept, a realistic description of subgrid variability of atmospheric parameters and an appropriate description of glacier-atmosphere interactions) a biased atmospheric forcing would still lead to errors in the simulated glacier mass balance. On the other hand, errors in the imposed atmospheric parameters (e.g., precipitation) could compensate for shortcomings of the glacier parameterisation scheme itself (e.g., subgrid snow redistribution) and thereby lead to a realistic simulation of glacier mass balance despite a biased atmospheric forcing on a grid box scale. The same is true for errors in more than one atmospheric parameter which, in principle, could compensate each other (e.g., too high temperatures vs. too large amounts of precipitation).

Hence, in order to assess the performance of the new glacier parameterisation scheme it is necessary to validate the simulated climatic parameters involved in glacier mass and energy balance. The following section will focus on precipitation, air temperature and incoming solar radiation which have been identified as strongly influencing the interannual variability of glacier mass balance (Chapter 5.2.1) and for which observational data is available. The validation of the atmospheric parameters has not been carried out for the entire REMO model domain but focusses on a sub-domain covering the Alpine region as well as parts of the surrounding forelands (Figure 5.32). In the following section this area is simply referred to as the "Alps". In some cases it has additionally been subdivided into three altitudinal belts based on the underlying REMO orography (grid box altitude < 1000, 1000-2000 and > 2000 m a.s.l.).

5.3.1 Precipitation

Observational Datasets

For the validation of the simulated precipitation two gridded observational datasets have been used:

- **CRU TS 2.1** (referred to as CRU)
  The CRU TS 2.1 dataset (Mitchell et al., submitted) comprises monthly grids of five climatic parameters (precipitation, temperature, cloud cover, diurnal temperature range and vapour pres-

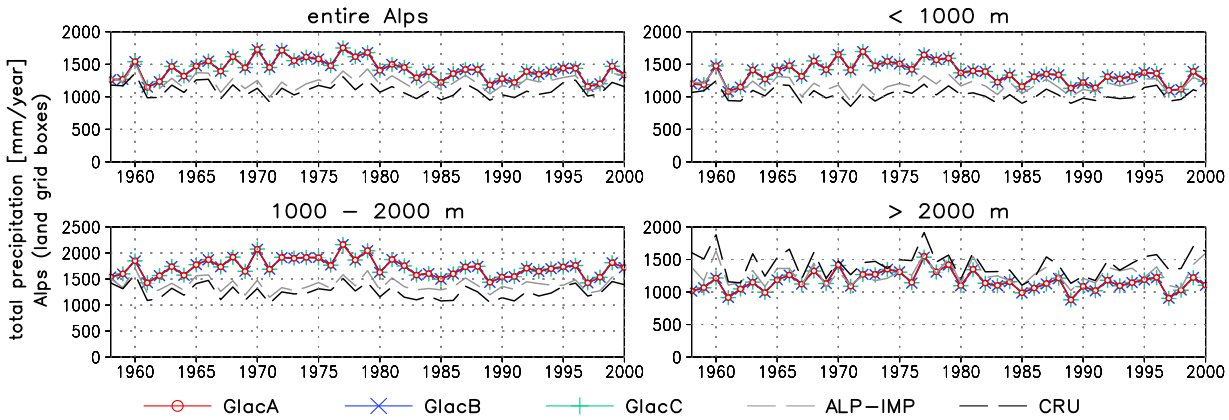

Figure 5.33: Spatial mean of total precipitation (1958-2000) [mm/year] for the entire Alpine region (land grid boxes only) and three altitudinal intervals as simulated by the three baseline simulations (GlacA, GlacB, GlacC) and as derived from two observational datasets (ALP-IMP, CRU).

sure) for the period 1901-2000. It has been been developed by the Climate Research Unit (CRU) of the University of East Anglia and covers the European land surface at a regular 10 min ($^1/_6^\circ$) resolution. This roughly corresponds to the rotated $^1/_6^\circ$ resolution used for all REMO simulations within the present study. The basic methodology for constructing a regular grid of a climate parameter out of an irregular station network is described in New et al. (2000). For validation purposes the original regular $^1/_6^\circ$ CRU precipitation dataset for the sub-period 1958-2000 was conservatively interpolated to the rotated $^1/_6^\circ$ REMO grid. The monthly precipitation sums in the CRU dataset are not corrected for the systematic bias of rain-gauge measurements, the most significant of which is undercatch of solid precipitation (snowfall; New et al., 2000).

▷ **ALP-IMP / HISTALP** (referred to as ALP-IMP)
The ALP-IMP/HISTALP precipitation dataset provides monthly precipitation totals for the period 1800-2003 (Efthymiadis et al., 2006). It has been developed within the ALP-IMP project and covers the so-called "Greater Alpine Region" (4-19°E, 43-49°N) on a regular 10 min ($^1/_6^\circ$) grid. The dataset is mainly based on 192 long-term, homogenised precipitation series from meteorological stations across the study domain (HISTALP station-mode dataset; Auer et al., 2005) and a high-resolution gridded precipitation climatology for the period 1971-1990 (Schwarb, 2000). Within the present study only the sub-period 1958-2000 has been investigated. The precipitation sums of the original $^1/_6^\circ$ grid were conservatively interpolated to the rotated $^1/_6^\circ$ REMO grid prior to the analysis. The ALP-IMP/HISTALP dataset does not account for the systematic bias of rain-gauge measurements.

Entire Alps

The comparison of the temporal evolution of simulated and observed annual precipitation for the period 1958-2000 for the entire Alps (Figure 5.33, upper left panel) reveals a systematic positive bias of $\text{REMO}_{\text{glacier}}$ which is strongest in the late 1960s and the 1970s (up to +45%). In this

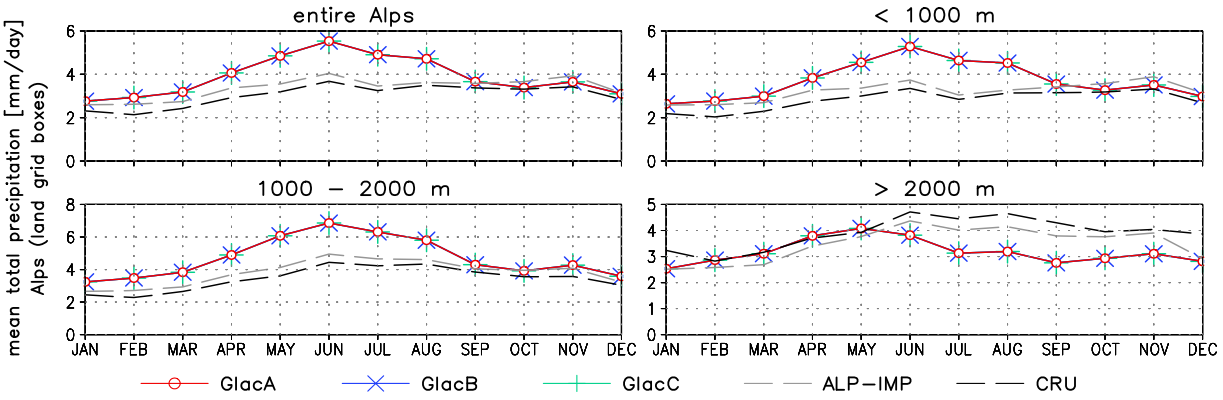

Figure 5.34: Climatological spatial mean of monthly precipitation (1958-2000) [mm/day] for the entire Alpine region (land grid boxes only) and three altitudinal intervals as simulated by the three baseline simulations (GlacA, GlacB, GlacC) and as derived from two observational datasets (ALP-IMP, CRU).

respect, it has to be considered that both observational datasets do not account for the systematic rain-gauge undercatch. The interannual variability of the observed precipitation sums is relatively well captured by the model. While the simulated amount of precipitation does not differ between the three REMO simulations (i.e., the use of a specific area adjustment method has virtually no influence on the simulated precipitation) the two observational datasets slightly differ from each other (higher amounts of precipitation in the ALP-IMP dataset). Looking at the mean precipitation for the three altitudinal belts (Figure 5.33, upper right and lower panels) it becomes evident that the positive bias of the simulated precipitation sums is mainly due to an overestimation in grid boxes with an altitude of less than 2000 m a.s.l., which cover more than 93% of the total area under investigation and thus dominate the Alpine mean value. In grid cells above this altitude the observed amounts of precipitation are slightly underestimated by the model. This negative bias at high-altitude grid boxes primarily stems from an underestimation of precipitation of up to 35% in summer, autumn and winter (June to January, Figure 5.34, lower right panel).[6] On the other hand, the general positive bias at grid boxes below 2000 m is due to a clear overestimation of precipitation of up to 50% in spring and especially in summer (Figure 5.34, upper right and lower left panels). The described shortcomings, i.e., an overestimation of spring and summer precipitation at grid boxes below 2000 m and an underestimation of summer and autumn precipitation at high-altitude boxes, do not only apply to the spatial mean over the entire Alpine area but are, in principle, also valid for each individual main Alpine catchment (not shown).

[6]Regarding the model evaluation at high altitudes it should be noted that the uncertainty of the observational datasets is largest in these regions since the underlying rain-gauge networks only contain very few high-altitude stations. Hence, the estimated grid box precipitation is often a result of interpolation from out-of-the-grid-cell station data (Efthymiadis et al., 2006). Furthermore, the combination of wind exposure and a high contribution from solid precipitation makes precipitation measurements extremely difficult at these altitudes, which is especially true for summit sites (Auer et al., 2005).

Glaciated Grid Boxes

As most glaciers in the Alps are found in high-altitude grid boxes (see Figure 5.8) the described precipitation biases at high elevations should, in principle, also apply for most parts of the glaciated area. In order to verify this assumption a more detailed model evaluation has been carried out for the glaciated grid boxes in the Alps. For reasons of simplicity only the analysis for the glacier simulation GlacA is presented. As the simulated amounts of precipitation are almost identical for the three baseline simulations (see analysis of spatial means above) very similar results are obtained for GlacB and GlacC (not shown).

Figures 5.35 and 5.36 show the mean seasonal precipitation bias of GlacA with respect to both observational datasets for glaciated grid boxes only. The spatial patterns are very similar in both cases which points to a good accordance between the CRU and the ALP-IMP datasets for the investigated period. In all seasons a mixture between grid boxes with a positive and grid boxes with a negative precipitation bias arises. An overestimation of precipitation generally prevails in spring while most glaciated grid boxes show a negative bias in autumn. Presumably, the most prominent influence on glacier mass balance is exerted by precipitation biases in wintertime since they are associated with important changes in snowfall, i.e., in snow accumulation on glaciated surfaces. In this season, most grid boxes along the northern slope of the main Alpine ridge show a strong positive precipitation bias of more than 50%. The same is true for grid cells in the southern and eastern parts, especially when compared to the ALP-IMP dataset. On the other hand, precipitation is clearly underestimated for most high-elevation grid boxes in the central and western part of the Alps (compare to model orography, Figure 5.1).

A more detailed picture of the relation between the precipitation bias and the glaciated grid box fraction in the four main Alpine catchments is given by Figure 5.37. In all four catchments most grid boxes with a mean glacier cover of more than 10% show a clear underestimation of precipitation in summer and autumn (lower panels). In winter and spring (upper panels) the relation is more complex. While the strongly glaciated grid boxes in the Rhone catchment exhibit a large negative precipitation bias of up to 65%, the simulated amounts of precipitation are too high for most grid boxes in the Rhine catchment. These boxes are mainly found along the northern Alpine slopes (see above). A similar overestimation of precipitation in strongly glaciated grid boxes is found in the Danube catchment in springtime.

Interestingly, the winterly precipitation bias (Figures 5.35 and 5.36, upper left panels) closely resembles the net change of the glaciated grid box area in GlacA (Figure 5.24), especially in the western part of the Alps. In this area, a strong overestimation of precipitation seems to be associated with a growing glacier area and vice versa. For strong positive biases of simulated precipitation this assumption is confirmed by Figure 5.38. The extraordinary growth of the glaciated grid box area of more than 200% in grid boxes along the northern slopes of the main Alpine crest is clearly associated with a strong overestimation of precipitation of more than 100% (left panel). However, no clear relation can be found for smaller changes of the glaciated grid box area (right panel).

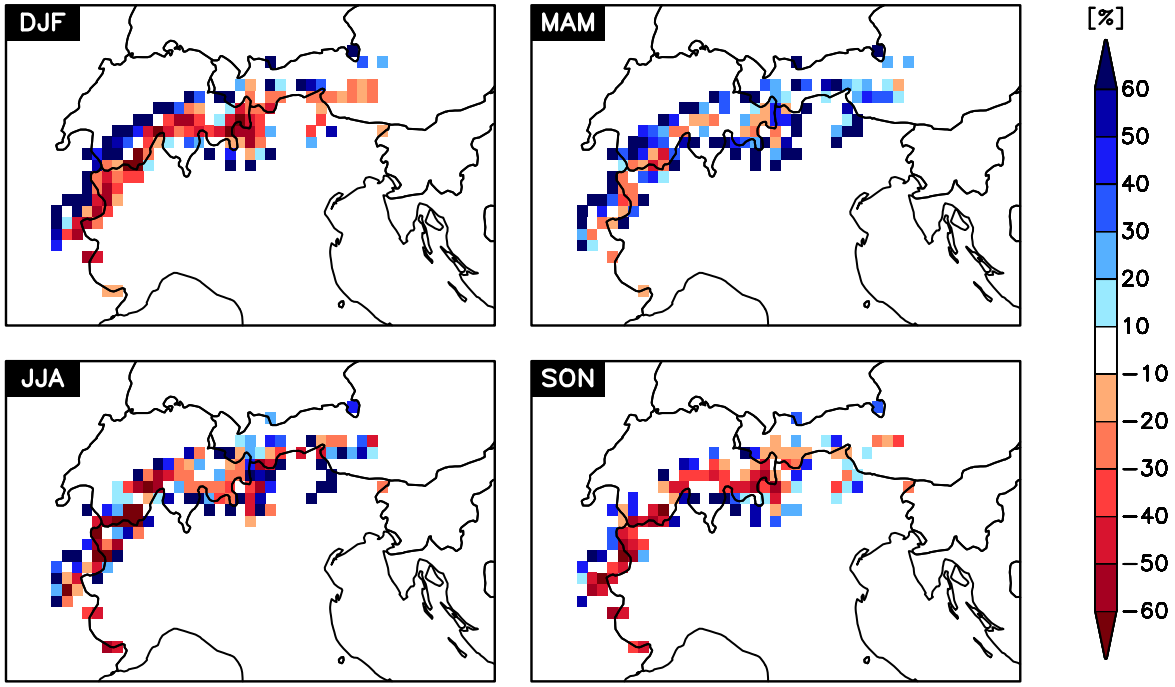

Figure 5.35: Mean seasonal bias of total precipitation (1958-2000) [%] in GlacA with respect to the CRU dataset. Only grid boxes with an initial glacier cover of more than 0.1% of the total grid box area are shown.

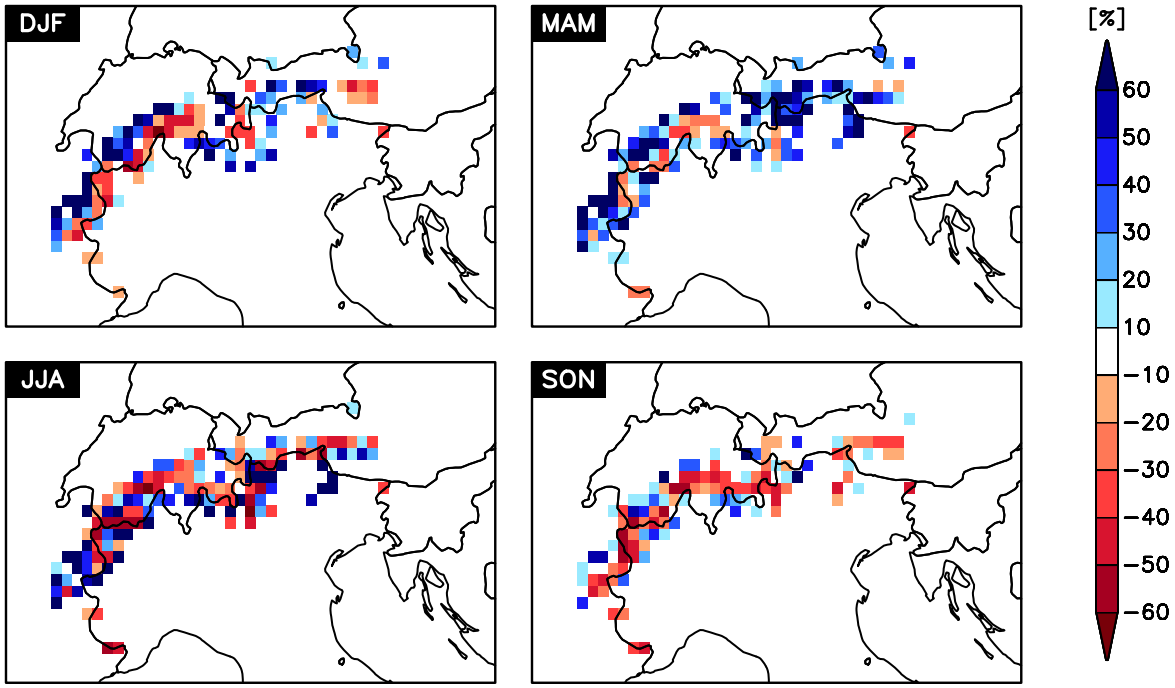

Figure 5.36: Mean seasonal bias of total precipitation (1958-2000) [%] in GlacA with respect to the ALP-IMP dataset. Only grid boxes with an initial glacier cover of more than 0.1% of the total grid box area are shown.

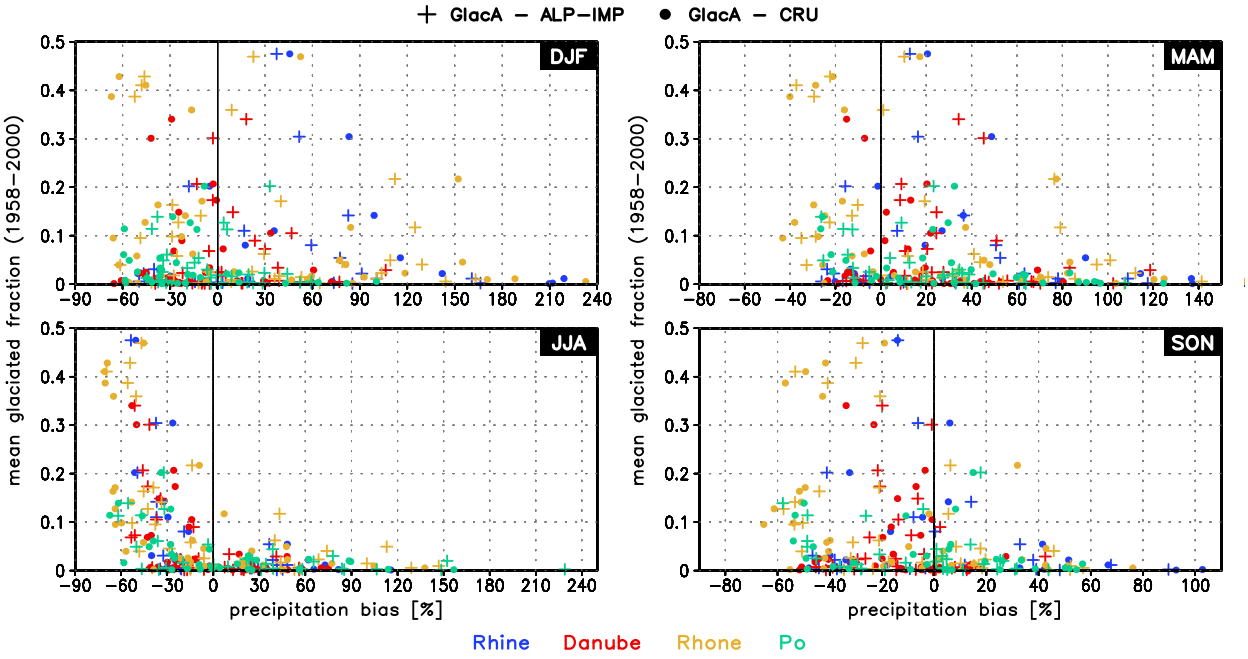

Figure 5.37: Relation between the mean glaciated grid box fraction and the seasonal precipitation bias (1958-2000) [%] of GlacA with respect to the ALP-IMP (crosses) and CRU (circles) datasets. Each cross/circle represents one glaciated REMO grid box and is colour-coded according to the respective catchment.

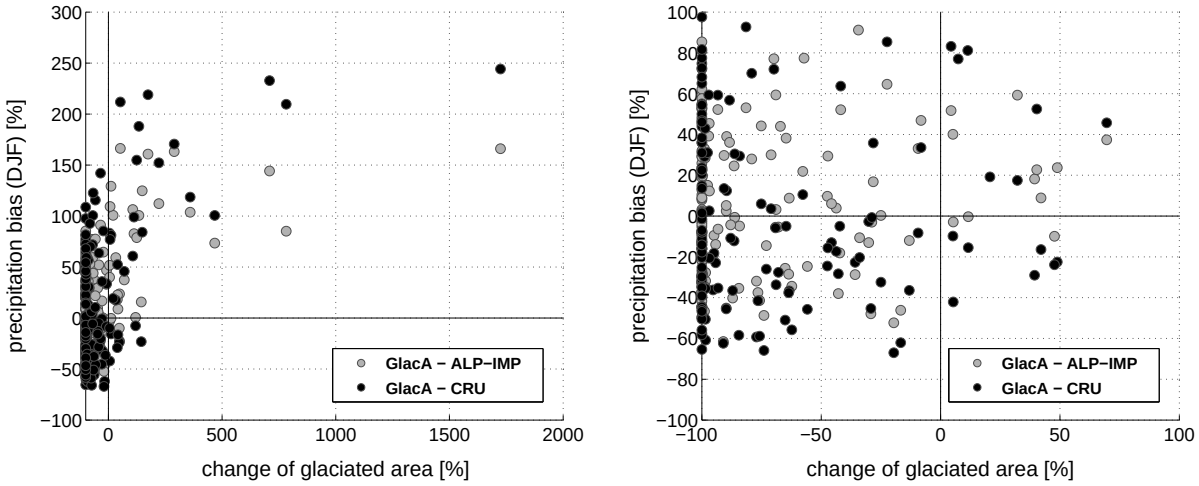

Figure 5.38: Percentage change of the glaciated grid box area in GlacA (1958-2003) [%] versus DJF precipitation bias (1958-2000) with respect to the ALP-IMP (grey) and the CRU (black) datasets. Each circle represents one glaciated REMO grid box. Left panel: All glaciated grid boxes. Right panel: Only grid boxes with changes between -100 and 100% for both parameters are shown.

Synthesis: Simulated Precipitation

While the simulated amounts of annual precipitation are generally overestimated in grid boxes below 2000 m a.s.l., precipitation in high-altitude boxes is too low compared to the two observational datasets. The latter is primarily due to an underestimation of precipitation of up to 35% from June to January. In the winter season this negative bias can reach up to -65% in individual glaciated grid cells in the Danube, Rhone and Po catchment which could, in principle, be associated with a pronounced negative bias of the simulated glacier mass balance (too low snow accumulation). In contrast to this, wintertime precipitation in glaciated grid cells of the Rhine catchment is mostly overestimated by $\text{REMO}_{\texttt{glacier}}$ which leads to a strong growth of glaciers in individual grid cells along the northern slopes of the main Alpine crest. Generally, the differences in the simulated amount of precipitation between the three baseline simulations are negligible.

5.3.2 Temperature

Observational Datasets

The validation of the simulated near-surface air temperature (here: 2m temperature) has been carried out using two observational datasets as reference:

- **CRU TS 2.1** (referred to as CRU)
  The gridded monthly temperature climatology of the CRU TS 2.1 dataset (Mitchell et al., submitted, see above) has been used as a first reference data source. In order to facilitate the spatial analysis the original regular $^1/_6^\circ$ CRU dataset for the sub-period 1958-2000 was interpolated to the rotated $^1/_6^\circ$ REMO grid applying the following procedure: In a first step the original monthly CRU temperature values were reduced to mean sea level (based on the CRU grid orography) applying a uniform lapse rate of -0.65°C/100m. Afterwards the resulting temperature fields were conservatively interpolated to the rotated $^1/_6^\circ$ REMO grid. In a final step, temperatures were adjusted to the REMO orography applying the same lapse rate of -0.65°C/100m. In this way, the general height dependence of air temperature and the difference between the CRU and the REMO orography are explicitly accounted for.

- **MeteoSwiss** (referred to as MS)
  As a second data source, the mean monthly temperature climatology of 10 high-altitude stations of the Swiss automatic network (ANETZ, see Figure 5.39, blue circles) for the period 1961-1990 has been used. This dataset is provided by MeteoSwiss, the Swiss Federal Office of Meteorology and Climatology.[7].

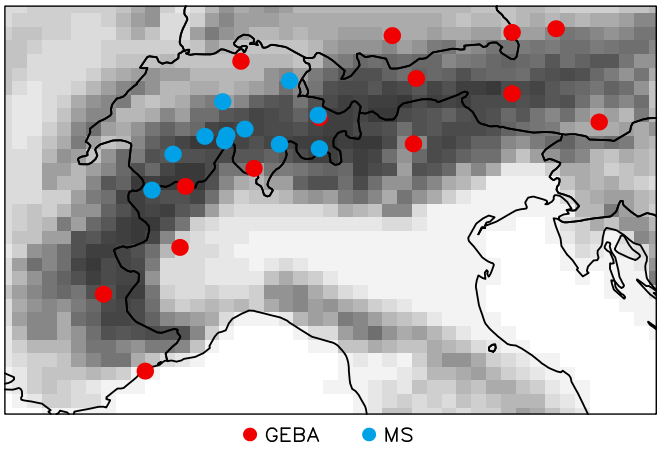

Figure 5.39: Location of the MeteoSwiss (MS, blue) and GEBA stations (red) used for validation of the simulated near-surface air temperature and the simulated global radiation. In the case of global radiation the MS temperature station Grimsel (Hospiz) has been replaced by the nearby station Ulrichen.

Entire Alps

In general, the temporal evolution of the simulated mean Alpine 2m temperature for the period 1958-2000 is in good accordance with the CRU dataset (Figure 5.40, upper left panel). This is especially true for the interannual and the decadal variability. Both the comparatively cold period in the 1970s and the early 1980s and the rising temperatures towards the end of the century are captured by the model simulations. However, in most years the observed mean temperature is underestimated by $\text{REMO}_{\text{glacier}}$ with largest differences of up to 1°C in the 1970s and the late 1990s. This negative temperature bias is mainly due to a strong underestimation of observed temperatures in grid boxes above 1000 m a.s.l. (Figure 5.40, upper right and lower panels). Largest biases of more than 2°C occur in high-elevation boxes with an altitude of more than 2000 m a.s.l.). In all altitudinal belts the simulated temperature does not differ between the three REMO simulations, i.e., the choice of a specific area adjustment method does hardly influence the mean near-surface air temperature. The strong underestimation of the observed temperatures in high-elevation areas can primarily be attributed

[7] The dataset can be obtained from the website
http://www.meteoswiss.ch/web/en/climate/climate_norm_values/tabellen.html

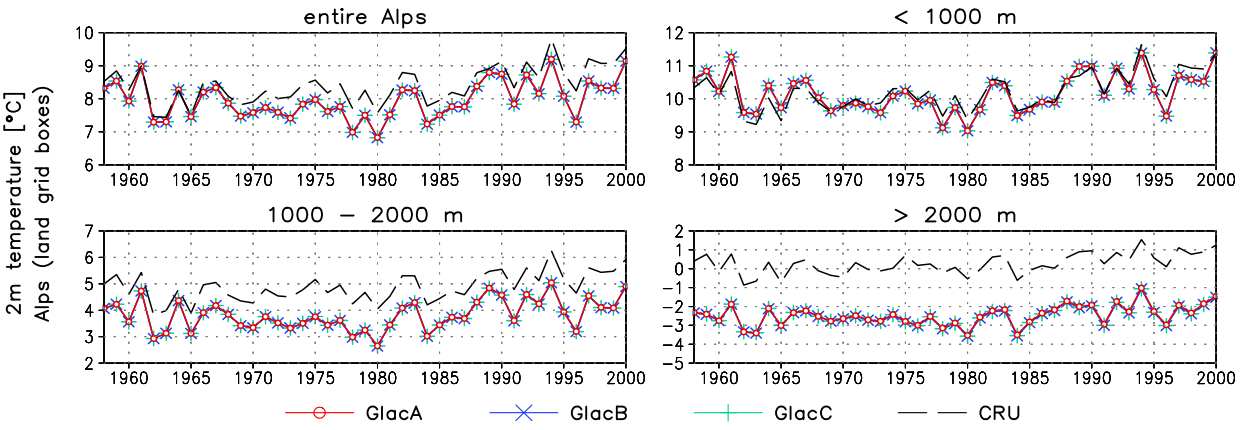

Figure 5.40: Spatial mean of 2m temperature (1958-2000) [°C] for the entire Alpine region (land grid boxes only) and three altitudinal intervals as simulated by the three baseline simulations (GlacA, GlacB, GlacC) and as derived from the CRU dataset.

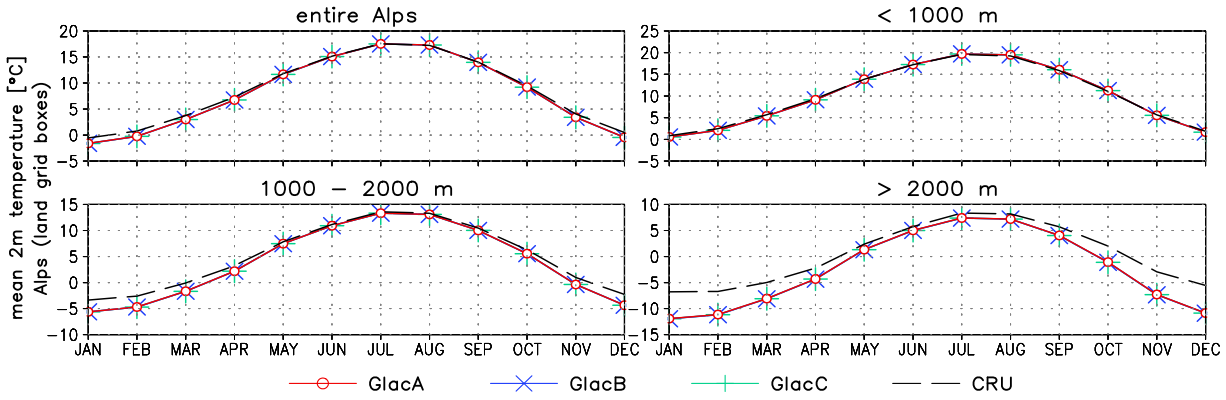

Figure 5.41: Climatological spatial mean of the monthly 2m temperature (1958-2000) [°C] for the entire Alpine region (land grid boxes only) and three altitudinal intervals as simulated by the three baseline simulations (GlacA, GlacB, GlacC) and as derived from the CRU dataset.

to the winter months. In this season the simulated 2m temperature shows a negative bias of about 2°C for the altitudinal interval 1000-2000 m a.s.l. and an even larger bias of up to 5°C in grid boxes above 2000 m (Figure 5.41, lower panels). In these high-elevation areas also the mean summer temperature is underestimated by about 1°C. In grid boxes below 1000 m a.s.l., i.e., in more than 90% of the investigated area, the spatial average of the mean annual cycle of temperature is very well reproduced (upper right panel in Figure 5.41).

In principle, the results described above are not only valid for the spatial mean over the entire Alpine region but do also apply for each individual main Alpine catchment. The only exception is the Po catchment, where the summer temperature in grid boxes below 2000 m a.s.l. is systematically underestimated by about 1°C (not shown). Nonetheless, a strong negative bias of the simulated winter temperatures in areas above 1000 m a.s.l. is also found in this catchment.

Individual Stations

In order to verify the negative bias of the simulated 2m temperature in wintertime and to check the usefulness of the gridded CRU dataset for high-elevation areas the model results have also been compared to individual station data. For reasons of simplicity, only the baseline simulation GlacA has been considered. Figure 5.42 shows the comparison between the mean annual cycle of temperature (1961-1990) for 10 high-elevation sites in Switzerland (MS) and the simulated temperature for the respective REMO grid box (i.e., the grid box in which the meteorological station is located). In order to account for the elevation difference between an individual station and the respective REMO grid box altitude, the model results have been height-corrected by applying a constant temperature lapse rate of -0.65°C/100m (dashed line). In general, the results obtained for the comparison of REMO and CRU (see above) are confirmed in this analysis. At all sites the height-corrected REMO temperature shows a strong negative bias with respect to the observations in the winter half of the year. This is true both for stations which lie above the mean grid box altitude (e.g., Pilatus, Saentis, Weissfluhjoch) and for stations with a lower elevation compared to the respective REMO grid box (e.g., Grimsel, San

Bernardino). Hence, the obvious underestimation of wintertime temperature is probably not due to wrong assumptions concerning the temperature lapse rate in this season (which is applied during the height-correction procedure) but seems to be a systematic model bias. In summer, on the other hand, the simulated temperature is relatively close to the observations (except for Grimsel, Jungfraujoch and Montana).

Glaciated Grid Boxes

The evaluation of the simulated 2m temperature in the baseline simulation GlacA for glaciated grid boxes only (Figures 5.43 and 5.44) confirms the results obtained above for high-elevation grid cells. Throughout most parts of the year the observed temperature (as derived from the CRU dataset) is generally underestimated with largest negative biases of up to 10°C occurring in autumn and winter and in a variety of grid boxes with different initial glacier cover (Figure 5.44, upper left and lower right panels). Only in summer a considerable fraction of glaciated grid boxes shows a positive bias of the simulated temperature. These boxes are mainly located south of the main Alpine ridge in the Po catchment (green colour in Figure 5.44).

Synthesis: Simulated Temperature

With respect to the simulated near-surface air temperature hardly any differences exist between the three baseline simulations. While the performance of all $\text{REMO}_{\texttt{glacier}}$ experiments is very good at low-elevation sites, problems arise in high-altitude grid cells where most glaciers are located. Here, the simulated air temperature shows a clear negative bias with respect to observations throughout the entire year. This bias is most pronounced in autumn and winter (up to -10°C). In principle, it has a positive effect on glacier mass balance via a reduced flux of sensible heat towards the glacier surface and an increase in the fraction of solid precipitation (snowfall).

5.3.3 Solar Radiation

Observational Datasets

As observation-based gridded datasets were not available, the validation of the simulated incoming solar radiation (i.e., global radiation, consisting of a direct and a diffuse part) relies on quality-checked observational data for individual stations. The mean annual cycle of global radiation has been computed for 24 sites in the Alpine area based on the following two data sources:

- **GEBA Database** (referred to as GEBA)
  Incoming shortwave radiation fluxes for 14 stations within the Alpine area (see Figure 5.39, red circles) were extracted from the Swiss Federal Institute of Technology's Global Energy Balance Archive (GEBA; Gilgen et al., 1998; Gilgen and Ohmura, 1999). The GEBA database contains quality-controlled monthly means of different energy fluxes that have been instrumentally measured at the surface. Prior to the analysis the mean annual cycle of global radiation has been calculated for each of the 14 stations based on the monthly means extracted from the database.

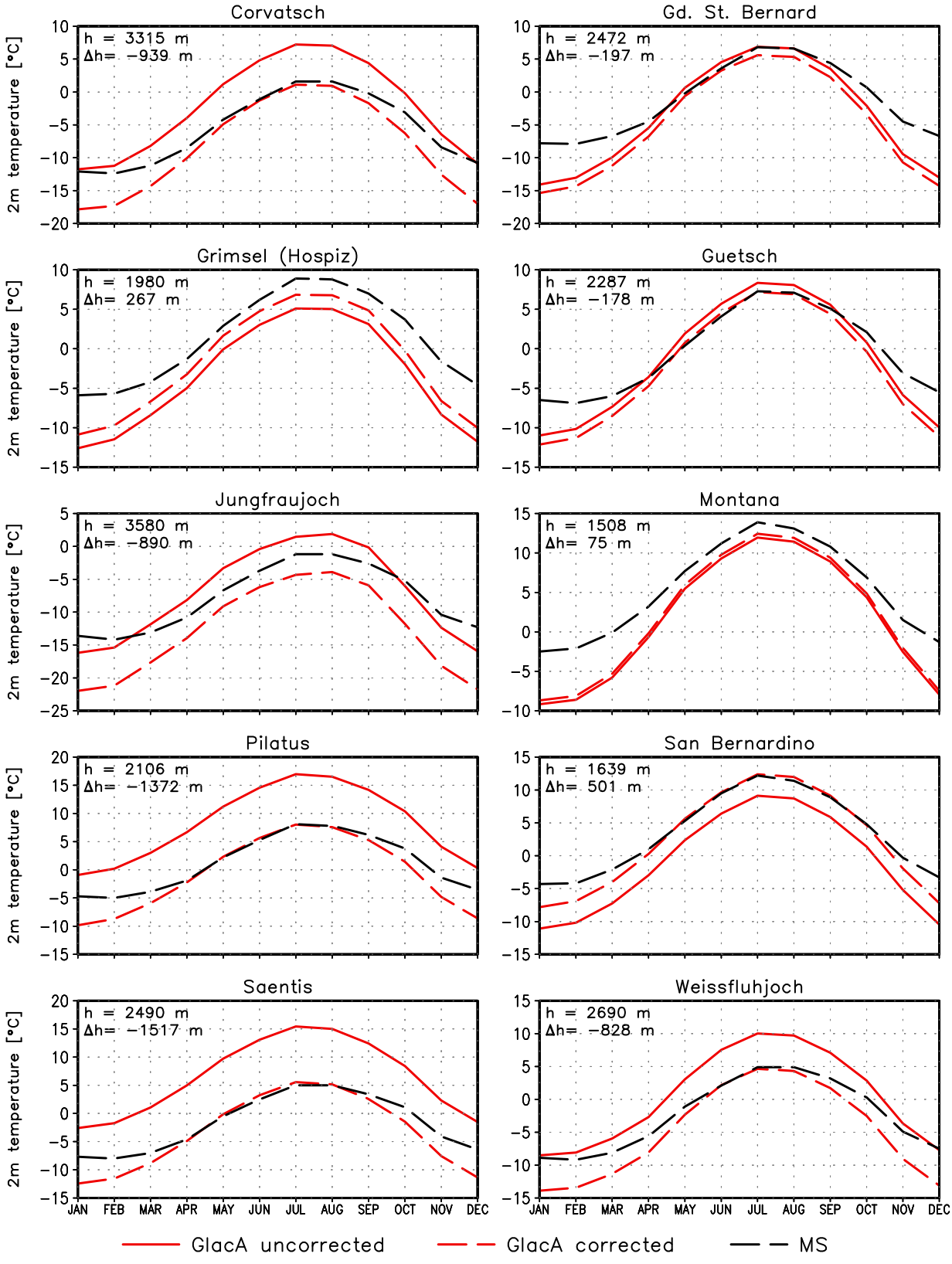

Figure 5.42: Comparison between the simulated (GlacA) and the observed (MS) mean annual cycle of temperature (1961-1990) [°C] for 10 high-elevation sites in Switzerland. h: Elevation of the meteorological station. Δh: Elevation difference REMO grid box - station. The dashed red line represents the height-corrected simulated temperature (applying a uniform lapse rate of -0.65°C/100m).

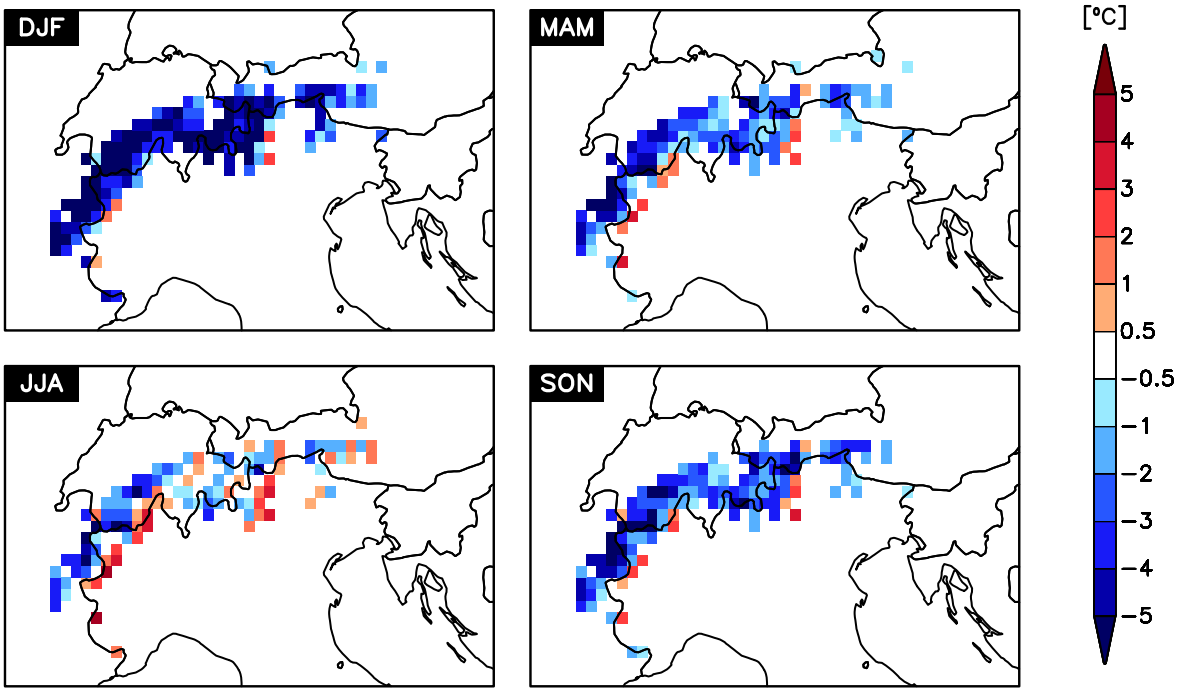

Figure 5.43: Mean seasonal temperature bias (1958-2000) [°C] in GlacA with respect to the CRU dataset. Only grid boxes with an initial glacier cover of more than 0.1% of the total grid box area are shown.

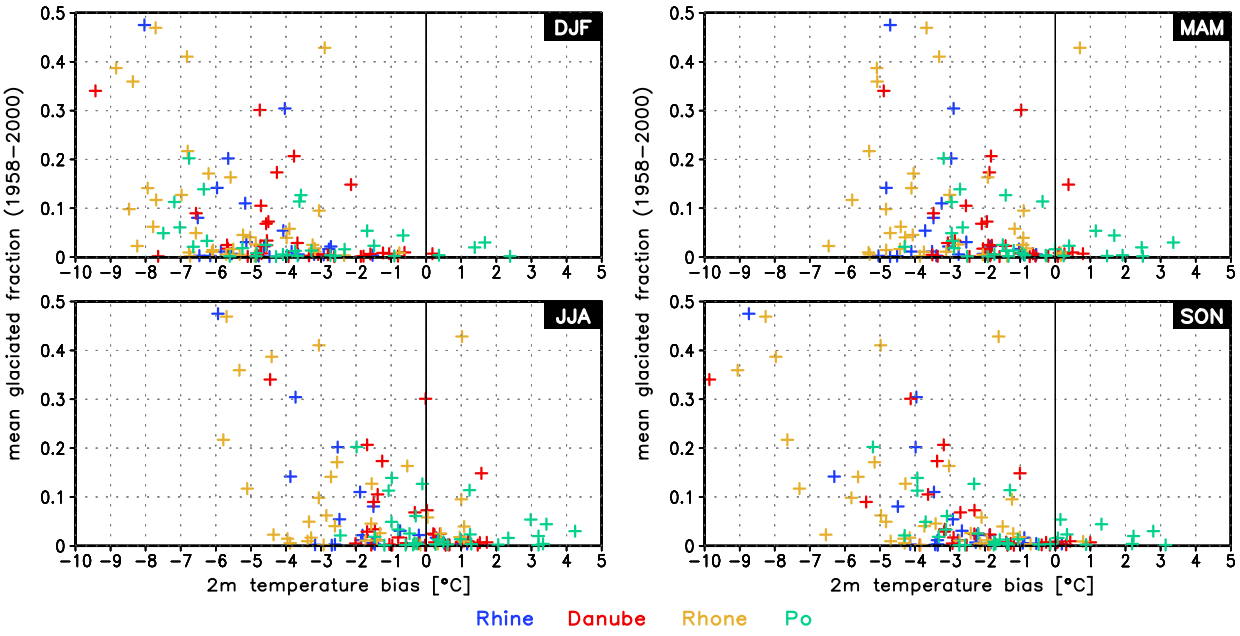

Figure 5.44: Relation between the mean glaciated grid box fraction and the seasonal temperature bias (1958-2000) [%] of GlacA with respect to the CRU dataset. Each cross/circle represents one glaciated REMO grid box and is colour-coded according to the respective catchment.

The underlying time period differs from station to station but has, in all cases, a length of at least 12 years.

▷ **MeteoSwiss** (referred to as MS)
As additional data source, the mean annual cycle of global radiation for 10 high-altitude stations in Switzerland (see Figure 5.39, blue circles) for the period 1981-2000 has been extracted from the MeteoSwiss dataset (see above).

Individual Stations

Figures 5.45 and 5.46 show the comparison between the observed (GEBA and MS) and the simulated (GlacA, GlacB and GlacC) mean annual cycle of global radiation for the 24 sites. The REMO values represent the simulated global radiation flux in the grid box in which the respective station is located. An additional height-correction of the solar radiation flux, i.e., a correction for the difference between station altitude and REMO grid box altitude, has not been applied. Based on station measurements at elevations between 370 m a.s.l. and 3580 m a.s.l. Marty et al. (2002) found an annual mean altitudinal gradient of global radiation of 1.3 $Wm^{-2}/100m$ in the Swiss Alps. This gradient strongly depends on the season and on the specific height interval under investigation. Its positive sign is caused by the decrease of the atmospheric optical depth with altitude.

As for precipitation and temperature, the simulated radiation fluxes do not differ between the three baseline simulations. The simulated and the observed mean monthly radiation fluxes show a relatively good agreement for the 14 GEBA sites (Figure 5.45). Nonetheless, in some cases (Feuerkogel, Hohenpeissenberg, Salzburg, Bolzano, Nice) the maximum solar radiation flux in summer is overestimated by several tens of W/m^2. In wintertime, REMO slightly underestimates the observed radiation flux at most sites. A systematic negative bias of the simulated global radiation seems to prevail in winter and especially in springtime at high-elevation sites (Feuerkogel, Sonnblick, Pian Rosa M., Davos). Here, the observed radiation flux is underestimated by up to 80 W/m^2 in the model simulations. The same phenomenon appears in case of the 10 MeteoSwiss sites, which are all located above 1300 m a.s.l. (Figure 5.46). Except for the valley station of Ulrichen the springtime global radiation flux is systematically underestimated. In contrast to this, the observed radiation flux in the summer months is overestimated at most sites. Both phenomena can possibly be attributed to errors in the simulated cloud cover since clouds exert a primary influence on the incoming surface radiation fluxes. The larger observed solar radiation flux in winter and spring could also be caused by multiple reflection of solar radiation on surrounding snow-covered slopes, a process which is not accounted for in REMO.

The described shortcomings of the simulated solar radiation flux directly affect the surface energy balance of the $REMO_{glacier}$ glacier cuboids and, via changes in snow and ice ablation, the simulated glacier mass balance. Generally, biases in the summer radiation flux can be thought to have the largest influence since the absorbed fraction of the total radiation flux is larger due to a lower surface albedo (disappearance of snow and exposure of the darker ice surfaces). Hence, the overestimation of summertime global radiation will probably lead to a net negative bias of glacier mass balance (enhanced ablation). In contrast, the underestimation of wintertime and springtime global radiation in $REMO_{glacier}$ will be less effective and the associated positive mass balance bias (reduced ablation) will probably not compensate for the enhanced summer melting.

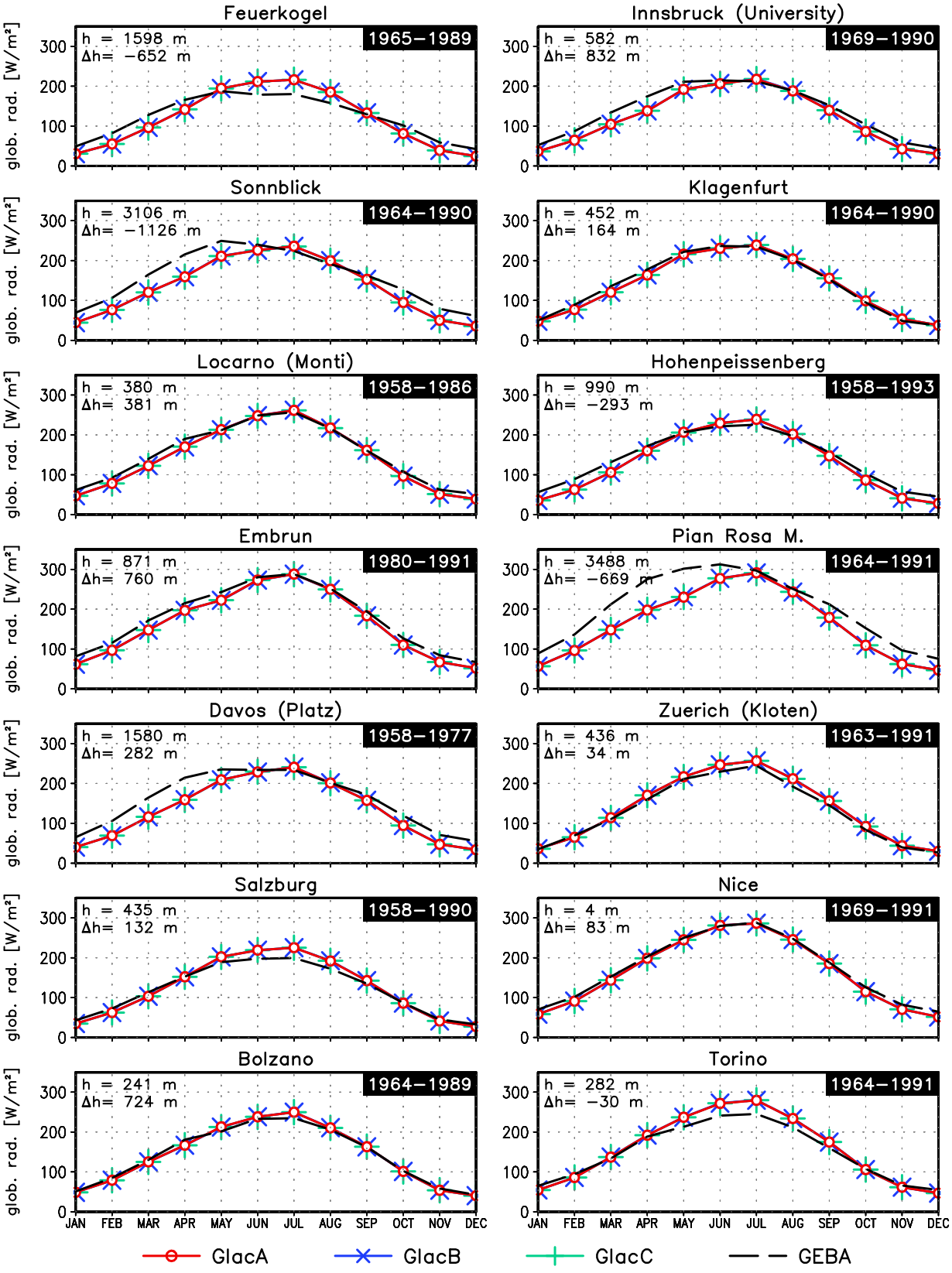

Figure 5.45: Comparison between the simulated (GlacA, GlacB, GlacC) and the observed (GEBA) mean annual cycle of global radiation [W/m^2] for 14 stations in the Alpine area. The underlying time period for both the observations and the model results is shown in the upper right corner of each panel. h: Elevation of the meteorological station. Δh: Elevation difference REMO grid box - station.

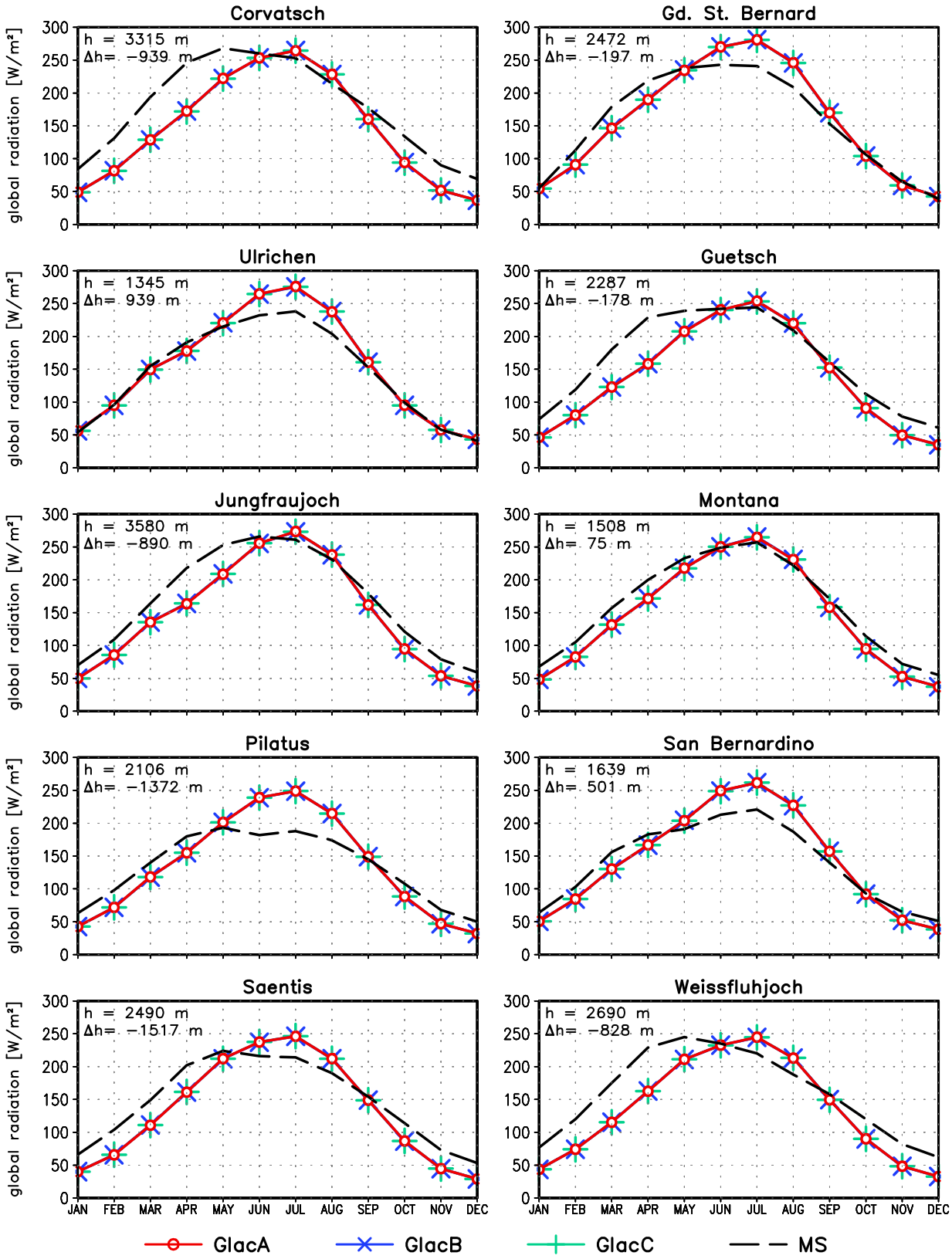

Figure 5.46: Comparison between the simulated (GlacA, GlacB, GlacC) and the observed (MS) mean annual cycle of global radiation (1981-2000) [W/m^2] for 10 high-elevation stations in Switzerland. h: Elevation of the meteorological station. Δh: Elevation difference REMO grid box - station.

5.3.4 Discussion

As the vast majority of glaciated surfaces is located in grid boxes with a mean altitude of more than 1000 m a.s.l., shortcomings in the simulated climatic forcing in high-altitude boxes will inevitably influence the simulation of glacier mass balance and the corresponding area changes. In this respect, one of the most important parameters is winter precipitation which is responsible for the majority of snow accumulation on Alpine glaciers. The validation of the simulated amounts of precipitation in this season indicates a strong positive bias in the Rhine catchment, especially during the 1970s and 1980s (not shown). Probably, this overestimation of winter precipitation is one reason for the positive bias of the simulated glacier mass balance in the Rhine catchment for the respective period (see Chapter 5.2.1). In contrast to this, strongly glaciated grid cells in the other catchments mostly show a negative wintertime precipitation bias which, in general, would lead to a negative bias of the simulated glacier mass balance. However, it is possible that for glaciated surfaces a negative bias of wintertime precipitation is partly compensated by the choice of a too large snow redistribution factor κ (see Chapter 4.2.7). A further compensating factor is the negative temperature bias in most high-altitude grid boxes for most parts of the year. This bias generally leads to an overestimation of the fraction of solid precipitation (snowfall) and, hence, to an increase in snow accumulation with a positive effect on glacier mass balance. Additionally, the general underestimation of temperature will reduce melt rates. The same is true for the negative bias of springtime global radiation at high-altitude sites. If the latter is related to an overestimation of cloud cover in $\text{REMO}_{\texttt{glacier}}$ the negative bias of global radiation might in parts be compensated by an increase in incoming longwave radiation due to the enhanced presence of clouds. This assumption cannot be verified since the simulated incoming longwave radiation flux has not been validated within the present study due to the lack of observational data on an Alpine-wide scale.

Again, it should be pointed out that in the areas of interest, i.e., in high-altitude Alpine regions, the coverage of meteorological stations is usually very sparse and errors of meteorological measurements themselves are largest. The uncertainty of observation-based datasets used for model validation is thus comparatively large.

5.4 Climatic Effect of Glacier Scheme

In order to investigate the effect of the new glacier parameterisation scheme on the simulated climate a control experiment (CTRL) using the standard version REMO 5.3 has been carried out for the period 1958-2003. The same model setup as in case of the $\text{REMO}_{\texttt{glacier}}$ simulations has been used. Since the simulated climatic conditions are very similar for all $\text{REMO}_{\texttt{glacier}}$ experiments (see above) only the simulation GlacA has been analysed and compared to the control simulation.

As described in Chapter 3 REMO 5.3 does not explicitly account for glaciers covering a subgrid fraction of a model grid box. Even the comparatively high albedo of snow-free glacier surfaces does not contribute to the mean grid box background albedo (see Chapter 3.3.6). From this point of view, the comparison of atmospheric quantities between GlacA and CTRL does not only reveal the (model-specific) effect of including the glacier subgrid parameterisation scheme into REMO but also the general influence of mountain glaciers on the regional climate. In $\text{REMO}_{\texttt{glacier}}$ this effect is

primarily exerted by the special surface characteristics of the glaciated grid box fraction. Compared to standard REMO experiments in which the entire land fraction of a grid box is covered by vegetated and bare soil surfaces (see Chapter 3) a part of the total grid box area in $\text{REMO}_{\texttt{glacier}}$ can be covered by a non-vegetated ice surface with a comparatively high background albedo and a surface temperature never exceeding 0°C. These effects should be most pronounced during the summer half of the year since in winter the presence of snow can mask differences of the underlying surfaces to a large degree.

However, differences in atmospheric parameters between GlacA and CTRL are not necessarily a result of the distinct surface characteristics of the glacier cuboid itself but can, in principle, also arise from the redistribution of incoming solar radiation and snowfall on a subgrid scale (Chapter 4). For instance, the redistribution of snow alone can lead to shifts in the annual cycle of the grid box mean surface albedo. A larger amount of snow is accumulated on the glaciated fraction and, hence, can persist for a longer period of time while the non-glaciated fractions become exposed earlier in the year. Differences between GlacA and CTRL can therefore only partly be interpreted as the general effect of glaciers on the regional climatic conditions.

5.4.1 Albedo

The seasonal difference of the mean grid box surface albedo between GlacA and CTRL is shown in Figure 5.47. Notable differences only exist in the glacier-covered part of the Alps. In all seasons, glaciated grid boxes generally have a higher surface albedo in the glacier experiment compared to the control simulation. Differences are most pronounced in summer and autumn with more than 90% of the glaciated grid cells showing a significantly higher mean grid box summer albedo in GlacA (99% confidence level). In this season, deviations of more than 0.2 occur and clearly depend on the glaciated grid box fraction (largest increases of albedo in strongly glaciated grid boxes, Figure 5.48). They are independent of the specific catchment under consideration. As stated above, these results can in parts be explained by the higher surface background albedo of the glaciated fractions in GlacA which becomes important as soon as the overlying snow has melted. A further point is that, due to the subgrid snow redistribution, a snow cover can generally persist for a longer period of time on the glaciated fraction and thereby increase the mean grid box surface albedo in summer.

In winter and spring, on the other side, albedo differences are far less pronounced and the positive relation between the albedo deviation and the glaciated grid box fraction only seems to hold for a mean glacier cover of less than 25% (Figure 5.48, upper panels). The interplay of several processes is responsible for this result. At first, grid boxes with a low glaciated fraction are mostly located at lower altitudes with higher temperatures where the winter snow will disappear fastest. Hence, in these boxes, the effect of the higher background albedo and the longer persistence of snow on the glaciated fraction in GlacA can slightly raise the mean grid box albedo already in late winter and in spring. On the other hand, grid cells with a high glaciated fraction are usually found at higher altitudes and are often covered by snow throughout the entire winter and far into spring. Therefore, differences in the background albedo probably only play a minor role in winter and spring. However, the lower winterly surface temperature in GlacA compared to CTRL (see below) and the dependence of the snow albedo on the surface temperature (Chapter 4.2.3) will lead to an albedo increase in strongly glaciated grid cells in case of a complete snow cover. This effect can be offset by the redistribution of snow in

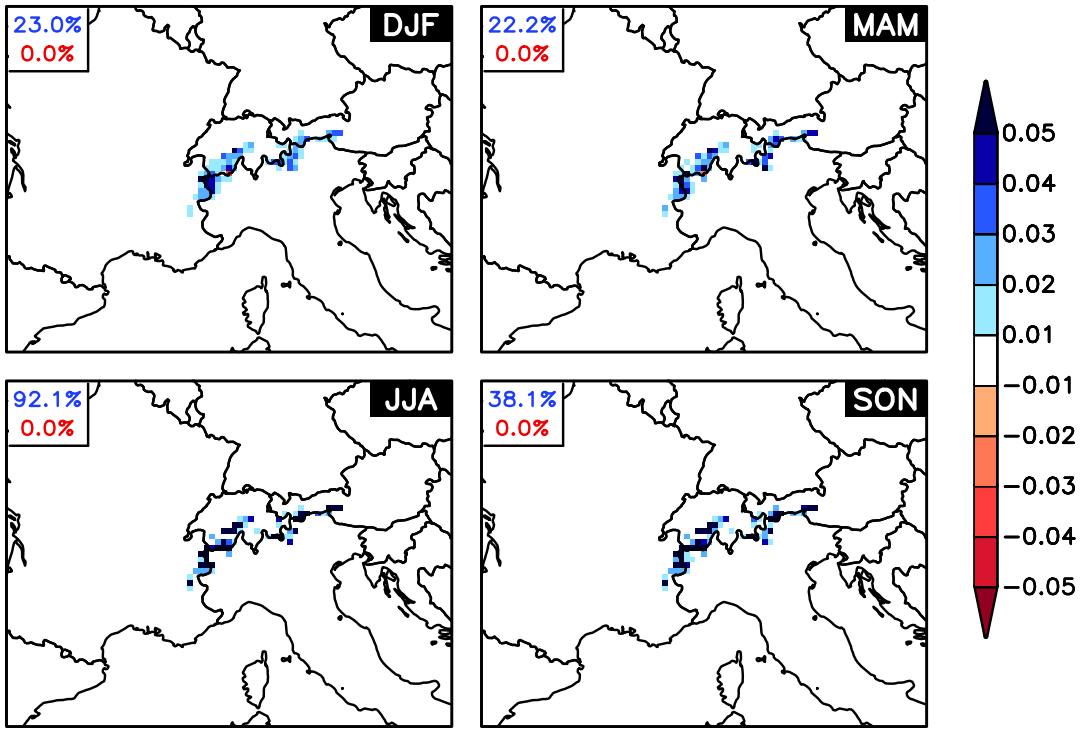

Figure 5.47: Seasonal difference of the mean grid box surface albedo GlacA - CTRL (1958-2003). The upper (lower) number in each panel represents the percentage of glaciated grid boxes showing a significant positive (negative) difference of the seasonal mean (99% confidence level, one-sided test).

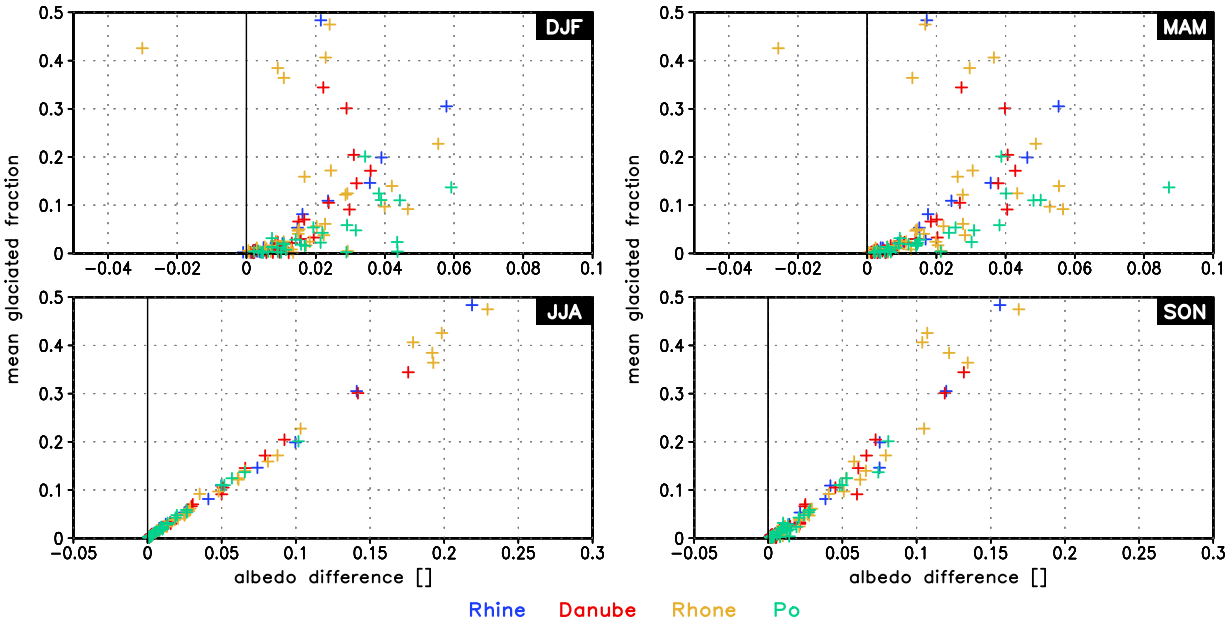

Figure 5.48: Relation between the mean glaciated grid box fraction and the seasonal difference of the mean grid box surface albedo GlacA - CTRL (1958-2003). Each cross represents one glaciated REMO grid box and is colour-coded according to the respective catchment.

GlacA which can, in principle, have a negative effect on the mean winterly grid box surface albedo. The larger the glaciated grid box fraction the higher the amount of snow that is substracted from the non-glaciated parts and shifted to the glacier fraction in order to maintain a fixed redistribution factor (see Chapter 4). As a consequence, the non-glaciated parts could become exposed earlier in the year in GlacA compared to CTRL which results in a lower mean grid box surface albedo.

5.4.2 Temperature

The spatial patterns of the mean seasonal difference in the 2m temperature between GlacA and CTRL are shown in Figure 5.49. The general effect of the inclusion of the glacier parameterisation scheme is a cooling of the near-surface air masses. Again, it is restricted to glaciated grid boxes in the Alps and shows a clear dependency on the glaciated grid box fraction with largest differences occurring in strongly glaciated grid cells (Figure 5.50).[8] The strongest influence is exerted in summer and autumn with temperature deviations of up to -7°C. In autumn more than 50% of the glaciated grid cells show a significant negative temperature deviation in GlacA. This cooling effect is due to the combination of a comparatively high albedo of snow-free glacier surfaces, a glacier surface temperature never exceeding 0°C and the longer persistence of snow on glaciated surfaces (due to the subgrid snow redistribution). Large negative temperature deviations of up to -4°C with respect to the control simulation are also found in the winter season. At first sight, the reason for this behaviour is less clear than in case of summer and autumn. The presence of an often continuous snow cover in winter should generally mask differences of the underlying surfaces and, hence, differences between the two simulations. Several processes can still be held responsible for this negative deviation of the winter 2m temperature. One of them is the presence of an isolating ice layer on a part of the grid box in the GlacA experiment. During summer, this layer cannot be warmed above 0°C and, hence, cannot store excess energy in this season. On the other hand, the soil column of the entire land fraction in the CTRL simulation is warmed during the summer half of the year and, later on, releases this excess energy in wintertime and counteracts the negative surface energy balance to some part. In order for this process to become significant the thickness of an isolating snow layer on top of the soil/ice surface must not be too large.

A second explanation for the negative winterly temperature bias in GlacA lies in the subgrid redistribution of the incoming solar radiation in $\text{REMO}_{\texttt{glacier}}$ and the corresponding differential warming of the glaciated and the non-glaciated grid box fraction. In winter, the glaciated part of a grid box only receives about 50% of the grid box mean incoming solar radiation while the incoming radiation flux over the non-glaciated fraction is increased accordingly (see Chapter 4.2.6 and Figure 4.8). Hence, the glaciated parts receive less energy and the daytime warming will be less pronounced (which, additionally, leads to a positive albedo deviation due to the dependence of the snow albedo on the snow surface temperature). The non-glaciated fraction on the other hand receives a larger amount of solar radiation compared to the CTRL experiment and will warm up faster during daytime, which probably also leads to an increase in the amount of snow melt. However, as long as a snow layer is present the surface temperature cannot exceed 0°C even if more energy would be available. The net effect on the mean grid box surface temperature and, hence, on the 2m temperature compared to the CTRL experiment might then be a cooling.

[8] Almost identical results are obtained for the mean grid box surface temperature (not shown here).

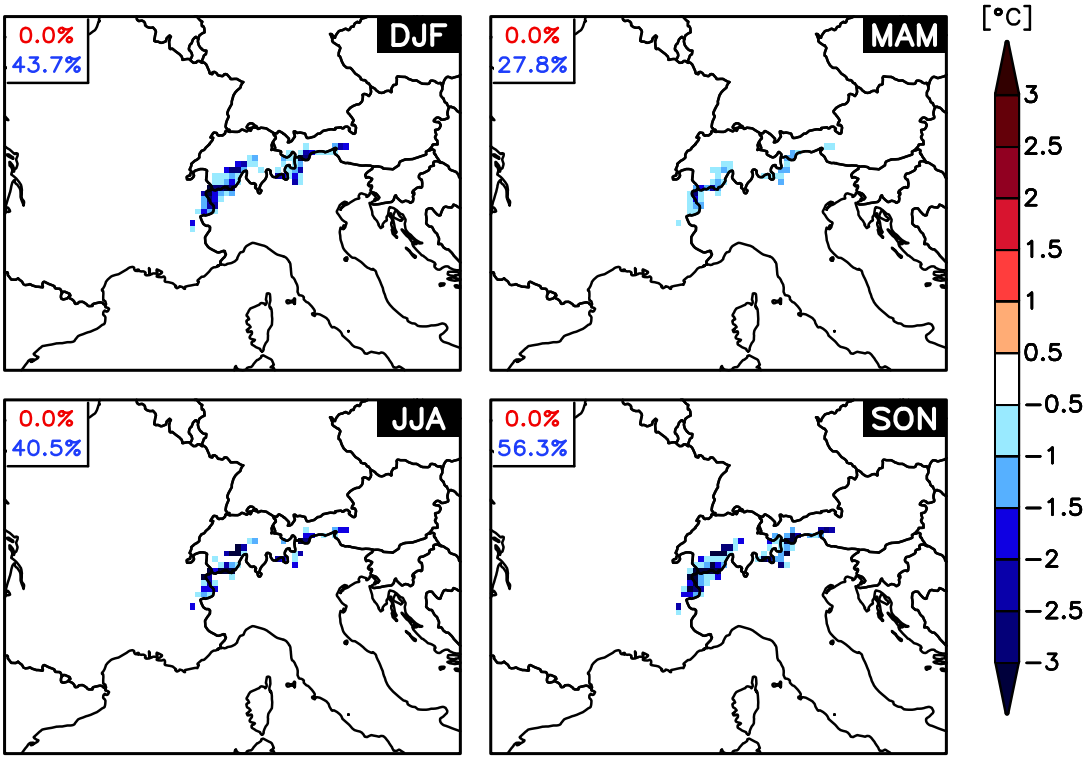

Figure 5.49: Seasonal difference of the mean grid box 2m temperature GlacA - CTRL (1958-2003) [°C]. The upper (lower) number in each panel represents the percentage of glaciated grid boxes showing a significant positive (negative) difference of the seasonal mean (99% confidence level, one-sided test).

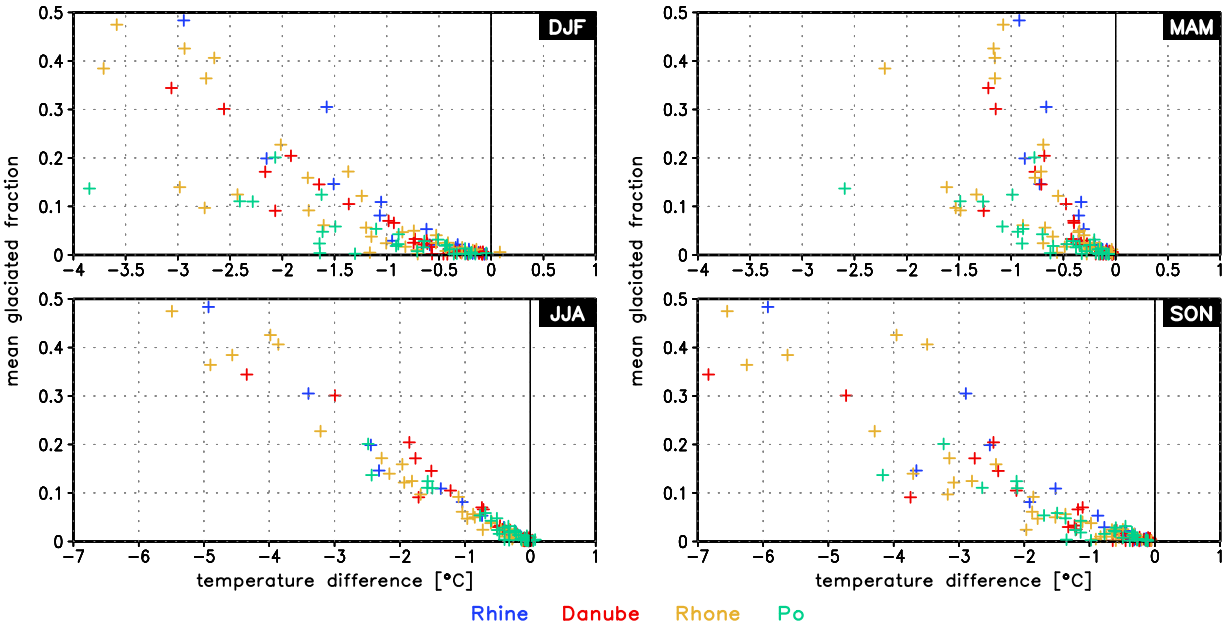

Figure 5.50: Relation between the mean glaciated grid box fraction and the seasonal difference of the mean grid box 2m temperature GlacA - CTRL (1958-2003) [°C]. Each cross represents one glaciated REMO grid box and is colour-coded according to the respective catchment.

The described cooling effect of the new glacier parameterisation is restricted to the lowest model levels, i.e., to the lower troposphere. In the 500 hPa level no significant temperature deviation is simulated (not shown).

5.4.3 Precipitation

The influence of the new glacier subgrid parameterisation scheme on the total amount of precipitation is strongest in the summer season and is mainly restricted to the Alpine area (Figure 5.51). In summer more than 66% of the glaciated grid boxes show a significant negative deviation with a maximum reduction of more than 50% in single grid boxes (Figure 5.52). In wintertime, on the other side, no significant differences can be found. Compared to the surface albedo and the 2m temperature the dependence of the summer precipitation difference on the glaciated grid box fraction is relatively weak. Furthermore, the spatial pattern of the precipitation signal is generally more diffuse and grid boxes in the vicinity of the glaciated areas in the Alps show distinct signals as well. The reduction of total precipitation in GlacA compared to CTRL is mainly due to a decrease of convective precipitation (i.e., precipitation generated by the model's convection parameterisation scheme) which, in summertime, is reduced by up to 90% in grid cells with a high glacier cover (not shown). The influence on the resolved large-scale precipitation on the other side is much weaker (maximum reduction of about -16% in single grid cells in summertime). Hence, the relatively week dependence of the difference in total precipitation on the glaciated grid box fraction can, at least in parts, be explained by the different contribution of convectively generated and large-scale precipitation to the total amount of grid box precipitation. In grid cells with a large contribution of convective precipitation to the total amount of precipitation the influence of glaciers on summer precipitation will generally be stronger.

The described reduction of summer precipitation in GlacA compared to the control simulation is partly caused by the lower surface temperature in glaciated grid cells (i.e., by the cooling effect of the glaciers, see above) which reduces the near-surface temperature gradient and hinders the initiation of convective processes. Furthermore, the supply of humidity by surface evaporation is strongly reduced with more than 70% of the glaciated grid boxes showing a significant reduction in GlacA compared to CTRL (Figure 5.53). This leads to a significantly lower near-surface specific humidity in more than 60% of the glaciated grid cells (not shown). The reduction of surface evaporation is mainly due to the existence of non-vegetated snow and ice surfaces in GlacA compared to vegetated / bare soil surfaces in the CTRL experiment. As a consequence, the local and regional recycling of humidity in summer by precipitation and evaporation is obviously reduced in $\text{REMO}_{\texttt{glacier}}$.

5.4.4 Further Parameters

Besides air temperature and precipitation further atmospheric parameters are affected by the inclusion of the new glacier subgrid parameterisation scheme. In the following section, only a summary of the most important changes is given.

The significant reduction of the near-surface specific humidity in summer due to the reduced supply of humidity by surface evaporation has already been mentioned above (maximum deviation: -24% for individual grid cells). Also in autumn more than 60% of the glaciated grid cells show a significantly

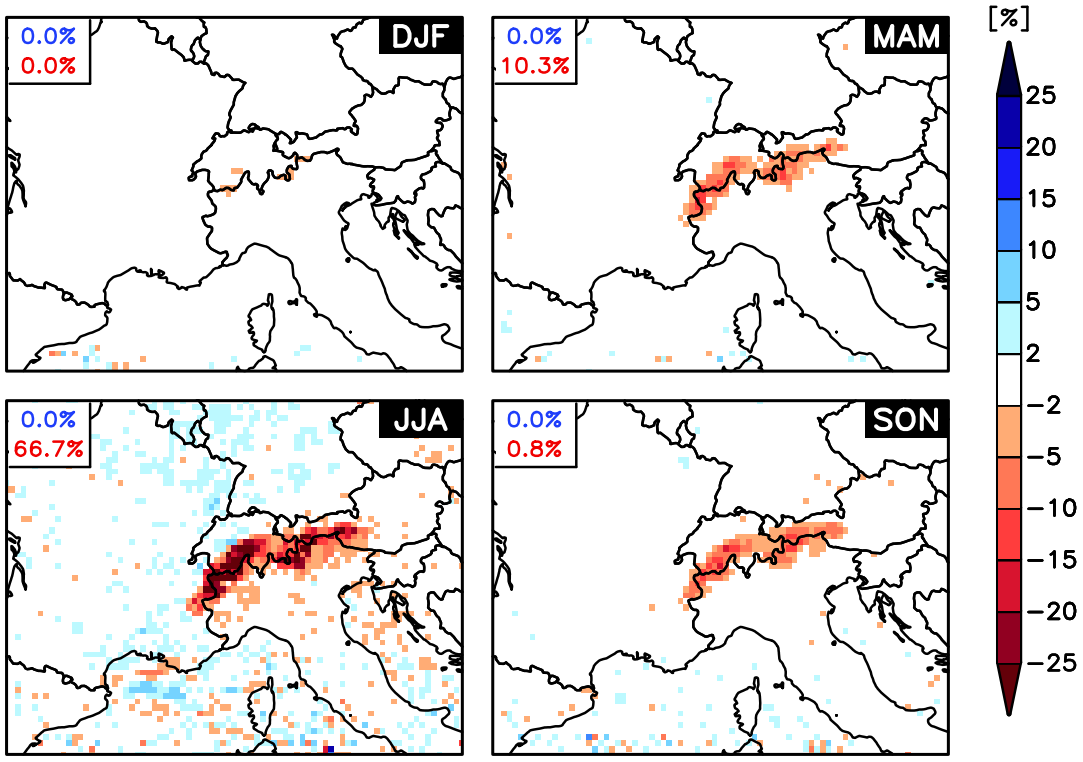

Figure 5.51: Seasonal difference of total precipitation GlacA - CTRL (1958-2003) [%]. The upper (lower) number in each panel represents the percentage of glaciated grid boxes showing a significant positive (negative) difference of the seasonal mean (99% confidence level, one-sided test).

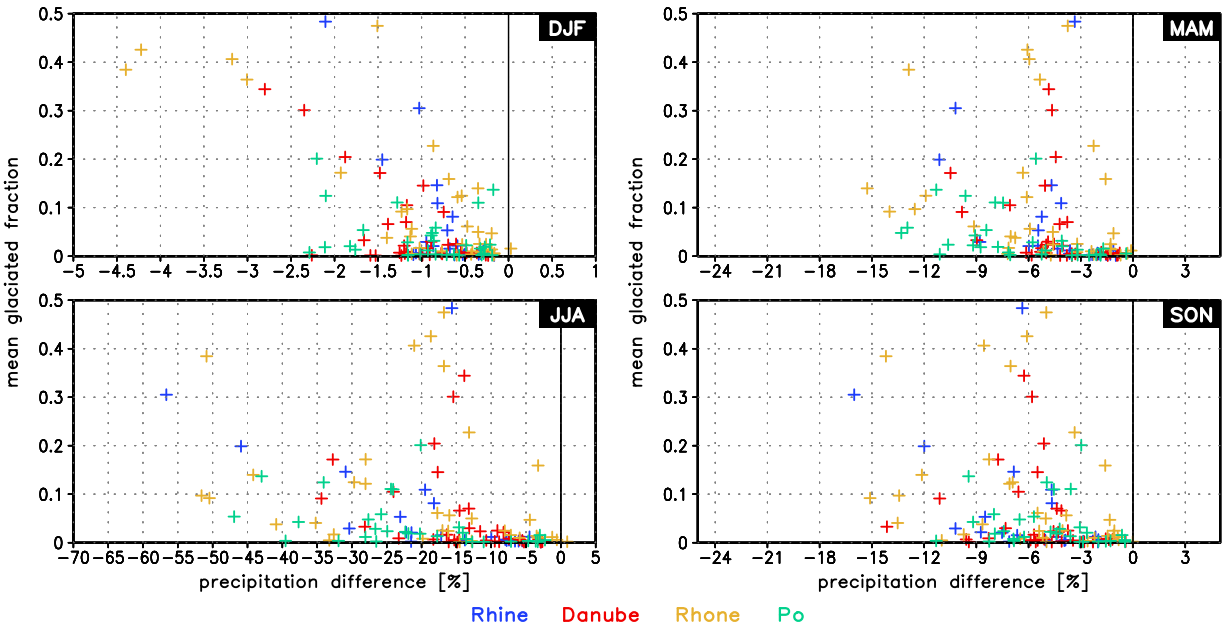

Figure 5.52: Relation between the mean glaciated grid box fraction and the seasonal difference of total precipitation GlacA - CTRL (1958-2003) [%]. Each cross represents one glaciated REMO grid box and is colour-coded according to the respective catchment.

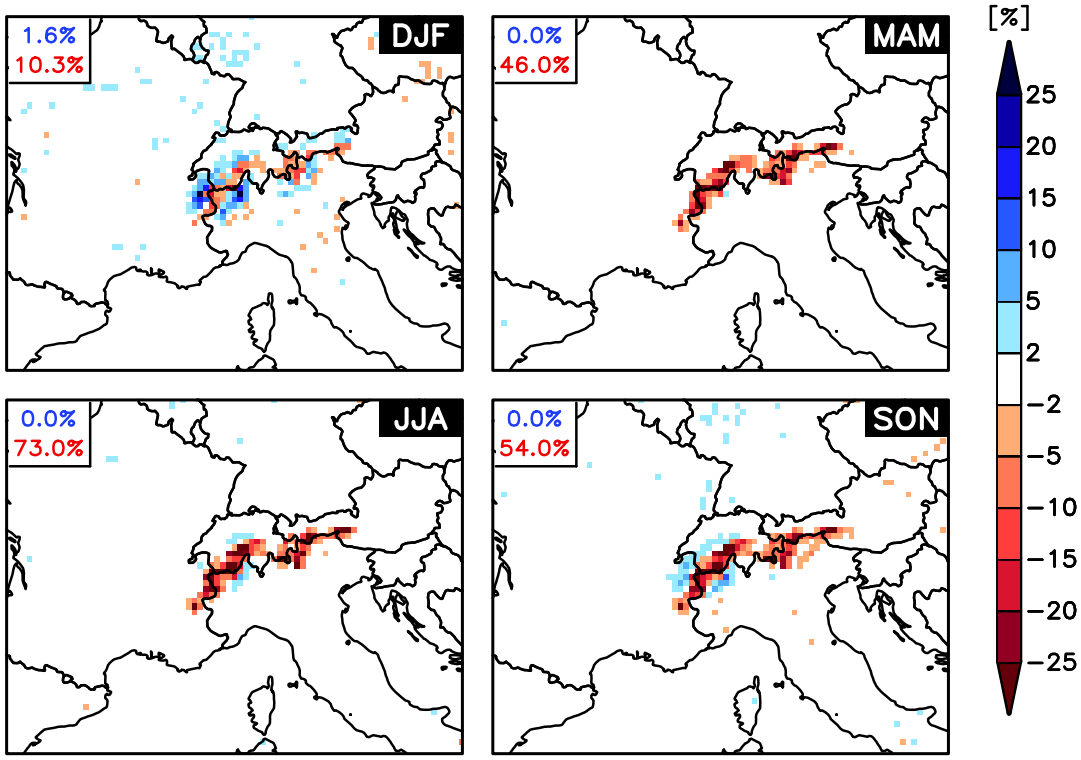

Figure 5.53: Seasonal difference of surface evaporation GlacA - CTRL (1958-2003) [%]. The upper (lower) number in each panel represents the percentage of glaciated grid boxes showing a significant positive (negative) difference of the seasonal mean (99% confidence level, one-sided test).

lower near surface humidity in the glacier simulation with maximum deviations of -28% on the grid box scale. Again, the influence on humidity is mainly restricted to the lower troposphere. In the 500 hPa level GlacA only shows a slight reduction of humidity with respect to CTRL which is not significant. Integrated over the entire atmospheric column only a very small reduction of humidity can be observed in summer (up to -4.5% in single grid boxes) and no significant changes occur during the rest of the year. The mean grid box cloud cover is slightly reduced in summertime which is in line with the lower humidity and with the reduction of both convective and large-scale precipitation. Also the amount of incoming longwave radiation in summer is slightly lower in GlacA compared to CTRL, which is probably caused by the lower air temperature.

The large scale flow conditions, expressed by the spatial patterns of mean sea level pressure, surface pressure and geopotential height, are not significantly affected by the new glacier subgrid parameterisation. Obviously, the glaciated surfaces in the Alps are too small in order to influence these parameters. In this respect, it has to be kept in mind that the integration domain used in the present study (Figure 5.1) is comparatively small and that the large-scale flow conditions are thus strongly determined by the lateral boundary conditions (which are identical in GlacA and CTRL).

5.4.5 Discussion

Summarising the results described above, the main effect of the inclusion of the new glacier parameterisation scheme into REMO is a lowering of the near-surface air temperature and a reduction

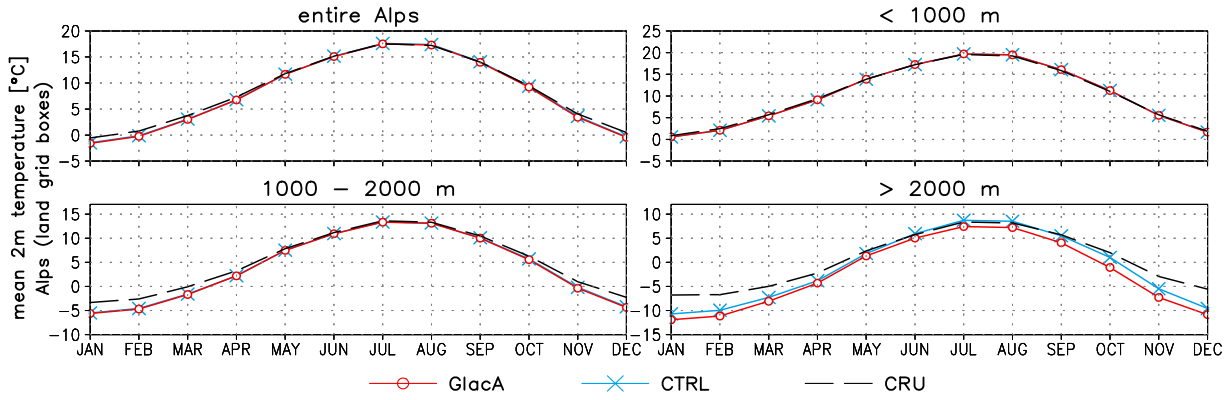

Figure 5.54: Climatological spatial mean of the monthly 2m temperature (1958-2000) [°C] for the entire Alpine region (land grid boxes only) and three altitudinal intervals as simulated by the GlacA (red) and CTRL (blue) and as derived from the CRU dataset.

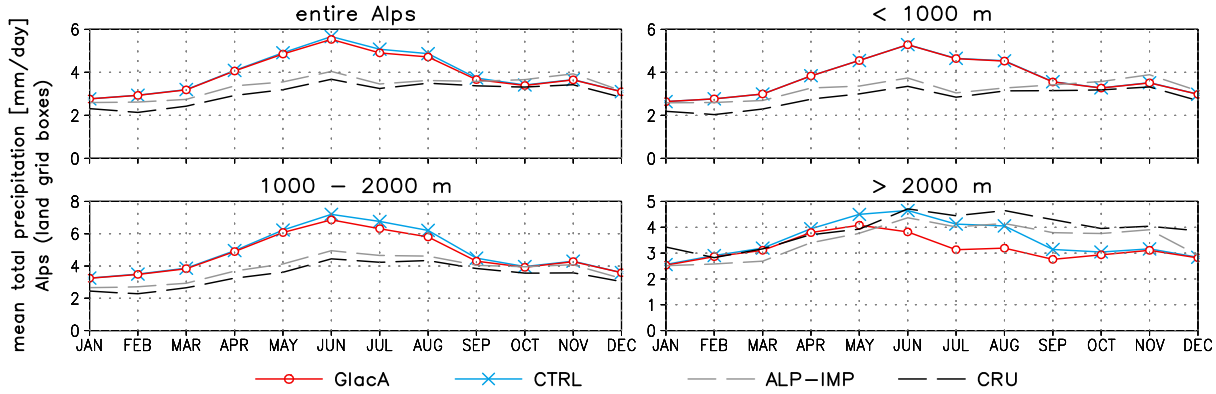

Figure 5.55: Climatological spatial mean of monthly precipitation (1958-2000) [mm/day] for the entire Alpine region (land grid boxes only) and three altitudinal intervals as simulated by GlacA (red) and CTRL (blue) and as derived from two observational datasets (ALP-IMP, CRU).

of precipitation. Both effects are most pronounced in summer and autumn. The lowering of the air temperature compared to the control simulation has to be attributed to a number of factors, mainly the comparatively high surface albedo of the glaciated grid box fractions and a surface temperature never exceeding 0°C. These effects are not only caused by the surface characteristics of the glacier cuboid itself, but partly arise from the longer persistence of snow due to the subgrid redistribution of snowfall. The decrease of precipitation is associated with a general decline of the intensity of the local recycling of water by surface evaporation and precipitation. Generally, the influence of the new parameterisation scheme is mainly restricted to glaciated areas in the Alps and their direct vicinity. Furthermore, only conditions in the lower troposphere are significantly influenced. The large-scale flows conditions are not affected, at least not in the chosen model setup.

At this point it should also be noted that, recalling the biases of the $\text{REMO}_{\texttt{glacier}}$ simulations with respect to observations (Chapter 5.3), the new glacier parameterisation scheme does not improve the

quality of the model simulations in high-altitude areas but generally leads to larger biases. Both the underestimation of winter temperatures and of summer precipitation in grid boxes above 2000 m a.s.l. are stronger in GlacA than in the CTRL experiment (Figures 5.54 and 5.55).

5.5 Model Sensitivities

In order to assess the main sensitivities of $\text{REMO}_{\texttt{glacier}}$ with respect to individual model parameters and regarding the inclusion of specific processes in the model, several sensitivity studies have been performed. The general setup of these experiments is identical to that of the baseline simulations (see Chapter 5.1) and in all cases AAM 1 has been used. Hence, the model sensitivities can be derived from a comparison between the respective sensitivity experiment and the baseline simulation GlacA. An emphasis is laid on the simulated Alpine-wide glacier mass balance and the evolution of the total glaciated area in the model domain. In some cases, differences between the sensitivity experiment and the baseline simulation GlacA are additionally exemplified by the mean annual cycle of individual model variables in three grid boxes in different parts of the Alps (Box1, Box2, Box3; see Figure 5.56) with a comparatively large initial glacier cover (24.7, 35.5 and 28.8%, respectively). Table 5.5 gives an overview of the sensitivity experiments carried out within the present study. Due to restrictions in computing time not all simulations cover the entire period 1958-2003.

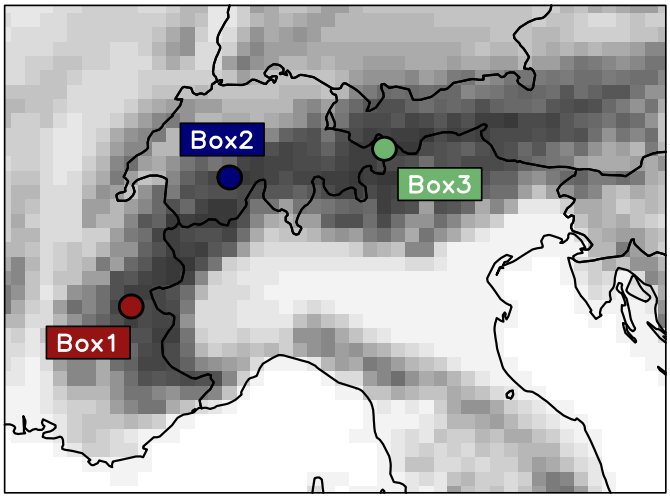

Figure 5.56: Orography of the Alpine area and location of the three benchmark REMO grid boxes used for illustrating the model sensitivities.

5.5.1 Ice Albedo (SensA)

An important control on the total surface energy budget of a glacier and, hence, on the ablation of snow and ice is exerted by the glacier surface albedo in the solar spectrum α_{surf}. In case of an exposed ice surface (no snow on top of the glacier cuboid) α_{surf} equals the ice albedo α_{ice}. In the sensitivity experiment SensA the constant value of $\alpha_{ice} = 0.4$ (Method A) has been replaced by Method B in which α_{ice} varies between 0.3 and 0.4 depending on the ice surface temperature (see Chapter 4.2.3).

Figure 5.57 shows the evolution of the simulated total Alpine glacier mass balance and of the total ice area for the sensitivity experiment SensA and the baseline simulation GlacA. The annual specific mass balance differs only slightly between both simulations and the interannual variability is almost identical. However, in years of a negative mass balance the glacier mass loss is slightly larger in the sensitivity experiment. The mean specific mass balance over the entire period decreases by 0.04 m w.e./year (-0.17 compared to -0.13 m w.e./year in GlacA) which, at the end of the simulation, leads to a considerably larger net mass loss (-5.13 m w.e., 1960-2003) compared to the baseline simulation (-

Name	Characteristics	Period	AAM	Direct control on
SensA	Ice albedo varies between 0.3 and 0.4, depending on surface temperature (Method B, see Chapter 4.2.3). **GlacA**: Ice albedo is fixed at 0.4.	1958 - 2003	1	ablation
SensB	SRAD ratio = 1.0 in all months (no radiation scaling). **GlacA**: Radiation scaling is applied.	1958 - 2003	1	ablation
SensC$_1$ **SensC$_2$**	No / less redistribution of snow. Redistribution factor κ_{eff} = 1.0 (SensC$_1$) and <= 1.5 (SensC$_2$). **GlacA**: κ_{eff} <= 2.0.	1958 - 1987	1	accumulation
SensD	Critical snow age for transformation into ice $ZACRIT$ = 5 years. **GlacA**: $ZACRIT$ = 2 years.	1958 - 1992	1	ablation
SensE$_1$ **SensE$_2$**	Subgrid transformation of rainfall into snowfall at mean glacier altitude. Temperature threshold: 0°C (SensE$_1$), 1°C (SensE$_2$). **GlacA**: No transformation.	1958 - 1987	1	accumulation
SensF	Snow redistribution factor κ_{eff} = 1.0 (as in SensC$_1$) plus modification of the sensible heat flux over glaciated surfaces. Glaciers are shifted to the mean glacier altitude of the respective grid box where a different air temperature prevails. **GlacA**: The mean grid box air temperature is assumed over glaciated surfaces.	1958 - 1987	1	ablation
SensG	Aerodynamic roughness length of glacier ice $z_{0,ice}$ = 0.01 m. **GlacA**: $z_{0,ice}$ = 0.001 m.	1958 - 1996	1	ablation

Table 5.5: Sensitivity studies carried out within the present study.

3.53 m w.e.). Accordingly, the decrease of the total Alpine ice area is larger in SensA (-28.4%) than in GlacA (-23.8%). The total amount of Alpine ice melt increases by 10.5%.

Hence, the general effect of the modified albedo parameterisation, which lowers the ice surface albedo especially during melt periods (ice surface temperature close to 0°C), is a slightly increased glacier mass loss due to an increased absorption of solar radiation. The effect is most pronounced in years of a negative total mass balance which are often associated with below-than-average snow accumulation (see Chapter 5.2.1). In these years, the glacier surfaces get exposed earlier and changes of the ice surface albedo are more effective. In periods of high snow accumulation the glaciated grid box fractions are often covered by snow with its comparatively high albedo for the entire year. As a consequence, the role of α_{ice} is far less important and differences in the simulated mass balance between GlacA and SensA are small. The same is generally true for the second half of the simulated period, in which large fractions of the total Alpine ice area are permanently covered by snow in the REMO$_{\texttt{glacier}}$ experiments (see Figure 5.31).

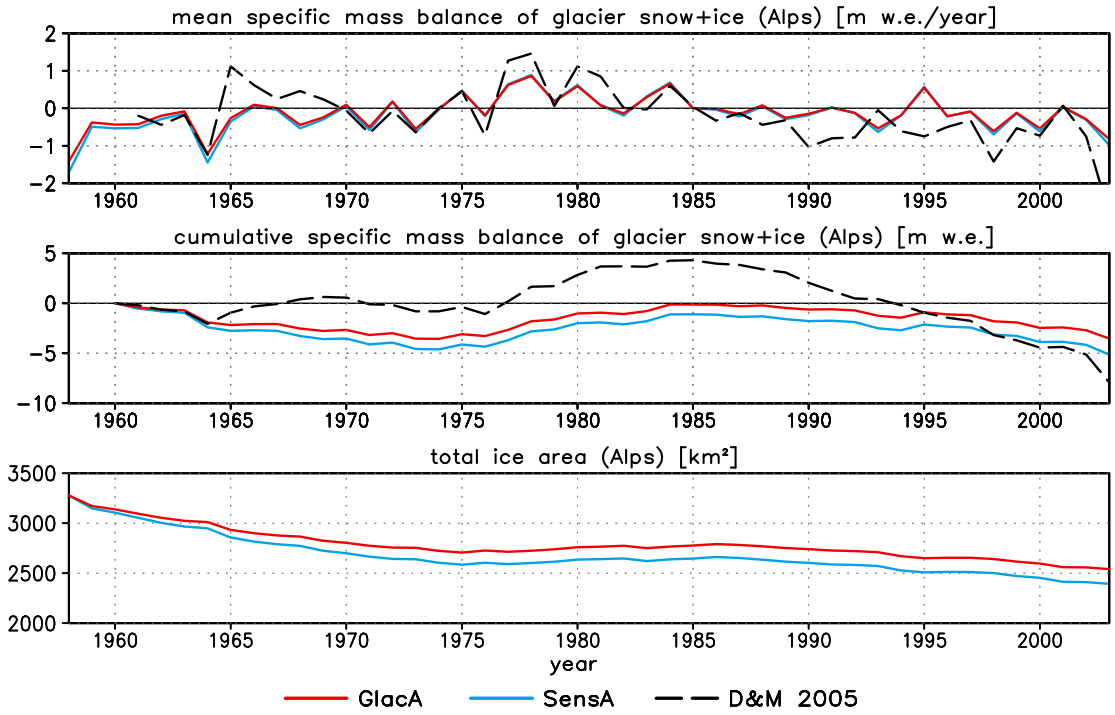

Figure 5.57: Evolution of the mean specific mass balance (upper panel), cumulative mass balance (middle panel) and total ice area in the model domain (lower panel) for the simulations GlacA and SensA. D&M 2005: observed mass balance as derived from Dyurgerov and Meier (2005).

5.5.2 Radiation Scaling (SensB)

On most glaciers solar radiation is the main source of energy with a dominant influence on ablation (see Chapter 4.2.3). In order to account for topographic effects on a subgrid scale (inclined surfaces, topographic shading), the incoming solar radiation (global radiation) flux on glaciated surfaces is scaled in $\text{REMO}_{\text{glacier}}$ using the monthly SRAD ratio $r_{G,i}$ (Chapter 4.2.6). This ratio is smaller than 1 for most grid boxes and for most parts of the year (Figure 4.8) which means that glaciers receive less solar radiation than the grid box average. The sensitivity experiment SensB allows to assess the influence of the radiation scaling on the simulated glacier mass balance since $r_{G,i}$ is set to the constant value of 1.0 and, hence, topographic effects are not accounted for in this simulation.

The comparison of the experiments GlacA and SensB reveals that the radiation scaling has a very strong influence on the simulated mass balance. In SensB the increased incoming flux of solar radiation leads to a strong negative deviation of the mean Alpine mass balance throughout the entire simulated period (Figure 5.58, upper panel). The mean specific mass balance decreases by 0.66 m w.e./year (-0.79 m w.e. compared to -0.13 m w.e. in GlacA) and, accordingly, the cumulative balance for the period 1960-2003 decreases drastically (-30.87 m w.e. compared to -3.53 m w.e.). After 46 years of continuous simulation the total Alpine glaciated area in the sensitivity experiment has declined by as much as 66% (-23.8% in GlacA). The change in global radiation over glaciated surfaces and the induced increase of ablation is illustrated in Figure 5.59 for the three benchmark boxes. Throughout the entire year the incoming solar radiation flux is considerably larger in SensB with maximum deviations of up to 50 W/m^2 from March to September. This energy surplus leads to a strong increase of snow

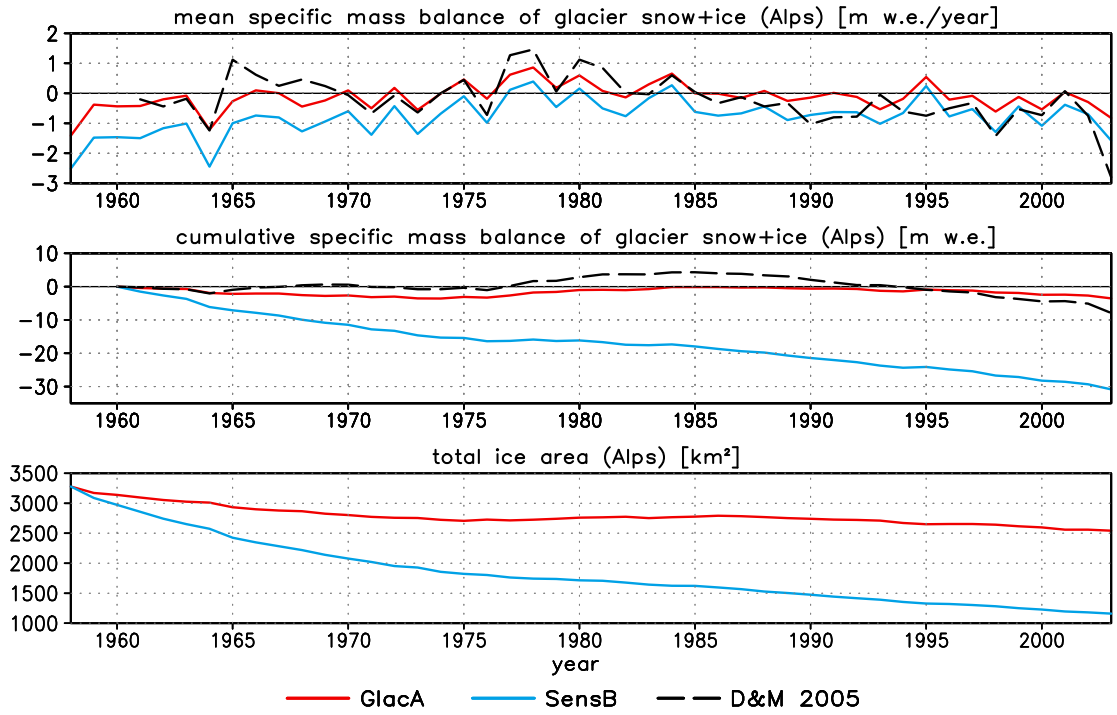

Figure 5.58: Evolution of the mean specific mass balance (upper panel), cumulative mass balance (middle panel) and total ice area in the model domain (lower panel) for the simulations GlacA and SensB. D&M 2005: observed mass balance as derived from Dyurgerov and Meier (2005).

and ice ablation, which is largest in late summer when the surface temperature is close to the melting point and the dark ice surfaces with their low albedo become exposed. In these times an increase in global radiation is most effective regarding meltwater production.

The strong influence of the radiation scaling on the simulated glacier mass balance underlines the need for an explicit consideration of topographic effects on a subgrid level in the new parameterisation scheme. A neglection of these effects can potentially lead to strong biases of the surface energy balance and, hence, of the simulated melt rates.

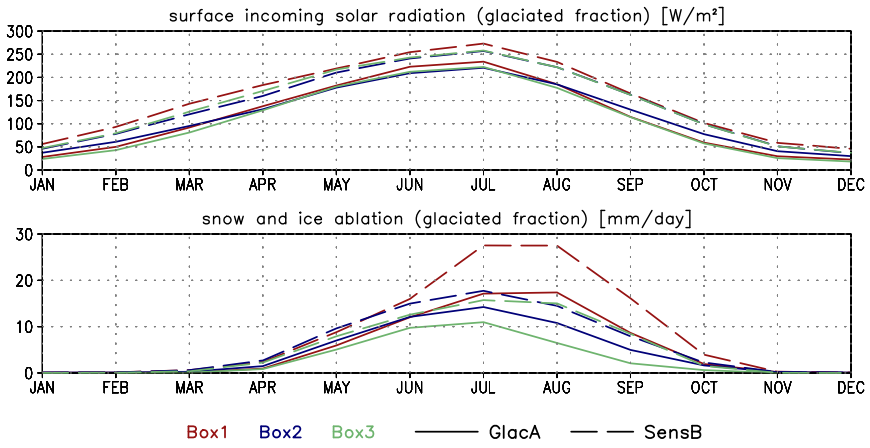

Figure 5.59: Mean annual cycle (1958-2003) of incoming solar radiation on the glaciated grid box fraction [W/m^2] (upper panel) and total ablation [mm/day] (lower panel) for the three benchmark grid boxes (see Figure 5.56) in the simulations GlacA and SensB.

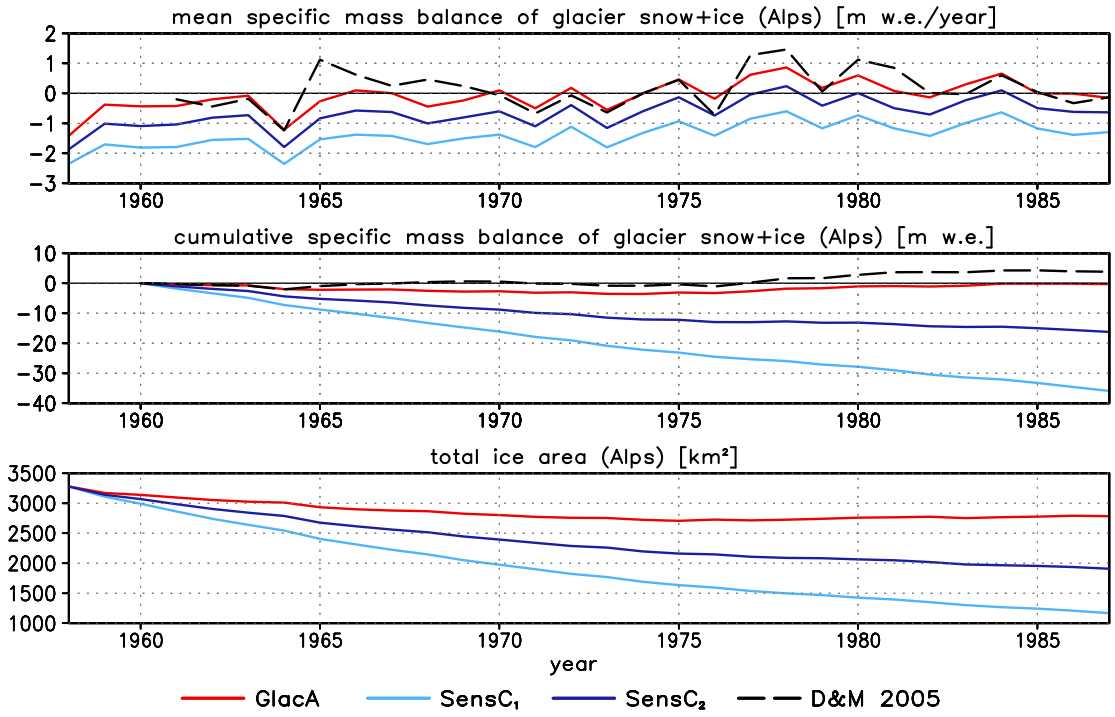

Figure 5.60: Evolution of the mean specific mass balance (upper panel), cumulative mass balance (middle panel) and total ice area in the model domain (lower panel) for the simulations GlacA, SensC$_1$ and SensC$_2$. D&M 2005: observed mass balance as derived from Dyurgerov and Meier (2005).

5.5.3 Snow Redistribution (SensC$_1$, SensC$_2$)

In order to account for the subgrid variability of snow accumulation caused by

a) the spatial variability of the amount and the phase of precipitation

b) the redistribution of fallen snow by wind and avalanches

the mean grid box snowfall is redistributed in REMO$_{\texttt{glacier}}$ from non-glaciated to glaciated surfaces (see Chapter 4.2.7). The redistribution factor κ_{eff} denotes the relation between the amount of snow falling onto the glaciated grid box fraction and the mean grid box snowfall. In the standard parameterisation its maximum value is $\kappa = 2$, i.e., the glaciated grid box fraction receives twice as much snow (expressed as snow column height) compared to the grid box mean. In order to assess the sensitivity of the simulated mass balance to the redistribution of snow two sensitivity experiments have been carried out in which the maximum redistribution factor is set to $\kappa = 1$ (i.e., no redistribution of snow; SensC$_1$) and $\kappa = 1.5$ (SensC$_2$), respectively.

From Figure 5.60 it can be clearly seen that the redistribution of snow plays a major role for the simulated glacier mass balance and the evolution of the total Alpine ice area. In case that no redistribution is carried out (SensC$_1$) the mean specific mass balance decreases by as much as 1.32 m w.e./year for the period 1958-1987 (-1.40 m w.e. compared to -0.08 m w.e. in the baseline experiment GlacA) and the cumulative mass loss for the same period amounts to -35.90 m w.e. (compared to -0.30 m w.e. in GlacA). In SensC$_1$ no single year with a positive mean specific mass balance occurs. The general temporal evolution of the annual mass balance does not change with respect to the baseline experiment, although the amplitude of interannual mass balance variations is slightly dampened. By the year 1987

65.9% of the glaciated area at initialisation is lost, which is considerably more than the area loss in GlacA (-15.6%). The respective values for SensC$_2$ lie in between those for SensC$_1$ and GlacA (mean specific mass balance: -0.67 m w.e./year, cumulative mass balance: -16.23 m w.e., area loss: -43.0%).

Generally, the strong influence of changes of the snow redistribution factor on the simulated glacier mass balance can be explained by two effects. On one hand, a smaller factor κ_{eff} reduces the amount of snow accumulation on glaciated surfaces (if the mean grid box snowfall rate is assumed to be identical in both simulations) with a direct negative effect on the net balance. In SensC$_1$ the average amount of snow accumulation on glaciated surfaces in the Alps is about 49.5% lower than in GlacA (SensC$_2$: -24.0%). A second, indirect effect is the earlier exposure of ice surfaces in spring/summer due to the reduced amount of winter accumulation. The lower albedo of ice compared to snow causes an enhanced melting with an additional negative effect on the net mass balance.

Summarising the results described above, the sensitivity studies SensC$_1$ and SensC$_2$ have shown that the subgrid variability of precipitation and snow accumulation is one of the major factors controlling the simulated glacier mass balance. The simple concept of snow redistribution as applied in the present study is one possible way of incorporating these effects. At the same time the choice of a specific redistribution factor κ being constant both in time and in space is a major factor of uncertainty with respect to the glacier mass balance as simulated by REMO$_{\texttt{glacier}}$.

5.5.4 Critical Snow Age (SensD)

REMO$_{\texttt{glacier}}$ generally discriminates between the glacier cuboid itself and a snow layer on top of the cuboid. If snow on the glaciated or the non-glaciated grid box fraction has reached the critical age of $ZACRIT = 2$ years it is partly transformed into ice. This transformation process adds mass to the glacier cuboid (see Chapter 4.2.4). The threshold of 2 years has been chosen as a compromise between the time it takes for snow to be transformed into firn (which is not accounted for explicitly) and the total time necessary for the transformation of snow into ice. In temperate regions, the latter amounts to 5 to 10 years at minimum and therefore $ZACRIT = 2$ years has to be considered as a lower boundary for real-world conditions.

In the sensitivity experiment SensD $ZACRIT$ has been increased to 5 years. The higher critical snow age has only minor effects on the simulated specific mass balance in the Alps (not shown). The mean mass balance for the period 1958-1992 amounts to -0.07 m w.e./year in SensD compared to -0.08 m w.e./year in GlacA. The slightly reduced glacier mass loss can be explained by the difference in the surface albedo of snow and ice. In the sensitivity experiment, snow with its high albedo generally persists for a longer period before being transformed into dark ice which, obviously, slightly increases the mean albedo and reduces ablation.

The minor effect of variations in $ZACRIT$ on the simulated glacier mass balance underlines the comparatively low importance of this model parameter.

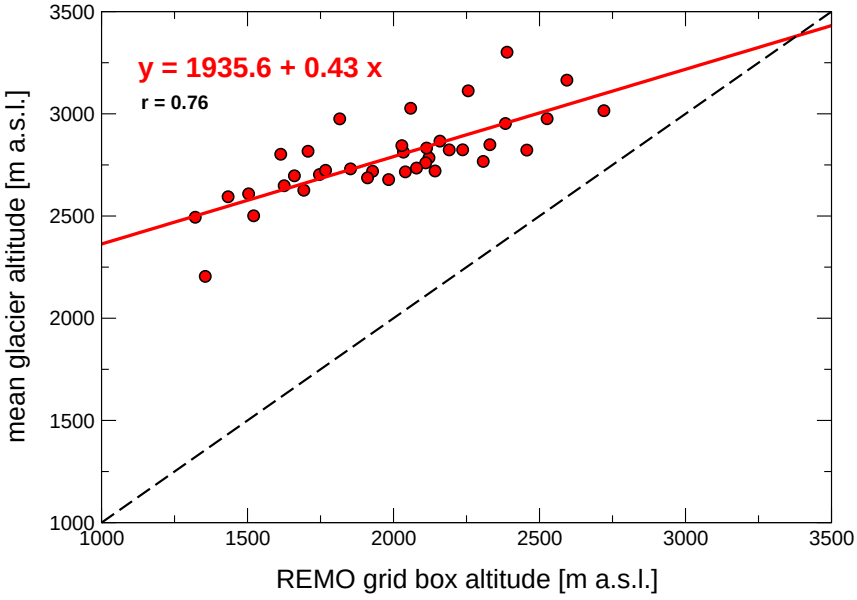

Figure 5.61: Relation between the REMO grid box altitude (x-axis) and the area-weighted mean glacier altitude (y-axis) for the Swiss part of the model domain. Each dot represents one glaciated REMO grid box. The dashed line denotes the 1:1 relation, the red line shows the best linear fit as obtained by linear regression.

5.5.5 Transformation of Rainfall (SensE$_1$, SensE$_2$)

In REMO$_{\texttt{glacier}}$ the altitude of the glacier cuboid surface is assumed to be identical to the mean grid box altitude (see Chapter 4.2.2). This is a strong simplification since, on the $^1/_6^\circ$ scale glaciers in the Alps can be expected to be located at higher altitudes than the grid box average. Figure 5.61 illustrates this fact for glaciers in the Swiss Alps: For all glaciated grid boxes the area-weighted mean glacier altitude is considerably higher than the corresponding REMO grid box altitude. The difference diminishes towards higher elevations. A linear regression analysis of the relationship yields a correlation coefficient r of 0.76 and the linear relation

$$\overline{h}_{glac} = 1935.6 + 0.43 \cdot h_{REMO} \tag{5.6}$$

between the area-weighted mean glacier altitude $\overline{h}_{glac}$ [m a.s.l.] and the corresponding REMO grid box altitude h_{REMO} [m a.s.l.].

Assuming a negative relation between air temperature and elevation (i.e., a negative temperature lapse rate), the fact that glaciers are located at higher altitudes means that they are usually exposed to a lower air temperature. This can have several implications, for instance in terms of the exchange of sensible heat between the glacier surface and the overlying air mass (sensitivity study SensF, see below). A further effect is related to the spatial variability of the phase of precipitation in mountainous terrain. While precipitation can fall as rain in the relatively warm valleys, high-elevation sites can receive snowfall at the same time. Hence, under certain conditions high-elevated glaciated surfaces in REMO$_{\texttt{glacier}}$ can be assumed to receive snowfall while rainfall occurs in the remaining part of the grid box. Presumably, this subgrid effect is most pronounced in spring and autumn when mean grid box air temperatures are above the freezing point but temperatures at high-elevation sites are still below 0°C.

The standard version of REMO$_{\texttt{glacier}}$ does not account for the subgrid variability of the phase of precipitation, but its effect is investigated in the sensitivity studies SensE$_1$ and SensE$_2$. In both experiments the near-surface air temperature T_{glac} [°C] at the mean glacier altitude is computed in each model timestep based on the temperature T_{lev20} [°C] of the lowest atmospheric level and assuming

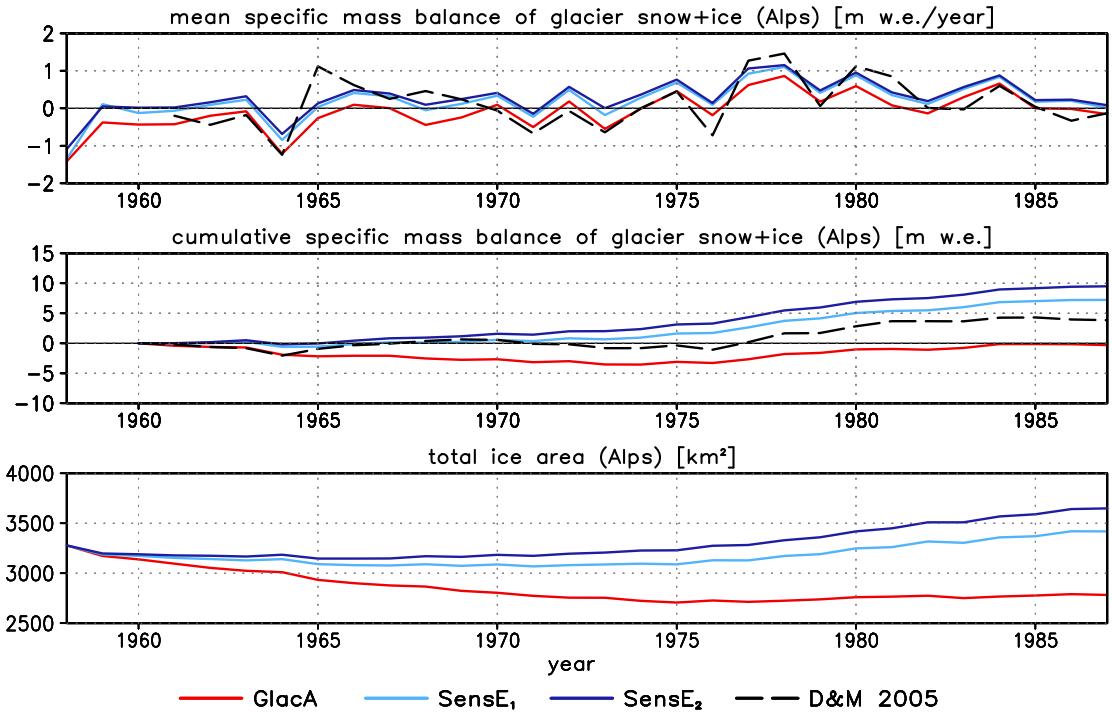

Figure 5.62: Evolution of the mean specific mass balance (upper panel), cumulative mass balance (middle panel) and total ice area in the model domain (lower panel) for the simulations GlacA, SensE$_1$ and SensE$_2$. D&M 2005: observed mass balance as derived from Dyurgerov and Meier (2005).

- ▷ the validity of Equation 5.6 not only for Switzerland but for the entire model domain and for the entire simulated period
- ▷ a constant temperature lapse rate of -0.65°C/100m :

$$T_{glac} = T_{lev20} - 0.0065 \cdot (\overline{h}_{glac} - h_{REMO}) \tag{5.7}$$

In the model domain, the maximum difference between $\overline{h}_{glac}$ and h_{REMO} is slightly larger than 1100 m, i.e., the mean glacier altitude in the corresponding grid box is about 1100 m higher than the mean grid box altitude! Accordingly, the mean air temperature at glacier altitude T_{glac} is up to 7.5°C lower than T_{lev20}. If in any given timestep T_{glac} falls below the critical threshold of 0°C (SensE$_1$) or +1°C (SensE$_2$) the liquid precipitation (rain) falling onto the grid box surface in the respective timestep is assumed to entirely fall in the form of snow over the glaciated grid box fraction. Over the non-glaciated part no modifications are carried out and the phase of precipitation remains unchanged. Given identical amounts of total precipitation in GlacA, SensE$_1$ and SensE$_2$, the amount of snow accumulation on glaciers is thus "artificially" increased in the sensitivity studies with respect to the baseline simulation. SensE$_1$ and SensE$_2$ serve as first test simulations towards the explicit inclusion of subgrid elevation classes in REMO$_{\texttt{glacier}}$ which is planned at a later stage (see Chapter 6).

Over the entire simulated period, the increase of mean snow accumulation on glaciated surfaces with respect to the baseline experiment amounts to +14% in SensE$_1$ and +19.1% in SensE$_2$. The larger value for SensE$_2$ is due to the higher temperature threshold for the transformation of rain into snow in this experiment. On a monthly basis, the largest relative changes of more than 70% in SensE$_1$ and

even more than 100% in SensE$_2$ occur in August. As expected, the absolute increases of mean snow accumulation are largest in spring and autumn (not shown). The net effect of the enhanced snow accumulation is a noticeable increase of the simulated glacier mass balance (Figure 5.62). The mean net balance for the period 1958-1987 changes from a negative value in GlacA (-0.08 m w.e./year) to a net mass gain in SensE$_1$ (0.20 m w.e./year) and SensE$_2$ (0.28 m w.e./year). Accordingly, the cumulative mass balance increases clearly (7.24 and 9.61 m w.e. compared to -0.30 m w.e. in GlacA). In both sensitivity studies the total glacier-covered area increases in the course of the model simulation (+4.6% and +11.9%, respectively).

The pronounced differences between the simulated glacier mass balance in SensE$_1$ and SensE$_2$ on one side and in GlacA on the other side point to the strong need for incorporating subgrid variability of elevation and, hence, of air temperature into the new parameterisation scheme. So far, these features are not explicitly accounted for in the standard version of REMO$_{\text{glacier}}$ but the simple concept used in SensE$_1$ and SensE$_2$ proposes one way of doing so in terms of the phase of precipitation. Presumably, a major point of uncertainty is the choice of a constant temperature lapse rate. In principle, this lapse rate could also be computed separately for each grid box and each time step based on the simulated vertical temperature gradient in REMO$_{\text{glacier}}$.

5.5.6 Air Temperature Adjustment (SensF)

Presumably, the neglection of subgrid scale variability of temperature in REMO$_{\text{glacier}}$ causes an overestimation of the air temperature above glaciated surfaces (see above). In addition to the effect on the phase of precipitation (SensE$_1$, SensE$_2$) this has also implications for the exchange of sensible and latent heat between the glacier surface and the overlying air. In order to assess the importance of this shortcoming in the model formulation on the simulated glacier mass balance a further sensitivity study (SensF) has been carried out. In this experiment the air temperature at the mean glacier altitude (T_{glac}) is computed according to Equation 5.7 in each timestep. T_{glac} is then used instead of T_{lev20} for the computation of the turbulent transfer coefficient C_χ (sensible and latent heat) and for the near-surface temperature gradient used for the calculation of the sensible heat flux (Equation 4.5). In addition, the snowfall redistribution factor is set to $\kappa = 1.0$, i.e., no redistribution is carried out.

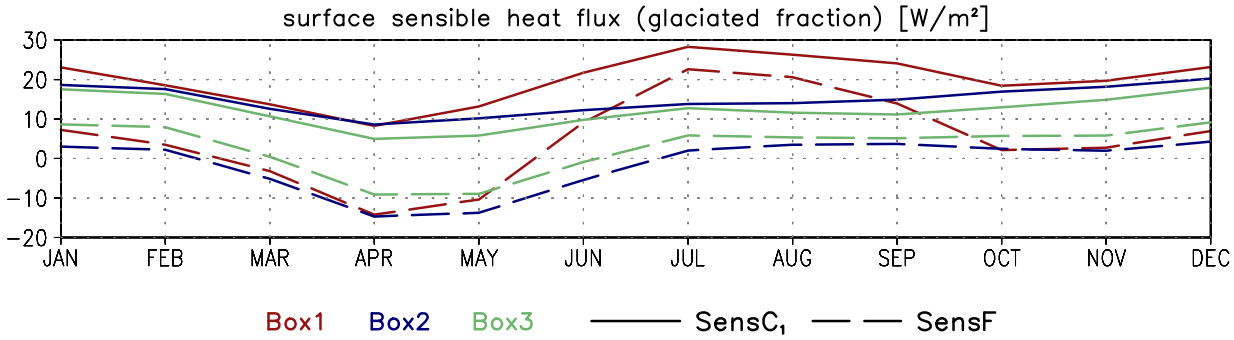

Figure 5.63: Mean annual cycle (1958-1987) of the surface sensible heat flux over the glaciated grid box fraction [W/m^2] for the three benchmark grid boxes (see Figure 5.56) in the simulations SensC$_1$ and SensF. Positive values denote a gain of energy for the surface, i.e., a downward flux of sensible heat.

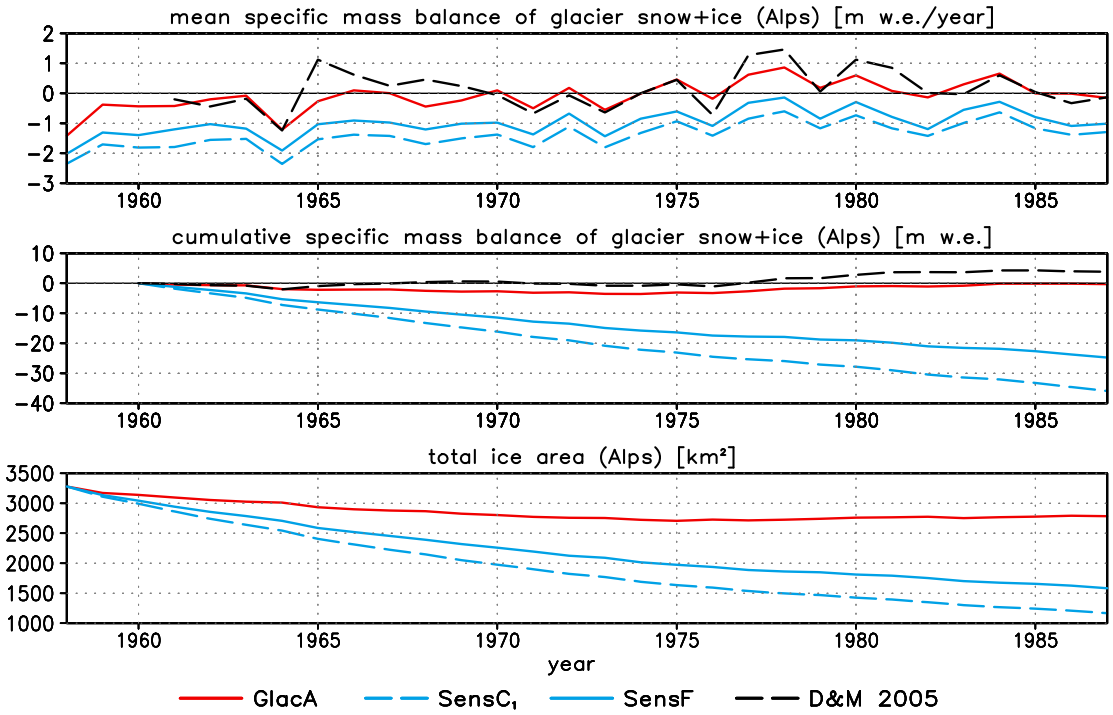

Figure 5.64: Evolution of the mean specific mass balance (upper panel), cumulative mass balance (middle panel) and total ice area in the model domain (lower panel) for the simulations GlacA, SensC$_1$ and SensF. D&M 2005: observed mass balance as derived from Dyurgerov and Meier (2005).

Therefore, the results of SensF have to be compared to those of SensC$_1$. Similarly to the sensitivity experiments SensE$_1$ and SensE$_2$ (see above) SensF can be considered as one further step towards the explicit inclusion of subgrid variability of elevation and, hence, of air temperature in REMO$_{\texttt{glacier}}$.

The effect of the consideration of a temperature lapse rate on the subgrid level on the sensible heat flux over glaciated surfaces is shown in Figure 5.63 for the three benchmark grid boxes. Throughout the entire year the sensible heat flux in SensF decreases by several W/m^2 compared to SensC$_1$ in all three boxes. In the positive co-domain this denotes a smaller supply of energy from the air towards the surface which can be explained by the lower air temperature above glaciated surfaces in SensF. Largest differences of more than 10 W/m^2 occur in springtime. In this part of the year the sign of the mean sensible heat flux even changes to negative values which denotes an energy loss of the surface due to a negative near-surface temperature gradient (surface warmer than air).

The surface latent heat flux, on the other side, slightly increases (not shown). This increase is of a lower magnitude than the change in the sensible heat flux and, hence, the net effect is a reduced total heat flux towards the glacier surface compared to SensC$_1$. This decrease in the supply of energy leads to a reduction of ablation and, consequently, to a considerably increased specific mass balance (Figure 5.64). Compared to the experiment SensC$_1$ the mean specific mass balance of the period 1958-1987 rises from -1.40 m w.e./year to -0.98 m w.e./year and the cumulative balance from -35.9 m w.e. to -24.8 m w.e.. The decrease of the total glaciated area in the Alps is reduced from -65.9% to -53.1%.

The results obtained for the sensitivity experiment SensF underline the high importance of the subgrid variability of air temperature due to its prominent effect on the simulated

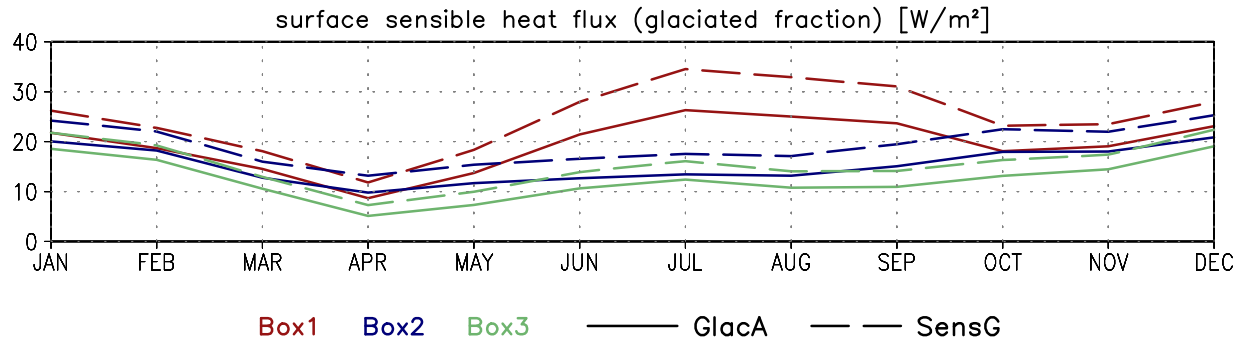

Figure 5.65: Mean annual cycle (1958-1996) of the surface sensible heat flux over the glaciated grid box fraction [W/m^2] for the three benchmark grid boxes (see Figure 5.56) in the simulations GlacA and SensG. Positive values denote a gain of energy for the surface, i.e., a downward flux of sensible heat.

glacier mass balance. The overall effect of incorporating this feature into REMO$_{\texttt{glacier}}$ is an increase of accumulation (SensE$_1$ and SensE$_2$) and a reduced ablation (SensF), hence, a general increase of glacier mass balance. Also in the case of SensF the choice of a constant atmospheric temperature lapse rate has to be considered as a major point of uncertainty (see above).

5.5.7 Roughness Length (SensG)

The turbulence structure in the near-surface air layer is often strongly influenced by the inhomogeneous nature of the underlying surface. The aerodynamic roughness length z_0 is a measure of the roughness of the terrain with its corresponding effects on turbulent exchange processes. In REMO$_{\texttt{glacier}}$ the roughness length of glacier ice $z_{0,ice}$ is by default set to 0.001 m (see Chapter 4.2.3). This value approximately corresponds to the roughness length commonly applied for a flat, snow-covered surface but probably underestimates the value for a melting ice surface in the ablation zone (e.g., Kuhn, 1979). In order to test the sensitivity of glacier mass balance in REMO$_{\texttt{glacier}}$ to this parameter, $z_{0,ice}$ has been multiplied by 10 and set to 0.01 m in the sensitivity experiment SensG.

As can be seen from figure 5.65 the direct effect of the increase of $z_{0,ice}$ is an increase of the sensible heat flux over glaciated surfaces by several W/m^2 throughout the entire year which is probably related to an intensification of the near-surface turbulent activity. Also the latent heat flux is increased, but differences between GlacA and SensG are of a lower magnitude (not shown). The corresponding energy surplus at the surface leads to a stronger ablation of snow and ice and, consequently, to a decrease of the mean alpine glacier mass balance for the period 1958-1996 from -0.09 m w.e./year in GlacA to -0.33 m w.e./year in SensG (Figure 5.66). By the year 1996 this enhanced glacier mass loss in the sensitivity experiment leads to a strong negative cumulative balance of -9.42 m w.e. (compared to -1.11 m w.e. in GlacA). The total area loss in the Alps increases from -19.2% to -37.2%.

This strong influence of $z_{0,ice}$ on the simulated glacier mass balance and the changes in ice area points to the high importance of this parameter. However, it should be noted that the clear negative effect of an increased roughness length on the simulated mass balance is partly due to the fact that the mean surface sensible heat flux over glaciers is usually positive throughout the entire

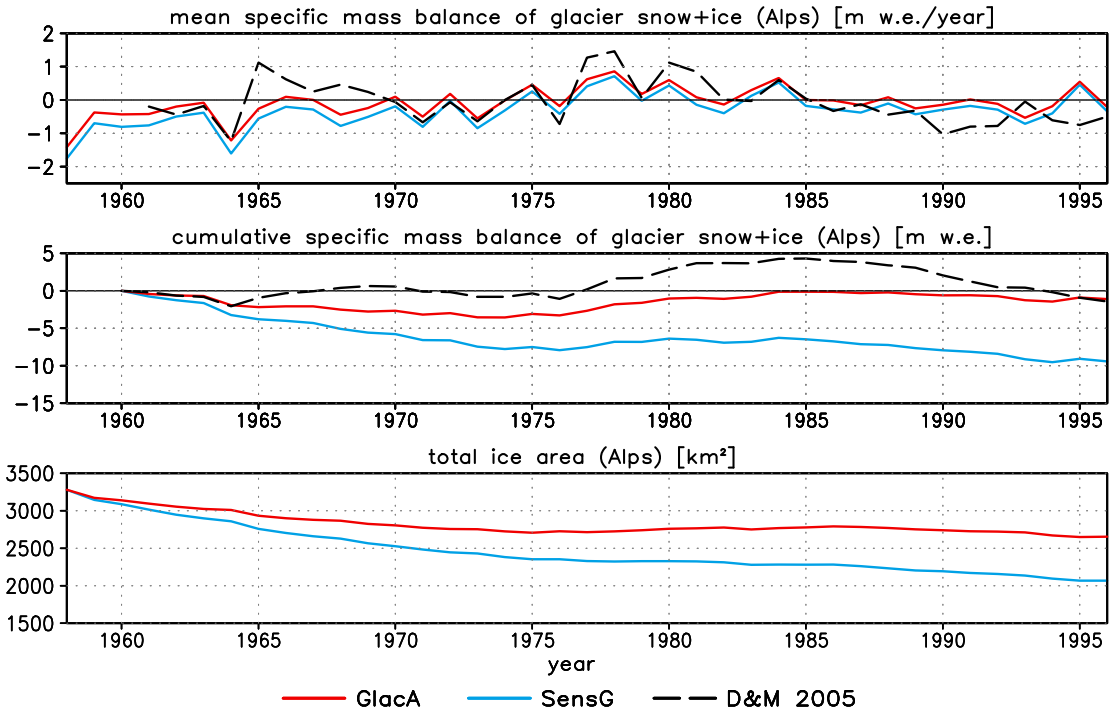

Figure 5.66: Evolution of the mean specific mass balance (upper panel), cumulative mass balance (middle panel) and total ice area in the model domain (lower panel) for the simulations GlacA and SensG. D&M 2005: observed mass balance as derived from Dyurgerov and Meier (2005).

year. The increase of $z_{0,ice}$ amplifies the corresponding gain of energy for the surface. If SensG would be combined with the sensitivity experiment SensF (adjustment of air temperature, see above) the effect of a larger roughness length can be expected to be less clear since also the loss of energy by the turbulent exchange of sensible heat (due to a negative near-surface temperature gradient) is likely to be amplified.

5.5.8 Discussion

The sensitivity experiments described above reveal that the simulated glacier mass balance and the corresponding glacier area changes in $\text{REMO}_{\texttt{glacier}}$ are strongly dependent on

a) the chosen value for a number of model parameters

b) the inclusion of subgrid processes which are so far not part of the standard parameterisation scheme.

Apparently, a crucial point in the model formulation is the adequate description of the subgrid variability of global radiation, snow accumulation and air temperature. While in the first two cases simple concepts have been incorporated into the standard parameterisation scheme the subgrid variability of air temperature is not yet accounted for explicitly. Given the clear dependency of the simulated glacier mass balance on air temperature variations via direct and indirect effects (sensible heat flux and phase of precipitation, respectively) the subgrid variability of elevation and, hence, of air temperature should be introduced in a next step. The sensitivity experiments SensE_1, SensE_2 and SensF propose one possibility of doing so. Generally, the subgrid variation of air temperature and of snow accumulation

as induced by the respective subgrid parameterisation concepts (up to 7.5°C and 100%, respectively) is of the same order of magnitude as the bias of the simulated temperature and precipitation with respect to observations (Chapter 5.3).

As the explicit consideration of glacier elevations on a subgrid scale with its positive effect on glacier mass balance is not yet incorporated in $\text{REMO}_{\texttt{glacier}}$, the general positive bias of the simulated mass balance with respect to observations (Chapter 5.2.1) points to shortcomings in the formulation of other processes. Here, one obvious candidate is the subgrid redistribution of snow accumulation. Large differences in the simulated mass balance can be achieved by variations in the controlling parameter κ (see SensE_1 and SensE_2). In principle, a too strong redistribution of snow could more or less easily compensate for the neglection of subgrid temperature variations. At the same time, the maximum redistribution factor of $\kappa = 2.0$ in the standard parameterisation (independent of the season and applied in the entire model domain) is not more than a rough estimate and could well be considerably lower or higher than the chosen value. By definition, κ accounts both for the subgrid variation of the amount and the phase of precipitation and for the redistribution of fallen snow by wind and avalanches (see Chapter 4.2.7). A more physically based concept which discriminates between both features and which considers spatial and temporal variations of κ would be desirable. An explicit consideration of variations in the phase of precipitation can also be achieved by accounting for the subgrid variability of air temperature (SensE_1 and SensE_2).

Concerning the assessment of the optimal combination of model parameters, the standard parameterisation (as applied in GlacA) performs comparatively well with respect to the simulated glacier mass balance. However, the use of a temperature-dependent ice albedo (Method B as applied in SensA) would slightly improve the results by enhancing melt rates and thereby leading to a better reproduction of the observed cumulative mean Alpine mass balance (Figure 5.57). Furthermore, an ice albedo α_{ice} lower than 0.4 is more physically based since it is closer to the albedo of exposed real-world glacier surfaces which often contain at least some amount of impurities (see Chapter 2.4.2). The chosen combination of subgrid radiation scaling (which is based on the application of the radiation model SRAD for the Swiss part of the model domain) and snow redistribution (which is not more than a rough estimate) also yields more or less realistic results. Problems occur along the north-facing slopes of the main Alpine ridge (Rhine catchment) where the amount of snow accumulation is very high and simulated mass balances are strongly positive (Chapter 5.2.1). Apart from biases of the simulated amount of precipitation with respect to observations (Chapter 5.3.1) this fact could also partly arise from a too large snow redistribution factor κ. The incorporation of subgrid elevation classes with its positive effect on glacier mass balance (SensE_1, SensE_2, SensF) would generally allow for a smaller value of κ which would, in turn, reduce the amount of snow accumulation in these areas and would probably lead to smaller biases of the simulated glacier mass balance.

5.6 Glacier Hydrology

Due to their storage characteristics on a variety of timescales, the presence of glaciers can have a considerable influence on catchment hydrology (see Chapter 2.8). The long- to intermediate-term storage function of glaciers, i.e., their influence on interannual variations of runoff and its seasonal cycle due to the storage of water in the form of snow and ice, are represented in $\text{REMO}_{\texttt{glacier}}$ and

should, in principle, be reproduced. On the other hand, the short-term to intermediate-term retention capacity of the englacial and subglacial drainage system and of firn aquifers is so far not accounted for in $\text{REMO}_{\texttt{glacier}}$.

This section investigates the influence of glaciers on the catchment hydrology in $\text{REMO}_{\texttt{glacier}}$ on seasonal and interannual timescales. As the simulated glacier mass balances are very similar in the three glacier baseline simulations (see Chapter 5.2.1), only the experiment GlacA is analysed. In a simplifying manner, the hydrological behaviour is expressed in terms of the temporal evolution of the amount of water draining from a partly glaciated area. In this respect it is generally distinguished between

- **grid box runoff**, i.e., the total amount of water leaving a certain REMO grid box in a specific time step. This quantity includes both surface runoff and subsurface drainage as produced by the climate model's land surface scheme on a local grid box scale (see Chapter 3.3).
- **river discharge**, i.e., the amount of water draining from a specified catchment area within the surface river system during a certain period of time. This quantity is simulated by the lateral routing scheme (HD model, see Chapter 3.4) which is coupled to REMO in an offline mode and which explicitly accounts for the travel time of water in the river system.

5.6.1 Grid Box Runoff

In glaciated $\text{REMO}_{\texttt{glacier}}$ grid boxes the total amount of runoff produced within a given timestep is the sum of the contribution from the non-glaciated part of the grid box and the contribution from the glaciated fraction. In the latter case, it originates from snow and ice melt and from liquid precipitation falling onto the surface of the glacier cuboid (which might additionally be covered by a snow layer). The mean seasonal contribution of runoff originating from the glaciated fraction to the total grid box runoff in the simulation GlacA is compared to the mean glaciated grid box fraction itself in Figure 5.67. In case that the amount of runoff (expressed as volume per unit area or as water column) would be identical on both fractions, the glaciated grid box fraction would equal the runoff contribution from this fraction and the markers in Figure 5.67 would be aligned along the line denoting the 1:1 relation. This is approximately the case in winter and spring (upper panels). In winter the location of the grid box markers slightly above the 1:1-line denotes a disproportionately higher contribution from the non-glaciated fraction which is probably caused by an enhanced snow melt due to subgrid radiation scaling (see Chapter 4.2.6). During summer and autumn, on the other hand, the glaciated grid box fractions contribute to a disproportionately larger degree to the total grid box runoff in all catchments. In strongly glaciated boxes values close to 100% are reached, i.e., the total amount of grid box runoff almost exclusively stems from the glaciated part. This large contribution of the glaciated fraction is mainly caused by snow and ice melt, i.e., by meltwater originating from the snow layer on top of the glacier cuboid and from the cuboid itself. Due to the subgrid redistribution of snow, the non-glaciated fractions are already snow-free in these seasons and meltwater is not produced. Additionally, the potential evapotranspiration is largest in this period and, hence, evapotranspiration

indirectly consumes a large portion of the liquid precipitation falling onto the non-glaciated fraction which minimises the production of runoff.

The comparatively large amounts of runoff in summer and autumn originating from the glaciated grid box fractions are not exclusively a result of enhanced ice melt in these seasons. The subgrid redistribution of snow alone can have a very strong effect. Snow is explicitly shifted from the non-glaciated to the glaciated fraction where, as a consequence, the presence of snow is extended into spring and summer. Hence, additional amounts of meltwater are available in this period. This effect is further enhanced by the subgrid radiation scaling, i.e., the reduction of incoming solar radiation on the glaciated fraction which causes a general delay of snow melt (which is probably not too large due to the high albedo of snow). Therefore, in order to assess the importance of glacial meltwater alone, the runoff component originating from ice melt has to be investigated separately. For the experiment GlacA this is done in Figure 5.68 which shows the mean monthly contribution of ice melt to the total amount of runoff in three altitudinal belts and for the entire Alpine area. In grid boxes below 2000 m a.s.l. the influence of ice melt is negligible. Only in high-altitude grid cells glacial meltwater contributes an important fraction to the total amount of runoff in summer and autumn with up to 26.7% in August. Averaged over the entire Alpine region (upper left panel) this fraction is much lower and reaches a maximum of 2.9% in August.

Depending on the percentage glacier cover and the simulated mass balance the contribution of ice melt to the total amount of runoff differs between the four main Alpine catchments (Figure 5.69). Largest contributions of more than 34% in August are simulated in grid boxes above 2000 m a.s.l. in the Rhone and the Po catchment. For the Rhine and the Danube the respective numbers are considerably

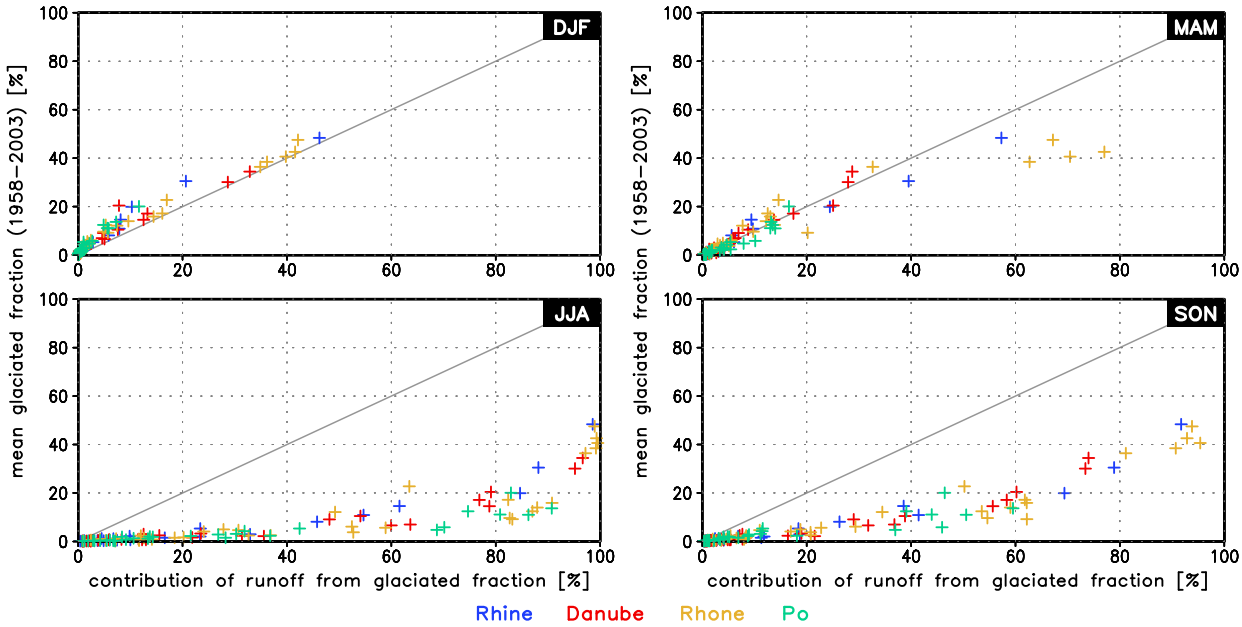

Figure 5.67: Relation between the mean glaciated grid box fraction (1958-2003) [%] and the mean seasonal contribution of runoff originating from the glaciated grid box fraction to the total amount of runoff [%] in the baseline simulation GlacA. Each cross represents one glaciated REMO grid box and is colour-coded according to the respective catchment. The grey line denotes the 1:1 relation.

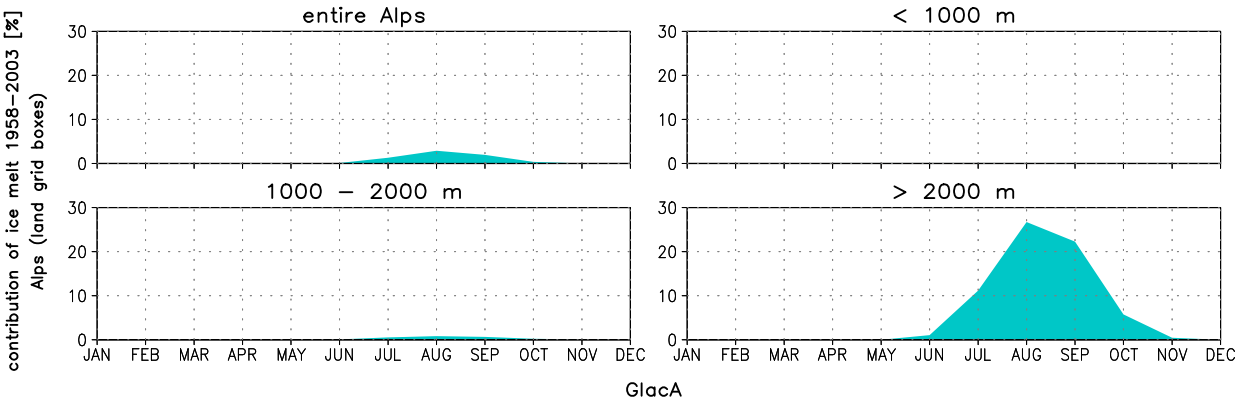

Figure 5.68: Mean monthly contribution of ice melt (1958-2003) [%] to the total amount of runoff in the experiment GlacA for the entire Alpine region (land grid boxes only) and three altitudinal intervals.

lower (14.3 and 20.5%, respectively). Averaged over the entire catchment area the influence of glacial meltwater is largest in the Rhone catchment (8.5% in August) and lowest for the Danube (1.3%).

The overall effect of the new glacier parameterisation scheme on the simulated runoff can be assessed by a comparison between the glacier simulation GlacA and the control experiment CTRL (see Table 5.1). Runoff differences between both simulations are not only caused by snow and ice melt from the glaciated grid box fractions in GlacA (i.e., by the redistribution of snow and by glacial meltwater) but can also stem from the influence of glaciers on precipitation and evaporation (see Chapter 5.4). The mean monthly difference of the simulated runoff between both simulations is shown in Figure 5.70 for the entire Alps and for the three altitudinal intervals. At elevations above 2000 m a.s.l. the simulated amount of summer runoff is considerably higher in GlacA with largest increases of up to 60% occurring in July. This positive deviation originates from snow melt (about 2/3) and ice melt (about 1/3) on the glaciated grid box fractions in GlacA. From October to May, on the other hand, less runoff is produced in GlacA which is probably due to the general decrease of precipitation (see Chapter 5.4) and the negative effect of snow redistribution on total runoff in these months. In grid boxes below 2000 m a.s.l. the simulated runoff in GlacA is generally lower compared to the control experiment. The same is true for the average over the entire Alpine region (upper left panel). Obviously, the reduction of evaporation in the Alpine area in GlacA cannot compensate for the general decrease of precipitation compared to the control simulation. The corresponding negative deviation in the amount of water available for runoff, in turn, is able to compensate for the additional amount of glacial meltwater in GlacA, leading to a net reduction of the average amount of runoff. In total, the runoff from the Alps is reduced by 2.1% in GlacA compared to CTRL.

In both simulations the annual amount of Alpine runoff is strongly controlled by the annual sum of precipitation (not shown). The respective correlation coefficients r amount to 0.98 (GlacA) and 0.97 (CTRL). For grid boxes above 2000 m a.s.l. coefficients of 0.82 (GlacA) and 0.84 (CTRL) are obtained. Hence, there is almost no indication of a general shift from a precipitation-dominated runoff regime to an energy-dominated regime due to the explicit consideration of glaciers in REMO (see also Chapter 2.8). In both REMO and $\text{REMO}_{\texttt{glacier}}$ the interannual variability of runoff is strongly controlled by the annual precipitation sums.

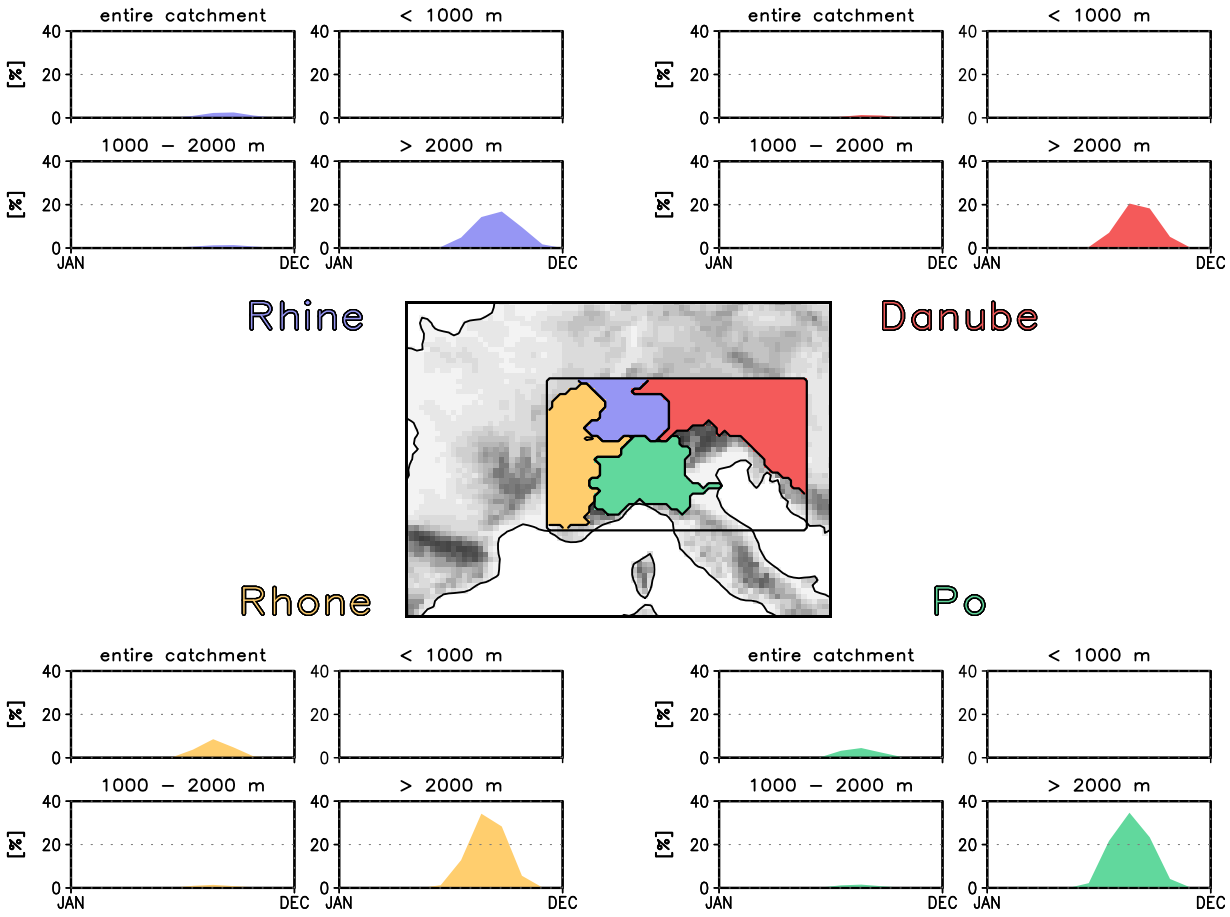

Figure 5.69: Mean monthly contribution of ice melt (1958-2003) [%] to the total amount of runoff in the experiment GlacA for the entire catchment and three altitudinal intervals. Upper left: Rhine catchment. Upper right: Danube catchment. Lower left: Rhone catchment. Lower right: Po catchment.

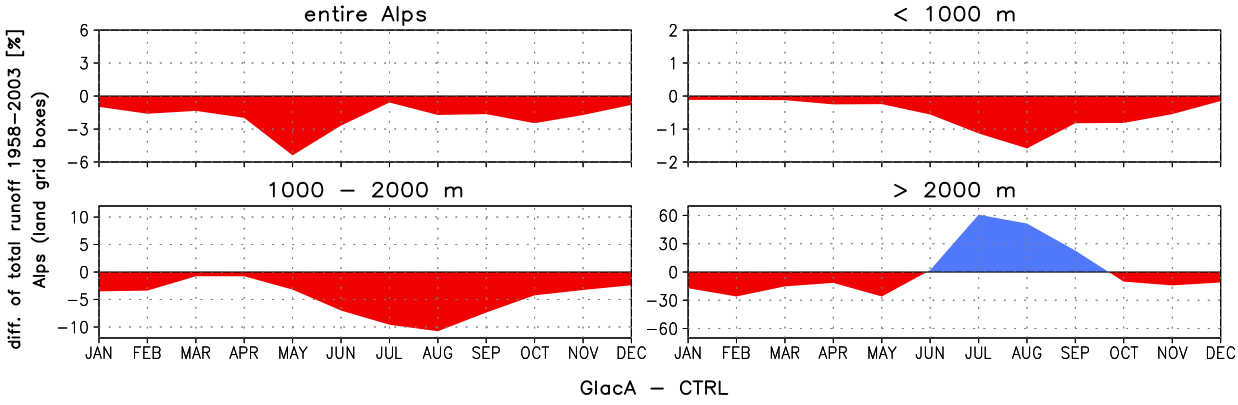

Figure 5.70: Mean monthly difference of runoff (1958-2003) [%] between GlacA and CTRL for the entire Alpine region (land grid boxes only) and three altitudinal intervals.

5.6.2 River Discharge

The analysis of the grid box runoff as presented above does not account for the travel time of water within the surface river system and for the retention capacity of several large lakes in the study area (e.g., Lake of Constance, Lake Geneva, Lac de Neuchâtel). For meso- to macroscale catchments, glaciers in the Alps can be expected to be located in remote high-altitude regions. This implies a comparatively large travel and residence time of locally generated runoff in the surface river and lake system until the catchment outlet is reached.

In order to explicitly account for this transport of water in the horizontal direction the HD routing scheme (Chapter 3.4) has been coupled to $\text{REMO}_{\texttt{glacier}}$ in an offline mode. In total, three HD simulations have been carried out for the entire model domain for the period 1958-2003 (Table 5.6). The experiments differ with respect to the input of surface runoff and drainage as provided by REMO's land surface scheme. While HD A is directly forced with the runoff components simulated by the $\text{REMO}_{\texttt{glacier}}$ experiment GlacA, also HD B is forced by GlacA but excluding the amount of runoff originating from ice melt. Hence, the comparison between the simulated discharge in HD A and HD B reveals the contribution of ice melt to the total amount of discharge. The third experiment (HD CTRL) is forced by the runoff components derived from the standard REMO control simulation CTRL (see Table 5.1).

The simulated discharge in the three HD simulations has been analysed at eight grid boxes in the Alpine region, draining areas of different size and with a different initial glacier cover. The chosen grid boxes correspond to the location of gauging stations in three of the four main Alpine catchments (Rhine, Danube, Rhone). Their position as well as the respective catchments including the HD flow directions are shown in Figure 5.71. Table 5.7 summarises the main characteristics of the eight catchments.

Mean Annual Cycle

The simulated mean annual cycle of river discharge at the eight gauging stations for the experiments HD A, HD B and HD CTRL is shown in the Figures 5.72 (Rhine), 5.73 (Danube) and 5.74 (Rhone). At all locations, the discharge in spring and early summer is considerably lower in HD A and HD B compared to the control simulation. This reduction is most pronounced in the small, high-altitude catchments of Thun, Brugg, Martinsbruck and Porte du Scex. For the large catchments of Rheinfelden and Schaerding the effect is comparatively small. The negative deviation of river discharge in HD A and HD B compared to the control experiment is partly caused by the smaller amount of precipitation in the REMO simulation GlacA compared to CTRL (see Chapter 5.4.3). However, the major part

Name	Period	REMO runoff input
HD A	1958 - 2003	GlacA
HD B	1958 - 2003	GlacA without ice melt
HD CTRL	1958 - 2003	CTRL

Table 5.6: HD discharge simulations carried out within the present study.

has to be attributed to the redistribution of snow on a subgrid level in GlacA. This generally causes an extension of the snow melt period and, consequently, a less pronounced springtime snow melt peak. In springtime and early summer the amount of melting snow decreases since the non-glaciated fractions become snow-free relatively early in the year. On the other hand, the snow cover on the glaciated grid box fractions lasts for a longer period and increases the amount of snow melt and, hence, discharge in summer and early autumn compared to the control simulation. The increase of discharge especially in July and August is clearly visible in the smaller catchments (Thun, Brugg, Martinsbruck, Porte du Scex, Chancy). Except for Thun and Brugg it is further enhanced by the additional contribution of melting ice in this period (difference between HD A and HD B). The positive effect of the redistribution of snow and of ice melt on the discharge in late summer and early autumn is partly offset by the considerably smaller amount of summer precipitation in GlacA compared to CTRL. In the large catchments of Rheinfelden and Schaerding this negative bias of precipitation in GlacA even leads to a slight reduction of the discharge in HD A and HD B in late summer and autumn with respect to HD CTRL. As it has been shown in Chapter 5.6.1 the decrease of evapotranspiration in GlacA compared to CTRL cannot fully compensate for the decrease of precipitation, resulting in a smaller amount of grid box runoff on an Alpine wide scale and, hence, in a decrease of river discharge

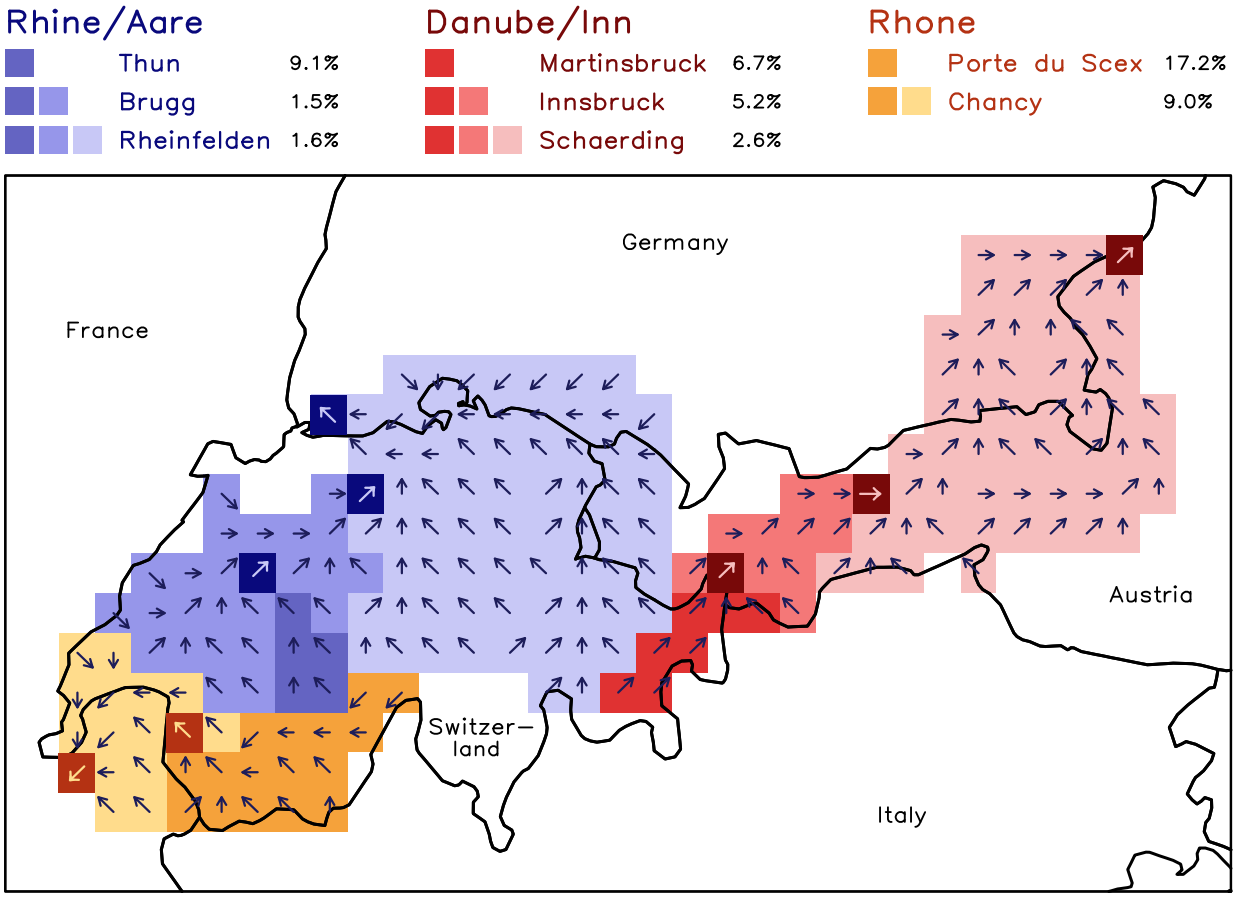

Figure 5.71: Location of the eight Alpine gauging stations investigated in the present study (dark boxes) and the corresponding HD catchments, including flow directions. Blue: Rhine catchment. Red: Danube catchment. Orange: Rhone catchment. The numbers in black (legend) denote the initial glacier cover of the respective catchment (January 1958).

Name	River	Main catchment	A_{HD} [km^2]	Initial glacier cover [%]
Thun	Aare	**Rhine**	1687	9.1
Brugg	Aare	**Rhine**	10128	1.5
Rheinfelden	Rhine	**Rhine**	33785	1.6
Martinsbruck	Inn	**Danube**	2362	6.7
Innsbruck	Inn	**Danube**	6078	5.2
Schaerding	Inn	**Danube**	25365	2.6
Porte du Scex	Rhone	**Rhone**	5389	17.2
Chancy	Rhone	**Rhone**	10444	9.0

Table 5.7: Basic characteristics of the eight HD catchments (corresponding to the catchment of eight gauging stations) analysed within the present study.

for the largest catchments.

Contribution of Ice Melt

Generally, the contribution of ice melt to the total amount of river discharge strongly depends on the glaciated surface fraction in the catchment under investigation. A high degree of glacier cover will in most cases lead to an important contribution of glacial meltwater especially in summer and autumn. Further factors which can cause differences in the meltwater contribution between different catchments as well as large interannual variations for the same catchment are the magnitude of ice melt in the respective balance period (as expressed, for instance, by the summer mass balance) and the amount of discharge originating from precipitation and snow melt. A dry summer with a negative precipitation anomaly will usually result in a comparatively high contribution of glacial meltwater to the total amount of river discharge.

The combination of these factors leads to a pronounced variability of the simulated contribution of ice melt at the investigated gauging stations in both space (i.e., between different catchments) and time (seasonal and interannual scale; Figure 5.75). At all locations, the maximum contribution is simulated in August and September. In the small, strongly glaciated catchments of Thun, Martinsbruck and Porte du Scex glacial meltwater is responsible for more than 50% of the total discharge in individual months (light-shaded area). The mean contribution is considerably lower (dark-shaded area). Values of more than 10% are reached in August and partly in September in the catchments of Martinsbruck, Porte du Scex and Chancy. These catchments have a comparatively large glaciated surface fraction (see Table 5.7) and show a considerable decline of the total glaciated area in the course of the underlying $\text{REMO}_{\texttt{glacier}}$ simulation GlacA (-11.7, -12.9 and -11.4% from 1958 to 2003, respectively). The largest percentage glacier area loss is simulated for the catchment of Schaerding (-23.6%). However, due to the comparatively small glaciated surface fraction of this catchment the mean contribution of ice melt to the total amount of discharge is lower than 5% in all months.

A special phenomenon appears in the catchments of Thun and Brugg: While the maximum contribution of glacial meltwater in individual months is relatively large (about 60 and 40% in August,

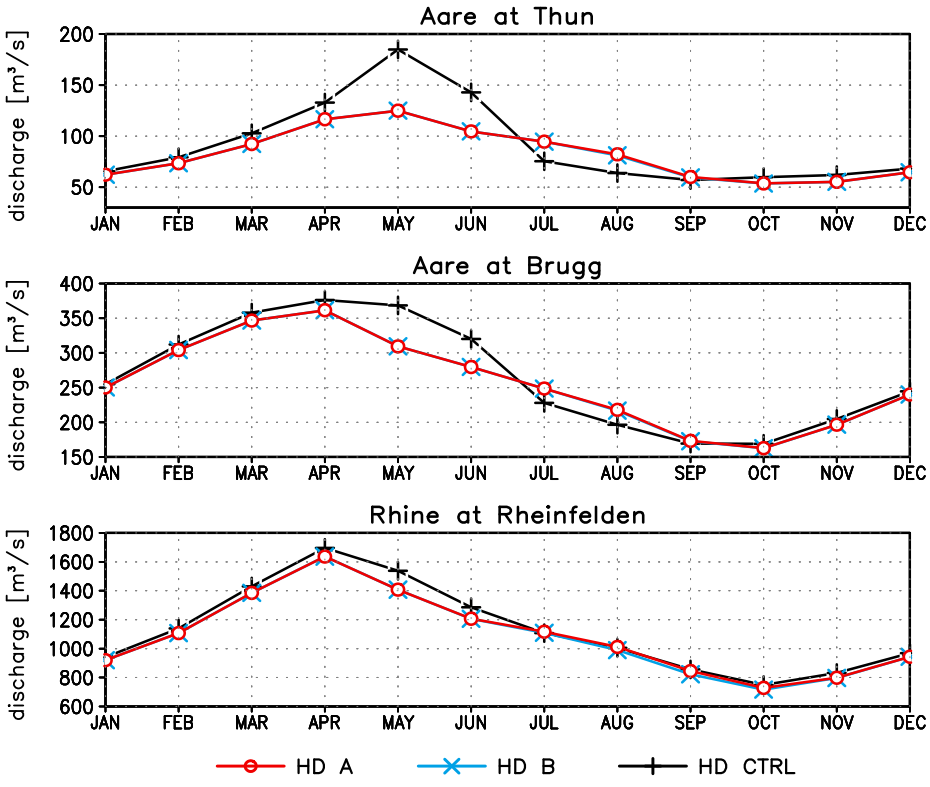

Figure 5.72: Mean annual cycle (1958-2003) of the simulated discharge [m^3/s] for three gauges in the Rhine catchment in the simulations HD A, HD B and HD CTRL.

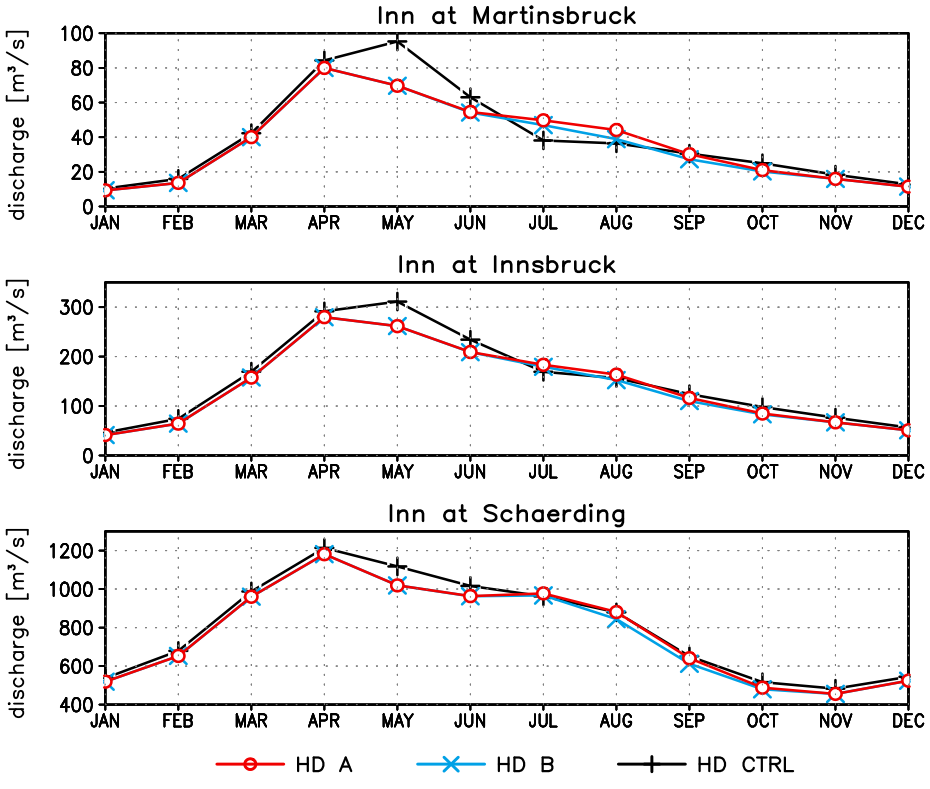

Figure 5.73: Mean annual cycle (1958-2003) of the simulated discharge [m^3/s] for three gauges in the Danube catchment in the simulations HD A, HD B and HD CTRL.

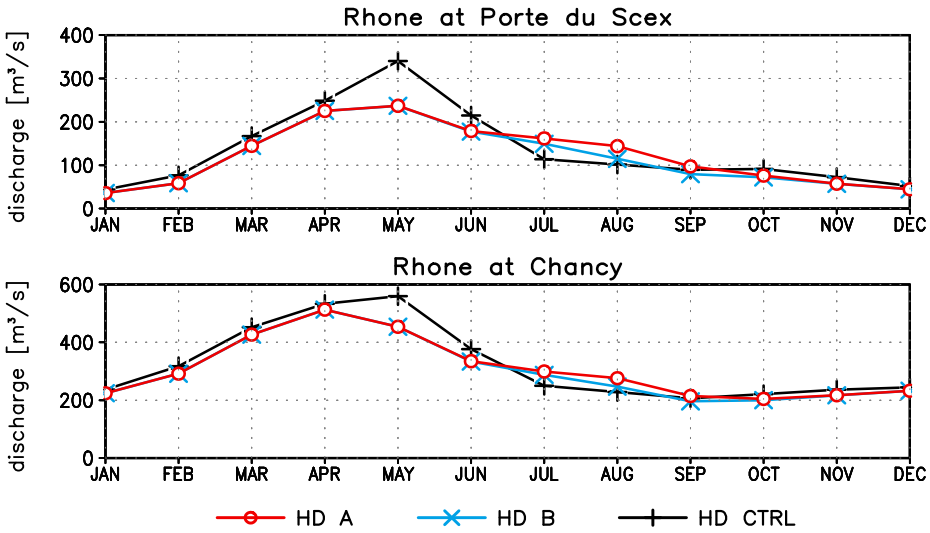

Figure 5.74: Mean annual cycle (1958-2003) of the simulated discharge [m^3/s] for three gauges in the Rhone catchment in the simulations HD A, HD B and HD CTRL.

respectively) the mean contribution is almost negligible (less than 2% in all months, not visible from Figure 5.75). This behaviour is caused by a considerable growth of glaciers in GlacA in this region of the Alps (see Chapter 5.2.2, especially Figures 5.24 and 5.26). In the course of the experiment the mean glaciated grid box fraction increases by more than 70% in both catchments. This growth is associated with a strong positive mass balance and with a persistent snow cover on top of the glacier cuboid in the respective grid cells. During summer this snow layer is not melting entirely which enables the transformation of snow into ice and the growth of the glacier cuboid with respect to both volume and surface area. A further effect of the continuous presence of a snow layer is that ice melt does not occur and, hence, glacial meltwater (defined as meltwater from the glacier cuboid, excluding the overlying snow layer) does not contribute to the locally produced runoff. Only in years in which the cuboids become exposed ice melt occurs and, given the relatively high glaciated surface fraction, strongly contributes to the total grid box runoff and to the total river discharge. The absence of ice melt in $\text{REMO}_{\texttt{glacier}}$ due to the persistence of a snow layer in years of high snow accumulation is a direct consequence of the simple cuboid concept which assumes a uniformly distributed snow layer on top of the cuboid. In reality, the spatial variability of the presence of snow on a glacier's surface is much higher, especially during the melt period. Also in years of a strongly positive mass balance the tongues of Alpine glaciers usually become exposed in the course of the melt season and ice melt does occur.

Validation

The results presented in the two previous subsections on glacier discharge are exclusively based on the HD experiments carried out within the present study. In order to assess the overall quality of the discharge simulations a validation against observational data is necessary. In Figure 5.76 the mean annual cycle of river discharge at the eight Alpine gauging stations as simulated by HD A and HD CTRL is compared to observations.[9] For all stations, the monomodal, snow melt-dominated character of the observed mean monthly discharge is captured by the simulations and, in most cases, the magnitude of the observed discharge peak is approximately reproduced. However, a systematic model bias appears with respect to the timing of the annual peak discharge. At all stations the simulated maximum of

[9]Note that, following the availability of discharge measurements, the validation is based on different periods of time for the individual gauging stations.

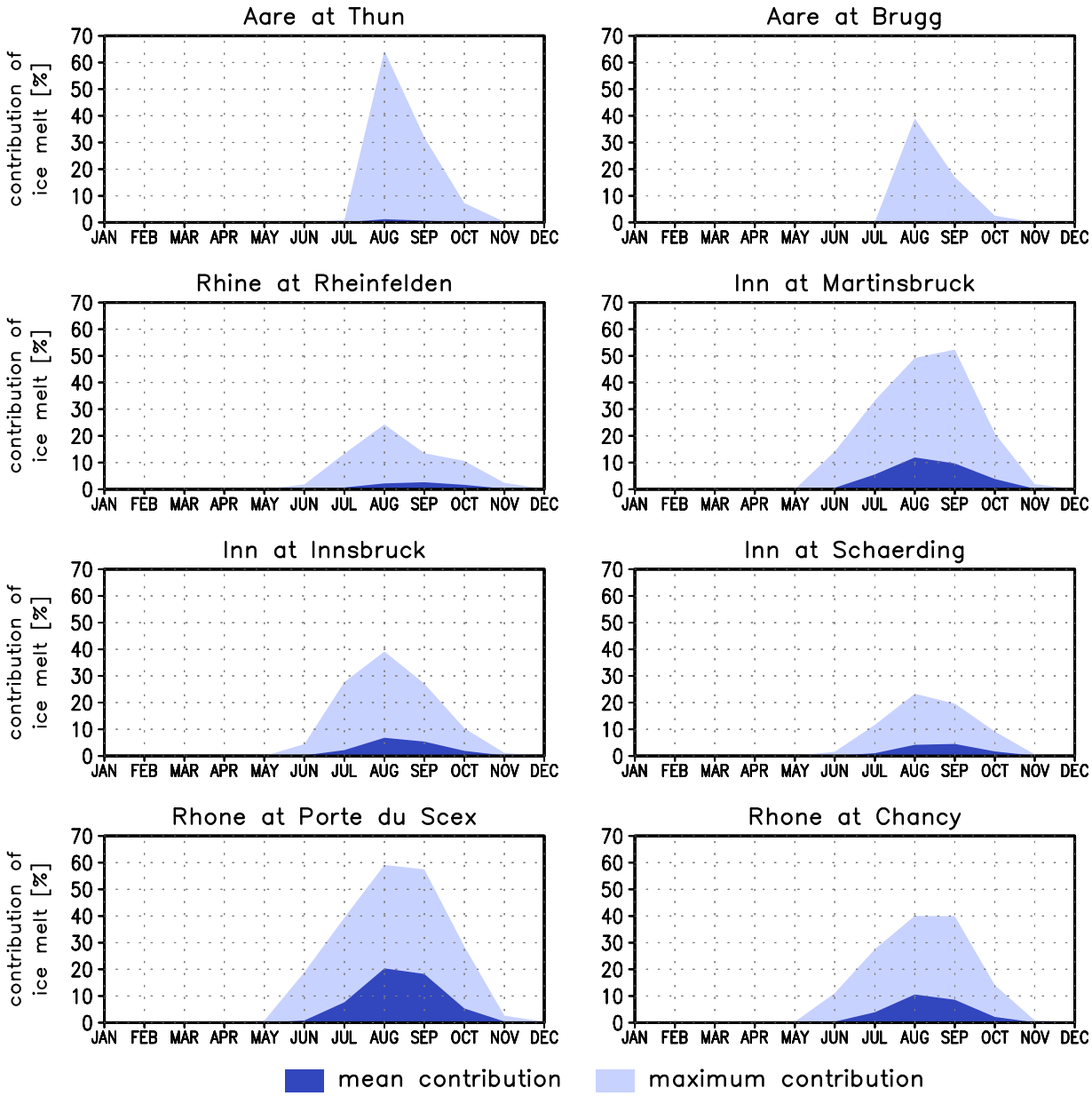

Figure 5.75: Mean (dark blue) and maximum (light blue) monthly contribution of ice melt to the total amount of river discharge (1958-2003) [%] for the eight investigated Alpine gauging stations as derived by the comparison between HD A and HD B.

river flow appears in April or May while the observed peak occurs about one to two months later. The inclusion of the glacier subgrid parameterisation (difference between HD A and HD CTRL) does only slightly improve the quality of the simulation by lowering the springtime discharge peak and shifting parts of the total discharge to early summer.

5.6.3 Discussion

The analysis of the simulated grid box runoff and river discharge shows that the effect of the new glacier parameterisation scheme on surface hydrology is mainly restricted to strongly glaciated areas

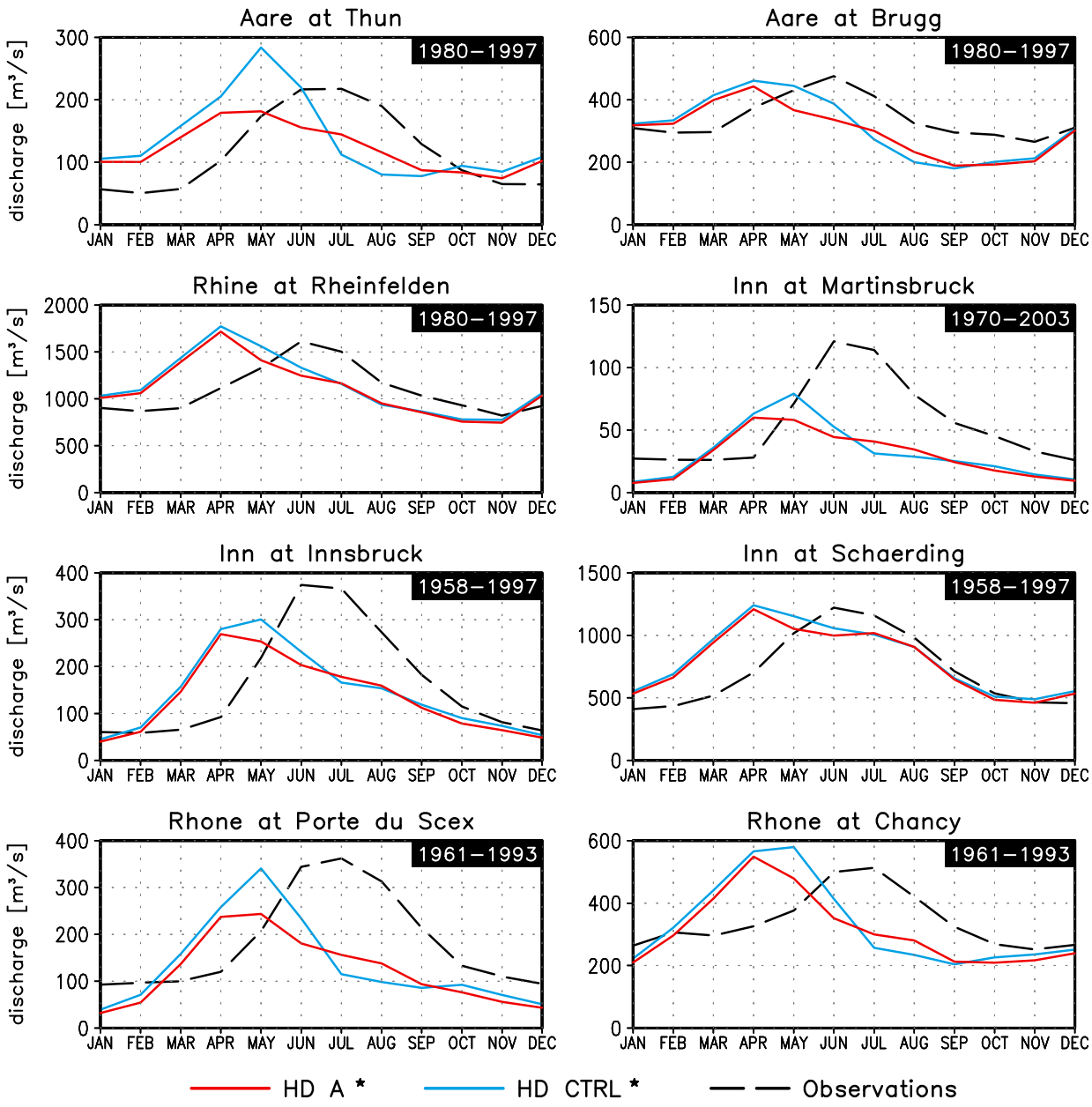

Figure 5.76: Mean monthly discharge [m^3/s] for the eight investigated Alpine gauging stations as simulated by the experiments HD A and HD CTRL and as observed. The underlying period of time is indicated in the upper right part of each panel. ★: The model results have been scaled in order to account for slight differences between the real catchment area and the area of the respective HD model catchment.

in high-altitude regions of the Alps. Here, glacial meltwater can play an important role especially in late summer and early autumn by contributing a large fraction (more than 20%) to the total amount of grid box runoff and river discharge. On the scale of large Alpine catchments (Rheinfelden, Schaerding) the mean influence is relatively small, though not negligible. Nonetheless, in individual summer months the meltwater contribution can surpass 20% of the total river discharge even for these large catchments with a comparatively small glacier-covered surface fraction. Regarding the annual regime of river discharge, the pure effect of glacial meltwater is small compared to the effect of snow redistribution in $\text{REMO}_{\texttt{glacier}}$ and the influence of the new glacier parameterisation scheme

on summer precipitation. The subgrid redistribution of snow leads to an extended melt season in glaciated grid cells and decreases the amount of river discharge in spring while increasing river flows in early summer. Still, the general characteristics of the annual cycle of discharge are only slightly modified compared to the control simulation (standard REMO forcing HD). The general bias in the timing of the springtime/summer snow melt peak of discharge compared to observations persists. In all HD simulations it occurs too early. In principle, this temporal bias can be caused by

- ▷ shortcomings of the regional climate model, especially related to the annual cycle of precipitation, the contribution of snowfall to total precipitation and the period of snow melt
- ▷ shortcomings of the HD routing scheme, especially related to the residence time of water within the surface river and lake system.

Probably, the latter point is in parts responsible for the temporal bias of the simulated discharge peak. Especially in the Rhine catchment (Thun, Brugg, and Rheinfelden) and the Rhone catchment at Chancy (which is located downstream of Lake Geneva), the discharge conditions are strongly influenced by the delaying and dampening effect of large lakes. In the HD model these processes are represented by a relatively simple parameterisation which increases the mean residence time of water in the linear reservoirs for overland flow and riverflow in the presence of lakes (see Chapter 3.4). This parameterisation has been developed on a global scale and can be expected to be associated with comparatively large biases if individual sub-catchments with their special characteristics regarding the retention capacity of lakes are investigated. Furthermore, the management of artificial reservoirs, which is of high importance in the Alpine region, is not accounted for in the HD model.

However, the too early occurrence of the simulated discharge peak by one to two months seems to be a robust signal. It appears for large catchments with a long travel time of water as well as for smaller ones (e.g., Rheinfelden compared to Thun) and for catchments with a different retention capacity of large lakes (e.g., Chancy compared to Innsbruck). If only the routing parameterisation of the HD model would be responsible for the model bias, larger differences between catchments of different size and with different retention characteristics could be expected. Therefore, the major problem probably lies in the regional climate model itself, i.e., in the simulated amount of locally generated runoff as a response to rainfall and snow melt. As the observed annual cycle of precipitation in the Alps is approximately reproduced by REMO and summer precipitation is even overestimated in most parts (see Figure 5.55) biases in the total amount of precipitation are probably not responsible for the temporal bias of the discharge peak. Hence, there is a strong indication of major shortcomings in the simulated amount and especially the timing of snow melt. Obviously, snow melt generally peaks too early in the year in large parts of the Alps both in REMO and $\text{REMO}_{\texttt{glacier}}$. In order to further investigate these shortcomings a detailed validation of the simulated evolution of snow cover throughout the year especially in the low- and mid-altitude areas of the Alps (which represent the majority of the total surface area) would be necessary. In the frame of the present study this has so far not been carried out. Given the high spatial variability of snow cover in complex terrain, the obvious shortcomings in the simulation of snow cover and snow melt in the Alps are presumably related to the poor resolution of topographical structures by the model orography. Giorgi et al. (2003) showed that the inclusion of a subgrid topography scheme in an RCM leads to a more realistic simulation of snow

cover as driven by complex features of the Alpine terrain, potentially leading to a better simulation of the seasonal evolution of the surface hydrology.

Given the general bias in the timing of the simulated discharge peak the question arises if the simulated contributions of ice melt to the total amount of monthly discharge are realistic. On one side the interannual variability of glacier mass balance and its general magnitude are comparatively well captured by the model, except for the Rhine catchment in the 1980s and early 1990s (see Figure 5.14). Furthermore, in terms of the total discharge volume originating from ice melt, the general underestimation of glacier mass loss towards the end of the simulation period is partly compensated by a positive bias of the simulated glacier area (see Chapter 5.2.2). Hence, the total amount of glacial meltwater (in this case originating from snow melt plus ice melt) can be assumed to be simulated in a reasonable way. On the other side, discharge in summer and autumn is generally underestimated by the model system $\text{REMO}_{\texttt{glacier}}$ + HD (Figure 5.76). Combining both points a too large contribution of glacial meltwater to total discharge in summer and autumn is likely. However, if only ice melt is considered (melt water originating from the glacier cuboid, excluding the snow layer) an underestimation of the total volume of meltwater has to be assumed for the last two decades of the 20^{th} century. In this period the reduction of ice volume is underestimated by the model (in the Rhine catchment even a net growth is simulated, see Chapter 5.2.2) and glacial meltwater mainly stems from snow melt on top of the ice cuboids.

The general assessment of the simulated contribution of ice melt to river discharge is difficult since only very few studies based on observed amounts of river discharge and observed mass balances exist for the Alpine area. A recent study by Frauenfelder et al. (2006) suggests that in the Upper Rhine catchment at Ilanz (A=778 km^2, glacier-covered surface fraction in 2000: 2.7%) glacial meltwater contributed less than 1% to the total amount of river discharge in the period 1850 to 2000. Also in the HD simulations for slightly glaciated catchments for the period 1958 to 2003 this value is not surpassed (annual mean of the blue areas in Figure 5.75). A seasonal analysis has so far not been carried out by the authors.

Based on simplifying assumptions of glacier mass balance the range of the contribution of pure ice melt to the total summer discharge at Basel (Rhine, downstream of Rheinfelden) and Porte du Scex (Rhone) can be estimated by the following procedure: If one assumes

- a total glaciated area in the catchment of Basel between 430 km^2 (1970s) and 320 km^2 (year 2000) and in the catchment of Porte du Scex between 750 km^2 (1970s) and 620 km^2 (year 2000)
- a 3-month summer melt period (July to September)
- a mean exposed ice area in summer between 30% and 70% of the total glaciated area
- an amount of pure ice ablation on the exposed area between 2 cm/day (corresponding to about 2 m w.e./3 months) in normal years and 5 cm/day in hot years
- a negligible influence of evaporation and of the temporary storage of water within the surface river and lake system

the mean amount of summer discharge originating from pure ice melt varies between 22 and 174 m^3/s at Basel and between 43 and 304 m^3/s at Porte du Scex, depending on the specific year under consideration. If these values are related to the long-term (1891-2003) mean summer discharge at the two gauging stations (Basel: 1273 m^3/s, Porte du Scex: 296 m^3/s) the contribution of ice melt at Basel ranges from 2 to 14% and from 15 to 100% at Porte du Scex. Assuming the maximum amount of ice melt (174 m^3/s, see above) the contribution of glacial meltwater to total discharge at Basel could have been as high as 27% in the extraordinary warm and dry summer of 2003 (mean summer discharge 650 m^3/s). Regarding the strong simplifications of this analysis the numbers obtained are subject to a large uncertainty. Still, they can be considered as a first-order approach and can be compared to the respective values as simulated by the model system $\text{REMO}_{\texttt{glacier}}$ + HD (Figure 5.75). The comparison reveals that both the mean and the maximum contribution of glacial meltwater to the total amount of discharge at Basel/Rheinfelden and at Porte du Scex are approximately reproduced by $\text{REMO}_{\texttt{glacier}}$ + HD. Only the estimated maximum contribution of 100% at Porte du Scex is never reached in the model simulation. It has to be noted that this extreme case (i.e., river discharge exclusively originating from ice melt during the entire summer) has very probably never occurred in reality which generally points to the large uncertainties of the analysis presented above.

6 Conclusions and Outlook

6.1 Conclusions

Within the present study a glacier parameterisation scheme has been developed and implemented into the regional climate model REMO. The new scheme simulates the mass balance as well as changes of the areal extent of glaciers on a subgrid scale. For the first time a complete simulation of glacier-climate interactions, including the effect of glaciers on catchment hydrology, is possible. The European Alps were chosen as a test region and a number of simulations have been carried out for the second half of the 20th century in order to assess the performance and the main sensitivities of the new model system REMO$_{\texttt{glacier}}$.

Regarding the main scientific questions of this work (see Chapter 1.2) the results obtained indicate that it is possible to approximately reproduce observed regional glacier mass balances based on simplified concepts of glacier-climate interaction. However, it has been shown that realistic results can only be achieved if the subgrid variability of atmospheric parameters within a climate model grid box is explicitly accounted for. In the case of snowfall and solar radiation simple scaling techniques are applied in REMO$_{\texttt{glacier}}$. Also the variability of glacier characteristics within a climate model grid box as well as glacier dynamics are idealised to a very high degree in the new scheme. As a consequence, only a minimum amount of additional input data is required. Furthermore, the representation of the glacier-atmosphere interface itself is based on simplifying assumptions. A constant ice albedo of 0.4 is for instance used in the standard setup and snow is assumed to be uniformly distributed over the entire glacier cuboid surface.

On one side, the use of these simple concepts ensures a reasonable additional amount of required computing time and, even more important, allows for the application of the model system REMO$_{\texttt{glacier}}$ on the scale of entire mountain ranges. Furthermore, the comparatively low demand of glacier-specific input data facilitates the application of the model in regions other than the European Alps where the data coverage is usually much sparser. On the other hand, the high degree of simplification can obviously lead to important inaccuracies of the model. The strong glacier mass loss towards the end of the 20th century is, for instance, clearly underestimated by REMO$_{\texttt{glacier}}$. In the Rhine catchment even a net growth of glaciers is simulated compared to the observed glacier mass loss. Presumably, these deficiencies are at least partly associated with the assumption of a uniformly distributed snow layer on top of the glacier cuboid and the neglection of the equilibrium line concept, i.e., the coexistence of accumulation and ablation areas on the same glacier. This simplification is directly related to the fact that subgrid variability of orography is so far not explicitly accounted for in REMO$_{\texttt{glacier}}$ and that the entire glacier cuboid surface is located at the mean grid box altitude. In most cases this altitude is well below the steady state equilibrium line altitude in the Alps during the last decades of the 20th century ($>$ 2700 m a.s.l. in most areas; Zemp et al., 2007), i.e., glaciated surfaces located at the REMO grid box altitude would mostly experience a strong net ablation in reality. Hence, the

fact that the observed mass balances are nevertheless approximately reproduced by $\text{REMO}_{\texttt{glacier}}$ and that glaciers even considerably grow in some grid boxes points to

- ▷ biases in the simulated atmospheric forcing
- ▷ a possible overcompensation by other parts of the parameterisation scheme, namely by the redistribution of snow and the subgrid radiation scaling

resulting in an increase of glacier mass balance. Negative biases of the simulated air temperature in high-altitude grid boxes and incoming solar radiation in springtime have been identified and could, in principle, partly compensate for the too low glacier elevation. However, the main effect is presumably related to the subgrid redistribution of snow which is strongly increasing the amount of snow accumulation on the glaciated surface fraction compared to the grid box average. This process has a major influence on the simulated glacier mass balance and, at the same time, the corresponding snow redistribution factor of $\kappa = 2$ is not more than a rough estimate and could well overcompensate for the altitudinal bias. In this respect, a detailed validation of the simulated snow depths both on the resolved and the subgrid scale, which has so far not been carried out, is necessary.

Regarding the influence of glaciers on the regional climatic conditions, the effect of the new subgrid parameterisation on atmospheric parameters is generally restricted to the lower troposphere and to glaciated grid boxes themselves as well as their direct vicinity. The large scale flow conditions are not significantly affected. In glaciated grid cells the incorporation of the glacier scheme into REMO causes a lowering of the near surface air temperature by several degrees Celsius and a less intense local recycling of water by reducing both precipitation and evapotranspiration. These effects are generally most pronounced in summer and autumn. They are not exclusively due to the distinct surface characteristics of the glaciers themselves (i.e., of the grid box glacier cuboids) but are partly caused by the redistribution of snow and incoming solar radiation on a subgrid scale. The same is true for the influence of the new glacier scheme on catchment hydrology. In strongly glaciated catchments the most prominent effect on river discharge is caused by the partial delay of snow melt, which is a direct consequence of the subgrid redistribution of snowfall carried out in $\text{REMO}_{\texttt{glacier}}$. However, it was shown that in individual summer months ice melt can contribute an important fraction to the total amount of river discharge, even in large Alpine catchments.

Unfortunately, the inclusion of the new glacier parameterisation scheme in REMO does not improve the general quality of the model simulations but generally leads to larger biases of atmospheric parameters in high-altitude areas. Both the underestimation of winter temperatures and of summer precipitation in grid boxes above 2000 m a.s.l. are more pronounced in the glacier experiments compared to the control simulation. Assuming that the land surface characteristics and the corresponding exchange processes in high-altitude Alpine areas are described more realistically in $\text{REMO}_{\texttt{glacier}}$ than in standard REMO (due to the explicit inclusion of glaciated surfaces), this points to more general shortcomings of the RCM REMO in the Alpine region. In case of precipitation, these shortcomings are probably related to the distribution of rain and snowfall in space and especially with respect to altitude. The simulated amount of annual precipitation is, generally, too large in grid boxes below 2000 m and negative biases only occur in high-altitude areas. Hence, a slight redistribution of precipitation towards high elevations could improve the quality of the simulation in both altitudinal intervals.

Given the comparatively weak influence of the new glacier scheme on the simulated large scale climate

and the obvious problems in reproducing observed glacier area and volume changes the general question arises if the interactive coupling of a glacier scheme to an RCM is meaningful at all. For the European Alps the answer is "yes" in case that an emphasis is laid on the simulation and analysis of regional water cycles on a catchment scale. Both precipitation and evapotranspiration are significantly affected by the new parameterisation scheme. The same is true for river discharge. Even in large Alpine catchments with a comparatively small glacier-covered surface fraction ice melt can contribute more than 20% to the total amount of discharge in individual months. For small catchments this fraction is much larger. In order to obtain more reliable results a number of deficiencies of the new parameterisation scheme should be addressed in future studies, especially related to the area-altitude distribution of glaciers on a subgrid scale (see below). In this respect, the current version of the subgrid parameterisation should be seen as a first attempt to simulate glaciers as an interacting component of the climate system, which can serve as a fundament for future efforts. A further point is that the European Alps have been chosen as a test region mainly due to the comparatively large amount of observational data available for model development and model validation and due to the experience concerning the general performance of the RCM REMO in this area. Now, a next step is to transfer the approach to other regions where the glacier coverage is more prominent and glaciers can be expected to exert a stronger influence on the regional climate and on discharge conditions and might even be an important factor for global sea level rise (see Chapter 2.7.4).

6.2 Outlook

The above mentioned transfer of the model system $\text{REMO}_{\texttt{glacier}}$ to regions other than the European Alps and the assessment of its performance in these areas is a necessary step for gaining confidence in the new parameterisation scheme. The application of $\text{REMO}_{\texttt{glacier}}$ in parts of the Himalayas is planned for the near future. From a general point of view the transferability of the presented approach is given since the most important processes regarding accumulation and ablation conditions are represented on a physical basis. Also the amount of glacier-specific input data required by the model is comparatively small. Still, basic information on glacier location, extent and preferably glacier volume is necessary for the model initialisation and the subsequent evaluation of its performance. Also the availability of observation-based mass balance time series is a crucial element for model validation. For the application of $\text{REMO}_{\texttt{glacier}}$ in the European Alps very detailed observational data, namely glacier outline polygons for Switzerland and a high-resolution digital elevation model, were used for deriving the subgrid radiation factors. After the release of the Swiss glacier inventory of 2000 (Paul, 2004) and the forthcoming new Austrian glacier inventory (Lambrecht et al., 2005) such information will soon be available for most parts of the Alps for the end of the 20^{th} century. In other regions the data coverage is much worse and modified concepts might have to be applied (e.g., exposition classes). In this respect, an encouraging effort is the establishment of a satellite-derived global inventory of land ice within the GLIMS project (*Global Land Ice Measurements from Space*).[1]

An open question is, whether parts of the new parameterisation scheme will have to be modified or extended in order to be applicable on a global scale. For instance, internal accumulation (the refreezing of surface meltwater in deeper layers of the glacier) might have to be accounted for if the

[1] http://www.glims.org

model is applied in sub-polar regions. For very large glaciers and ice fields a parameterisation of ice flow between the RCM grid cells and an explicit consideration of changes in the glacier surface altitude might have to be introduced. At the same time, subgrid effects presumably become less significant in these cases. Hence, individual parameters of the new parameterisation scheme might have to be adjusted if $\text{REMO}_{\texttt{glacier}}$ is applied in regions other than the Alps (e.g., the snow redistribution factor κ).

In any case, future modifications of the subgrid parameterisation should put an emphasis on the incorporation of the subgrid variability of orography and on the representation of the area-elevation distribution of glaciers within a climate model grid cell. Only by doing so the mass balance gradient with elevation, which strongly determines the climatic sensitivity of a glacier, and changes in the equilibrium line altitude can be explicitly simulated. In this respect, a possible approach is the implementation of subgrid elevation classes which would require an additional amount of glacier-specific input data for the model. Further fields in which improvements of the current parameterisation scheme would probably be highly beneficial are

- an improved representation of the surface albedo of snow and ice, e.g., the explicit consideration of an ageing effect (decrease of the albedo with time) and the effect of supraglacial debris
- a more detailed representation of the transformation process of snow into ice, possibly accounting explicitly for the intermediate state of firn
- improvements of the concept of area adjustment, e.g., the explicit consideration of the surface slope as a controlling parameter and of response times
- an improved parameterisation of glacier hydrology, e.g., the consideration of the retention capacity of the glacier itself.

A further topic which has so far not been investigated is the dependency of the model results on the chosen horizontal resolution of the climate model. Presumably, a change of the resolution would require an adjustment of the parameters κ (snow redistribution factor) and r_G (SRAD ratio), controlling the subgrid variability of snowfall and global radiation. Furthermore, an increase in the climate model's horizontal resolution would hopefully result in a better representation of topographic effects on the regional climate and, hence, in an improved quality of the simulated atmospheric forcing. The fact that REMO simulations on the chosen $^1/_6^\circ$ resolution are obviously associated with comparatively large biases of temperature and precipitation in high-altitude grid boxes (as well as simulations of other state-of-the-art RCMs; e.g., Kotlarski et al., 2005) which directly influences the simulated glacier mass balance indicates the need for a stand-alone version of the new glacier scheme. The latter could be directly forced with observed meteorological quantities for individual grid cells which would minimise errors in the atmospheric forcing and would allow for a more thorough assessment of the performance of the glacier scheme itself. So far, such a stand-alone version has not been set up.

Despite the obvious shortcomings of the current parameterisation scheme, some degree of confidence has been gained in its ability to reproduce observed glacier mass balances. This gives the motivation to investigate the development of Alpine glaciers in a climate change scenario using the current model setup. A recent study by Zemp et al. (2006a) suggests that by 2100 the major part of Alpine ice cover will have disappeared. The question is if such results can be approximately reproduced by

$\text{REMO}_{\texttt{glacier}}$.

In this respect, the validity of the newly developed parameterisations under climate change conditions has to be challenged. This is especially true for the description of the subgrid variability of global radiation and of snow accumulation which both have a strong effect on the simulated glacier mass balance. In the first case, the scaling of incoming solar radiation on a subgrid level is based on the SRAD radiation model and digitised Swiss glacier outlines and clearly relies on a physically based process description which will be valid also under future climatic conditions. However, a retreating glacier may gradually become subject to different shading conditions which would, in principle, require a recalculation of the respective SRAD factors based on simplifying assumptions of changes in the glacier outlines and topography. Both are generally not resolved by $\text{REMO}_{\texttt{glacier}}$. Furthermore, the effects of future mass balance changes on glacier geometry and on the surface radiation balance are a current field of research and cannot be assessed reliably so far. They strongly depend on factors such as the general type of glacier (e.g., valley glacier or mountain glacier), the exposition (e.g., north-facing or south-facing) and on the specific characteristics of changes in glacier geometry (e.g., dynamic retreat or down-wasting). A further point is the subgrid variability of snow accumulation, which includes both the effect of the spatial variability of total precipitation and the redistribution of fallen snow. The latter generally depends on wind speed, which can in principle be expected to change under enhanced atmospheric greenhouse gas concentrations, and on the characteristics of the local wind field, which are usually not resolved by a climate model. The incorporation of these effects into the very simple concept of snow redistribution in $\text{REMO}_{\texttt{glacier}}$ would be a difficult task. Also changes in the subgrid variability of precipitation itself under future climatic conditions would be hard to assess. In principle they could be approximated via the simulated regional precipitation-altitude relationships.

References

Alley, R. B., P. U. Clark, P. Huybrechts and I. Joughin (2005). Ice-sheet and sea-level changes. *Science*, **310**, 456–460.

Arnold, N. (2005). Investigating the sensitivity of glacier mass-balance/elevation profiles to changing meteorological conditions: Model experiments for Haut Glacier D'Arolla, Valais, Switzerland. *Arctic, Antarctic, and Alpine Research*, **37**(2), 139–145.

Arya, S. P. (2001). Introduction to Micrometeorology. Academic Press.

Asselin, R. (1972). Frequency filter for time integrations. *Monthly Weather Review*, **100**, 487–490.

Auer, I., R. Böhm, A. Jurkovic, A. Orlik, R. Potzmann, W. Schöner, M. Ungersböck, M. Brunetti, T. Nanni, M. Maugeri, K. Briffa, P. Jones, D. Efthymiadis, O. Mestre, J.-M. Moisselin, M. Begert, R. Brazdil, O. Bochnicek, T. Cegnar, M. Gajic-Capka, K. Zaninovic, Z. Majstorovic, S. Szalai, T. Szentimrey and L. Mercalli (2005). A new instrumental precipitation dataset for the Greater Alpine Region for the period 1800-2002. *International Journal of Climatology*, **25**, 139–166.

Bahr, D. B., M. F. Meier and S. D. Peckham (1997). The physical basis of glacier volume-area scaling. *Journal of Geophysical Research*, **102**, 20355–20362.

Barnett, T. P., J. C. Adam and D. P. Lettenmaier (2005). Potential impacts of a warming climate on water availability in snow-dominated regions. *Nature*, **438**, 303–309. doi: 0.1038/nature04141.

Barry, R. G. (2003). Mountain cryospheric studies and the WCRP climate and cryosphere (CliC) project. *Journal of Hydrology*, **282**, 177–181.

Baumgartner, A. and J.-J. Liebscher (1990). Lehrbuch der Hydrologie. Band 1: Allgemeine Hydrologie, Quantitative Hydrologie. Gebrüder Borntraeger, 673 pp.

Beniston, M. (2003). Climatic change in mountain regions : A review of possible impacts. *Climatic Change*, **59**, 5–31.

Beniston, M. (2004). The 2003 heat wave in Europe: A shape of things to come? An analysis based on Swiss climatological data and model simulations. *Geophysical Research Letters*, **31**, L02202. doi: 0.1029/2003GL018857.

Beniston, M., F. Keller, B. Koffi and S. Goyette (2003). Estimates of snow accumulation and volume in the Swiss Alps under changing climatic conditions. *Theoretical and Applied Climatology*, **76**, 125–140. doi: 0.1007/s00704-003-0016-5.

Braithwaite, R. J. (1984). Can the mass balance of a glacier be estimated from its equilibrium-line altitude ? *Journal of Glaciology*, **30**, 364–368.

Braithwaite, R. J. (2002). Glacier mass balance: the first 50 years of international monitoring. *Progress in Physical Geography*, **26**(1), 76–95.

Braithwaite, R. J. and O. B. Olesen (1989). Calculation of glacier ablation from air temperature, West Greenland. In *Glacier Fluctuations and Climatic Change* (edited by J. Oerlemans), pp. 219–233. Kluwer Academic Publishers.

Braithwaite, R. J. and S. C. B. Raper (2002). Glaciers and their contribution to sea level change. *Physics and Chemistry of the Earth*, **27**, 1445–1454.

Braithwaite, R. J. and Y. Zhang (1999). Modelling changes in glacier mass balance that may occur as a result of climate changes. *Geografiska Annaler*, **81 A**(4), 489–496.

Braithwaite, R. J. and Y. Zhang (2000). Sensitivity of mass blance of five Swiss glaciers to temperature changes assessed by tuning a degree-day model. *Journal of Glaciology*, **46**(152), 7–14.

Braithwaite, R. J., Y. Zhang and S. C. B. Raper (2002). Temperature sensitivity of the mass balance of mountain glaciers and ice caps as a climatological characteristic. *Zeitschrift für Gletscherkunde und Glazialgeologie*, **38**(1), 35–61.

Braun, L. N. and M. Weber (2001). Wasserspende aus hochalpinen Gebieten. In *Die Alpen - Ein kostbares Wasserschloss. Fachtagung 26.-28. November, Bad Reichenhall*. Kommission für Glaziologie der Bayerischen Akademie der Wissenschaften, München.

Braun, L. N., M. Weber and M. Schulz (2000). Consequences of climate change for runoff from Alpine regions. *Annals of Glaciology*, **31**, 19–25.

BUWAL (2004). Auswirkungen des Hitzesommers 2003 auf die Gewässer. Dokumentation. In *Schriftenreihe Umwelt Nr. 369 - Gewässerschutz*. Bundesamt für Umwelt, Wald und Landschaft (BUWAL), in Zusammenarbeit mit dem Bundesamt für Wasser und Geologie (BWG) und dem Bundesamt für Meteorologie und Klimatologie (MeteoSchweiz), Schweiz.

Calov, R., A. Ganopolski, M. Claussen, V. Petoukhov and R. Greve (2005). Transient simulation of the last glacial inception. Part I: glacial inception as a bifurcation in the climate system. *Climate Dynamics*, **24**, 545–561.

Charnock, M. (1955). Wind stress on a water surface. *Quarterly Journal of the Royal Meteorological Society*, **81**, 639–640.

Chen, J. and A. Ohmura (1990a). Estimation of Alpine glacier water resources and their change since the 1870s. No. 193 in *Hydrology in Mountainous Regions, IAHS Publ.*.

Chen, J. and A. Ohmura (1990b). On the influence of Alpine glaciers on runoff. No. 193 in *Hydrology in Mountainous Regions, IAHS Publ.*.

Chinn, T., S. Winkler, M. J. Salinger and N. Haakensen (2005). Recent glacier advances in Norway and New Zealand: A comparison of their glaciological and meteorological causes. *Geografiska Annaler*, **87 A**(1), 141–157.

Chinn, T. J. (1996). New Zealand glacier responses to climate change of the past century. *New Zealand Journal of Geology and Geophysics*, **39**, 415–428.

Christensen, J. H., O. B. Christensen, P. Lopez, E. van Meijgaard and M. Botzet (1996). The HIRHAM4 regional atmospheric climate model. Scientific Report 96-4, Danish Meteorological Institute, Copenhagen.

Coe, M. T. (2000). Modeling terrestrial hydrological systems at the continental scale: Testing the accuracy of an atmospheric GCM. *Journal of Climate*, **13**(4), 686–704.

Cogley, J. G. and W. P. Adams (1998). Mass balance of glaciers other than the ice sheets. *Journal of Glaciology*, **44**(147), 315–325.

Collins, D. (2005). Climatic variation and runoff in mountain basins with differing proportions of glacier cover. In *15th International Northern Research Basins Symposium and Workshop. Lulea to Kvikkjokk, Sweden*, pp. 21–30.

Collins, D. N. (1989). Hydrometeorological conditions, mass balance and runoff from alpine catchments. In *Glacier Fluctuations and Climatic Change* (edited by J. Oerlemans), pp. 235–260. Kluwer Academic Publishers.

Collins, W. D., C. M. Bitz, M. L. Blackmon, G. B. Bonan, C. S. Bretherton, J. A. Carton, P. Chang, S. C. Doney, J. J. Hack, T. B. Henderson, J. T. Kiehl, W. G. Large, D. S. McKenna, B. D. Santer and R. D. Smith (2006). The Community Climate System Model Version 3 (CCSM3). *Journal of Climate*, **19**, 2122–2143.

Davies, H. C. (1976). A lateral boundary formulation for multi-level prediction models. *Quarterly Journal of the Royal Meteorological Society*, **102**, 405–418.

Déqué, M., R. G. Jones, M. Wild, F. Giorgi, J. H. Christensen, D. C. Hassell, P. L. Vidale, B. Rockel, D. Jacob, E. Kjellström, M. de Castro, F. Kucharski and B. van den Hurk (2005). Global high resolution versus Limited Area Model climate change projections over Europe: quantifying confidence level from PRUDENCE results. *Climate Dynamics*, **25**, 653–670.

Dickinson, R. E., K. W. Oleson, G. Bonan, F. Hoffman, P. Thornton, M. Vertenstein, Z.-L. Yang and X. Zeng (2006). The Community Land Model and its climate statistics as a component of the Community Climate System Model. *Journal of Climate*, **19**, 2302–2324.

DKRZ (1994). The ECHAM 3 atmospheric general circulation model. Technical Report 6, Deutsches Klimarechenzentrum, Hamburg.

Dümenil, L. and E. Todini (1992). A rainfall-runoff scheme for use in the Hamburg climate model. In *Advances in theoretical hydrology - A tribute to James Dooge* (edited by J. O'Kane), No. 1 in *European Geophysical Society Series on Hydrological Sciences*, pp. 129–157. Elsevier Science, Amsterdam.

Dyurgerov, M. (2003). Mountain and subpolar glaciers show an increase in sensitivity to climate warming and intensification of the water cycle. *Journal of Hydrology*, **282**, 164–176.

Dyurgerov, M. and M. Meier (2005). Glaciers and the changing earth system: A 2004 snapshot. Occasional Paper 58, Institute of Arctic and Alpine Research, University of Colorado.

EEA (2005). The European Environment - State and Outlook 2005. Technical report, European Environment Agency.

Efthymiadis, D., P. Jones, K. Briffa, I. Auer, R. Böhm, W. Schöner, C. Frei and J. Schmidli (2006). Construction of a 10-min-gridded precipitation data set for the Greater Alpine Region for 1800-2003. *Journal of Geophysical Research*, **111**, D01105. doi: 0.1029/2005JD006120.

Escher-Vetter, H. (2000). Modelling meltwater production with a distributed energy balance method and runoff using a linear reservoir approach - Results from Vernagtferner, Oetztal Alps, for the ablation seasons 1992 to 1995. *Zeitschrift für Gletscherkunde und Glazialgeologie*, **36**, 119–150.

Essery, R. (2004). Statistical representation of mountain shading. *Hydrology and Earth System Sciences*, **8**(6), 1045–1050.

FoG (1967). Fluctuations of Glaciers 1959-1965, Vol. I of *Permanent Service on Fluctuations on Glaciers*. IAHS (ICSI) - UNESCO, Paris, 52 pp.

Frauenfelder, R., M. Maisch and F. Paul (2006). Glacier recession in the Upper Rhine river catchment between 1850 and 2000 and its importance for regional runoff. *Geophysical Research Abstracts*, **8**, 10385.

Frauenfelder, R., M. Zemp, W. Haeberli and M. Hoelzle (2005). Worldwide glacier mass balance measurements: Trends and first results of an extraordinary year in Central Europe. *Ice and Climate News. The WCRP Climate and Cryosphere Newsletter*, (6), 9–10.

Frei, C. and C. Schär (1998). A precipitation climatology of the Alps from high-resolution rain-gauge observations. *International Journal of Climatology*, **18**, 873–900.

Gilgen, H. and A. Ohmura (1999). The Global Energy Balance Archive (GEBA). *Bulletin of the American Meteorological Society*, **80**, 831–850.

Gilgen, H., M. Wild and A. Ohmura (1998). Means and trends of shortwave irradiance at the surface estimated from Global Energy Balance Archive data. *Journal of Climate*, **11**, 2042–2061.

Giorgi, F., R. Francisco and J. Pal (2003). Effects of a subgrid-scale topography and land use scheme on the simulation of surface climate and hydrology. Part I: Effects of temperature and water vapour disaggregation. *Journal of Hydrometeorology*, **4**, 317–333.

Graham, L. P. and D. Jacob (2000). Using large-scale hydrologic modeling to review runoff generation processes in GCM climate models. *Meteorologische Zeitschrift*, **9**(1), 49–57.

Gregory, J. M. and J. Oerlemans (1998). Simulated future sea-level rise due to glacier melt based on regionally and seasonally resolved temperature changes. *Nature*, **391**, 474–476.

Greuell, W. and R. Böhm (1998). 2 m temperatures along melting mid-latitude glaciers, and implications for the sensitivity of the mass balance to variations in temperature. *Journal of Glaciology*, **44**(146), 9–20.

Greve, R. (2003). Inlandeismodelle. *promet*, **29**(1-4), 98–104.

Grove, J. M. (2001). The initiation of the "Little Ice Age" in regions round the North Atlantic. *Climatic Change*, **48**, 53–82.

Gruber, S. and M. Hoelzle (2001). Statistical modelling of mountain permafrost distribution: local calibration and incorporation of remotely sensed data. *Permafrost and Periglacial Processes*, **12**, 69–77.

Häckel, H. (1999). Meteorologie. Ulmer, 4th edition, 448 pp.

Haeberli, W. (1995). Glacier fluctuations and climatic change detection - operational elements of a worldwide monitoring strategy. *WMO-Bulletin*, **44**, 23–31.

Haeberli, W. and M. Beniston (1998). Climate change and its impacts on glaciers and permafrost in the Alps. *Ambio*, **27**(4), 258–265.

Haeberli, W., R. Frauenfelder, M. Hoelzle and M. Maisch (1999). On rates and acceleration trends of global glacier mass changes. *Geografiska Annaler*, **81A**, 585–591.

Haeberli, W. and M. Hoelzle (1995). Application of inventory data for estimating characteristics of and regional climate-change effects on mountain glaciers: a pilot study with the European Alps. *Annals of Glaciology*, **21**, 206–212.

Haeberli, W., M. Hoelzle and M. Maisch (2001). Glaciers as key indicator of global climate change. In *Climate of the 21st Century: Changes and Risks* (edited by J. Lozán, H. Graßl and P. Hupfer), pp. 212–220. Wissenschaftliche Auswertungen, 2nd edition.

Haeberli, W., M. Maisch and F. Paul (2002). Mountain glaciers in global climate-related observation networks. *WMO-Bulletin*, **51**(1), 18–25.

Haeberli, W., P. Müller, P. Lean and H. Bösch (1989). Glacier changes following the Little Ice Age - A survey of the international data basis and its perspectives. In *Glacier Fluctuations and Climatic Change* (edited by J. Oerlemans), pp. 77–101. Kluwer Academic Publishers.

Haeberli, W. and H. J. Zumbühl (2003). Schwankungen der Alpengletscher im Wandel von Klima und Perzeption. In *Welt der Alpen - Gebirge der Welt* (edited by F. Jeanneret, D. Wastl-Walter and U. Wiesmann), pp. 25–37. Haupt, Bern.

Hagemann, S. (1998). Entwicklung einer Parameterisierung des lateralen Abflusses für Landflächen auf der globalen Skala. PhD thesis, University of Hamburg.

Hagemann, S. (2002). An improved land surface parameter dataset for global and regional climate models. Report 336, Max Planck Institute for Meteorology, Hamburg.

Hagemann, S., M. Botzet, L. Dümenil and B. Machenhauer (1999). Derivation of global GCM boundary conditions from 1 km land use satellite data. Report 289, Max Planck Institute for Meteorology, Hamburg.

Hagemann, S. and L. Dümenil (1998a). Documentation for the Hydrological Discharge Model. Technical Report 17, Deutsches Klimarechenzentrum, Hamburg.

Hagemann, S. and L. Dümenil (1998b). A parametrization of the lateral waterflow for the global scale. *Climate Dynamics*, **14**, 17–31.

Hagemann, S. and L. Dümenil (1999). Application of a global discharge model to atmospheric model simulations in the BALTEX Region. *Nordic Hydrology*, **30**, 209–230.

Hagemann, S. and D. Jacob (2007). Gradient in the climate change signal of European discharge predicted by a multi-model ensemble. *Climatic Change*. Accepted.

Hall, A. (2004). The role of surface albedo feedback in climate. *Journal of Climate*, **17**, 1550–1568.

Hall, M. H. P. and D. B. Fagre (2003). Modeled climate-induced glacier change in Glacier National Park, 1850-2100. *BioScience*, **53**(2), 131–140.

Hambrey, M. and J. Alean (2004). Glaciers. Cambridge University Press, 2nd edition, 376 pp.

Herterich, K. (2001). The Ice of the Earth. In *Climate of the 21st Century: Changes and Risks* (edited by J. Lozán, H. Graßl and P. Hupfer), pp. 65–69. Wissenschaftliche Auswertungen, 2nd edition.

Hock, R. (2003). Temperature index melt modelling in mountain areas. *Journal of Hydrology*, **282**, 104–115.

Hock, R. (2005). Glacier melt: a review of processes and their modelling. *Progress in Physical Geography*, **29**(3), 362–391.

Hock, R., P. Jansson and L. N. Braun (2005). Modelling the response of mountain glacier discharge to climate warming. In *Global Change and Mountain Regions: An Overview of Current Knowledge* (edited by U. M. Huber, H. K. M. Bugmann and M. A. Reasoner), Vol. 23 of *Advances in Global Change Research*. Springer, Dordrecht.

Hoelzle, M., W. Haeberli, M. Dischl and W. Peschke (2003). Secular glacier mass balances derived from cumulative glacier length changes. *Global and Planetary Change*, **36**, 295–306.

Hutter, K. (1983). Theoretical Glaciology. D. Reidel Publishing Company, Dordrecht / Boston / Lancaster, 510 pp.

Huybrechts, P., J. Gregory, I. Janssens and M. Wild (2004). Modelling Antarctic and Greenland volume changes during the 20th and 21st centuries forced by GCM time slice integrations. *Global and Planetary Change*, **42**, 83–105.

IPCC (2001). Climate Change 2001: The Scientific Basis. Contribution of Working Group I to the Third Assessment Report. Cambridge University Presss.

Jacob, D. (2001). A note to the simulation of the annual and inter-annual variability of the water budget over the Baltic Sea drainage basin. *Meteorology and Atmospheric Physics*, **77**, 61–73.

Jacob, D., L. Bärring, O. Christensen, J. Christensen, S. Hagemann, M. Hirschi, E. Kjellström, G. Lenderink, B. Rockel, C. Schär, S. Seneviratne, S. Somot, A. van Ulden and B. van den Hurk (2007). An inter-comparison of regional climate models for Europe: Design of the experiments and model performance. *Climatic Change*. Accepted.

Jacob, D. and R. Podzun (1997). Sensitivity studies with the regional climate model REMO. *Meteorology and Atmospheric Physics*, **63**, 119–129.

Jacob, D., B. J. J. M. Van den Hurk, U. Andrae, G. Elgered, C. Fortelius, L. P. Graham, S. D. Jackson, U. Karstens, C. Köpken, R. Lindau, R. Podzun, B. Rockel, F. Rubel, B. H. Sass, R. N. B. Smith and X. Yang (2001). A comprehensive model inter-comparison study investigating the water budget during the BALTEX-PIDCAP period. *Meteorology and Atmospheric Physics*, **77**, 19–43.

Jaedicke, C. and A. D. Sandvik (2002). High resolution snow distribution data from complex Arctic terrain: a tool for model validation. *Natural Hazards and Earth System Sciences*, **2**, 147–155.

Jansson, P., R. Hock and T. Schneider (2003). The concept of glacier storage: a review. *Journal of Hydrology*, **282**, 116–129.

Johannesson, T., C. F. Raymond and E. D. Waddington (1989). A simple method for determining the response time of glaciers. In *Glacier Fluctuations and Climatic Change* (edited by J. Oerlemans), pp. 343–352. Kluwer Academic Publishers.

Jonsell, U., R. Hock and B. Holmgren (2003). Spatial and temporal variations in albedo on Storglaciären, Sweden. *Journal of Glaciology*, **49**(164), 59–68.

Jungclaus, J., N. Keenlyside, M. Botzet, J.-J. Haak, H.and Luo, M. Latif, J. Marotzke, U. Mikolajewicz and E. Roeckner (2006). Ocean Circulation and Tropical Variability in the Coupled Model ECHAM5/MPI-OM. *Journal of Climate*, **19**, 3952–3972.

Kageyama, M., S. Charbit, C. Ritz, M. Khodri and G. Ramstein (2004). Quantifying ice-sheet feedbacks during the last glacial inception. *Geophysical Research Letters*, **31**, L24203. doi: 0.1029/2004GL021339.

Kaser, G. (2001). Glacier-climate interaction at low latitudes. *Journal of Glaciology*, **47**(157), 195–204.

Kaser, G., J. G. Cogley, M. B. Dyurgerov, M. F. Meier and A. Ohmura (2006). Mass balance of glaciers and ice caps: Consensus estimates for 1961-2004. *Geophysical Research Letters*, **33**, L19501. doi: 0.1029/2006GL027511.

Klok, E. J. (2003). The response of glaciers to climate change. PhD thesis, Institute for Marine and Atmospheric Research Utrecht, University of Utrecht.

Klok, E. J. and J. Oerlemans (2002). Model study of the spatial distribution of the energy and mass balance of Morteratschgletscher, Switzerland. *Journal of Glaciology*, **48**(163), 505–518.

Klok, E. J. and J. Oerlemans (2004). Modelled climate sensitivity of the mass balance of Morteratschgletscher and its dependence on albedo parameterization. *International Journal of Climatology*, **24**, 231–245.

Kotlarski, S., A. Block, U. Böhm, D. Jacob, K. Keuler, R. Knoche, D. Rechid and A. Walter (2005). Regional climate model simulations as input for hydrological applications: Evaluation of uncertainties. *Advances in Geosciences*, **5**, 119–125.

Kuhn, M. (1979). On the computation of heat transfer coefficients from energy-balance gradients on a glacier. *Journal of Glaciology*, **22**(87), 263–272.

Kuhn, M. (1981). Climate and glaciers. In *Sea level, ice, and climatic change* (edited by I. Allison), IAHS Publication No. 131, pp. 3–20. International Association of Hydrological Sciences.

Kuhn, M. (2003). Redistribution of snow and glacier mass balance from a hydrometeorological model. *Journal of Hydrology*, **282**, 95–103.

Kuhn, M., G. Markl, G. Kaser, U. Nickus, F. Obleitner and H. Schneider (1985). Fluctuations of climate and mass balance: Different responses of two adjacent glaciers. *Zeitschrift für Gletscherkunde und Glazialgeologie*, **21**, 409–416.

Lambrecht, A., R. Würländer and M. Kuhn (2005). The new Austrian glacier inventory: a tool for the analysis of modern glacier change. *Geophysical Research Abstracts*, **7**, 03097.

Latif, M., E. Roeckner, M. Botzet, M. Esch, H. Haak, S. Hagemann, J. Jungclaus, S. Legutke, S. Marsland and U. Mikolajewicz (2003). Reconstructing, monitoring, and predicting decadal-scale changes in the North Atlantic thermohaline circulation with sea surface temperature. *Journal of Climate*, **17**, 1605–1613.

Lehmann, A., P. Lorenz and D. Jacob (2004). Modelling the exceptional Baltic Sea inflow events in 2002-2003. *Geophysical Research Letters*, **31**, L21308. doi: 0.1029/2004GL020830.

Letréguilly, A. and L. Reynaud (1990). Space and time distribution of glacier mass-balance in the Northern Hemisphere. *Arctic and Alpine Research*, **22**(1), 43–50.

Lohmann, D., R. Nolte-Holube and E. Raschke (1996). A large-scale horizontal routing model to be coupled to land surface parametrization schemes. *Tellus*, **48A**, 708–721.

Lorenz, P. and D. Jacob (2005). Influence of regional scale information on the global circulation: A two-way nesting climate simulation. *Geophysical Research Letters*, **32**, L18706. doi: 0.1029/2005GL023351.

Loth, B. (1995). Die Schneedecke als Komponente des Klimasystems und ihre Modellierung. PhD thesis, University of Hamburg.

Louis, J. F. (1979). A parametric model of vertical eddy fluxes in the atmosphere. *Boundary-Layer Meteorology*, **17**, 187–202.

Loveland, T. R., B. C. Reed, J. F. Brown, D. O. Ohlen, J. Zhu, L. Yang and J. W. Merchant (2000). Development of a global land cover characteristics database and IGBP DISCover from 1-km AVHRR data. *International Journal of Remote Sensing*, **21**, 1303–1330.

Machguth, H., F. Paul, M. Hoelzle and W. Haeberli (2006). Distributed glacier mass balance modelling as an important component of modern multi-level glacier monitoring. *Annals of Glaciology*, **43**, 335–343. In press.

Maisch, M. (1992). Die Gletscher Graubündens - Rekonstruktion und Auswertung der Gletscher und deren Veränderungen seit dem Hochstand von 1850 im Gebiet der Östlichen Schweizer Alpen. Teil A: Grundlagen -Analysen - Ergebnisse. PhD thesis, Geographisches Institut der Universität Zürich.

Maisch, M., A. Wipf, B. Denneler, J. Battaglia and C. Benz (2000). Die Gletscher der Schweizer Alpen. Gletscherhochstand 1850 - Aktuelle Vergletscherung - Gletscherschwund-Szenarien. Schlussbericht NFP 31, Geographisches Institut der Universität Zürich.

Majewski, D. (1991). The Europa-Modell of the Deutscher Wetterdienst, Vol. 2 of *ECMWF Seminar on numerical methods in atmospheric models*.

Manabe, S. (1969). Climate and the ocean circulation, 1: The atmospheric circulation and the hydrology of the Earth's surface. *Monthly Weather Review*, **97**, 739–805.

Marty, C., R. Philipona, C. Fröhlich and A. Ohmura (2002). Altitude dependence of surface radiation fluxes and cloud forcing in the alps: Results from alpine surface radiation budget network. *Theoretical and Applied Climatology*, **72**, 137–155.

MBB (2005). Glacier Mass Balance Bulletin No. 8 (2002-2003). IUGG (CCS) - UNEP - UNESCO - WMO, Zürich, 100 pp.

McGregor, J. L. (1997). Regional Climate Modelling. *Meteorology and Atmospheric Physics*, **63**, 105–117.

Meier, M. F. and D. B. Bahr (1996). Counting glaciers: Use of scaling methods to estimate the number and size distribution of the glaciers of the world. In *Glaciers, Ice Sheets and Volcanoes: A Tribute to Mark F. Meier* (edited by S. C. Colbeck), No. 96-27 in *CRREL Special Report*, pp. 89–94. U.S. Army Hanover, New Hampshire.

Meier, M. F., M. B. Dyurgerov and G. J. McCabe (2003). The health of glaciers: Recent changes in glacier regime. *Climatic Change*, **59**, 123–135.

Miller, J. R., G. L. Russell and G. Caliri (1994). Continental-scale river flow in climate models. *Journal of Climate*, **7**, 914–928.

Mitchell, T. D., T. R. Carter, P. D. Jones, M. Hulme and M. New (submitted). A comprehensive set of high-resolution grids of monthly climate for Europe and the globe: the observed record (1901-2000) and 16 scenarios (2001-2100). *Journal of Climate*.

Mölg, T. and D. R. Hardy (2004). Ablation and associated energy balance of a horizontal glacier surface on Kilimanjaro. *Journal of Geophysical Research*, **106**, D16104. doi: 0.1029/2003JD004338.

Moore, I. D., T. W. Norton and J. E. Williams (1993). Modelling evironmental heterogeneity in forested landscapes. *Journal of Hydrology*, **150**, 717–747.

Mountain Agenda (1998). Mountains of the world. Water towers for the 21st century. Prepared for the United Nations Commission on Sustainable Development. Paul Haupt Publishers, Bern, Switzerland, 32 pp.

Müller, F., T. Caflish and G. Müller (1976). Firn und Eis der Schweizer Alpen, Gletscherinventar. Report 57, Geographisches Institut, ETH Zürich.

Müller, M. D. and D. Scherer (2005). A grid- and subgrid-scale radiation parameterization of topographic effects for mesoscale weather forecast models. *Monthly Weather Review*, **133**, 1431–1442.

Munro, D. S. (1990). Comparison of melt energy computations and ablatometer measurements on melting ice and snow. *Arctic and Alpine Research*, **22**(2), 153–162.

Nakawo, M. and B. Rana (1999). Estimate of ablation rate of glacier ice under a supraglacial debris layer. *Geografiska Annaler*, **81 A**, 695–701.

Nesje, A., Ø. Lie and S. O. Dahl (2000). Is the North Atlantic Oscillation reflected in Scandinavian glacier mass balance records? *Journal of Quaternary Science*, **15**(6), 587–601.

New, M., M. Hulme and P. Jones (2000). Representing Twentieth-Century Space-Time Climate Variability. Part II: Development of 1901-96 Monthly Grids of Terrestrial Surface Climate. *Journal of Climate*, **13**, 2217–2238.

NSIDC (1999). World glacier inventory. Digital media, World Glacier Monitoring Service and National Snow and Ice Data Center/World Data Center for Glaciology, Boulder.

Oerlemans, J. (1989). On the response of valley glaciers to climatic change. In *Glacier Fluctuations and Climatic Change* (edited by J. Oerlemans), pp. 353–371. Kluwer Academic Publishers.

Oerlemans, J. (1991). A model for the surface balance of ice masses: Part I. Alpine Glaciers. *Zeitschrift für Gletscherkunde und Glazialgeologie*, **27/28**, 63–83.

Oerlemans, J. (1993). Modelling of glacier mass balance. In *Ice in the Climate System* (edited by W. Peltier), Vol. 12 of *NATO ASI series. Series I, Global Environmental Change*. Springer.

Oerlemans, J. (1994). Quantifying global warming from the retreat of glaciers. *Science*, **264**, 243–245.

Oerlemans, J. (2001). Glaciers and climate change. A.A. Balkema Publishers, Lisse, Abingdon, Exton (PA), Tokyo.

Oerlemans, J. (2005). Extracting a climate signal from 169 glacier records. *Science*, **308**, 675–677.

Oerlemans, J., B. Anderson, A. Hubbard, P. Huybrechts, T. Johannesson, W. H. Knap, M. Schmeits, A. P. Stroeven, R. S. W. van de Wal, J. Wallinga and Z. Zuo (1998). Modelling the response of glaciers to climate warming. *Climate Dynamics*, **14**, 267–274.

Oerlemans, J. and J. P. F. Fortuin (1992). Sensitivity of glaciers and small ice caps to greenhouse warming. *Science*, **258**, 115–117.

Oerlemans, J. and N. C. Hoogendoorn (1989). Mass-balance gradients and climate change. *Journal of Glaciology*, **35**(121), 399–405.

Oerlemans, J. and E. J. Klok (2004). Effect of summer snowfall on glacier mass balance. *Annals of Glaciology*, **38**, 97–100.

Oerlemans, J. and W. H. Knap (1998). A 1 year record of global radiation and albedo in the ablation zone of Morteratschgletscher, Switzerland. *Journal of Glaciology*, **44**(147), 231–238.

Oerlemans, J. and B. K. Reichert (2000). Relating glacier mass balance to meteorological data by using a seasonal sensitivity characteristic. *Journal of Glaciology*, **46**(152), 1–6.

Ohmura, A. (2001). Physical basis for the temperature-based melt-index method. *Journal of Applied Meteorology*, **40**, 753–761.

Oke, T. (1978). Boundary layer climates. Methuen & Co Ltd.

Oleson, K. W., Y. Dai, G. Bonan, M. Bosilovich, R. Dickinson, P. Dirmeyer, F. Hoffman, P. Houser, S. Levis, G.-Y. Niu, P. Thornton, M. Vertenstein, Z.-L. Yang and X. Zeng (2004). Technical Description of the Community Land Model (CLM). NCAR Technical Note NCAR/TN-461+STR, National Center for Atmospheric Research.

Oliphant, A. J., R. A. Spronken-Smith, A. P. Sturman and I. F. Owens (2003). Spatial variability of surface radiation fluxes in mountainous terrain. *Journal of Applied Meteorology*, **42**(1), 113–128.

Østrem, G. (1975). ERTS data in glaciology - An effort to monitor glacier mass balance from satellite imagery. *Journal of Glaciology*, **15**, 403–415.

Paterson, W. S. B. (1994). The physics of glaciers. Butterwort-Heinemann, Oxford, 3rd edition, 481 pp.

Paul, F. (2004). The New Swiss Glacier Inventory 2000. Application of remote sensing and GIS. PhD thesis, Universität Zürich.

Paul, F., C. Huggel and A. Kääb (2004a). Combining satellite multispectral image data and a digital elevation model for mapping debris-covered glaciers. *Remote Sensing of Environment*, **89**, 510–518.

Paul, F., A. Käab, M. Maisch, T. Kellenberger and W. Haeberli (2004b). Rapid disintegration of Alpine glaciers observed with satellite data. *Geophysical Research Letters*, **31**, L21402. doi: 0.1029/2004GL020816.

Paul, F., H. Machguth and A. Kääb (2005). On the impact of glacier albedo under conditions of extreme glacier melt: The summer of 2003 in the Alps. *EARSeL eProceedings*, **4**(2), 139–149.

Pedersen, C. A. and J.-G. Winther (2005). Intercomparison and validation of snow albedo parameterization schemes in climate models. *Climate Dynamics*, **25**, 351–362.

Pitman, A. (2003). Review: The evolution of, and revolution in, land surface schemes designed for climate models. *International Journal of Climatology*, **23**, 479–510.

Press, F. and R. Siever (1994). Understanding Earth. W.H. Freeman and Company, 602 pp.

Radić, V. and R. Hock (2006). Modeling future glacier mass balance and volume changes using ERA-40 reanalysis and climate models: A sensitivity study at Storglaciären, Sweden. *Journal of Geophysical Research*, **111**, F03003. doi: 0.1029/2005JF000440. Hello.

Ranzi, R. and R. Rosso (1995). Distributed estimation of incoming direct solar radiation over a drainage basin. *Journal of Hydrology*, **166**, 461–478.

Raper, S. C. B. and R. J. Braithwaite (2005). The potential for sea lvel rise: New estimates from glacier and ice cap area and volume distributions. *Geophysical Research Letters*, **32**, L05502. doi: 0.1029/2004GL021981.

Raper, S. C. B. and R. J. Braithwaite (2006). Low sea level rise projections from mountain glaciers and icecaps under global warming. *Nature*, **439**, 311–313. doi: 0.1038/nature04448.

Raper, S. C. B., O. Brown and R. J. Braithwaite (2000). A geometric glacier model for sea-level change calculations. *Journal of Glaciology*, **46**(154), 357–368.

Raymond, C. F. (1980). Dynamics of snow and ice masses, chapter 2, pp. 80–139. Academic Press, Inc., New York.

Rechid, D. and D. Jacob (2006). Influence of seasonally varying vegetation on the simulated climate in Europe. *Meteorologische Zeitschrift*. In press.

Reichert, B. K., L. Bengtsson and J. Oerlemans (2001a). Midlatitude forcing mechanisms for glacier mass balance investigated using general circulation models. *Journal of Climate*, **14**, 3767–3784.

Reichert, B. K., L. Bengtsson and J. Oerlemans (2001b). Natural climate variability as indicated by glaciers and implications for climate change: A modeling study. Report 328, Max Planck Institute for Meteorology, Hamburg.

Reichert, B. K., L. Bengtsson and J. Oerlemans (2002). Recent glacier retreat exceeds internal variability. *Journal of Climate*, **15**, 3069–3081.

Ridley, J. K., P. Huybrechts, J. M. Gregory and J. A. Lowe (2005). Elimination of the Greenland Ice Sheet in a High CO_2 Climate. *Journal of Climate*, **18**, 3409–3427.

Roeckner, E., K. Arpe, L. Bengtsson, M. Christoph, M. Claussen, L. Dümenil, M. Esch, M. Giorgetta, U. Schlese and U. Schulzweida (1996). The atmospheric general circulation model ECHAM-4: Model description and simulation of present-day climate. Report 218, Max Planck Institute for Meteorology, Hamburg.

Roeckner, E., G. Bäuml, L. Bonaventura, R. Brokopf, M. Esch, M. Giorgetta, S. Hagemann, I. Kirchner, L. Kornblueh, E. Manzini, A. Rhodin, U. Schlese, U. Schulzweida and A. Tompkins (2003). The atmospheric general circulation model ECHAM5 - Part I: Model description. Report 349, Max Planck Institute for Meteorology, Hamburg.

Schädler, B. (2003). Effects of global climate change on alpine aquatic systems. No. 55 in *EAWAG News*.

Schär, C., T. D. Davies, C. Frei, H. Wanner, M. Widmann, M. Wild and H. C. Davies (1998). Current alpine climate. In *Views from the Alps - Regional perspectives on climate change* (edited by P. Cebon, U. Dahinden, H. Davies, D. Imboden and C. Jaeger). MIT Press.

Schär, C., P. Vidale, D. Lüthi, C. Frei, C. Häberli, M. Liniger and C. Appenzeller (2004). The role of increasing temperature variability in European summer heatwaves. *Nature*, **427**, 332–336.

Schneeberger, C., O. Albrecht, H. Blatter, M. Wild and R. Hock (2001). Modelling the response of glaciers to a doublig in atmospheric CO_2: a case study of Storglaciären, northern Sweden. *Climate Dynamics*, **17**, 825–834.

Schneeberger, C., H. Blatter, A. Abe-Ouchi and M. Wild (2003). Modelling changes in the mass balance of glaciers of the northern hemisphere for a transient 2 x CO_2 scenario. *Journal of Hydrology*, **282**, 145–163.

Schwarb, M. (2000). The Alpine Precipitation Climate - Evaluation of a high-resolution analysis scheme using comprehensive rain-gauge data. PhD thesis, Swiss Federal Institute of Technology, Zürich.

Schwarb, M., C. Daly, C. Frei and C. Schär (2001). Mean annual and seasonal precipitation throughout the European Alps 1971-1990. In *Hydrological Atlas of Switzerland*. Plates 2.6 and 2.7.

Semmler, T. (2002). Der Wasser- und Energiehaushalt der arktischen Atmosphäre. PhD thesis, University of Hamburg.

Sevruk, B. (1997). Regional dependency of precipitation-altitude relationship in the Swiss Alps. *Climatic Change*, **36**, 355–369.

Simmons, A. J. and D. M. Burridge (1981). An energy and angular-momentum conserving vertical finite-difference scheme and hybrid vertical coordinate. *Monthly Weather Review*, **109**, 758–766.

Singh, P. and V. P. Singh (2001). Snow and glacier hydrology. In *Water Science and Technology Library*, Vol. 37. Kluwer Academic Publishers.

Smith, I. N. and W. F. Budd (1981). The derivation of past climate changes from observed changes in glaciers. In *Sea level, ice, and climatic change* (edited by I. Allison), IAHS Publication No. 131, pp. 31–52. International Association of Hydrological Sciences.

SWISSTOPO (2001). DHM25 - Das digitale Hhenmodell der Schweiz Level 2. Technical report, Bundesamt für Landestopographie, Schweiz.

Takeuchi, N., S. Kohshima and K. Seko (2001). Structure, formation, and darkening process of albedo-reducing material (cryoconite) on a Himalayan glacier: A granular algae mat growing on the glacier. *Arctic, Antarctic, and Alpine Research*, **33**(2), 115–122.

UNESCO (1970). Perennial ice and snow masses. A guide for compilation and assemblage of data for a World Glacier Inventory. No. 1 in *UNESCO/IAHS Technical Papers in Hydrology*.

Uppala, S. M., P. W. Kallberg, A. J. Simmons, U. Andrae, V. da Costa Bechtold, M. Fiorino, J. K. Gibson, J. Haseler, A. Hernandez, G. A. Kelly, X. Li, K. Onogi, S. Saarinen, N. Sokka, R. P. Allan, E. Andersson, K. Arpe, M. A. Balmaseda, A. C. M. Beljaars, L. van de Berg, J. Bidlot, N. Bormann, S. Caires, F. Chevallier, A. Dethof, M. Dragosavac, M. Fisher, M. Fuentes, S. Hagemann, E. Holm, B. J. Hoskins, L. Isaksen, P. A. E. M. Janssen, R. Jenne, A. P. McNally, J.-F. Mahfouf, J.-J. Morcrette, N. A. Rayner, R. W. Saunders, P. Simon, A. Sterl, K. E. Trenberth, A. Untch, D. Vasiljevic, P. Viterbo and J. Woollen (2005). The ERA-40 re-analysis. *Quarterly Journal of the Royal Meteorological Society*, **131**, 2961–3012.

van de Wal, R. S. W. and M. Wild (2001). Modelling the response of glaciers to climate change by applying volume-area scaling in combination with a high resolution GCM. *Climate Dynamics*, **18**, 359–366.

Verbunt, M., J. Gurtz, K. Jasper, H. Lang, P. Warmerdam and M. Zappa (2003). The hydrological role of snow and glaciers in alpine river basins and their distributed modeling. *Journal of Hydrology*, **282**, 36–55.

Vincent, C. (2002). Influence of climate change over the 20th Century on four French glacier mass balances. *Journal of Geophysical Research*, **107**(D19), 4375. doi: 0.1029/2001JD00832.

Vizcaino, M. (2006). Long-term interactions between ice sheets and climate under anthropogenic greenhouse forcing - Simulations with two complex Earth System Models. PhD thesis, Max Planck Institute for Meteorology. Reports on Earth System Science No. 30.

Wang, J., K. White and J. Robinson (2000). Estimating surface net solar radiation by use of Landsat-5 TM and digital elevation models. *International Journal of Remote Sensing*, **21**(1), 31–43.

Wang, Z. and L. A. Mysak (2002). Simulation of the last glacial inception and rapid ice sheet growth in the McGill Paleoclimate Model. *Geophysical Research Letters*, **29**(23). doi: 0.1029/2002GL015120.

Weber, M. (2005). Mikrometeorologische Prozesse bei der Ablation eines Alpengletschers. PhD thesis, Institut für Meteorologie und Geophysik, Universität Innsbruck.

WGI (1989). World glacier inventory - Status 1988. IAHS (ICSI) - UNEP - UNESCO, compiled by the World Glacier Monitoring Service (WGMS), Nairobi, 458 pp.

Wilson, J. P. and J. C. Gallant (2000). Terrain analysis - Principles and applications, chapter 4: Secondary Topographic Attributes, pp. 51–86. John Wiley & Sons, Inc.

Winguth, A., U. Mikolajewicz, M. Gröger, E. Maier-Reimer, G. Schurgers and M. Vizcaíno (2005). Centennial-scale interactions beween the carbon cycle and anthropogenic climate change using a dynamic Earth system model. *Geophysical Research Letters*, **32**, L23714. doi: 0.1029/2005GL023681.

Zemp, M. (2006). Glaciers and Climate Change - Spatio-temporal Analysis of Glacier Fluctuations in the European Alps after 1850. PhD thesis, Universität Zürich.

Zemp, M., W. Haeberli, M. Hoelzle and F. Paul (2006a). Alpine glaciers to disappear within decades ? *Geophysical Research Letters*, **33**, L13504. doi: 0.1029/2006GL026319.

Zemp, M., M. Hoelzle and W. Haeberli (2007). Distributed modelling of the regional climatic equilibrium line altitude of glaciers in the European Alps. *Global and Planetary Change*, **56**, 83–100. doi: 0.1016/j.gloplacha.2006.07.2002.

Zemp, M., F. Paul, M. Hoelzle and W. Haeberli (2006b). Glacier fluctuations in the European Alps 1850 - 2000: An overview and spatio-temporal analysis of available data. In *The darkening peaks: Glacial retreat in scientific and social context* (edited by B. Orlove, E. Wiegandt and B. Luckman). University of California Press. In press.

A New Variables

The following listing gives an overview on the 46 grid box variables that have been introduced in REMO in order to account for glaciers on a subgrid scale.

Name	Internal Code	Description	Unit
TGLAC1	16	Temperature of the upper ice layer	[K]
TGLAC2	17	Temperature of the lower ice layer	[K]
GLD	18	Total ice depth	[m w.e.]
GLRUN	19	Surface runoff originating from the glaciated fraction (reference area: total grid box land surface area)	[mm]
GLDRAIN	20	Subsurface drainage originating from the glaciated fraction (reference area: total grid box land surface area)	[mm]
GLACIER	21	Fractional glacier coverage (glacier-covered fraction of the total grid box surface area)	[ ]
TD3G	22	Temperature of the first (= uppermost) soil layer of the glaciated fraction	[K]
TD4G	23	Temperature of the second soil layer of the glaciated fraction	[K]
TD5G	24	Temperature of the third soil layer of the glaciated fraction	[K]
TDG	25	Temperature of the fourth soil layer of the glaciated fraction	[K]
TDCLG	26	Temperature of the fifth (= lowermost) soil layer of the glaciated fraction	[K]
WI3G	27	Fraction of frozen soil water of the first (= uppermost) soil layer of the glaciated fraction	[ ]
WI4G	28	Fraction of frozen soil water of the second soil layer of the glaciated fraction	[ ]
WI5G	29	Fraction of frozen soil water of the third soil layer of the glaciated fraction	[ ]
WIG	30	Fraction of frozen soil water of the fourth soil layer of the glaciated fraction	[ ]
WICLG	31	Fraction of frozen soil water of the fifth (= lowermost) soil layer of the glaciated fraction	[ ]
GLACCI	32	Ice accumulation on the glaciated fraction (reference area: glaciated surface area)	[mm w.e.]
GLABLI	33	Ice ablation on the glaciated fraction (reference area: glaciated surface area)	[mm w.e.]
GLACCS	34	Snow accumulation on the glaciated fraction (reference area: glaciated surface area)	[mm w.e.]

GLABLS	35	Snow ablation on the glaciated fraction (reference area: glaciated surface area)	[mm w.e.]
GLVOL	36	Total ice volume	[m^3 w.e.]
SRADSGI	37	Surface incoming solar radiation on the glaciated fraction	[W/m^2]
SRADSGO	38	Surface outgoing solar radiation on the glaciated fraction	[W/m^2]
TSGECH	111	Surface temperature of the glaciated fraction	[K]
AZ0G	113	Surface roughness length of the glaciated fraction	[m]
TMCHG	114	Turbulent exchange coefficient for sensible and latent heat on the glaciated fraction	[ ]
AHFSG	115	Sensible heat flux on the glaciated fraction (model physics)	[W/m^2]
BFLHSG	116	Sensible heat flux on the glaciated fraction (model dynamics)	[W/m^2]
BFLQDSG	117	Latent heat flux on the glaciated fraction (model dynamics)	[W/m^2]
EVAPG	118	Surface evaporation on the glaciated fraction (reference area: glaciated surface area)	[mm w.e.]
QDBG	119	Surface specific humidity on the glaciated fraction	[kg/kg]
USTRG	120	Surface u-stress on the glaciated fraction	[Pa*s]
VSTRG	121	Surface v-stress on the glaciated fraction	[Pa*s]
ALSOG	122	Surface albedo of the glaciated fraction	[ ]
SNG	123	Snow depth on the glaciated fraction	[m w.e.]
TSNG	124	Snow temperature (centre) on the glaciated fraction	[K]
SNAGEL	125	Age of the snow cover on the non-glaciated fraction	[days]
SNAGEG	126	Age of the snow cover on the glaciated fraction	[days]
SNMDL	127	Mean snow depth on the non-glaciated fraction over the period SNAGEL	[m w.e.]
SNMDG	128	Mean snow depth on the glaciated fraction over the period SNAGEG	[m w.e.]
SNMELG	252	Snow melt on the glaciated fraction (reference area: total grid box land surface area)	[mm w.e.]
AHFLG	253	Latent heat flux on the glaciated fraction (model physics)	[W/m^2]
GLDLAST	254	Total ice depth after the previous area adjustment (AAM=2,3,4)	[m w.e.]
GLIMELT	255	Ice melt on the glaciated fraction (reference area: total grid box land surface area)	[mm w.e.]
TRADSGI	256	Surface incoming thermal radiation on the glaciated fraction	[W/m^2]
TRADSGO	256	Surface outgoing thermal radiation on the glaciated fraction	[W/m^2]

List of Abbreviations and Acronyms

AAM	Area Adjustment Method
AAR	Accumulation Area Ratio
ALP-IMP	Multi-Centennial Climate Variability in the Alps based on Instrumental Data, Model Simulations and Proxy Data
AOGCM	Atmosphere-Ocean General Circulation Model
CRU	Climate Research Unit (University of East Anglia)
DEM	Digital Elevation Model
DJF	winter season (December, January, February)
ECMWF	European Centre for Medium-Range Weather Forecasts
ELA	Equilibrium Line Altitude
EM	Europa-Modell
FoG	Fluctuations of Glaciers
GCM	General Circulation Model
GEBA	Global Energy Balance Archive (Swiss Federal Institute of Technology)
GLIMS	Global Land Ice Measurements from Space
HD	Hydrological Discharge
IPCC	Intergovernmental Panel on Climate Change
JJA	summer season (June, July, August)
LAI	Leaf Area Index
LBC	Lateral Boundary Condition
LSS	Land Surface Scheme
MAM	spring season (March, April, May)
MODIS	Moderate Resolution Imaging Spectroradiometer
MS	MeteoSwiss
N, E, S, W	North, East, South, West
NSIDC	National Snow and Ice Data Center
NWP	Numerical Weather Prediction
RCM	Regional Climate Model
REMO	Regional Model
SON	autumn season (September, October, November)
SRAD	Solar Radiation
SSC	Seasonal Sensitivity Characteristic
SST	Sea Surface Temperature
UNESCO	United Nations Educational, Scientific and Cultural Organization
WGI	World Glacier Inventory
WGMS	World Glacier Monitoring Service
WCRP	World Climate Research Programme
w.e.	water equivalent

Acknowledgements

The present work has only been made possible by the support and the help of a large number of persons. Some of them are mentioned below, most of them are not. This last section is dedicated to all who contributed to this work, might it be on a scientific level or in every-day life. I am truly thankful and greatly acknowledge their support.

Mentioning a number of special contributions, I would like to thank first of all the members of my supervising panel, Prof. Hartmut Graßl, Dr. Daniela Jacob and Dr. Stefan Hagemann for offering scientific guidance and advice and for giving me the opportunity to work on this interesting topic. In particular, the support of Dr. Daniela Jacob during the long-lasting final phase of the PhD work is greatly acknowledged. Dr. Stefan Hagemann kindly offered his help concerning the application of the HD model.

All reviewers of the manuscript are thanked for their useful comments.

A number of major problems as well as smaller but still annoying obstacles arose along the way. Both would not have been overcome without the help and the advice of the (former and current) members of the regional climate modelling group at the MPI-M and of Ralf Podzun at the Model & Data Group. Thanks to all of you ! Also the partners of the QUIRCS project are thanked for the interesting and pleasant time in the project.

A special thank goes to Dr. Frank Paul and the Glaciology and Geomorphodynamics Group of the University of Zurich for hosting me in summer 2005 and for taking me out to the field. Their scientific advice has been extremely helpful for this work. I will not forget the pleasant time in Zurich ! That cooperation has been made possible by the financial support of the International Max Planck Research School on Earth System Modelling (IMPRS). I greatly appreciate the possibility to take part in the IMPRS program in the course of my PhD work.

I am deeply thankful to my parents and my family for their lifelong support and confidence.

Most of all, I thank Tanja for all her love and encouragement and for being the light in the dark. Without your support I would have got lost.

Publikationsreihe des MPI-M
„Berichte zur Erdsystemforschung“ , „*Reports on Earth System Science*“, ISSN 1614-1199
Sie enthält wissenschaftliche und technische Beiträge, inklusive Dissertationen.

Berichte zur Erdsystemforschung Nr.1 Juli 2004	**Simulation of Low-Frequency Climate Variability in the North Atlantic Ocean and the Arctic** Helmuth Haak
Berichte zur Erdsystemforschung Nr.2 Juli 2004	**Satellitenfernerkundung des Emissionsvermögens von Landoberflächen im Mikrowellenbereich** Claudia Wunram
Berichte zur Erdsystemforschung Nr.3 Juli 2004	**A Multi-Actor Dynamic Integrated Assessment Model (MADIAM)** Michael Weber
Berichte zur Erdsystemforschung Nr.4 November 2004	**The Impact of International Greenhouse Gas Emissions Reduction on Indonesia** Armi Susandi
Berichte zur Erdsystemforschung Nr.5 Januar 2005	**Proceedings of the first HyCARE meeting, Hamburg, 16-17 December 2004** Edited by Martin G. Schultz
Berichte zur Erdsystemforschung Nr.6 Januar 2005	**Mechanisms and Predictability of North Atlantic - European Climate** Holger Pohlmann
Berichte zur Erdsystemforschung Nr.7 November 2004	**Interannual and Decadal Variability in the Air-Sea Exchange of CO2 - a Model Study** Patrick Wetzel
Berichte zur Erdsystemforschung Nr.8 Dezember 2004	**Interannual Climate Variability in the Tropical Indian Ocean: A Study with a Hierarchy of Coupled General Circulation Models** Astrid Baquero Bernal
Berichte zur Erdsystemforschung Nr9 Februar 2005	**Towards the Assessment of the Aerosol Radiative Effects, A Global Modelling Approach** Philip Stier
Berichte zur Erdsystemforschung Nr.10 März 2005	**Validation of the hydrological cycle of ERA40** Stefan Hagemann, Klaus Arpe and Lennart Bengtsson
Berichte zur Erdsystemforschung Nr.11 Februar 2005	**Tropical Pacific/Atlantic Climate Variability and the Subtropical-Tropical Cells** Katja Lohmann
Berichte zur Erdsystemforschung Nr.12 Juli 2005	**Sea Ice Export through Fram Strait: Variability and Interactions with Climate**- Torben Königk
Berichte zur Erdsystemforschung Nr.13 August 2005	**Global oceanic heat and fresh water forcing datasets based on ERA-40 and ERA-15** Frank Röske
Berichte zur Erdsystemforschung Nr.14 August 2005	**The** HAM**burg** O**cean** C**arbon** C**ycle Model HAMOCC5.1 - Technical Description Release 1.1** Ernst Maier-Reimer, Iris Kriest, Joachim Segschneider, Patrick Wetzel
Berichte zur Erdsystemforschung Nr.15 Juli 2005	**Long-range Atmospheric Transport and Total Environmental Fate of Persistent Organic Pollutants - A Study using a General Circulation Model** Semeena Valiyaveetil Shamsudheen

Publikationsreihe des MPI-M
„Berichte zur Erdsystemforschung“ , „*Reports on Earth System Science*“, ISSN 1614-1199
Sie enthält wissenschaftliche und technische Beiträge, inklusive Dissertationen.

Publikationsreihe des MPI-M
„Berichte zur Erdsystemforschung“ , „*Reports on Earth System Science*“, ISSN 1614-1199
Sie enthält wissenschaftliche und technische Beiträge, inklusive Dissertationen.



ISSN 1614-1199